AD NUMBER

AD912519

NEW LIMITATION CHANGE

TO

Approved for public release, distribution unlimited

FROM

Distribution authorized to U.S. Gov't. agencies only; Test and Evaluation; MAR 1973. Other requests shall be referred to Air Force Armament Laboratory, Attn: DLDL, Eglin AFB, FL 32542.

AUTHORITY

AFATL ltr, 17 Oct 1975

AFATL-TR-73-69

STUDY OF HEAT TRANSFER AND EROSION IN GUN BARRELS

SCHOOL OF MECHANICAL ENGINEERING
GEORGIA INSTITUTE OF TECHNOLOGY

TECHNICAL REPORT AFATL-TR-73-69

MARCH 1973

AIR FORCE ARMAMENT LABORATORY
AIR FORCE SYSTEMS COMMAND • UNITED STATES AIR FORCE
EGLIN AIR FORCE BASE, FLORIDA

Study Of Heat Transfer And Erosion In Gun Barrels

S. Shelton

A. Bergles

P. Saha

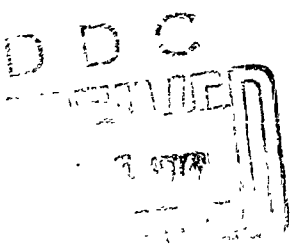

FOREWORD

This report details the work performed under the direction of Dr. S. V. Shelton at the School of Mechanical Engineering, Georgia Institute of Technology, Atlanta, Georgia, under Contract No. F08635-70-C-0129 with the Air Force Armament Laboratory, Eglin Air Force Base, Florida 32542. Lieutenant William S. Bulpitt (DLDL) was program manager for the Armament Laboratory. This effort was conducted during the period from 15 July 1970 to 15 July 1972. The first 12 months were devoted to modeling the heat transfer mechanism in gun barrels; during the second 12 months this model and its results were used to aid in understanding erosion in gun barrels and its reduction by particle seeding (TiO_2) of the propellants.

This report is divided into two parts. Part I - Analytical Model of Heat Transfer in Gun Barrels consists of Section II through VI, and Part II - Particle Seeding Effects on Gun Barrel Heat Transfer and Erosion consists of Sections VII through XI.

This technical report has been reviewed and is approved.

DALE M. DAVIS
Director, Guns and Rockets Division

ABSTRACT

This study models the combustion, solid propellant movement, gas dynamics, projectile dynamics, transient boundary layer, heat transfer, and barrel metal temperatures in a gun barrel. This is accomplished by rigorous development of the coupled partial differential equations and carrying out a detailed numerical solution to these equations. Comparison of barrel temperature solutions to experimental data is shown. Erosion mechanisms are discussed in the light of these solutions. This model is then used to study hypotheses concerning the heat transfer, temperature, and erosion effects of submicron size solid particle additives (TiO_2) to gun propellants. A mechanism not previously studied offers excellent theoretical results in explaining the reduced erosion.

(The reverse of this page is blank.)

TABLE OF CONTENTS

TABLE OF CONTENTS (Concluded)

LIST OF FIGURES

LIST OF FIGURES (Continued)

LIST OF FIGURES (Continued)

LIST OF FIGURES (continued)

LIST OF FIGURES (Concluded)

LIST OF TABLES

NOMENCLATURE

English notations

A	coefficient in wall shear stress expression (59),
A_m	series coefficient defined by Equation (146),
A_p	cross-sectional area of tube
a	sonic velocity in gas media
a_p	piston acceleration
B	exponent of Reynolds number in (59),
B_I	function defined by Equation (11),
B_{II}	function defined by Equation (38),
B_m	series coefficient defined by Equation (146),
C_1	ratio of boundary layer thickness and momentum thickness, δ/δ^*
C_I	function defined by Equation (12),
C_{II}	function defined by Equation (39),
C_f	local wall friction coefficient
C_m	series coefficient defined by Equation (152),
c_s	specific heat of solids
c_p	specific heat of gas at constant pressure
c_v	specific heat of gas at constant volume
D	tube inside diameter
D_1'	function defined by Equation (78),
D_2'	function defined by Equation (79),
D_3'	function defined by Equation (3.21),
E_I	function defined by Equation (13),
E_{II}	function defined by Equation (40),
E'	function defined by Equation (77),

NOMENCLATURE (continued)

English notations

e	internal energy per unit mass
G'	function defined by Equation (83),
H	profile shape factor, δ^*/θ
H'_I	function defined by Equation (84),
H'_{II}	function defined by Equation (94),
h	enthalpy per unit mass film heat transfer coefficient
h_m	mean heat transfer coefficient at the inner surface, $(h_{ij}^{n} + h_{ij}^{n+1})/2$
J	mechanical equivalent of heat
j	axial position of a nodal point in finite difference grid
L_o	initial piston distance from tube head end
L_p	piston distance from tube head end at any instant
L_t	tube length
M	molecular weight of gas
M_p	piston mass
m_{s_i}	initial charge of propellant
n	time in finite difference grid reciprocal of exponent in power-law velocity profile
P	pressure
Pr	Prandtl number
$\dot{q}''$	heat flux or rate of heat transfer per unit area
R	tube inside radius

NOMENCLATURE (continued)

English notations

R_o	tube outside radius
R_g	gas constant, R_u/M
R_u	universal gas constant
Re_θ	Reynolds number based on momentum thickness, $(\frac{\rho_f U\theta}{\mu_f})$
r	radial distance from tube axis
r_b	linear speed of burning
S_{b_t}	total burning surface
St	Stanton number, $(\frac{h}{\rho_f U c_p})$
s	entropy
T	one-dimensional gas temperature
T_o	explosion temperature
T_w	tube wall temperature
T_∞	free stream gas temperature
T_f	film temperature, $(T_\infty + T_{w,i})/2$
$T_{w,i}$	inner surface temperature of tube wall
t	time
U	one-dimensional velocity
U_p	piston velocity
U_∞	free stream velocity
u	velocity within boundary layer
v	specific volume
V_o	initial chamber volume
$\dot{v}_{d_s}$	volume rate of decrease of solids

English notations

W	potential of propellant per unit mass, $\frac{R_g T_o}{(\gamma-1)}$
w_{s_i}	initial web thickness of a solid particle
x	axial distance from tube head end

Greek notations

α	thermal diffusivity
β	coefficient of thermal expansion
γ	ratio of specific heats, c_p/c_v
ΔE	additional energy available per unit mass during conversion of solids into gases
Δf	change of function f
δ	boundary layer thickness
δ^*	displacement thickness
η	covolume in Equation of state (6), Part I
η, ξ	characteristic directions corresponding to positive and negative value of λ respectively
θ	function defined by Equation (61), Part I
θ	momentum thickness
κ	thermal conductivity
λ	arbitrary multiplier to determine η, ξ characteristics
λ_m	mth root of Equation (151), Part II
μ	viscosity
ν_s	volume fraction of solids
ρ_g	one-dimensional gas density
ρ_s	density of propellant material

Greek notations

ρ_f	gas density at film temperature T_f
ρ_m	mixture density, $[\nu_s\rho_s + (1-\nu_s)\rho_g]$
τ_w	wall shear stress
ζ	characteristic direction along a particle path

Subscripts

f	value at film temperature T_f
g	value for gas
i	value at inner surface of tube wall
o	initial value
p	value at piston base
s	value for solids
w	value for wall material
∞	free stream value

Superscripts

'	corresponding non-dimensional form

Special notations

$\tilde{(\ )}$	first estimated value of a function after time $\Delta t'$
$\tilde{\tilde{(\ )}}$	second estimated value of a function after time $\Delta t'$
$(\ )'$	differentiation with respect to r
$(\ )_j^n$	value at node n,j in time-space finite difference grid
$\frac{D}{Dt}$	$\frac{\partial}{\partial t} + U\frac{\partial}{\partial x}$

(The reverse of this page is blank)

SECTION I

SUMMARY

The objective of this study is to (1) provide a mathematical model which can be used to predict the performance and heat transfer characteristics of guns, or devices which produce high pressure and temperatures in an enclosed but expanding volume by burning solid propellant and (2) utilize this model to study the heat transfer and erosion effects of adding solid micron size particles, such as titanium dioxide, to the propellant.

The internal ballistic model is developed by deriving the time-dependent one-dimensional conservation equations, including the effect of skin friction and wall heat transfer. A boundary layer analysis is carried out by deriving the boundary layer momentum equation for a non-steady, developing compressible flow in a tube. As a first approximation, the profile shape fraction (ratio of the displacement thickness and the momentum thickness) is assumed to be a constant. The conduction heat transfer equations for the tube itself are written and coupled with this boundary layer heat transfer analysis. Two limiting cases of solids velocity, namely (1) the same velocity as the combustion gases and (2) zero velocity, are considered.

Numerical techniques are used to solve the above equations together with the equation of state of the combustion gas and to determine all the ballistic properties, namely pressure, velocity, gas density, gas temperature, volume fraction of solids, and the boundary layer thickness at each point along the length of the tube at every time step. The heat transfer coefficient at the inside surface of the tube is obtained from Colburn's analogy and the tube wall temperature is determined simultaneously, and coupled with, the interior ballistic solution.

Results are obtained for a typical set of input data which show that the final projectile velocity and the time of travel for the two extreme cases of solids velocity are quite close. The total heat loss to the tube wall is found to be five to six percent of the input energy. Very high values of the heat transfer coefficient (50 kcal/m^2-sec-°K on the average) are found, which produce peak tube wall surface temperatures of 800 to 1000°K near the projectile standing position.

Excellent agreement between predicted and experimentally measured single shot tube wall temperatures are found. This agreement is produced without the use of experimentally measured interior ballistics data such as chamber pressure versus time.

Repetitive firing calculations were made for ten to fifty repeated firings with the tube heat transfer analysis yielding tube wall temperatures. For fifty firings over a three second period (0.060 second/firing) the inside tube wall peak temperature reaches 1500°K. Repeated firing bursts would produce temperatures high enough to cause melting of a very thin layer of metal. This verifies the importance of heat transfer in the gun tube erosion process.

The possible effects of solid micron size particles on the heat transfer from the combustion gases to the tube wall are investigated. A review of the existing literature concerning experimental measurements on dusty gases reveal that a reduction in wall friction and convective heat transfer is possible in many cases. In fact, reductions up to 30 percent have been measured, but no experimental heat transfer or friction data at the Reynolds number, particle loading, and particle sizes applicable to the gun tube problem are available. If it is assumed that the particles cause a reduction of the convective heat transfer coefficient of 20 percent, the inside

tube wall temperature is reduced by about 100°K, which appears as insufficient to cause a significant reduction in erosion.

All data on wear-reducing gun propellant additives reveal that a coating remains on the tube wall after numerous firings. A study of the insulation effect of micron size particles forming a packed bed in the surface roughness crevices of the tube wall showed that the tube metal temperatures would be reduced by up to 300°K. This occurs for a surface roughness of ten microns. It is found that sufficient particle loadings are contained in propellants used in actual practice to supply this coating material.

This insulation mechanism hypothesis is upheld by all calculations and is concluded to be the most probable predominate wear-reducing mechanism of wax with Titanium dioxide particles. This deposition of particles should therefore be optimized.

PART I: ANALYTICAL MODEL OF HEAT TRANSFER IN GUN BARRELS

SECTION II

INTRODUCTION

Definition of the Problem

Devices which produce high pressure in an enclosed but expanding volume by burning combustible mixture of gases or solid propellant with the objective of performing work are common in practice. Internal ballistics of these devices, for example the problem of the gun, have been solved experimentally since the fourteenth century when gunpowder first came into use [1]*. But surprisingly enough, an analytical solution which may be used to accurately predict the performance of such devices has not been found. This lack of mathematical model compels a designer to choose the comparatively expensive path of experimentation, although only limited information can be obtained from these experiments. Moreover, a large number of experiments have to be performed before a set of optimum design parameters can be determined for a particular purpose, and still the final result remains in question as to whether a truly optimum condition has been achieved.

The problem of internal ballistics requires a modeling of the fluid flow phenomena and heat transfer to the wall inside the expanding volume. For simplicity, throughout this work we shall be restricted to the special geometry of a closed cylindrical tube with a sliding piston

---

*Number in [ ] refers to the references in Bibliography.

at one end, as shown in Figure 1. The combustible mixture is burnt inside the enclosed volume whereby the pressure is increased and the piston is set into motion. The products of combustion which flow down the cylinder behind the piston impart a considerable amount of its energy to the piston and a fraction is lost to the tube wall. This cools the combustion gases and modifies the pressure and flow conditions.

While heat transfer has some effect on the ballistic properties, this is probably more important with respect to the material properties of the tube. Since the combustion gases are usually at a temperature of 2000-3000^{o}K, after repeated use of the device at high frequency the wall temperature of the tube may reach a value high enough to cause appreciable wear as the piston slides down the tube. A model of heat transfer, which can be used to predict the wall temperature, will help a designer to choose the optimum design parameters which will minimize the erosion rate.

The purpose of the present research is, therefore, to provide a working analytical model which shall be able to predict all the ballistic properties, namely velocity, pressure, temperature and density of the combustion gas mixture as a function of space and time. The heat loss to the tube wall shall be considered and the temperature distribution at the wall shall be determined. This model will then allow study and optimization of various parameters without expensive trial and error experimentation.

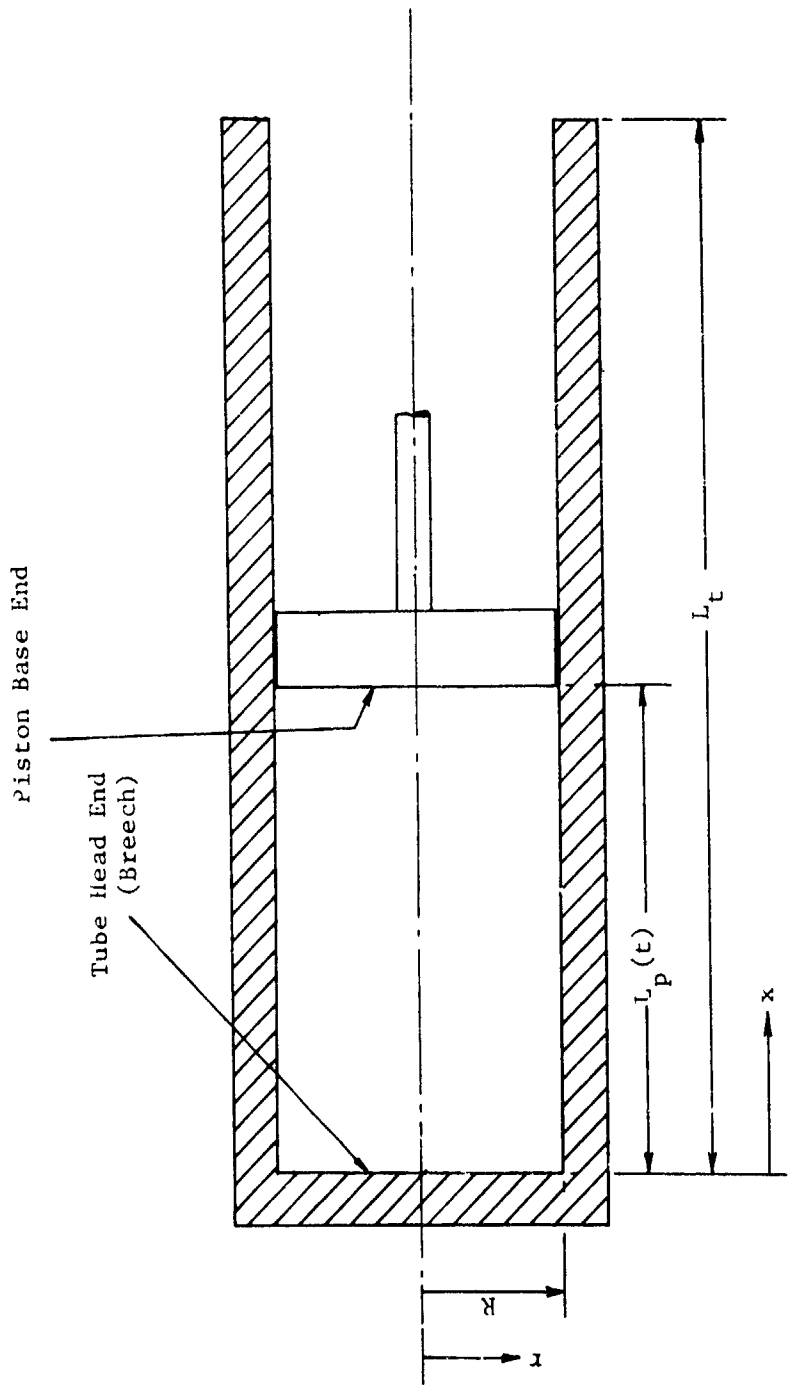

Figure 1. Schematic of the Piston-Cylinder Arrangement

Related Work

Theoretical solutions to the problem of interior ballistics have been attempted since the days of Lagrange who in 1793 first tried to determine the spatial distribution of pressure, density and gas velocity in the tube at all times after the combustion. The work available until now can be divided into two broad categories:

(1) Semiempirical solutions which may have practical utility in the study of familiar devices.

(2) Exact theories which attempt to include the predominate phenomena up to a certain order of magnitude by formulating a simple mathematical model of the flow.

Semiempirical Solutions

The major works in this area with special application to the guns using solid propellant are described in references 1 and 2 The main purpose of these works is to obtain a solution which matches with the experimental values of peak chamber pressure and muzzle velocity of the projectile. Only a few of the number of solutions shall be discussed here.

Isothermal Solution. The solution as described by Corner [2] is based on the following assumptions:

(1) The propellant stays in the chamber burning under the tube head end (breech) pressure and the rate of burning is proportional to that pressure.

(2) During the period of burning of the propellant, the progressive cooling of the combustion gases due to the work done on the projectile can be approximated by taking a mean gas temperature over this time

interval, corresponding to an effective mean force constant λ.

(3) Uniform gas density and linear velocity distribution in the space between the tube head end and piston base.

(4) Resistance to motion of the projectile can be taken into account by introducing an increased effective projectile mass instead of actual mass.

(5) The covolume η (volume correcting term in the equation of state of the combustion gas) is equal to the specific volume of the propellant material.

The expressions for breech pressure P, projectile velocity V, and projectile distance from breech face x, are given as a function of "convenient variable" f, the form factor θ, the force constant λ, burning rate β, and central ballistic parameter M. The central ballistic parameter M itself is a function of λ, β, initial mass and web size of propellant, effective projectile mass, and tube diameter. The form factor θ depends on the geometrical shape of the propellant and the variable "f" goes from one to zero as the propellant is burnt. Other parameters, namely λ, M and β are chosen following a trial and error procedure until good agreement is obtained with the experimental values of peak pressure and muzzle velocity. The solution, however, does not take into account the heat loss to the tube wall.

Coppock's Solution [2]. This is an extension to the isothermal solution described above with the following modifications:

(1) Instead of taking a mean gas temperature during burning, the analysis takes into account the kinetic energy of the projectile and that of the gases, assuming that the combustion gases are uniform in density

between the breech and the projectile and that their velocity at any point is proportional to the distance from the breech face. The total heat loss to the tube wall up to a particular instance of time is assumed to be a certain fraction of the total kinetic energy of the projectile and the gases at that instant. In practice, the effect of heat loss is incorporated in the energy equation by a proper choice of γ (ratio of specific heats at constant pressure and constant volume).

(2) The gases have a constant covolume η, not necessarily equal to the specific volume of the propellant material.

From the observed peak pressure it is possible to back-calculate the central ballistic parameter M, and thence the burning rate β.

The solution is superior to the isothermal solution because there is only one arbitrary parameter, namely the burning rate β, whose value is selected so that the peak pressure matches the experimental data. Moreover, the model takes into account the heat loss to the tube wall, though in a crude fashion.

Goldie's Solution [2]. The solution follows Coppock's solution described above with the only modification that the projectile is assumed to be motionless until a "shot-start pressure" is produced inside the chamber. If there is any resistance to motion at later times, the effect is simulated by a change in effective shot weight.

Apart from these solutions, there are solutions which attempt to use a better relationship between the burning rate and the corresponding pressure. But the solutions still need trial and error of one or more variables to match experimental data. Besides, there is no guarantee as to how good the solutions will be when prediction of performance of

a new device is desired. Also no information regarding the ballistic properties in between the breech face and the projectile is available from any of these models. Even a recent publication [3] fails to provide such informations.

Exact Theories

As mentioned earlier, Lagrange took the initiative to solve the one-dimensional problem of interior ballistics in 1793. He introduced the "Lagrange approximation" which assumes that the gas velocity at any instant increases linearly with distance along the tube, from zero at the tube head end to the full projectile velocity at the back of the piston. It is further assumed that all the propellant charge is in gaseous form from the start and at any time the gas density is the same at all points. It can be shown from the equation of continuity that if gas density is independent of position, the velocity distribution is linear; but the converse is not necessarily true.

In other work, Hugoniot in 1889 used the theory of waves of finite amplitude developed by Riemann in 1858, with the assumption that all the propellant was completely burnt when the piston began to move. He followed the resulting wave of rarefaction on its journey to the tube head end. The method was extended by Gossot and Liouville to follow the wave as it travels back to the piston after being reflected from the tube head end. Finally, Love [4] carried the analysis as far as the third wave traveling toward the breech and Pidduck [4] applied Love's solution in the special case of internal ballistics. But all these solutions, though completely analytical, hold good under two important assumptions:

(a) Instantaneous combustion.

(b) Adiabatic expansion of each element of gas.

The assumptions may be applicable for the devices which use gaseous fuel as propellant, say automobile engines, but for the devices using solid propellant the assumptions are far from the real situation. In this case, gradual burning of the propellant must be considered.

Analytical work based on most realistic assumptions has been done by Carriere [5]. For simplicity he assumed the propellant to be stationary in the combustion chamber at the time of burning which is a good assumption for cast propellant in a rocket-motor. From the basic concept of conservation of mass, momentum and energy, he derived three partial differential equations expressing gas density, gas velocity and entropy as a function of time and distance. He transformed those equations into three ordinary differential equations along three characteristic directions in the time-space co-ordinate. Then with proper choice of the equation of state for the combustion gas, he followed what is commonly known as the "method of characteristics" to determine the gas properties at any time and position. The effect of frictional losses and heat loss to the tube wall were disregarded in the analysis.

The problem of heat loss to the tube wall has been studied by Hicks and Thornhill in England. A fairly elaborate description of their method has been given in both references [1] and [2]. This work is also based on the Lagrange approximation of linear velocity distribution and uniform gas density in between the breech face and the piston.

It can be shown that at high velocity, heat is mainly transferred to the tube wall by convection. It is also evident that a boundary layer

is formed at the inner surface of the tube. The heat transfer rate per unit area through the boundary layer can be given as $h(T_g-T_s)$, where h, T_g and T_s are the film heat transfer coefficient, temperature of the gas, and temperature of the inner surface of the tube respectively. All three quantities depend on time as well as position along the tube.

Hicks and Thornhill considered the flow in the boundary layer to be the same as the flow over a flat plate. In internal ballistic applications the flow is in the turbulent region most of the time. Therefore, they used the analogy solution, as extended by Von Karman to cover Prandtl number other than unity, to obtain a relation between the heat transfer coefficient h and wall shear stress τ_w. To get the wall shear stress they first found a "best" power law for the velocity profile (non-dimensionalized with respect to the shear velocity $\sqrt{\tau_w/\rho}$) inside the boundary layer which was capable of giving the local wall shear stress τ_w within three per cent of the value that could be obtained by using more rigorous logarithmic form of the velocity profile when applied to steady and uniform flow situations. Then they used the boundary layer momentum integral, including the terms due to non-steady and non-uniform nature of the flow, and used the "best" power law found earlier to obtain the local wall shear stress at all points. The heat transfer coefficient h is then easily calculated from the analogy solution. They, however, omitted one boundary condition that the boundary layer thickness at the base of the piston be zero at all times.

The heat transfer in the tube wall has been calculated by using the differential equation for unsteady heat conduction with proper boundary conditions. For the case studied by Hicks and Thornhill, i.e.

the first round of firing from a cold gun, the curvature effect of the wall was neglected as the temperature rise was confined within one millimeter of the inside surface. Consequently, there was no heat loss from the outer surface of the tube which remained at ambient temperature. The heat conduction along the length of the barrel was also neglected. Knowing the tube material properties, namely thermal conductivity and diffusivity, it was possible to obtain the temperature distribution at the inner surface of the tube along the length at all times. The free stream values of the gas velocity, density and temperature were taken from the one-dimensional ballistic solution.

It has been indicated in reference [2] that frictional pressure drop is small compared to the inertia pressure drop needed to accelerate the gas. But no analysis until now indicates quantitatively the effect of skin friction on the ballistic properties. Even the heat transfer solution has not been fed back to study its effect on the one-dimensional solution.

Present Investigation

In the light of available theories, it is clear that a good one-dimensional solution is first required to replace the Lagrange approximation, or at least check its validity for the particular problem. The first and most formidable difficulty in writing down the one-dimensional continuity, momentum and energy equations during the burning of the solid propellant is due to the uncertainty of the relative velocity between the gas phase and the solid phase. It is extremely difficult to estimate the drag exerted on the burning solid particles by the accelerating

combustion gases. Therefore, two limiting cases of the solids velocity have been considered in the present work:

Case I. The solid particles move at the same velocity as the gas phase.

Case II. The solid particles remain at their initial positions throughout the period of burning.

For both cases the conservation of mass, momentum and energy results in four coupled partial differential equations expressing volume fraction of solid ν_s, gas density ρ_g, gas velocity U, and pressure P as a function of axial distance x and time t. The heat release due to gradual burning of the propellant is taken into account. A typical propellant geometry, namely a hollow cylinder, is considered whereby the total burning surface remains constant, although this assumption is not essential.

The ballistic properties at the internal points are calculated from these equations after writing the same in finite difference form. But to obtain the properties at the two ends, namely the tube head end and the piston base, the equations are transformed into ordinary differential equations along the characteristic directions. The covolume of the gas is assumed to be constant, and experimental data for burning rate is used. As one of the initial conditions, it is assumed that the piston does not start until a certain specified pressure is reached inside the chamber and thereafter the piston does not experience any resistance to motion.

The boundary layer momentum integral for a non-steady, non-uniform, developing flow inside a tube is derived. The profile shape factor H

(ratio between the displacement thickness δ^* and momentum thickness θ) is introduced and the Ludwieg-Tillmann [6] friction factor is used. As a first approximation, the shape factor is assumed to be constant in the present work. The flow is in the high Reynolds number region for which the boundary layer thickness is small compared to the tube radius. It is therefore legitimate to replace the free stream values of gas density and velocity by the values obtained from the one-dimensional solution neglecting the boundary layer thickness.

The local heat transfer coefficient h is calculated by using Colburn's analogy [7] between heat and momentum transfer. It covers Prandtl numbers other than unity and is simple to use. The values of viscosity and gas density at the film temperature are used. The heat transfer in the tube wall is computed from the unsteady one-dimensional (radial) heat conduction equation with appropriate boundary conditions. The wall temperature is also found as a function of axial distance and time.

The heat loss term is entered into the one-dimensional energy equation and a comparison of ballistic properties is made with the solution without heat loss. Effect of wall shear stress is also included. The ballistic efficiency of the piston-cylinder arrangement is compared by varying different design parameters.

SECTION III

MATHEMATICAL ANALYSIS

The mathematical analysis consists of two major parts:

(1) One-dimensional analysis with gradual burning of the solid propellant, including the effect of heat transfer and skin friction.

(2) Formulation of the boundary layer problem and determination of heat transfer to the tube wall.

As outlined in the previous chapter, the present analysis is carried out for two extreme cases of solid velocity. In the first case, it is assumed that a burning solid particle moves with the same velocity as the combustion gases. In the second case, however, the solid particles are assumed to be stationary at their initial positions throughout the period of burning. Henceforth these two cases are referred as Case I and Case II, respectively.

One-Dimensional Analysis Including Heat Transfer and Skin Friction

Case I

The assumptions, other than that regarding the solids velocity, which are made to simplify the model are as follows:

(1) At any instance of time, the linear speed of burning r_b is same for all the solid particles and it is a function of the

average pressure in the chamber (space in between the tube head end and the piston base).

(2) The solid propellants are single perforated circular cylinders in shape whereby the total burning surface remains constant during the whole period of burning.

(3) The burning rate is fast enough to consider that the temperature of the remaining solids at any instance of time remains constant at the initial temperature.

(4) The propellant material is incompressible and its coefficient of thermal expansion is negligible.

(5) The piston starts to move only when the chamber pressure reaches a certain value P_o, and thereafter the resistance to its motion is negligible compared to the pressure force exerted on it by the combustion gases in the chamber.

The conservation equations are as follows (for derivation see Appendix I):

Solid continuity:

$$\frac{\partial \nu_s}{\partial t} + U\frac{\partial \nu_s}{\partial x} + \nu_s \frac{\partial U}{\partial x} + \dot{\nu}_{d_s} = 0 \qquad (1)$$

Gas continuity:

$$\frac{\partial \rho_g}{\partial t} + U\frac{\partial \rho_g}{\partial x} + \frac{\rho_g}{(1-\nu_s)} \frac{\partial U}{\partial x} = \frac{(\rho_s - \rho_g)}{(1-\nu_s)} \dot{\nu}_{d_s} \qquad (2)$$

Momentum:

$$\frac{\partial U}{\partial t} + U \frac{\partial U}{\partial x} = - \frac{1}{\rho_m} \frac{\partial P}{\partial x} - \frac{2\tau_w}{\rho_m R} \tag{3}$$

Energy:

$$\nu_s \rho_s \frac{Dh_s}{Dt} + (1-\nu_s)\, \rho_g \frac{Dh_g}{Dt} - \frac{DP}{Dt}$$

$$= \rho_s (W + \frac{P}{\rho_s} - h_g)\dot{v}_{d_s} - \frac{2h_i}{R}(T-T_{w,i}) + \frac{2\tau_w U}{R} \tag{4}$$

where $\dot{v}_{d_s}$ is the volume rate of decrease of solids per unit cylinder volume and is given by:

$$\dot{v}_{d_s}(x,t) = (\frac{S_{b_t}}{A_p}) \frac{\nu_s(x,t) r_b}{\int_o^{L_P} \nu_s(x,t)dx} \tag{5}$$

The equation of state of the gas is:

$$P(v_g - \eta) = R_g T$$

or,

$$P(\frac{1}{\rho_g} - \eta) = R_g T \tag{6}$$

where the gas constant R_g is obtained from the ratio of the universal gas constant R_u and the molecular weight of the gas M.

It has been shown in Appendix I that under assumptions three and four as stated earlier, the differential of enthalpy of solids per unit

mass h_s and the differential of enthalpy of gases per unit mass h_g can be given by:

$$dh_s = \frac{1}{\rho_s} dP \tag{7}$$

$$dh_g = \frac{(\gamma-\eta\rho_g)}{\rho_g(\gamma-1)} dP - \frac{\gamma P}{(\gamma-1)\rho_g^2} d\rho_g \tag{8}$$

Substituting equations (7) and (8) into the energy equation (4):

$$\frac{(1-\nu_s)(1-\eta\rho_g)}{(\gamma-1)} \frac{DP}{Dt} - \frac{(1-\nu_s)\gamma P}{(\gamma-1)\rho_g} \frac{D\rho_g}{Dt}$$

$$= \rho_s(W + \frac{P}{\rho_s} - h_g)\dot{v}_{d_s}$$

$$- \frac{2h_i}{R}(T-T_{w,i}) + \frac{2\tau_w U}{R} \tag{9}$$

Using gas continuity, i.e. equation (2) to replace $\frac{D\rho_g}{Dt}$ in equation (9) the final form of the energy equation becomes:

$$\frac{(1-\nu_s)(1-\eta\rho_g)}{(\gamma-1)} \frac{DP}{Dt} + \frac{\gamma P}{(\nu-1)} \frac{\partial U}{\partial x} - \frac{\gamma P(\rho_s-\rho_g)}{(\gamma-1)\rho_g} \dot{v}_{d_s}$$

$$= \rho_s(W + \frac{P}{\rho_s} - h_g)\dot{v}_{d_s} - \frac{2h_i}{R}(T-T_{w,i})$$

$$+ \frac{2\tau_w U}{R}$$

or,

$$\frac{\partial P}{\partial t} + U\frac{\partial P}{\partial x} + B_I \frac{\partial U}{\partial x} = C_I \dot{v}_{d_s} - E_I \frac{2h_i}{R}(T-T_{w,i})$$

$$+ E_I \frac{2\tau_w U}{R} \tag{10}$$

where

$$B_I = \frac{\gamma P}{(1-\nu_s)(1-\eta\rho_g)} \tag{11}$$

$$C_I = \frac{\gamma P(\rho_s-\rho_g) + (\gamma-1)\rho_s\rho_g(W + \frac{P}{\rho_s} - h_g)}{\rho_g\{(1-\nu_s)(1-\eta\rho_g)\}} \tag{12}$$

$$E_I = \frac{(\gamma-1)}{(1-\nu_s)(1-\eta\rho_g)} \tag{13}$$

The initial conditions of the conservation equations are:

Position of the piston, $L_p(0) = L_o$

$$U(x,0) = 0 \;;\quad P(x,0) = P_o \;;\quad T(x,0) = T_o \;;\quad \rho_g(x,0) = \rho_{g_o} \tag{14}$$

$$\text{and} \quad \nu_s(x,0) = \nu_{s_o} \qquad \text{at } 0 \leq x \leq L_o$$

where P_o is the pressure at which the piston starts to move, and T_o is the adiabatic, stagnation flame temperature of the propellant. By knowing P_o and T_o it is possible to determine ρ_{g_o} from the equation of state (2.6):

$$\rho_{g_o} = \frac{1}{\frac{R T_{g_o}}{P_o} + \eta} \tag{15}$$

Neglecting the initial mass of air in the chamber, a mass balance gives:

$$m_{s_i} = \nu_{s_o} V_o \rho_s + (1-\nu_{s_o}) V_o \rho_{g_o}$$

or,

$$\nu_{s_o} = \frac{(m_{s_i}/V_o) - \rho_{g_o}}{\rho_s - \rho_{g_o}} \tag{16}$$

(m_{s_i}/V_o) is called the "loading density."

The boundary conditions are:

$$\text{at } x = 0, \qquad U(0,t) = 0$$

and (17)

$$\text{at } x = L_p, \qquad U(L_p,t) = U_p(t)$$

The piston velocity $U_p(t)$ is obtained from the equation of motion of the piston, which under the assumption five takes the following form:

$$\frac{dU_p}{dt} = a_p = \frac{P_p A_p}{M_p} \tag{18}$$

The position of the piston is obtained from:

$$\frac{d^2x_p}{dt^2} = a_p \tag{19}$$

The unknowns, and the corresponding equations from which they can be calculated are listed below:

Unknown	Equation
Volume fraction of solids, ν_s	Solid continuity, (1)
Gas density, ρ_g	Gas continuity, (2)
Velocity, U	Momentum equation, (3)
Pressure, P	Energy equation, (10)
Gas temperature, T	Equation of state, (6)

The conservation equations, i.e. (1), (2), (3) and (10) are written in finite difference form, and a numerical scheme which takes into account both forward and backward space derivatives are used to calculate the corresponding unknowns, i.e. ν_s, ρ_g, U and P, at all the interior points at an advanced time by knowing the present values at and around those points. The gas temperature, T, is then calculated from the equation of state (6). The details of the solution technique shall be discussed in Chapter IV.

The above solution technique, however, is not applicable to the boundary points, i.e. the piston base end and the tube head end, as space derivatives on both sides of these two points are not available. This necessitates the transformation of the conservation equations to ordinary differential equations along characteristic directions, i.e. to follow the "method of characteristics" [8].

P-U Charac ristic. The energy equation (10) is:

$$\frac{\partial P}{\partial t} + U\frac{\partial P}{\partial x} + B_I \frac{\partial U}{\partial x} = C_I \dot{v}_{d_s} - E_I \frac{2h_i}{R}(T-T_{w,i})$$

$$+ E_I \frac{2\tau_w U}{R}$$

Multiplying the momentum equation (3) by an arbitrary constant λ:

$$\lambda\frac{\partial P}{\partial x} + \lambda\rho_m \frac{\partial U}{\partial t} + \lambda\rho_m U\frac{\partial U}{\partial x} = -\lambda \frac{2\tau_w}{R} \qquad (20)$$

Adding equation (20) to equation (10):

$$\left[\frac{\partial P}{\partial t} + (U+\lambda)\frac{\partial P}{\partial x}\right] + \left[\lambda\rho_m \frac{\partial U}{\partial t} + (B_I + \lambda\rho_m U)\frac{\partial U}{\partial x}\right]$$

$$= C_I \dot{v}_{d_s} - E_I \frac{2h_i}{R}(T-T_{w,i})$$

$$+ \frac{2\tau_w}{R}\left[E_I U - \lambda\right] \qquad (21)$$

To obtain the characteristic directions, the value of λ shall be such that:

$$\frac{dt}{dx} = \frac{1}{U+\lambda} = \frac{\lambda\rho_m}{B_I+\lambda\rho_m U}$$

$$\lambda_{1,2} = \pm\sqrt{B_I/\rho_m} \qquad (22)$$

Dividing equation (2.21) by $\sqrt{1+(U+\lambda)^2}$ and using

$$\frac{1}{\sqrt{1+(U+\lambda)^2}}\frac{\partial}{\partial t}+\frac{(U+\lambda)}{\sqrt{1+(U+\lambda)^2}}\frac{\partial}{\partial x}=\frac{d}{d\eta,\xi}$$

where η corresponds to λ_1, i.e. positive sign of λ, and ξ corresponds to λ_2, i.e. negative sign of λ, the equation (21) becomes.

$$\frac{dP}{d\eta,\xi}+\lambda_{1,2}\rho_m\frac{dU}{d\eta,\xi}=\frac{1}{\sqrt{1+(U+\lambda)^2}}\left[C_I\dot{v}_{d_s}-E_I\frac{2h_i}{R}(T-T_{w,i})+\frac{2\tau_w}{R}(E_IU-\lambda)\right] \quad (23)$$

Now,

$$\Delta\eta,\xi=\sqrt{(\Delta x)^2+(\Delta t)^2}=\Delta t\sqrt{1+(U+\lambda)^2} \quad (24)$$

Therefore, along η-characteristic, i.e. $\frac{dt}{dx}=\frac{1}{U+\sqrt{B_I/\rho_m}}$:

$$\Delta P+\rho_m\sqrt{B_I/\rho_m}\,\Delta U=\left[C_I\dot{v}_{d_s}-E_I\frac{2h_i}{R}(T-T_{w,i})+\frac{2\tau_w}{R}(E_IU-\sqrt{B_I/\rho_m})\right]\Delta t \quad (25)$$

and along ζ-characteristic, i.e. $\frac{dt}{dx}=\frac{1}{U-\sqrt{B_I/\rho_m}}$:

$$\Delta P - \rho_m \sqrt{B_I/\rho_m}\,\Delta U = \left[C_I \dot{v}_{d_s} - E_I \frac{2h_i}{R}(T-T_{w,i}) + \frac{2\tau_w}{R}(E_I U + \sqrt{B_I/\rho_m})\right] \Delta t \qquad (26)$$

P-ρ_g Characteristic. By rearranging equation (9),

$$\frac{\partial \rho_g}{\partial t} + U\frac{\partial \rho_g}{\partial x} = \frac{\rho_g(1-\eta\rho_g)}{\gamma P}\left[\frac{\partial P}{\partial t} + U\frac{\partial P}{\partial x}\right] + \frac{(\gamma-1)\rho_s\rho_g(h_g - \frac{P}{\rho_s} - W)}{(1-\nu_s)\gamma P}\dot{v}_{d_s}$$

$$+ \frac{(\gamma-1)\rho_g}{(1-\nu_s)\gamma P}\left[\frac{2h_i}{R}(T-T_{w,i}) - \frac{2\tau_w U}{R}\right] \qquad (27)$$

Dividing this equation by $\sqrt{1+U^2}$ and using,

$$\frac{1}{\sqrt{1+U^2}}\frac{\partial}{\partial t} + \frac{U}{\sqrt{1+U^2}}\frac{\partial}{\partial x} = \frac{d}{d\zeta}$$

and

$$\Delta\zeta = \sqrt{(\Delta x)^2+(\Delta t)^2} = \Delta t\sqrt{1+U^2}$$

along a particle path, i.e. $\frac{dt}{dx} = \frac{1}{U}$:

$$\Delta\rho_g = \frac{\rho_g(1-\eta\rho_g)}{\gamma P}\Delta P + \frac{(\gamma-1)\rho_s\rho_g(h_g - \frac{P}{\rho_s} - W)}{(1-\nu_s)\gamma P}\dot{v}_{d_s}\Delta t$$

$$+ \frac{(\gamma-1)\rho_g}{(1-\nu_s)\gamma P}\left[\frac{2h_i}{R}(T-T_{w,i}) - \frac{2\tau_w}{R}U\right]\Delta t \qquad (28)$$

ν_s-ρ_g Characteristic. From equation (2)

$$\frac{\partial U}{\partial x} = -\frac{(1-\nu_s)}{\rho_g}\left[\frac{\partial \rho_g}{\partial t} + U\frac{\partial \rho_g}{\partial x}\right] + \frac{(\rho_s-\rho_g)}{\rho_g}\dot{v}_{d_s} \qquad (29)$$

Substituting this expression for $\frac{\partial U}{\partial x}$ in solid continuity (1):

$$\frac{\partial \nu_s}{\partial t} + U\frac{\partial \nu_s}{\partial x} - \frac{\nu_s(1-\nu_s)}{\rho_g}\left[\frac{\partial \rho_g}{\partial t} + U\frac{\partial \rho_g}{\partial x}\right] + \left[\frac{\nu_s\rho_s+(1-\nu_s)\rho_g}{\rho_g}\right]\dot{v}_{d_s} = 0 \qquad (30)$$

Proceeding in the same fashion as for the P-ρ_g characteristic, one obtains:

Along a particle path, i.e. $\frac{dt}{dx} = \frac{1}{U}$:

$$\Delta\nu_s = -\frac{\nu_s(1-\nu_s)}{\rho_g}\Delta\rho_g - \frac{\rho_m}{\rho_g}\dot{v}_{d_s}\Delta t \qquad (31)$$

The procedure of solving the above characteristic equations are discussed in Chapter IV.

Case II

In this case the solid propellant particles are assumed to be stationary at their initial positions throughout the period of burning. The linear speed of burning r_b, is same for all the solid particles and is a function of the average pressure in the space between the tube head end and the initial position of the piston L_o. The rest of the assumptions are the same as those for Case I.

The conservation equations in this case are (See Appendix I for derivation):

Solid continuity:

$$\frac{\partial \nu_s}{\partial t} + \dot{v}_{d_s} = 0 \tag{32}$$

Gas continuity:

$$\frac{\partial \rho_g}{\partial t} + U\frac{\partial \rho_g}{\partial x} + \rho_g \frac{\partial U}{\partial x} = \frac{(\rho_s - \rho_g)}{(1-\nu_s)} \dot{v}_{d_s} + \frac{\rho_g U}{(1-\nu_s)} \frac{\partial \nu_s}{\partial x} \tag{33}$$

Momentum:

$$\frac{\partial U}{\partial t} + U\frac{\partial U}{\partial x} = -\frac{1}{\rho_g}\frac{\partial P}{\partial x} - \frac{\rho_s U}{(1-\nu_s)\rho_g} \dot{v}_{d_s} - \frac{2\tau_w}{(1-\nu_s)\rho_g R} \tag{34}$$

Energy:

$$(1-\nu_s)\rho_g \frac{Dh_g}{Dt} - (1-\nu_s)\frac{DP}{Dt} = \rho_s\left(W + \frac{P}{\rho_s} + \frac{U^2}{2} - h_g\right)\dot{v}_{d_s}$$

$$- \frac{2h_i}{R}(T - T_{w,i}) + \frac{2\tau_w U}{R} \tag{35}$$

As none of the solid particles moves beyond L_o, $\dot{v}_{d_s}$ can be expressed as:

$$\dot{v}_{d_s} = \left(\frac{S_{b_t}}{A_p}\right) \frac{\nu_s r_b}{\int_0^{L_o} \nu_s dx} \tag{36}$$

The same equation of state, i.e. equation (6) is used and by successive use of equation (8) and (33) the final form of the energy equation (35) becomes:

$$\frac{\partial P}{\partial t} + U\frac{\partial P}{\partial x} + B_{II}\frac{\partial U}{\partial x} = C_{II}\dot{v}_{d_s} + \frac{B_{II}U}{(1-\nu_s)}\frac{\partial \nu_s}{\partial x}$$

$$- E_{II}\frac{2h_i}{R}(T-T_{w,i}) + E_{II}\frac{2\tau_w U}{R} \qquad (37)$$

where

$$B_{II} = \frac{\gamma P}{(1-\eta\rho_g)} \qquad (38)$$

$$C_{II} = \frac{\gamma P(\rho_s-\rho_g) + (\gamma-1)\rho_s\rho_g\left(W + \frac{P}{\rho_s} + \frac{U^2}{2} - h_g\right)}{\rho_g\{(1-\nu_s)(1-\eta\rho_g)\}} \qquad (39)$$

$$E_{II} = E_I = \frac{(\gamma-1)}{(1-\nu_s)(1-\eta\rho_g)} \qquad (40)$$

The initial and boundary conditions are the same as those for Case I. The characteristic equations are also required to calculate the ballistic properties at the two ends.

P-U Characteristic. The procedure is exactly same as Case I. Multiplying the momentum equation (34) by an arbitrary constant λ, and adding to the energy equation (37) one obtains:

$$\left[\frac{\partial P}{\partial t} + (U+\lambda)\frac{\partial P}{\partial x}\right] + \left[\lambda\rho_g \frac{\partial U}{\partial t} + (B_{II}+\lambda\rho_g U)\frac{\partial U}{\partial x}\right]$$

$$= C_{II}\dot{v}_{d_s} + \frac{B_{II}U}{(1-\nu_s)}\frac{\partial \nu_s}{\partial x} - \lambda\frac{\rho_s U}{(1-\nu_s)}\dot{v}_{d_s}$$

$$- E_{II}\frac{2h_i}{R}(T-T_{w,i}) + \frac{2\tau_w}{R}\left[E_{II}U - \frac{\lambda}{(1-\nu_s)}\right] \quad (41)$$

The characteristic directions are such that:

$$\frac{dt}{dx} = \frac{1}{U+\lambda} = \frac{\lambda\rho_g}{B_{II}+\lambda\rho_g U}$$

$$\therefore \quad \lambda_{1,2} = \pm\sqrt{\frac{B_{II}}{\rho_g}} = \pm\sqrt{\frac{\gamma P}{\rho_g(1-\eta\rho_g)}} = \pm a \quad (42)$$

From solid continuity, i.e. equation (32)

$$\frac{\partial \nu_s}{\partial t} = -\dot{v}_{d_s} \quad (43)$$

By adding and substracting $\frac{B_{II}U}{(1-\nu_s)(U+\lambda)}\frac{\partial \nu_s}{\partial t}$ on the right hand side of equation (41)

$$\left[\frac{\partial P}{\partial t} + (U+\lambda)\frac{\partial P}{\partial x}\right] + \lambda\rho_g\left[\frac{\partial U}{\partial t} + (U+\lambda)\frac{\partial U}{\partial x}\right]$$

$$= \frac{B_{II}U}{(1-\nu_s)(U+\lambda)}\left[\frac{\partial \nu_s}{\partial t} + (U+\lambda)\frac{\partial \nu_s}{\partial x}\right] - \frac{B_{II}U}{(1-\nu_s)(U+\lambda)}\frac{\partial \nu_s}{\partial t}$$

$$+ C_{II}\dot{v}_{d_s} - \lambda\frac{\rho_s U}{(1-\nu_s)}\dot{v}_{d_s} - E_{II}\frac{2h_i}{R}(T-T_{w,i}) + \frac{2\tau_w}{R}\left[E_{II}U - \frac{\lambda}{(1-\nu_s)}\right]$$

(44)

Dividing equation (2.44) by $\sqrt{1+(U+\lambda)^2}$ and using

$$\frac{1}{\sqrt{1+(U+\lambda)^2}}\frac{\partial}{\partial t}+\frac{(U+\lambda)}{\sqrt{1+(U+\lambda)^2}}\frac{\partial}{\partial x}=\frac{d}{d\eta,\xi}$$

yields the relation:

$$\frac{dP}{d\eta,\xi}+\lambda_{1,2}\rho_g\frac{dU}{d\eta,\xi}=\frac{B_{II}U}{(1-\nu_s)(U+\lambda)}\frac{d\nu_s}{d\eta,\xi}$$

$$+\frac{1}{\sqrt{1+(U+\lambda)^2}}\left[\{C_{II}-\frac{\rho_s U\lambda}{(1-\nu_s)}+\frac{B_{II}U}{(1-\nu_s)(U+\lambda)}\}\dot{v}_{d_s}\right.$$

$$\left.-E_{II}\frac{2h_i}{R}(T-T_{w,i})+\frac{2\tau_w}{R}\{E_{II}U-\frac{\lambda}{(1-\nu_s)}\}\right] \qquad (45)$$

Therefore, along η-characteristic, i.e. $\frac{dt}{dx}=\frac{1}{U+a}$:

$$\Delta P+\rho_g\, a\,\Delta U=\frac{B_{II}U}{(1-\nu_s)(U+a)}\Delta\nu_s$$

$$+\left[C_{II}-a\frac{\rho_s U}{(1-\nu_s)}+\frac{B_{II}U}{(1-\nu_s)(U+a)}\right]\dot{v}_{d_s}\,\Delta t$$

$$-E_{II}\frac{2h_i}{R}(T-T_{w,i})\Delta t+\frac{2\tau_w}{R}\left[E_{II}U-\frac{a}{(1-\nu_s)}\right]\Delta t \qquad (46)$$

and along ξ-characteristic, i.e. $\frac{dt}{dx}=\frac{1}{U-a}$:

$$\Delta P - \rho_g a \Delta U = \frac{B_{II} U}{(1-\nu_s)(U-a)} \Delta \nu_s$$

$$+ \left[C_{II} + a\frac{\rho_s U}{(1-\nu_s)} + \frac{B_{II} U}{(1-\nu_s)(U-a)} \right] \dot{v}_{d_s} \Delta t$$

$$- E_{II} \frac{2h_i}{R}(T-T_{w,i})\Delta t + \frac{2\tau_w}{R}\left[E_{II} U + \frac{a}{(1-\nu_s)} \right] \Delta t \qquad (47)$$

P-ρ_g Characteristic. Using equation (8) in equation (35) an alternative form of energy equation is:

$$\frac{\partial \rho_g}{\partial t} + U\frac{\partial \rho_g}{\partial x} = \frac{\rho_g(1-\eta\rho_g)}{\gamma P}\left[\frac{\partial P}{\partial t} + U\frac{\partial P}{\partial x} \right]$$

$$+ \frac{(\gamma-1)\rho_s \rho_g (h_g - W - \frac{P}{\rho_s} - \frac{U^2}{2})}{(1-\nu_s)\gamma P} \dot{v}_{d_s}$$

$$+ \frac{(\gamma-1)\rho_g}{(1-\nu_s)\gamma P}\left[\frac{2h_i}{R}(T-T_{w,i}) - \frac{2\tau_w U}{R} \right] \qquad (48)$$

Proceeding in exactly the same manner as for Case I, along a particle path, i.e. $\frac{dt}{dx} = \frac{1}{U}$:

$$\Delta \rho_g = \frac{\rho_g(1-\eta\rho_g)}{\gamma P} \Delta P + \frac{(\gamma-1)\rho_s \rho_g (h_g - W - \frac{P}{\rho_s} - \frac{U^2}{2})}{(1-\nu_s)\gamma P} \dot{v}_{d_s} \Delta t$$

$$+ \frac{(\gamma-1)\rho_g}{(1-\nu_s)\gamma P}\left[\frac{2h_i}{R}(T-T_{w,i}) - \frac{2\tau_w U}{R} \right] \Delta t \qquad (49)$$

v_s at the piston base is always zero after the piston starts moving and v_s at the tube head end can be obtained from equation (32) alone.

Boundary Layer Analysis

The boundary layer part of the entire analysis did not receive much attention in the past because of the nonsteady and nonuniform nature of the free stream flow. The flow is generally in the turbulent region with pressure gradient in the direction of the flow and a large temperature difference across the boundary layer. Also, in Case I a gas-solid mixture flows down the tube; hence the analysis is more complicated. A number of attempts [8, 10, 11, 12] have been made in the past to model the mechanism of heat transfer in a gas-solid mixture with various solid particle sizes and loading ratios (w_s/w_g). It has been found that the effect of the solids on convective heat transfer is prominent for micron-size particles whereas for millimeter size the effect is not appreciable. The present problem deals with the solid propellant of millimeter size and most of the time it burns out completely long before the piston reaches the end of the tube. It has also been found from the study of Hicks and Thornhill [2] that the boundary layer thickness is small compared to the tube radius. Therefore, to simplify the model, it is assumed that the solids always stay in the core of the flow and never enter into the thin boundary layer at the wall.

In the present study, an integral approach is preferred to a differential approach to keep the model relatively simple and tractable. The boundary layer momentum integral for the nonsteady and nonuniform compressible flow inside a tube as derived in Appendix II is:

$$\frac{\partial}{\partial t}\left[\int_{R-\delta}^{R}\rho(U_\infty-u)r\,dr\right]+\frac{\partial}{\partial x}\left[\int_{R-\delta}^{R}\rho u(U_\infty-u)r\,dr\right]+\int_{R-\delta}^{R}\rho(U_\infty-u)r\,dr\;\frac{\partial U_\infty}{\partial x}$$

$$=\left(R\delta-\frac{\delta^2}{2}\right)\left[\frac{\partial P}{\partial x}+\rho_f\frac{\partial U_\infty}{\partial t}+\rho_f U_\infty\frac{\partial U_\infty}{\partial x}\right]$$

$$+\tau_w R \qquad (50)$$

Defining δ^* = Displacement thickness

and θ = Momentum thickness

such that,

$$\rho_f U_\infty\int_{R-\delta^*}^{R}2\pi r\,dr=\int_{R-\delta}^{R}\rho 2\pi r(U_\infty-u)dr$$

or,

$$\rho_f U_\infty R\delta^*\left(1-\frac{\delta^*}{2R}\right)=\int_{R-\delta}^{R}\rho r(U_\infty-u)dr \qquad (51)$$

and

$$\rho_f U_\infty^2\int_{R-\theta}^{R}2\pi r\,dr=\int_{R-\delta}^{R}\rho\,2\pi r\,u(U_\infty-u)dr$$

or,

$$\rho_f U_\infty^2 R\theta\left(1-\frac{\theta}{2R}\right)=\int_{R-\delta}^{R}\rho\,u\,r(U_\infty-u)dr \qquad (52)$$

and using the definition of the profile shape factor $H=\frac{\delta^*}{\theta}$, and for a thin boundary layer $\frac{\delta}{2R}\ll 1$, $\frac{\delta^*}{2R}\ll 1$, $\frac{\theta}{2R}\ll 1$, the momentum integral equation (50) becomes,

$$\frac{\partial}{\partial t}\left[\rho_f U_\infty RH\theta\right] + \frac{\partial}{\partial x}\left[\rho_f U_\infty^2 R\theta\right] + (\rho_f U_\infty RH\theta)\frac{\partial U_\infty}{\partial x}$$

$$= R\delta\left[\frac{\partial P}{\partial x} + \rho_f \frac{\partial U_\infty}{\partial t} + \rho_f U_\infty \frac{\partial U_\infty}{\partial x}\right] + \tau_w R$$

or,

$$\rho_f U_\infty RH\frac{\partial \theta}{\partial t} + \rho_f U_\infty R\theta\frac{\partial H}{\partial t} + \rho_f RH\theta\frac{\partial U_\infty}{\partial t} + U_\infty RH\theta\frac{\partial \rho_f}{\partial t} + \rho_f U_\infty^2 R\frac{\partial \theta}{\partial x}$$

$$+ 2\rho_f U_\infty R\theta\frac{\partial U_\infty}{\partial x} + U_\infty^2 R\theta\frac{\partial \rho_f}{\partial x} + \rho_f U_\infty RH\theta\frac{\partial U_\infty}{\partial x}$$

$$= R\delta\left[\frac{\partial P}{\partial x} + \rho_f \frac{\partial U_\infty}{\partial t} + \rho_f U_\infty\frac{\partial U_\infty}{\partial x}\right] + \tau_w R \qquad (53)$$

Dividing equation (53) by $\rho_f U_\infty RH\theta$:

$$\frac{1}{\theta}\frac{\partial \theta}{\partial t} + \frac{1}{H}\frac{\partial H}{\partial t} + \frac{1}{U_\infty}\frac{\partial U_\infty}{\partial t} + \frac{1}{\rho_f}\frac{\partial \rho_f}{\partial t} + \frac{U_\infty}{H\theta}\frac{\partial \theta}{\partial x} + \frac{2}{H}\frac{\partial U_\infty}{\partial x} + \frac{U_\infty}{\rho_f H}\frac{\partial \rho_f}{\partial x} + \frac{\partial U_\infty}{\partial x}$$

$$= \frac{\delta}{\rho_f U_\infty H\theta}\left[\frac{\partial P}{\partial x} + \rho_f \frac{\partial U_\infty}{\partial t} + \rho_f U_\infty \frac{\partial U_\infty}{\partial x}\right] + \frac{\tau_w}{\rho_f U_\infty H\theta} \qquad (54)$$

From the study of steady compressible turbulent boundary layers by Reshotko and Tucker [13], it is likely that for moderate Mach number flow encountered in this problem ($M < 1.5$), the percentage change in the shape factor, i.e. $\frac{1}{H}\frac{\partial H}{\partial t}$, is small compared to the percentage change in momentum thickness, $\frac{1}{\theta}\frac{\partial \theta}{\partial t}$. As a first approximation, therefore, the shape factor, H, is assumed to be a constant. A more rigorous approach would be to derive another auxiliary equation, say moment of momentum

integral [14] to obtain an expression for $\frac{\partial H}{\partial t}$. However, derivation of such an equation for the nonsteady case is extremely complicated and therefore neglected in the present work.

For thin boundary layers, $U_\infty \simeq U$; $T_\infty \simeq T$ and the film temperature,

$$T_f = \frac{T+T_{w,i}}{2} \tag{55}$$

The gas density at the film temperature, ρ_f, can be evaluated from the equation of state (6), and the final form is:

$$\rho_f = \frac{(\frac{T}{T_f})\rho_g}{\left[1 + \eta\rho_g(\frac{T}{T_f} - 1)\right]} \tag{56}$$

Equation (54) finally becomes:

$$\frac{\partial \theta}{\partial t} = -\frac{U}{H}\frac{\partial \theta}{\partial x} + \frac{\tau_w}{\rho_f UH} - \theta\left[\frac{1}{\rho_f}\frac{\partial \rho_f}{\partial t} + \frac{U}{\rho_f H}\frac{\partial \rho_f}{\partial x} + \frac{1}{U}\frac{\partial U}{\partial t} + \frac{(H+2)}{H}\frac{\partial U}{\partial x}\right]$$

$$+ \frac{\delta}{\rho_f UH}\left[\frac{\partial P}{\partial x} + \rho_f\frac{\partial U}{\partial t} + \rho_f U\frac{\partial U}{\partial x}\right] \tag{57}$$

The initial condition is: $\theta(x,0) = 0$.

The boundary condition at the piston end is $\theta(L_p,t) = 0$, which is obvious from the fact that all the particles at the piston base are at the full piston velocity all the time. The condition at the tube head end shall be established later.

It is assumed that the entire flow is in the turbulent region and the wall shear stress can be obtained from the Ludwieg-Tillmann

friction factor [6], which was developed from a series of experiments with all types of pressure gradients. The original expression which holds good for incompressible flow with small temperature differences across the boundary layer is:

$$C_f = \frac{\tau_w}{\frac{1}{2}\rho_\infty U_\infty^2} = 0.246 \times 10^{-0.678H} \left(\frac{\rho_\infty U_\infty \theta}{\mu_\infty}\right)^{-0.268} \qquad (58)$$

In the present work, the expression is slightly modified by using the fluid properties (ρ, μ) at the film temperature, T_f, instead of the free stream temperature, T_∞, to take into account the effect of property variation across the boundary layer. The expressions for local friction coefficient, C_f, and local shear stress at the tube wall, τ_w, used in the present work are:

$$C_f = 2A \frac{1}{(Re_\theta)^B}$$

$$\tau_w = A \rho_f U^2 \frac{1}{(Re_\theta)^B} \qquad (59)$$

where

$$A = \frac{0.123}{10^{0.678H}} \quad ; \qquad B = 0.268; \qquad Re_\theta = \frac{\rho_f U \theta}{\mu_f}$$

Using the above expression for wall shear stress in equation (57), and multiplying equation (57) by $(1+B)\theta^B$:

$$\frac{\partial \Theta}{\partial t} = - \frac{U}{H} \frac{\partial \Theta}{\partial x} + (1+B)\frac{A}{H} \frac{\mu_f^B}{\rho_f^B} U^{(1-B)}$$

$$- (1+B)\Theta \left[\frac{1}{\rho_f} \frac{\partial \rho_f}{\partial t} + \frac{U}{\rho_f H} \frac{\partial \rho_f}{\partial x} + \frac{1}{U} \frac{\partial U}{\partial t} + \frac{(H+2)}{H} \frac{\partial U}{\partial x} \right]$$

$$+ (1+B)\, C_1\, \Theta \left[\frac{1}{\rho_f U} \frac{\partial P}{\partial x} + \frac{1}{U} \frac{\partial U}{\partial t} + \frac{\partial U}{\partial x} \right] \qquad (60)$$

where

$$\Theta = \theta^{(1+B)} \qquad \text{or,} \quad \theta = \Theta^{\frac{1}{(1+B)}} \qquad (61)$$

and,

$$C_1 = \frac{\delta}{\delta^*}$$

At the tube head end, U = 0 and the equation (60) becomes:

$$\frac{\partial \Theta}{\partial t} = - (1+B)\, \Theta \left[\frac{1}{\rho_f} \frac{\partial \rho_f}{\partial t} + \frac{U}{\rho_f H} \frac{\partial \rho_f}{\partial x} + \frac{1}{U} \frac{\partial U}{\partial t} + \frac{(H+2)}{H} \frac{\partial U}{\partial x} \right]$$

$$+ (1+B)\, \Theta\, C_1 \left[\frac{1}{\rho_f U} \frac{\partial P}{\partial x} + \frac{1}{U} \frac{\partial U}{\partial t} + \frac{\partial U}{\partial x} \right] \qquad (62)$$

and at t = 0, Θ = 0. This implies that at the tube head end, θ, i.e. momentum thickness or boundary layer thickness is zero at all times.

The equation (60) is applicable to both Case I and II for computing momentum thickness θ, and thence the friction coefficient,

C_f, at each station in the axial direction at each time step.

Heat Transfer Analysis

As the flow is in the turbulent region, the analogy between the momentum transfer and the heat transfer provides the easiest way to determine the heat transfer coefficient, h_i, at the tube wall. Because of its simplicity, Colburn's analogy [7] has been used for Prandtl numbers other than unity as follows:

$$St\ Pr^{2/3} = \frac{C_f}{2}$$

or,

$$h_i = \rho_f U c_p \left(\frac{C_f}{2}\right)/Pr^{2/3} \tag{63}$$

where $Pr = \left(\frac{\mu_g c_p}{\kappa_g}\right)$ and all properties are evaluated at T_f.

The heat transfer in the tube wall is considered as a one-dimensional (radial) unsteady heat conduction problem in a hollow cylinder. Longitudinal heat conduction is neglected because the temperature gradient in the radial direction is expected to be steeper by several order of magnitude than in the axial direction. The differential equation can be written as [15]:

$$\frac{\partial T_w}{\partial t} = \alpha_w \left[\frac{\partial^2 T_w}{\partial r^2} + \frac{1}{r}\frac{\partial T_w}{\partial r}\right] \tag{64}$$

The material properties will be assumed constant with respect to temperature. The boundary conditions are:

$$\text{at} \quad r = R, \quad \dot{q}_i'' = h_i(T_\infty - T_{w,i}) = -\kappa_w \left.\frac{\partial T_w}{\partial r}\right|_{r=R}$$

$$\text{at} \quad r = R_o, \quad \dot{q}_o'' = h_o(T_{w,o} - T_{amb}) = -\kappa_w \left.\frac{\partial T_w}{\partial r}\right|_{r=R_o} \tag{65}$$

$$\text{at} \quad t = 0, \quad T(r) = T_{amb}$$

It is possible to solve equation (64) numerically and obtain the temperature at the inner surface of the tube $T_{w,i}$ at each station along the length of the tube at each time step. The local heat transfer rate to the wall per unit surface area is given by $h_i(T-T_{w,i})$, and integrating over the entire surface and the time, the total heat transfer to the tube wall can be determined. The values of local wall shear stress τ_w, heat transfer coefficient h_i, and inner surface temperature $T_{w,i}$ as calculated from (59), (63) and (64) are used in the one-dimensional analysis for the subsequent time step.

Non-dimensionalization

Before proceeding to the solution technique that can be applied to solve the equations derived so far, it is advantageous to non-dimensionalize the equations to obtain a general solution for the geometrically similar devices with the same initial conditions. The non-dimensionalized parameters are:

Axial distance, $x' = \frac{x}{L_t}$

Pressure, $P' = P/P_o$

Temperature, $T' = T/T_o$

Density, $\rho' = \rho/\rho_{g_o}$

Velocity, $U' = U/U_o \qquad U_o = \sqrt{P_o/\rho_{g_o}}$

Time, $t' = \dfrac{U_o t}{L_t}$

Linear speed of burning, $r_b' = r_b/U_o$ (66)

It can be noted that:

$$\dot{v}_{d_s} = \frac{U_o}{L_t}\left[\left(\frac{S_{b_t}}{Ap}\right)\frac{\nu_s r_b'}{\int_o^{L'} \nu_s dx'}\right] = \frac{U_o}{L_t}\,\dot{v}'_{d_s} \tag{67}$$

$$h_g = \frac{P_o}{\rho_{g_o}}\left[\frac{P'(\gamma-\eta\rho_{g_o}\rho_g')}{\rho_g'(\gamma-1)}\right] = \frac{P_o}{\rho_{g_o}}\,h_g' \tag{68}$$

$$W = \frac{R_g T_o}{(\gamma-1)} = \frac{P_o}{\rho_{g_o}}\left[\frac{\rho_{g_o}}{P_o}\,\frac{R_g T_o}{(\gamma-1)}\right] = \frac{P_o}{\rho_{g_o}}\,W' \tag{69}$$

$$\tau_w = A\,\rho_f U^2 \frac{1}{(Re_\theta)^B} = P_o\;A\rho_f' U'^2 \frac{1}{(Re_\theta)^B} \tag{70}$$

and, $\eta\rho_{g_o}$ is a constant non-dimensional quantity.

Finally, non-dimensional forms of the conservation equations are:

Case I

Continuity of solids:

$$\frac{\partial \nu_s}{\partial t'} + U'\frac{\partial \nu_s}{\partial x'} + \nu_s\frac{\partial U'}{\partial x'} + \dot{v}_{d_s}' = 0 \tag{71}$$

Continuity of gases:

$$\frac{\partial \rho_g'}{\partial t'} + U' \frac{\partial \rho_g'}{\partial x'} + \frac{\rho_g'}{(1-\nu_s)} \frac{\partial U'}{\partial x'} = \frac{(\rho_s'-\rho_g')}{(1-\nu_s)} \dot{v}_{d_s}' \tag{72}$$

Momentum:

$$\frac{\partial U'}{\partial t'} + U' \frac{\partial U'}{\partial x'} = - \frac{1}{\rho_m'} \frac{\partial P'}{\partial x'} - D_1' \frac{\rho_f' U'^2}{\rho_m'} \frac{1}{(Re_\theta)^B} \tag{73}$$

Energy:

$$\frac{\partial P'}{\partial t'} + U' \frac{\partial P'}{\partial x'} + B_I' \frac{\partial U'}{\partial x'} = C_I' \dot{v}_{d_s}'$$

$$- D_2' E' h_i (T-T_{w,i}) + D_1' E' \frac{\rho_f' U'^3}{(Re_\theta)^B} \tag{74}$$

where,

$$B_I' = \frac{\gamma P'}{(1-\nu_s)(1-\eta\rho_{g_o}\rho_g')} \tag{75}$$

$$C_I' = \frac{\gamma P'(\rho_s'-\rho_g')+(\gamma-1)\rho_s'\rho_g'(W' + \frac{P}{\rho_s'} - h_g')}{\rho_g'\{(1-\nu_s)(1-\eta\rho_{g_o}\rho_g')\}} \tag{76}$$

$$E' = \frac{(\gamma-1)}{(1-\nu_s)(1-\eta\rho_{g_o}\rho_g')} \tag{77}$$

$$D_1' = 2A(\frac{L_t}{R}) \tag{78}$$

$$D_2' = 2(\frac{L_t}{R}) \frac{J}{P_o U_o} \tag{79}$$

Equation of state:

$$T' = \frac{P'}{\rho_g'} \frac{(1-\eta\rho_{g_o}\rho_g')}{(1-\eta\rho_{g_o})} \tag{80}$$

Characteristic equations:

Along η', ξ' characteristic, i.e. $\frac{dt'}{dx'} = \frac{1}{U' \pm \sqrt{B_I'/\rho_m'}}$,

$$\Delta P' \pm \rho_m'\sqrt{B_I'/\rho_m'}\ \Delta U' = C_I'\dot{v}_{d_s}'\ \Delta t - D_2'E'h_i(T-T_{w,i})\Delta t'$$

$$+ D_1'\left[E'U' \mp \sqrt{B_I'/\rho_m'}\right]\frac{\rho_f'U'^2}{(Re_\theta)^B}\Delta t' \tag{81}$$

Along a particle path, i.e. $\frac{dt'}{dx'} = \frac{1}{U'}$,

$$\Delta\rho_g' = G'\ \Delta P' + H_I'\dot{v}_{d_s}'\Delta t' + D_2'\left[\frac{(\gamma-1)\rho_g'}{(1-\nu_s)\gamma P'}\right]h_i(T-T_{w,i})\Delta t'$$

$$- D_1'\left[\frac{(\gamma-1)\rho_g'}{(1-\nu_s)\gamma P'}\right]\frac{\rho_g'U'^3}{(Re_\theta)^B}\Delta t' \tag{82}$$

where,

$$G' = \frac{\rho_g'(1-\eta\rho_{g_o}\rho_g')}{\gamma P'} \tag{83}$$

$$H_I' = \frac{(\gamma-1)\rho_s'\rho_g'(h_g' - W' - \frac{P'}{\rho_s'})}{(1-\nu_s)\gamma P'} \tag{84}$$

Again along a particle path, i.e. $\frac{dt'}{dx'} = \frac{1}{U'}$,

$$\Delta\nu_s = \frac{\nu_s(1-\nu_s)}{\rho_g'}\,\Delta\rho_g' - \frac{\rho_m'}{\rho_g'}\,\dot{v}_{d_s}'\Delta t' \tag{85}$$

Case II

Continuity of solids:

$$\frac{\partial\nu_s}{\partial t'} + \dot{v}_{d_s}' = 0 \tag{86}$$

Continuity of gases:

$$\frac{\partial\rho_g'}{\partial t'} + U'\frac{\partial\rho_g'}{\partial x'} + \rho_g'\frac{\partial U'}{\partial x'} = \frac{(\rho_s'-\rho_g')}{(1-\nu_s)}\,\dot{v}_{d_s}' + \frac{\rho_g'U'}{(1-\nu_s)}\,\frac{\partial\nu_s}{\partial x'} \tag{87}$$

Momentum:

$$\frac{\partial U'}{\partial t'} + U'\frac{\partial U'}{\partial x'} = -\frac{1}{\rho_g'}\,\frac{\partial P'}{\partial x'} - \frac{\rho_s'U'}{(1-\nu_s)\rho_g'}\,\dot{v}_{d_s}' - D_1'\frac{\rho_f'U'^2}{(1-\nu_s)\rho_g'(Re_\theta)^B} \tag{88}$$

Energy:

$$\frac{\partial P'}{\partial t'} + U'\frac{\partial P'}{\partial x'} + B_{II}'\frac{\partial U'}{\partial x'} = C_{II}'\dot{v}_{d_s}' + \frac{B_{II}'U'}{(1-\nu_s)}\,\frac{\partial\nu_s}{\partial x'}$$

$$- D_2'E'h_i(T-T_{w,i}) + D_1'E'\frac{\rho_f'U'^3}{(Re_\theta)^B} \tag{89}$$

where,

$$B_{II}' = \frac{\gamma P'}{(1-\eta\rho_{g_o}\rho_g')} \tag{90}$$

$$C_{II}' = \frac{\gamma P'(\rho_s'-\rho_g') + (\gamma-1)\rho_s'\rho_g'(W' + \frac{P'}{\rho_s'} + \frac{U'^2}{2} - h_g')}{\rho_g'\{(1-\nu_s)(1-\eta\rho_{g_o}\rho_g')\}} \tag{91}$$

E', D_1', and D_2' are given by equations (77), (78), and (79), respectively. The equation of state for the gas is also same as equation (80).

Characteristic equations:

Along η', ξ' characteristic, i.e. $\frac{dt'}{dx'} = \frac{1}{U' \pm \sqrt{B_{II}'/\rho_g'}}$,

$$\Delta P' \pm \rho_g' \sqrt{B_{II}'/\rho_g'}\,\Delta U' = \frac{B_{II}'U'}{(1-\nu_s)(U' \pm \sqrt{B_{II}'/\rho_g'})}\Delta\nu_s$$

$$+ \left[C_{II}' \mp \sqrt{B_{II}/\rho_g'}\,\frac{\rho_s'U'}{(1-\nu_s)} + \frac{B_{II}'U'}{(1-\nu_s)(U' \pm \sqrt{B_{II}'/\rho_g'})}\right]\dot{v}_{d_s}'\Delta t'$$

$$- D_2'E'h_i(T-T_{w,i})\Delta t'$$

$$+ D_1'\left[E'U' \mp \frac{1}{(1-\nu_s)}\sqrt{B_{II}'/\rho_g'}\right]\frac{\rho_f'U'^2}{(Re_\theta)^B}\Delta t' \tag{92}$$

Along a particle path, i.e. $\frac{dt'}{dx'} = \frac{1}{U'}$,

$$\Delta\rho_g' = G'\,\Delta P' + H_{II}'\,\dot{v}_{d_s}'\,\Delta t' + D_2'\left[\frac{(\gamma-1)\rho_g'}{(1-\nu_s)\gamma P'}\right] h_i(T-T_{w,i})\Delta t'$$

$$- D_1'\left[\frac{(\gamma-1)\rho_g'}{(1-\nu_s)\gamma P'}\right]\frac{\rho_g' U'^3}{(Re_\theta)^B}\,\Delta t' \qquad (93)$$

where

$$H_{II}' = \frac{(\gamma-1)\rho_s'\rho_g'(h_g' - W' - \frac{P'}{\rho_s'} - \frac{U'^2}{2})}{(1-\nu_s)\gamma P'} \qquad (94)$$

Boundary Layer Equation

Using the non-dimensional momentum thickness, $\theta' = \frac{\theta}{R}$ and all the non-dimensionalized parameters listed in (66), the boundary layer equation (60) becomes:

$$\frac{\partial\theta'}{\partial t'} = -\frac{U'}{H}\frac{\partial\theta'}{\partial x'} + (1+B)\frac{A}{H}\left(\frac{L_t}{R}\right)\left(\frac{\mu_f}{\rho_{g_o} U_o R}\right)^B \frac{H'^{(1-B)}}{\rho_f'^B}$$

$$- (1+B)\theta'\left[\frac{1}{\rho_f'}\frac{\partial\rho_f'}{\partial t'} + \frac{U'}{\rho_f' H}\frac{\partial\rho_f'}{\partial x'} + \frac{1}{U'}\frac{\partial U'}{\partial t'} + \frac{H+2}{H}\frac{\partial U'}{\partial x'}\right]$$

$$+ (1+B)C_1\theta'\left[\frac{1}{\rho_f' U'}\frac{\partial P'}{\partial x'} + \frac{1}{U'}\frac{\partial U'}{\partial t'} + \frac{\partial U'}{\partial x'}\right] \qquad (95)$$

where

$$\theta' = \theta'^{(1+B)} \qquad \text{or} \qquad \theta' = \theta'^{\frac{1}{1+B}} \qquad (96)$$

Now U', ρ_g' and P' are taken from the one-dimensional solution and ρ_f' is obtained from the non-dimensional form of equation (56) i.e.:

$$\rho_f' = \frac{\left(\frac{2T}{T+T_{w,i}}\right)\rho_g'}{\left[1+n\rho_{g_o}\rho_g'\left(\frac{2T}{T+T_{w,1}} - 1\right)\right]} \qquad (97)$$

SECTION IV

SOLUTION PROCEDURE

Solution of Interior Points

As there is no analytical solution to the set of coupled non-linear partial differential equations derived in the previous chapter, numerical techniques have been used to solve the conservation equations along with the boundary layer momentum integral equation and the equation of state of the combustion gas. The differential equations are written in finite difference form and MacCormack's version [16] of Lax-Wendroff two step method [17] is followed. The procedure is shown by an example below:

Let,

$$\frac{\partial u}{\partial t} = -c \frac{\partial u}{\partial x} \tag{98}$$

where c is a constant.

Equation (3.1) can be written as,

$$\begin{aligned} \tilde{u}_j^{n+1} &= u_j^n - c \frac{\Delta t}{\Delta x} (u_{j+1}^n - u_j^n) \\ \tilde{\tilde{u}}_j^{n+1} &= u_j^n - c \frac{\Delta t}{\Delta x} (\tilde{u}_j^{n+1} - \tilde{u}_{j-1}^{n+1}) \end{aligned} \tag{99}$$

and finally,

$$u_j^{n+1} = \tfrac{1}{2} \left[\tilde{u}_j^{n+1} + \tilde{\tilde{u}}_j^{n+1} \right]$$

where $\tilde{u}_j^{n+1}$ and $\tilde{\tilde{u}}_j^{n+1}$ are the first and second estimated value of u_j^{n+1}. The integer n, and j denote the time and axial position of a nodal point shown in Figure 2. If c is a variable, i.e. c(u), $\tilde{c}(\tilde{u})_j^{n+1}$ is used in the second estimation of u_j^{n+1}. It can be recognized that both forward and backward space derivatives have been taken into account.

Case I

Using the MacCormack scheme, the non-dimensionalized conservation equations, i.e. (71) through (74) can be written as:

$$\tilde{\nu}_{s_j}^{n+1} = \nu_{s_j}^{n} - U'^{n}_{j} \frac{\Delta t'}{\Delta x'_o} (\nu_{s_{j+1}}^{n} - \nu_{s_j}^{n}) - \nu_{s_j}^{n} \frac{\Delta t'}{\Delta x'_o} (U'^{n}_{j+1} - U'^{n}_{j})$$

$$- \left[\dot{v}_{d_s}'\right]_j^n \Delta t' \qquad (100)$$

$$\tilde{\rho}_{g_j}'^{n+1} = \rho_{g_j}'^{n} - U'^{n}_{j} \frac{\Delta t'}{\Delta x'_o} (\rho_{g_{j+1}}'^{n} - \rho_{g_j}'^{n})$$

$$- \frac{\rho_{g_j}'^{n}}{(1-\nu_{s_j}^{n})} \frac{\Delta t'}{\Delta x'_o} (U'^{n}_{j+1} - U'^{n}_{j}) + \frac{(\rho_s' - \rho_{g_j}'^{n})}{(1-\nu_{s_j}^{n})} \left[\dot{v}_{d_s}'\right]_j^n \Delta t' \qquad (101)$$

$$\tilde{U}'^{n+1}_{j} = U'^{n}_{j} - U'^{n}_{j} \frac{\Delta t'}{\Delta x'_o} (U'^{n}_{j+1} - U'^{n}_{j})$$

$$- \frac{1}{\rho_{m_j}'^{n}} \frac{\Delta t'}{\Delta x'_o} (P'^{n}_{j+1} - P'^{n}_{j}) - ULF_j^n \Delta t' \qquad (102)$$

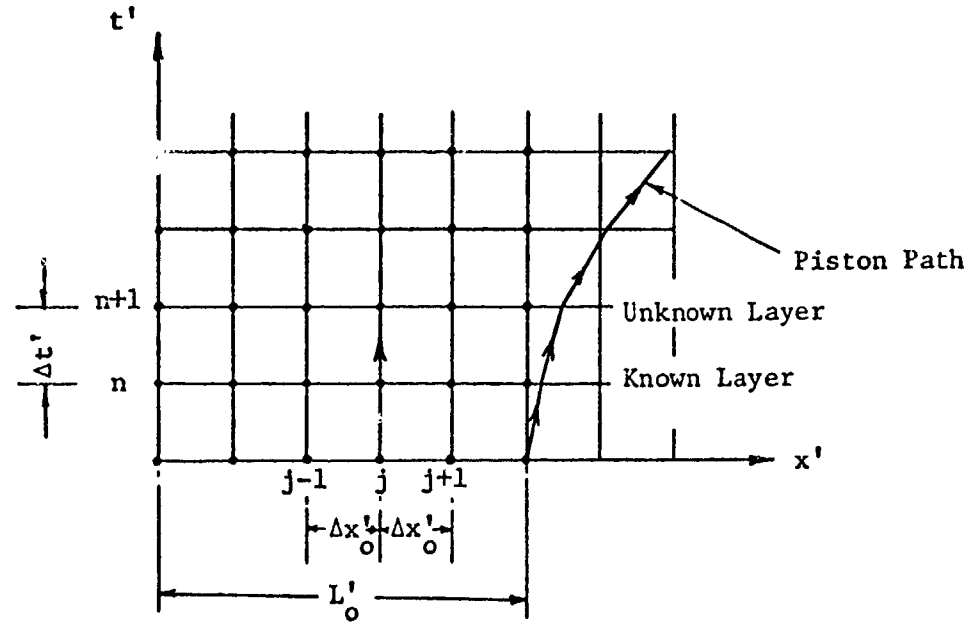

Figure 2. Numerical Scheme for Interior Points

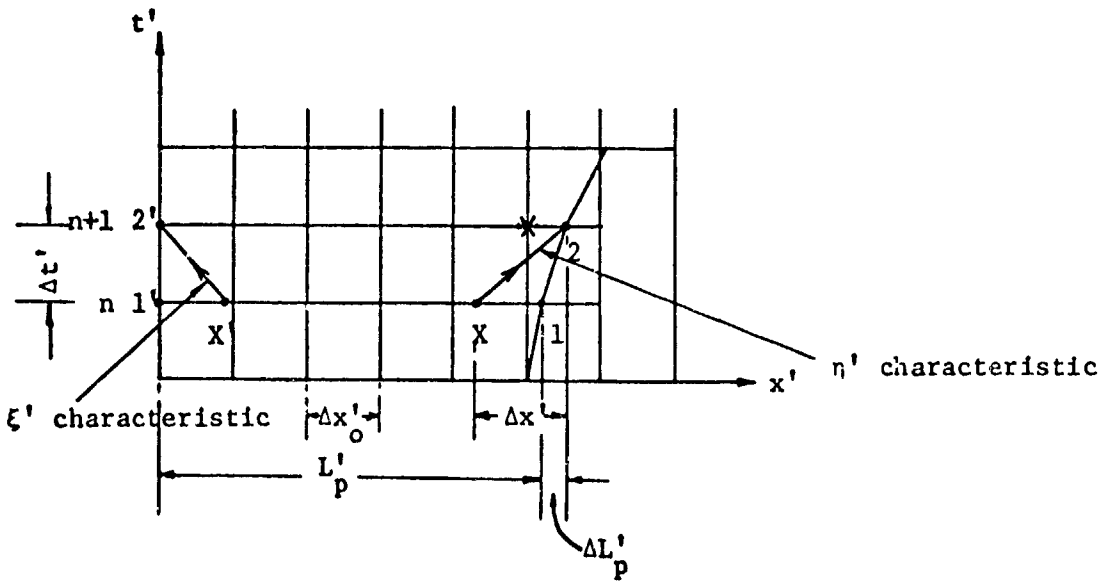

Figure 3. Scheme for End Points

$$\tilde{P}'^{n+1}_j = P'^{n}_j - U'^{n}_j \frac{\Delta t'}{\Delta x'_o} (P'^{n}_{j+1} - P'^{n}_j) - B'^{n}_I{}_j \frac{\Delta t'}{\Delta x'_o} (U'^{n}_{j+1} - U'^{n}_j)$$

$$+ C'^{n}_I{}_j \dot{v}'^{n}_{d_s}{}_j \Delta t' - E'^{n}_j D'_2 \dot{q}''^{n}_j \Delta t'$$

$$+ E'^{n}_j PGF^{n}_j \Delta t' \tag{103}$$

where,

$$\dot{v}'_{d_s} = \frac{S_{b_t}}{A_p} \frac{\nu_s r'_b}{\int_0^{L'_p} \nu_s dx'} \tag{104}$$

$$\dot{q}'' = h_i (T - T_{w,i}) \tag{105}$$

$$ULF = D'_1 \frac{\rho'_f U'^2}{\rho'_m} \frac{1}{(Re_t)^B} \tag{106}$$

$$PGF = D'_1 \frac{\rho'_f U'^3}{(Re_\theta)^B} \tag{107}$$

Thus, for all the nodal points (except the last point adjacent to the piston base) the first estimation regarding the ballistic properties after a time increment $\Delta t'$ is made by knowing the present values of the properties at the point of interest and at its forward nodal point. The second estimation is done as follows:

$$\tilde{\tilde{\nu}}_{s_j}^{n+1} = \nu_{s_j}^{n} - \tilde{U}_j'^{,n+1} \frac{\Delta t'}{\Delta x_o'} (\tilde{\nu}_{s_j}^{n+1} - \tilde{\nu}_{s_{j-1}}^{n+1})$$

$$- \tilde{\nu}_{s_j}^{n+1} \frac{\Delta t'}{\Delta x_o'} (\tilde{U}_j'^{,n+1} - \tilde{U}_{j-1}'^{,n+1}) - \dot{\nu}_{d_{s_j}}'^{n} \Delta t' \qquad (108)$$

$$\tilde{\tilde{\rho}}_{g_j}'^{,n+1} = \rho_{g_j}'^{,n} - \tilde{U}_j'^{,n+1} \frac{\Delta t'}{\Delta x_o'} (\tilde{\rho}_{g_j}'^{,n+1} - \tilde{\rho}_{g_{j-1}}'^{,n+1})$$

$$- \frac{\tilde{\rho}_{g_j}'^{,n+1}}{(1-\tilde{\nu}_{s_j}^{n+1})} \frac{\Delta t'}{\Delta x_o'} (\tilde{U}_j^{n+1} - \tilde{U}_{j-1}'^{,n+1}) + \frac{(\rho_s' - \tilde{\rho}_{g_j}'^{,n+1})}{(1-\tilde{\nu}_{s_j}^{n+1})} \dot{v}_{d_{s_j}}'^{n} \Delta t' \qquad (109)$$

$$\tilde{\tilde{U}}_j'^{,n+1} = U_j'^{,n} - \tilde{U}_j'^{,n+1} \frac{\Delta t'}{\Delta x_o'} (\tilde{U}_j'^{,n+1} - \tilde{U}_{j-1}'^{,n+1})$$

$$- \frac{1}{\tilde{\rho}_{m_j}'^{,n+1}} \frac{\Delta t'}{\Delta x_o'} (\tilde{P}_j'^{,n+1} - \tilde{P}_{j-1}'^{,n+1}) - ULF_j^{n} \Delta t' \qquad (110)$$

$$\tilde{\tilde{P}}_j'^{,n+1} = P_j'^{,n} - \tilde{U}_j'^{,n+1} \frac{\Delta t'}{\Delta x_o'} (\tilde{P}_j'^{,n+1} - \tilde{P}_{j-1}'^{,n+1})$$

$$- \tilde{B}_{I_j}'^{n+1} \frac{\Delta t'}{\Delta x_o'} (\tilde{U}_j'^{,n+1} - \tilde{U}_{j-1}'^{,n+1}) + \tilde{C}_{I_j}'^{n+1} \dot{v}_{d_{s_j}}'^{n} \Delta t'$$

$$- \tilde{E}_j'^{n+1} D_2' \dot{q}_j''^{n} \Delta t' + \tilde{E}_j'^{n+1} PGF_j^{n} \Delta t' \qquad (111)$$

and finally,

$$\nu_{s_j}^{n+1} = \tfrac{1}{2}\left[\tilde{\nu}_{s_j}^{n+1} + \tilde{\tilde{\nu}}_{s_j}^{n+1}\right] \qquad (112)$$

$$\rho'^{n+1}_{g_j} = \tfrac{1}{2}\left[\tilde{\rho}'^{n+1}_{g_j} + \overset{*}{\rho}'^{n+1}_{g_j}\right] \tag{113}$$

$$U'^{n+1}_{j} = \tfrac{1}{2}\left[\tilde{U}'^{n+1}_{j} + \tilde{\tilde{U}}'^{n+1}_{j}\right] \tag{114}$$

$$P'^{n+1}_{j} = \tfrac{1}{2}\left[\tilde{P}'^{n+1}_{j} + \tilde{\tilde{P}}'^{n+1}_{j}\right] \tag{115}$$

From the equation of state (80):

$$T'^{n+1}_{j} = \frac{P'^{n+1}_{j}}{\rho'^{n+1}_{g_j}} \frac{(1-\eta\rho_{g_o}\rho'^{n+1}_{g_j})}{(1-\eta\rho_{g_o})} \tag{116}$$

Similarly, to calculate the momentum thickness at a nodal point after increment $\Delta t'$, equation (95) is written as:

$$\tilde{\Theta}'^{n+1}_{j} = \Theta'^{n}_{j} - \frac{U'^{n}_{j}}{H}\frac{\Delta t'}{\Delta x'_o}(\Theta'^{n}_{j+1} - \Theta'^{n}_{j}) + D'_3 \frac{\left[U'^{n}_{j}\right]^{(1-B)}}{\left[\rho'^{n}_{f_j}\right]^{B}}\Delta t'$$

$$- (1+B)\,\Theta'^{n}_{j}\left[\frac{1}{\rho'^{n}_{f_j}}(\tilde{\rho}'^{n+1}_{f_j} - \rho'^{n}_{f_j}) + \frac{U'^{n}_{j}}{H\rho'^{n}_{f_j}}\frac{\Delta t'}{\Delta x'_o}(\rho'^{n}_{f_{j+1}} - \rho'^{n}_{f_j})\right.$$

$$\left. + \frac{(1-C_1)}{U'^{n}_{j}}(\tilde{U}'^{n+1}_{j} - U'^{n}_{j}) + \left\{\frac{H+2}{H} - C_1\right\}\frac{\Delta t'}{\Delta x'_o}(U'^{n}_{j+1} - U'^{n}_{j})\right]$$

$$+ (1+B)\,\Theta'^{n}_{j}\frac{C_1}{\rho'^{n}_{f_j}U'^{n}_{j}}\frac{\Delta t'}{\Delta x'_o}(P'^{n}_{j+1} - P'^{n}_{j}) \tag{117}$$

where

$$D_3' = (1+B)\frac{A}{H}\left(\frac{L_t}{R}\right)\left(\frac{\mu_{f_j}^{n}}{\rho_{g_o} U_o R}\right)^{B} \tag{118}$$

taking

$$\mu_f = \mu_{g_o}\left(\frac{T_f}{T_o}\right)^{m} , \tag{119}$$

m being a suitable constant.

The densities $\tilde{\rho}_{f_j}^{',n}$ and $\tilde{\rho}_{f_j}^{',n+1}$ are calculated from equation (97) with the assumption,

$$\left(\frac{\tilde{T}}{T_f}\right)_j^{n+1} \simeq \left(\frac{T}{T_f}\right)_j^{n}$$

again,

$$\tilde{\Theta}_j^{',n+1} = \Theta_j^{',n} - \frac{\tilde{U}_j^{',n+1}}{H}\frac{\Delta t'}{\Delta x_o'}\left(\tilde{\Theta}_j^{',n+1} - \tilde{\Theta}_{j-1}^{',n+1}\right) + D_3' \frac{\left(\tilde{U}_j^{',n+1}\right)^{(1-B)}}{\left(\tilde{\rho}_{f_j}^{',n+1}\right)^{B}}\Delta t'$$

$$- (1+B)\,\tilde{\Theta}_j^{',n+1}\left[\frac{1}{\tilde{\rho}_{f_j}^{',n+1}}\left(\tilde{\rho}_{f_j}^{',n+1} - \rho_{f_j}^{',n}\right) + \frac{\tilde{U}_j^{',n+1}}{H\tilde{\rho}_{f_j}^{',n+1}}\frac{\Delta t'}{\Delta x_o'}\left(\tilde{\rho}_{f_j}^{',n+1} - \tilde{\rho}_{f_{j-1}}^{',n+1}\right)\right.$$

$$\left. + \frac{(1-C_1)}{\tilde{U}_j^{',n+1}}\left(\tilde{U}_j^{',n+1} - U_j^{',n}\right) + \left\{\frac{H+2}{H} - C_1\right\}\frac{\Delta t'}{\Delta x_o'}\left(\tilde{U}_j^{',n+1} - \tilde{U}_{j-1}^{',n+1}\right)\right]$$

$$+ (1+B)\,\Theta_j^{',n+1}\,\frac{C_1}{\tilde{\rho}_{f_j}^{',n+1}\tilde{U}_j^{',n+1}}\frac{\Delta t'}{\Delta x_o'}\left[\tilde{P}_j^{',n+1} - \tilde{P}_{j-1}^{',n+1}\right] \tag{120}$$

finally,

$$\Theta'^{n+1}_j = \tfrac{1}{2}\left[\tilde{\Theta}'^{n+1}_j + \tilde{\tilde{\Theta}}'^{n+1}_j\right] \tag{121}$$

and,

$$\theta'^{n+1}_j = \left[\Theta'^{n+1}_j\right]^{\frac{1}{(1+B)}} \tag{122}$$

The heat transfer coefficient after time $\Delta t'$, $h_{i_j}^{n+1}$ can be calculated using equations (59) and (63) . The new inner surface temperature T_{w,i_j}^{n+1} is obtained from the solution of equation (64) using the mean heat transfer coefficient,

$$h_m = \frac{h_{i_j}^{n} + h_{i_j}^{n+1}}{2}$$

The same procedure is followed for Case II starting with appropriate conservation equations, namely equations (86) through (89), same equation of state (80) and boundary layer momentum equation (95). The only points of differences are: (1) no solid particles beyond L_o' and (2) the burning rate r_b is chosen corresponding to the average pressure in the space between the tube head end and L_o.

Solution for Boundary Points

It has been stated earlier that to calculate the ballistic properties at the tube head end and at the piston base end, one needs the characteristic equations. Typical characteristic directions are shown in Figure 3. Let, at any time t', the piston be at position 1 with

velocity $U'_{p,1}$. Its position and velocity after time $\Delta t'$ can be calculated by using equations (18) and (19) as follows:

$$U'_{p,2} = U'_{p,1} + \frac{1}{U_o} (a_p \Delta t)$$

and

$$\Delta L'_p = \frac{1}{L_t} \left[U_{p,1} \Delta t + \tfrac{1}{2} a_p (\Delta t)^2 \right] \tag{123}$$

where,

$$a_p = \frac{P_{p,m} A_p}{M_p} \qquad (P_{p,m} \text{ is mean of } P_1 \text{ and } P_2)$$

Then the η'-characteristic is traced back using the appropriate expression:

$$\begin{aligned} &\text{for Case I:} \quad \Delta x' = (U' + \sqrt{B'_I/\rho'_m})\, \Delta t' \\ &\text{for Case II:} \quad \Delta x' = (U' + \sqrt{B'_{II}/\rho'_g})\, \Delta t' \end{aligned} \tag{124}$$

The point X is thus determined and all the properties are interpolated between the nodal points in each side. Pressure at point 2 is calculated by applying equation (81) for Case I, and equation (92) for Case II,

$$\text{for Case I,} \quad P'_2 = P'_X - \rho'_m \sqrt{\frac{B'_I}{\rho'_m}} (U'_{P,2} - U'_X) + C'_I \dot{v}'_{d_s} \Delta t'$$

$$- D'_2 E' h_i (T - T_{w,i}) \Delta t' + D'_1 \left[E'U' - \sqrt{B'_I/\rho'_m} \right] \frac{\rho'_f U'^2}{(Re_\theta)^B} \Delta t' \tag{125}$$

for Case I', $P'_2 = P'_X - \rho'_g \sqrt{B'_{II}/\rho'_g}\,(U'_{p,2}-U'_X)$

$$+\frac{B'_{II}U'}{(1-\nu_s)(U'+\sqrt{B'_{II}/\rho'_g})}(\nu_{s,2}-\nu_{s,X})$$

$$+\left[C'_{II}-\sqrt{B'_{II}/\rho'_g}\,\frac{\rho'_s U'}{(1-\nu_s)}+\frac{B'_{II}U'}{(1-\nu_s)(U'+\sqrt{B'_{II}/\rho'_g})}\right]\dot{v}_{d_s}\,'\Delta t'$$

$$-D'_2E'h_i(T-T_{w,i})\Delta t'+D'_1\left[E'U'-\frac{1}{(1-\nu_s)}\sqrt{B'_{II}/\rho'_g}\right]$$

$$\frac{\rho'_f U'^2}{(Re_\theta)^B}\Delta t' \qquad (126)$$

The gas density and volume fraction of solids at the new base point 2 are determined from characteristic equations along a particle path as follows:

for Case I and II,

$$\rho'_{g,2}=\rho'_{g,1}+G'(P'_2-P'_1)+H'_{1,II}\dot{v}_{d_s}\,'\Delta t' \qquad (127)$$

for Case I,

$$\nu_{s,2}=\nu_{s,1}+\frac{\nu_s(1-\nu_s)}{\rho'_g}(\rho'_{g,2}-\rho'_{g,1})-\frac{\rho'_m}{\rho'_g}\dot{v}_{d_s}\,'\Delta t' \qquad (128)$$

for Case II,

$$\nu_{s,2}=0 \qquad (129)$$

For both points 1 and 2, the momentum thickness is zero, which implies that both friction factor and film heat transfer coefficient at point 1 and 2 are infinitely large. Therefore, the last two terms of equations (82) and (93) have been deleted while writing the equation (127) For the same reason, in equations (125) and (126) the values for $h_i(T-T_{w,i})$ and $\frac{\rho_f' U'^2}{(Re_\theta)^B}$ are taken corresponding to the nodal point adjacent to the first base point 1. All the coefficients used in equations (124) through (128) are mean values between point 2 and X or point 2 and 1 depending on the characteristic used. The properties at point 2 are first assumed to be the same as point 1 and then iteration is carried on until the values converge within the specified limit.

For the tube head end,

$$U_1' = U_2' = 0 \tag{130}$$

and the momentum thickness and heat transfer coefficient are also zero.

The ξ'-characteristic is traced by using,

$$\begin{aligned} &\text{for Case I:} \quad \Delta x' = (U' - \sqrt{B_I'/\rho_m'})\,\Delta t' \\ &\text{for Case II:} \quad \Delta x' = (U' - \sqrt{B_{II}'/\rho_g'})\,\Delta t' \end{aligned} \tag{131}$$

By knowing the properties at X' and 1', properties at point 2' are obtained in the following manner:

Case I

$$P'_{2'} = P'_{X'} + \rho'_m \sqrt{B'_I/\rho'_m}\,(0 - U'_{X'}) + C'_I\,\dot{v}_{d_s}{}'\,\Delta t' - D'_2 E'\,h_i(T-T_{w,i})\Delta t'$$

$$+ D'_1\left[E'U' + \sqrt{B'_I/\rho'_m}\right]\frac{\rho'_f U'^2}{(Re_\theta)^B}\,\Delta t' \qquad (132)$$

$$\rho'_{g,2'} = \rho'_{g,1'} + G'\,(P'_{2'} - P'_{1'}) + H'_I\,\dot{v}_{d_s}{}'\,\Delta t' \qquad (133)$$

$$\nu_{s,2'} = \nu_{s,1'} + \frac{\nu_s(1-\nu_s)}{\rho'_g}\,(\rho'_{g,2'}-\rho'_{g,1'}) - \frac{\rho'_m}{\rho'_g}\,\dot{v}_{d_s}{}'\,\Delta t' \qquad (134)$$

Case II

$$P'_{2'} = P'_{X'} + \rho'_g\sqrt{B'_{II}/\rho'_g}\,(0-U'_{X'}) + \frac{B'_{II}U'}{(1-\nu_s)(U'-\sqrt{B'_{II}/\rho'_g})}\,(\nu_{s,2'}-\nu_{s,1'})$$

$$+ \left[C'_{II} + \sqrt{B'_{II}/\rho'_g}\,\frac{\rho'_s U'}{(1-\nu_s)} + \frac{B'_{II}U'}{(1-\nu_s)(U'-\sqrt{B'_{II}/\rho'_g})}\right]\dot{v}_{d_s}{}'\,\Delta t'$$

$$- D'_2E'h_i(T-T_{w,i})\Delta t' + D'_1\left[E'U' + \frac{1}{(1-\nu_s)}\sqrt{B'_{II}/\rho'_g}\right]\frac{\rho'_f U'^2}{(Re_\theta)^B}\,\Delta t' \qquad (135)$$

and from (2.86),

$$\nu_{s,2'} = \nu_{s,1'} - \dot{v}_{d_s}{}'\,\Delta t' \qquad (136)$$

The expression for $\rho'_{g,2'}$ is obtained by replacing H'_I by H'_{II} in equation (133).

The iteration procedure for the tube head end is the same as that for the piston base end stated earlier.

The properties at the nodal point(s) adjacent to the base point (shown by * in Figure 3), which cannot be calculated from the Lax-Wendroff method,are determined by linear interpolation between the piston base point and the nearest point where properties have been calculated from the Lax-Wendroff method.

It is noted that the spatial interval $\Delta x'_o$ is fixed for the entire solution and can be chosen arbitrarily depending upon the desired accuracy. But, for the stability of the Law-Wendroff solution, the time interval $\Delta t'$ must be chosen such that $\frac{\Delta t'}{\Delta x'_o}$ nowhere exceeds the slope of any characteristic [17]. This implies that at every time step,

$$\Delta t' \leq \frac{\Delta x'_o}{|U'|+\sqrt{B'_I/\rho'_m}} \qquad \text{for Case I}$$

$$\Delta t' \leq \frac{\Delta x'_o}{|U'|+\sqrt{B'_{II}/\rho'_g}} \qquad \text{for Case II} \tag{137}$$

Therefore, before selecting a new time interval, the right hand side of (137) is calculated at each nodal point (including the end points) and then the lowest value is chosen as the next time step.

Determination of Wall Temperature

The differential equation (64) in finite difference form can be written as (see Figure 4 for notations):

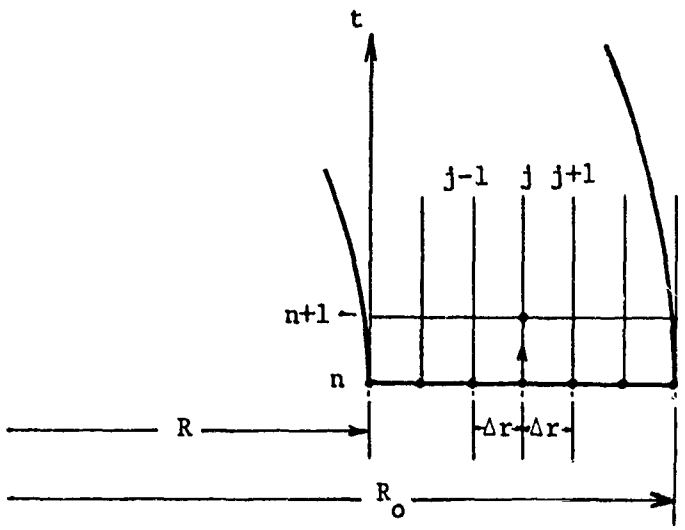

Figure 4. Numerical Scheme for Determination of Tube Wall Temperature.

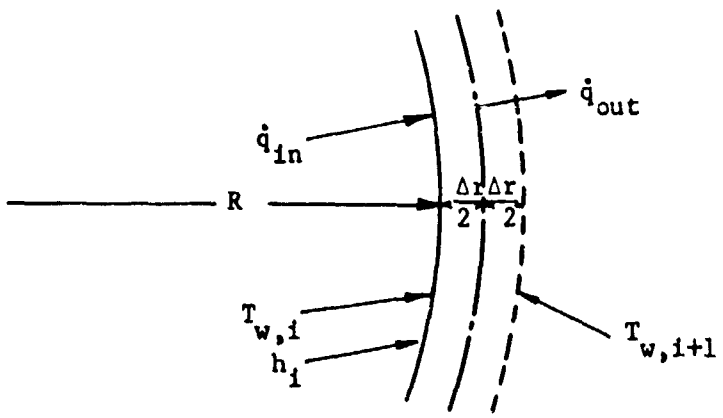

Figure 5. Heat Balance for a Thin Circular Element at the Inside Surface of the Tube

$$\frac{T^{n+1}_{w,j} - T^{n}_{w,j}}{\Delta t} = \alpha_w \left[\frac{T^{n}_{w,j+1} + T^{n}_{w,j-1} - 2T^{n}_{w,j}}{(\Delta r)^2} + \frac{1}{r_j} \frac{T^{n}_{w,j+1} - T^{n}_{w,j-1}}{2\Delta r} \right]$$

or,

$$T^{n+1}_{w,j} = \left[1 - \frac{2\alpha_w \Delta t}{(\Delta r)^2} \right] T^{n}_{w,j} + \frac{2\alpha_w \Delta t}{(\Delta r)^2} \left[\tfrac{1}{2} + \frac{\Delta r}{4r_j} \right] T^{n}_{w,j+1}$$

$$+ \frac{2\alpha_w \Delta t}{(\Delta r)^2} \left[\tfrac{1}{2} - \frac{\Delta r}{4r_j} \right] T^{n}_{w,j-1} \qquad (138)$$

Therefore, the temperature at any interior point in the tube wall after a time interval Δt can be calculated from the knowledge of present temperatures at and around the point of interest. For boundary points, however, a heat balance as described below is required:

Inner Surface: With reference to the Figure 5:

$$2\pi R \frac{\Delta r}{2} \rho_w c_w \frac{\partial T_{w,i}}{\partial t} = 2\pi R\, h_i (T_\infty - T_{w,i}) - 2\pi \left(R + \frac{\Delta r}{2}\right) \left(-\kappa_w \frac{\partial T_w}{\partial r} \right)\Bigg|_{r=R+\frac{\Delta r}{2}}$$

or,

$$\frac{\partial T_{w,i}}{\partial t} = \frac{2h_i}{\rho_w c_w \Delta r} (T_\infty - T_{w,i}) + \frac{2\kappa_w}{\rho_w c_w R\, \Delta r} \left(R + \frac{\Delta r}{2}\right) \frac{\partial T_w}{\partial r}\Bigg|_{r=R+\frac{\Delta r}{2}}$$

In finite difference form,

$$T_{w,i}^{n+1} = \left[1 - \frac{2\alpha_w \Delta t}{(\Delta r)^2}\left(\frac{h_m \Delta r}{\kappa_w} + 1 + \frac{\Delta r}{2R}\right)\right] T_{w,i}^{n}$$

$$+ \frac{2\alpha_w \Delta t}{(\Delta r)^2}\left(\frac{h_m \Delta r}{\kappa_w}\right) T_{\infty}^{n} + \frac{2\alpha_w \Delta t}{(\Delta r)^2}\left(1 + \frac{\Delta r}{2R}\right) T_{w,i+1}^{n} \qquad (139)$$

Similarly, for the outer surface,

$$T_{w,o}^{n+1} = \left[1 - \frac{2\alpha_w \Delta t}{(\Delta r)^2}\left(\frac{h_o \Delta r}{\kappa_w} + 1 - \frac{\Delta r}{2R_o}\right)\right] T_{w,o}^{n}$$

$$+ \frac{2\alpha_w \Delta t}{(\Delta r)^2}\left(\frac{h_o \Delta r}{\kappa_w}\right) T_{amb} + \frac{2\alpha_w \Delta t}{(\Delta r)^2}\left(1 - \frac{\Delta r}{2R_o}\right) T_{w,o-1}^{n} \qquad (140)$$

The stability conditions [18, 19] for the equations (138) through (140) are, respectively:

$$\Delta t \leq \frac{(\Delta r)^2}{2\alpha_w} \qquad (141)$$

$$\Delta t \leq \frac{(\Delta r)^2}{2\alpha_w\left[\frac{h_m \Delta r}{K_w} + 1 + \frac{\Delta r}{2R}\right]} \qquad (142)$$

and

$$\Delta t \leq \frac{(\Delta r)^2}{2\alpha_w\left[\frac{h_o \Delta r}{K_w} + 1 - \frac{\Delta r}{2R_o}\right]} \qquad (143)$$

Very small values of Δr (0.05 millimeter) are taken, and the selected Δt is the least of the values calculated from the right-hand side of (141), (142), and (143).

For a thick wall and initially cold tube, the temperature wave in a single shot does not generally reach the outer surface and, therefore, equation (140) can be disregarded.

Summary of the Procedure

Once the piston-cylinder arrangement, the initial conditions and all other input parameters are chosen, the solution proceeds according to the following steps:

(1) The time interval $\Delta t'$ is determined in accordance with expression (3.40) and the burning rate is taken corresponding to the average burning pressure.

(2) The new piston position and its velocity are calculated, and using the appropriate characteristic equations as indicated earlier the new ballistic properties at both the piston base end and the tube head end are determined.

(3) The interior points are solved either by the Lax-Wendroff method or by linear interpolation as discussed earlier.

(4) The new heat transfer coefficient is determined from the new ballistic properties and the momentum thickness at all the nodal points. The new wall temperature is also calculated using the mean heat transfer coefficient.

(5) All the calculated values are stored as the present values and reused for the next time step.

Thus the solution proceeds until the piston reaches the desired position. A computer program for the entire solution procedure was written in FORTRAN V and was run to obtain all of the results presented in the following chapter. The flow chart for the program has been shown in Appendix III. The computation time is approximately four minutes for the typical cases run on the Georgia Institute of Technology's UNIVAC 1108 machine.

SECTION V

RESULTS AND DISCUSSION

Standard Conditions

A set of realistic, but somewhat arbitrary, conditions is chosen as the input data to the computer program, and results are obtained for both cases of solid velocities. These conditions will be referred to as "standard conditions." They are:

Tube length, L_t	2 m
Tube inside diameter, D	3 cm
Piston mass, M_p	0.326 kg

Initial conditions:

Piston position, L_o	25 cm
Chamber pressure (piston start pressure), P_c	200 atm
Gas temperature (explosion temperature), T_o	3000°K
Charge of propellant, m_{s_i}	0.172 kg

Propellant properties:

Density, ρ_s	1670 Kg/m^3
Initial web thickness, w_{s_i}	0.711 mm
Type:	M-10, single perforated

Gas properties:

Molecular weight, M	24
Ratio of specific heats, γ	1.252

Covolume, η	0.00095 m^3/kg.
Specific heat at constant pressure, c_p	0.412 kcal/kg-^oK
Viscosity (at 3000^oK), μ_{g_o}	0.00007 kg/m-sec
Thermal conductivity (at 3000^oK), κ_{g_o}	0.000034 kcal/m-sec-^oK

Tube material properties:

Thermal diffusivity, α_w	0.126 cm^2/sec
Thermal conductivity, κ_w	0.0138 kcal/m-sec-^oK
Initial tube temperature, T_{amb}	300^oK

The initial gas density ρ_{g_o} as calculated from equation (2.15) is 19.14 kg/m^3 and the potential of the propellant is:

$$W = \frac{R_g T_o}{(\gamma-1)} = 985.66 \text{ kcal/kg}$$

The burning rate versus pressure data for the propellant has been taken from reference [20] and is presented in Table I. Linear interpolation is used to determine the burning rate at the desired pressure. To ensure the convergence of the solution, a single iteration on the burning rate is performed in each time step as shown in the flow diagram in Appendix III.

For Case I, the solid particles are initially assumed to be evenly distributed in the chamber. But, in Case II, a specific initial distribution, namely a constant value up to the second nodal point from the piston and then linearly to zero at the piston base, is chosen to avoid the discontinuity at x equal to L_o. This has been shown in Figure 6.

TABLE I. PRESSURE VERSUS BURNING RATE DATA FOR THE PROPELLANT [20]

Pressure X 10^{-5} Newton/m^2	Burning rate, r_b m/sec
20.68	0.00330
34.46	0.00508
48.25	0.00711
68.93	0.00965
103.39	0.01320
137.86	0.01727
172.32	0.02057
206.78	0.02438
275.71	0.03048
344.64	0.03683
413.57	0.04369
551.43	0.05588
689.28	0.06858
1378.57	0.11684
2067.86	0.17018
2757.14	0.21082
3446.43	0.24384
4825.00	0.30988
6892.86	0.40132
13785.71	0.63500

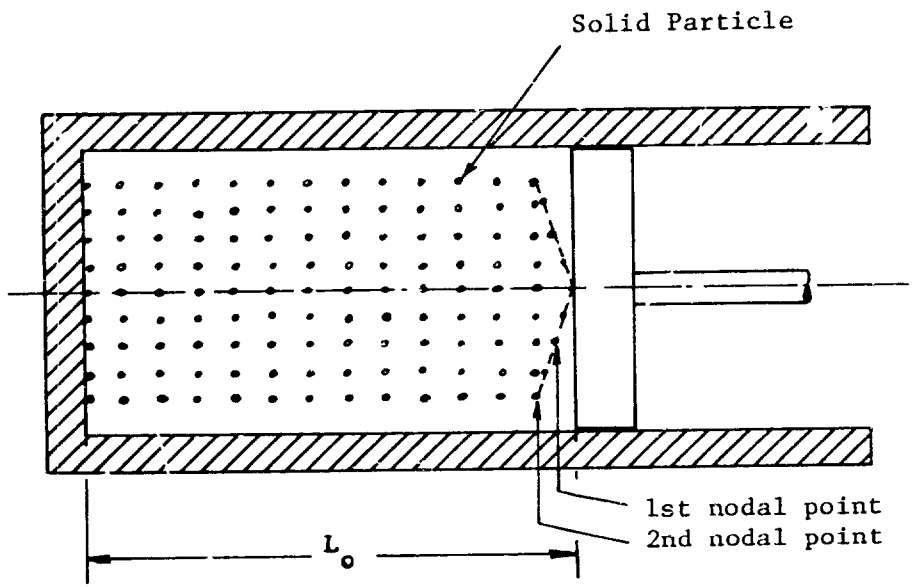

Figure 6. Assumed Initial Distribution of Solid Particles in Case II

The general power-law velocity profile, i.e. $\frac{u}{U_\infty} = (\frac{y}{\delta})^{\frac{1}{n}}$ yields the following relationships [21]:

$$\frac{\delta}{\delta^*} = n+1 \quad ; \qquad \frac{\delta}{\theta} = \frac{(n+1)(n+2)}{n} \tag{144}$$

and shape factor, $H = \frac{n+2}{n}$

The one-seventh profile has been used quite extensively in the past to compute the turbulent boundary layers with favorable pressure gradients [22, 23]. The same profile is assumed under the "standard conditions" and the corresponding value for the shape factor, i.e. 1.2857, is taken for the boundary layer computation.

The viscosity of the combustion gas is assumed to be proportional to the square root of the absolute temperature which implies that the value of m in (119) is 0.5. The same relation is assumed between the gas conductivity and its absolute temperature. These yield a constant value of 0.8482 for the Prandtl number of the gas.

One-Dimensional Solution

Case I. The results of the one-dimensional analysis have been presented in Figures 7 through 14. Comparison with the solution neglecting the heat transfer and skin friction shows insignificant effect of these phenomena on the ballistic properties of the piston-cylinder arrangement. But the following observations can be made from these results:

1) The Lagrange approximation of linear velocity distribution and constant gas density is not a good approximation of the real situation. It can be noted from Figure 10 that a considerable amount of time

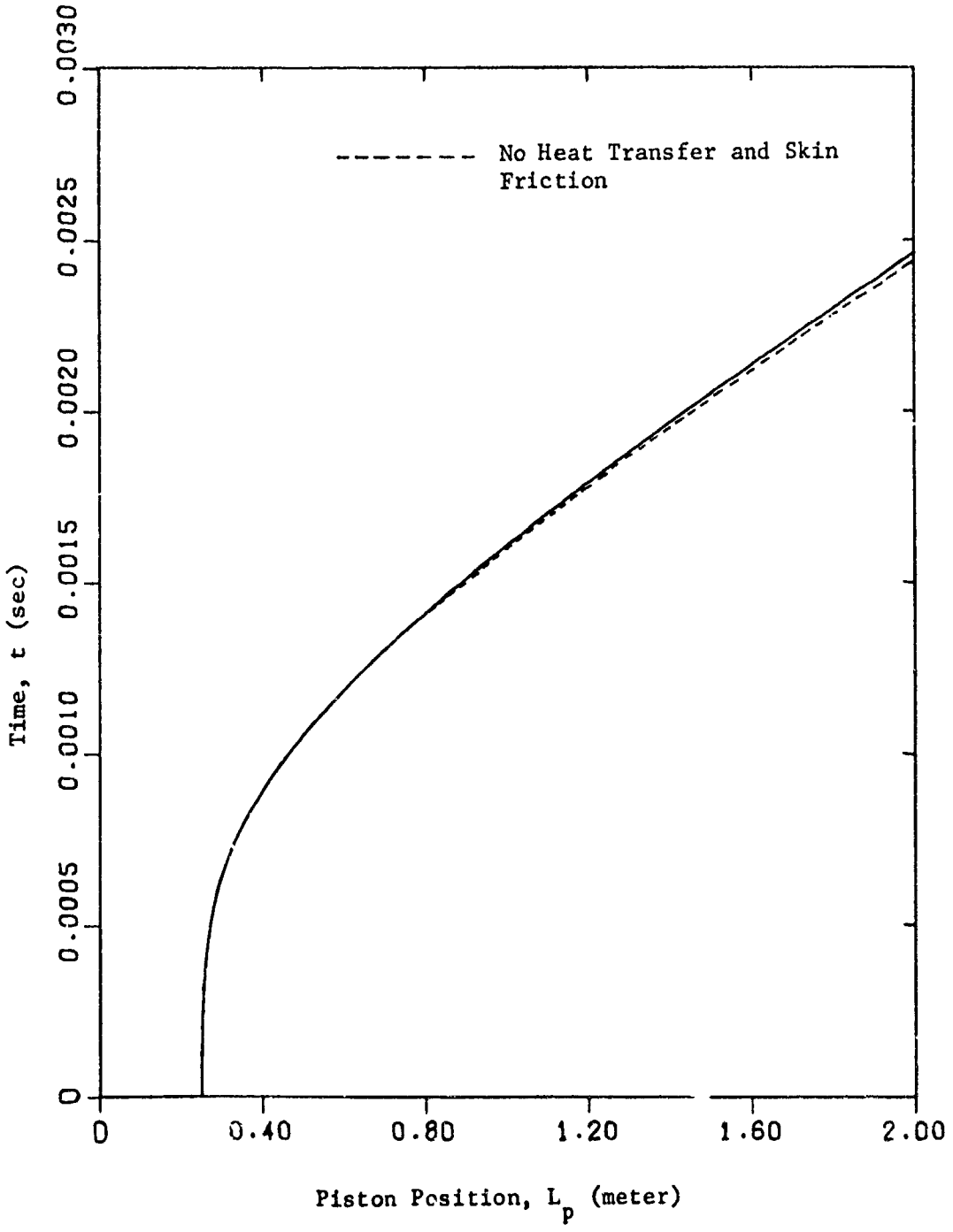

Figure 7. Piston Path for Case I.

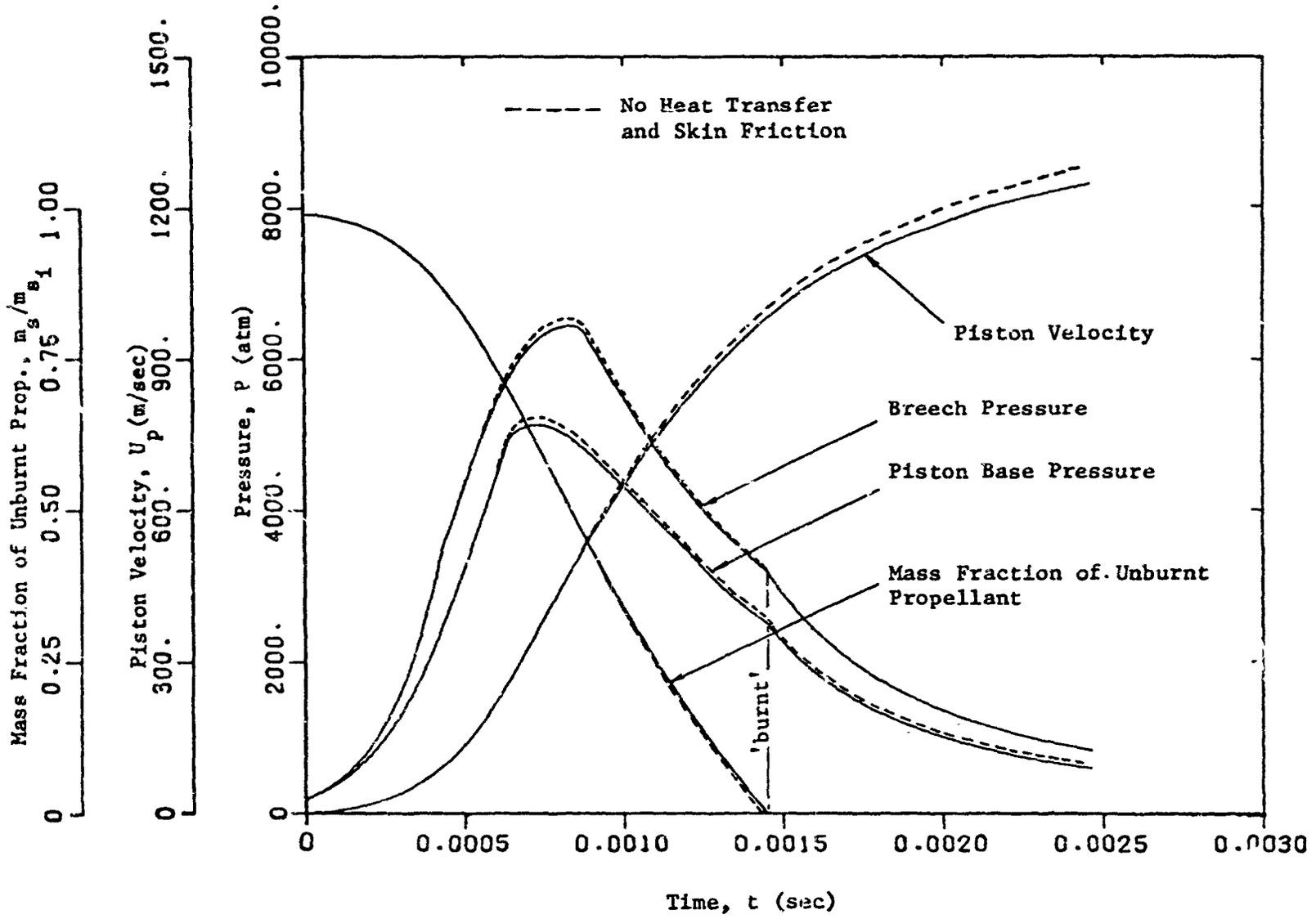

Figure 8. Variation of End Pressures, Piston Velocity and Mass Fraction of Solids with Time (Case I)

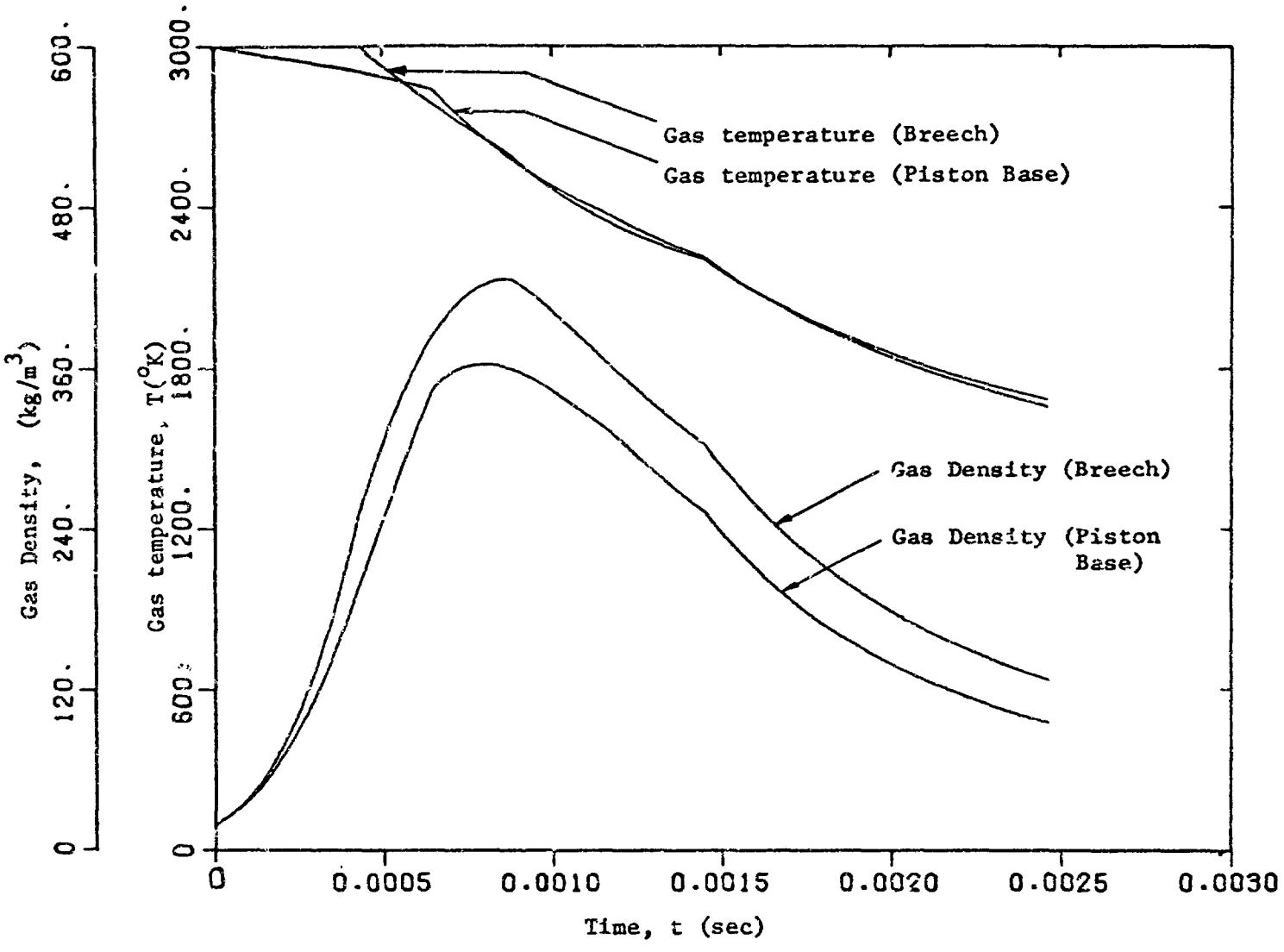

Figure 9. Variation of Gas Densities and Temperatures at the Breech and Piston Base End with Time (Case I)

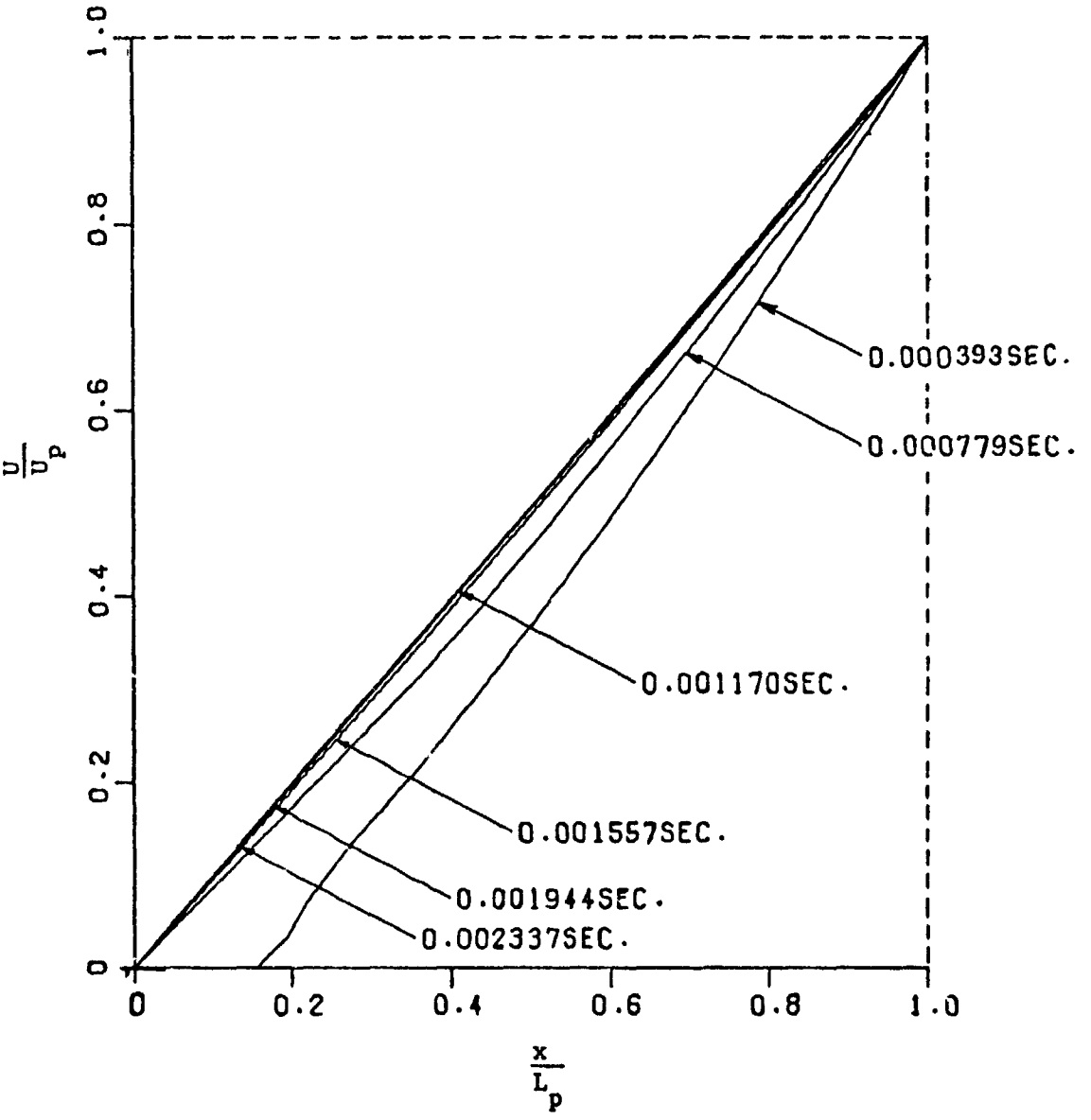

Figure 10. Spacewise Distribution of Velocity at Various Times (Case I)

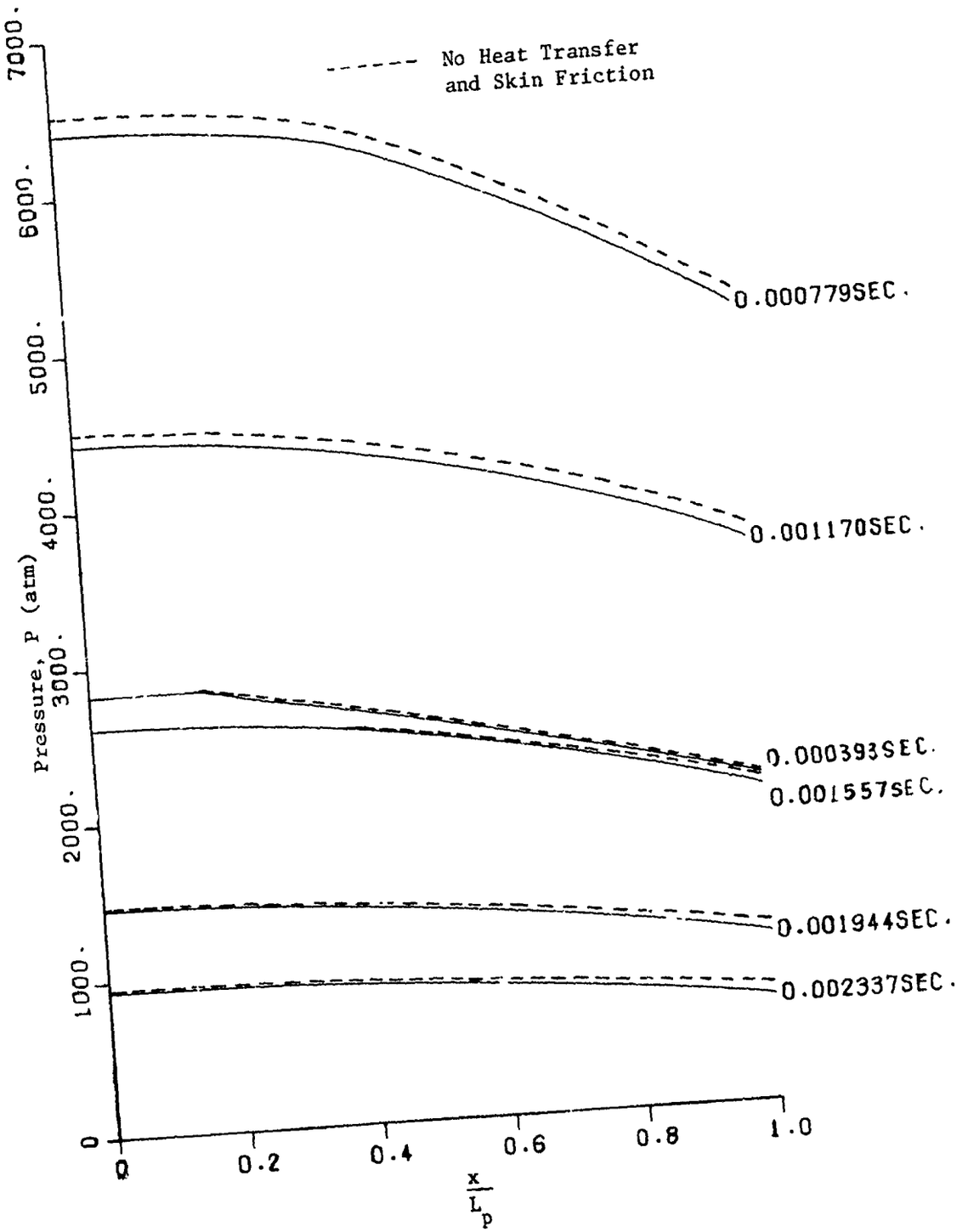

Figure 11. Spacewise Distribution of Pressure at Various Times (Case I)

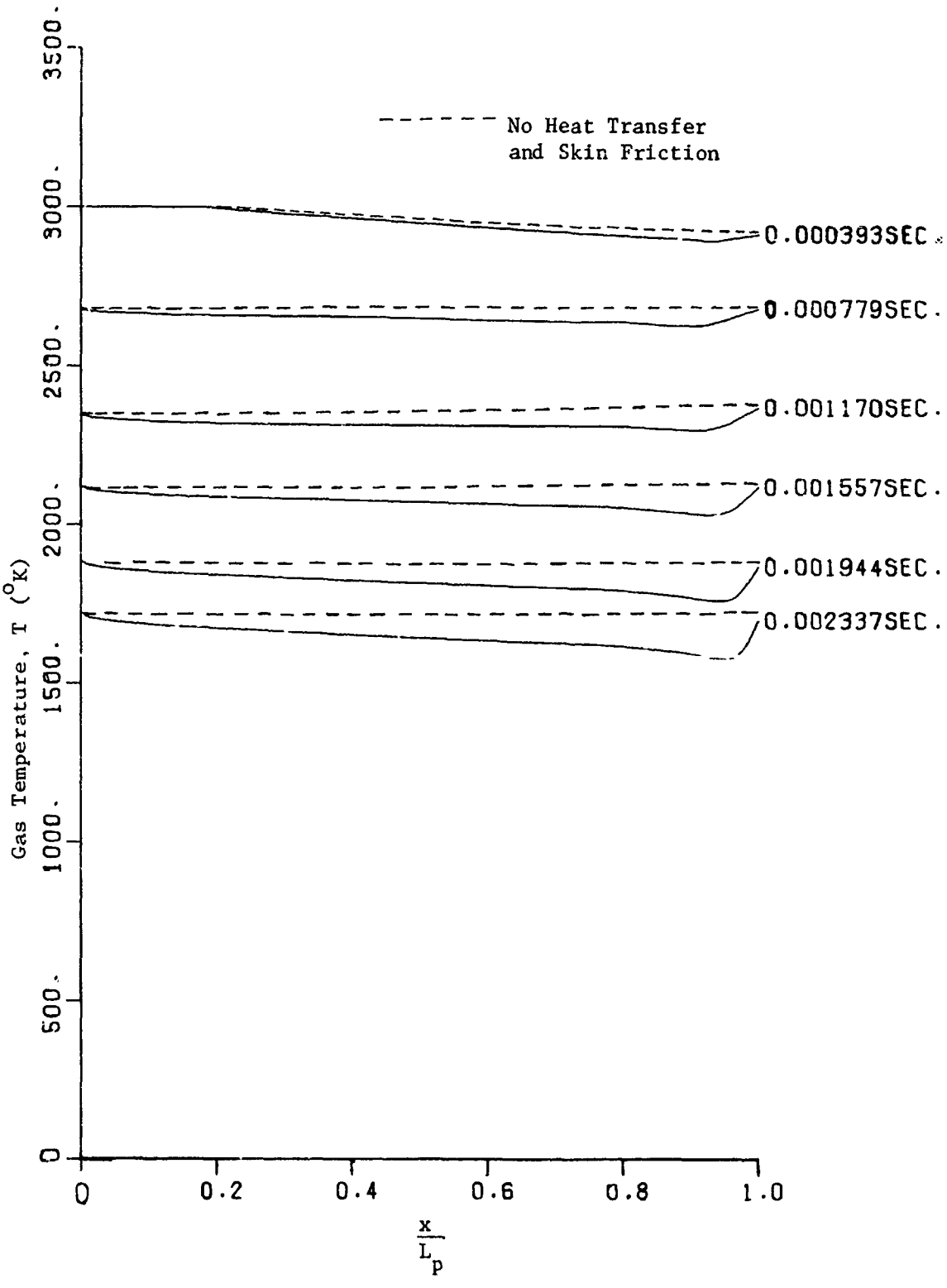

Figure 12. Spacewise Distribution of Gas Temperature at Various Times (Case I)

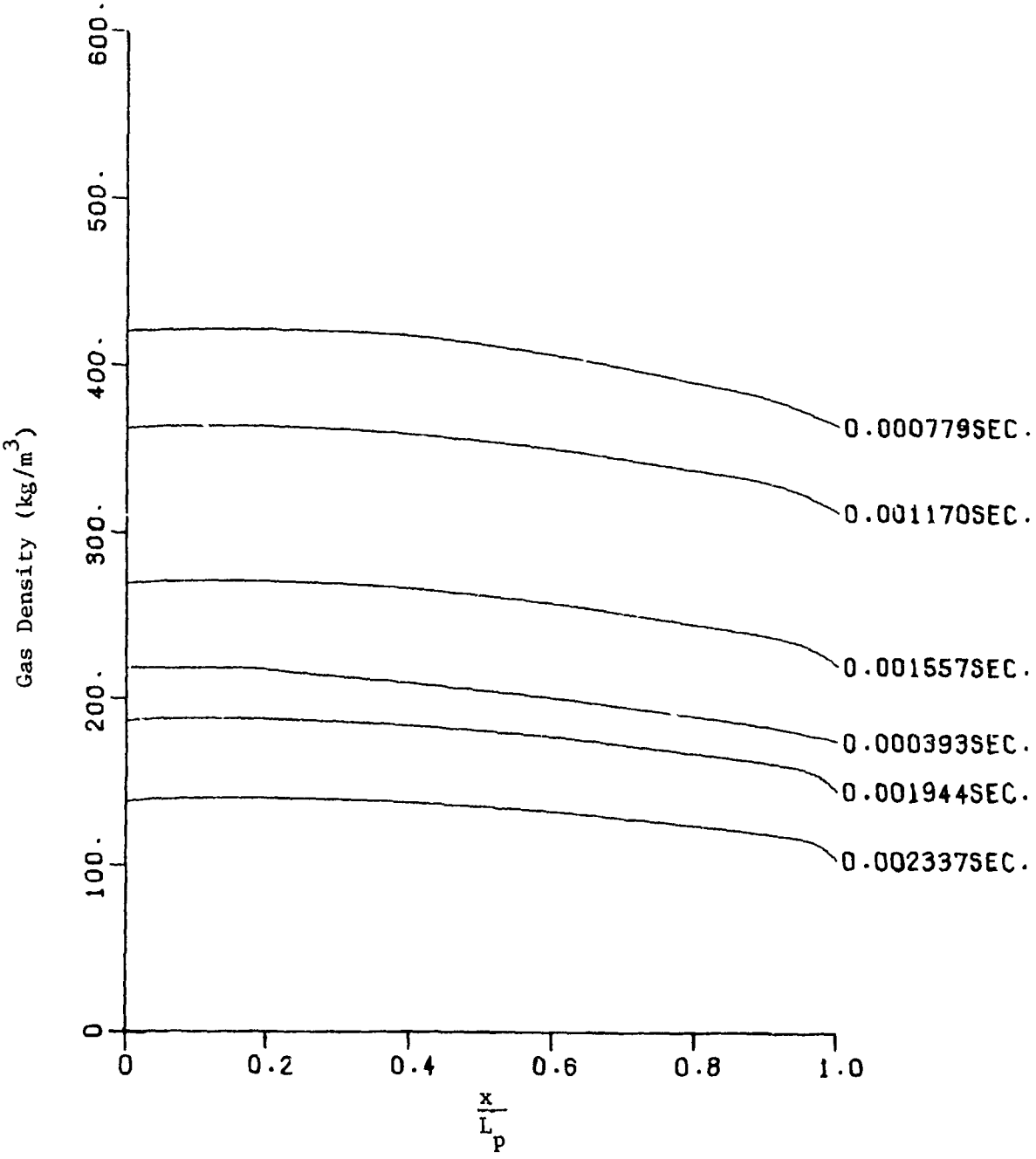

Figure 13. Spacewise Distribution of Gas Density at Various Times (Case I)

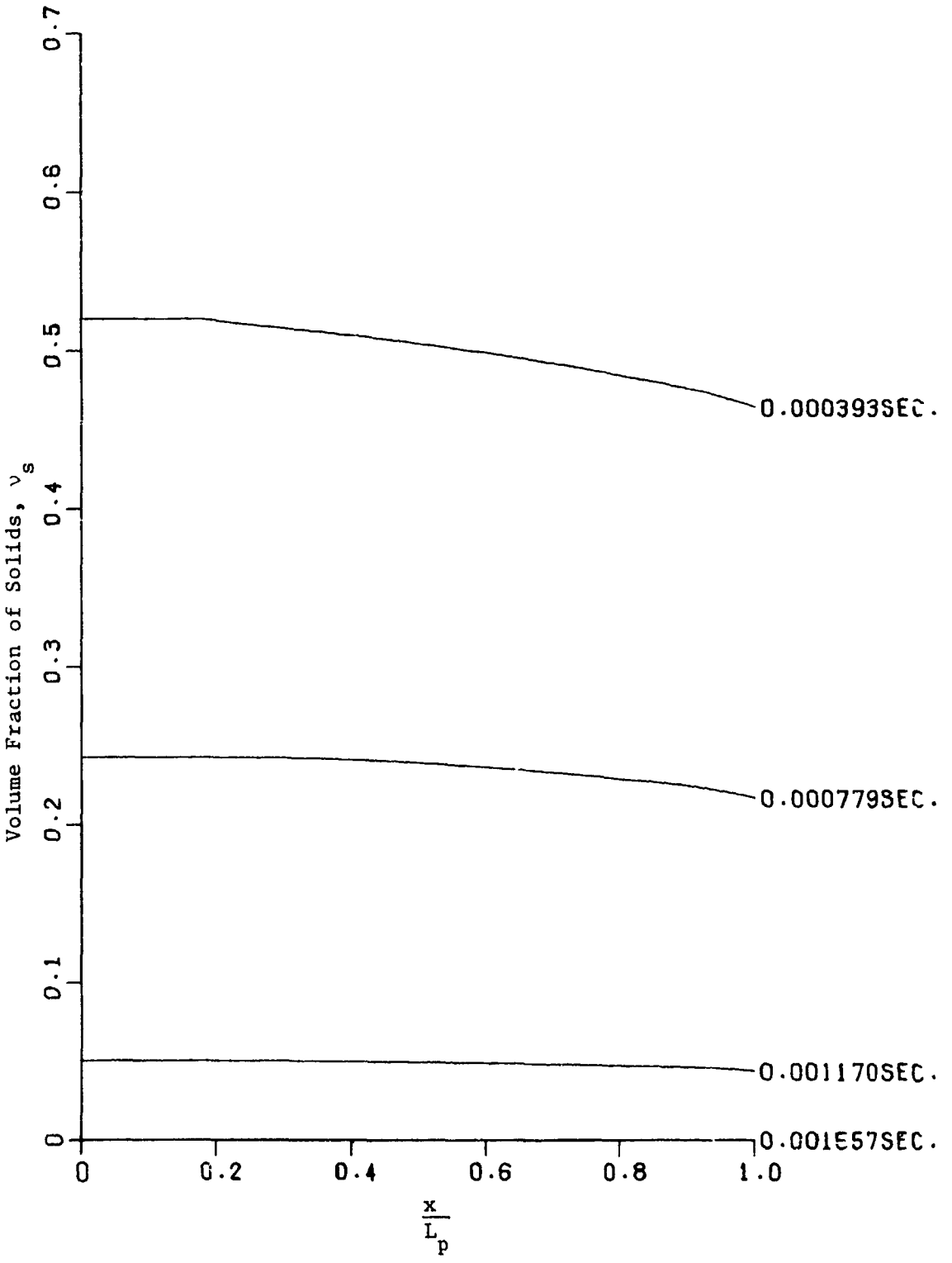

Figure 14. Spacewise Distribution of Volume Fraction of Solids at Various Times (Case I)

(approximately one-third of the total time) is elapsed before the velocity distribution along the length of the tube becomes linear. The gas density, on the other hand, has always a drooping characteristic from the breech end to the piston base end (Figure 9 and 13). The same characteristic is observed for the volume fraction of solids, ν_s (Figure 14).

(2) The gas pressure varies considerably along the length of the tube, and at the peak pressure, the difference between the pressures at the two ends is as high as 20 per cent of the breech pressure (Figures 8 and 11). The heat transfer to the tube wall reduces the pressure at all points, whereas the skin friction reduces the piston base pressure as the piston reaches the end of the tube. These two effects together reduce the final piston velocity to some extent.

(3) The gas temperatures at the breech and the piston base are of the same value all the time except for a short period in the beginning (Figure 9). There is, however, a sag in between the two end points due to the heat loss to the tube wall (Figure 12).

Case II. Similar results for Case II have been presented in Figures 15 through 21. A comparison with Case I reveals that the final values of piston velocity and total time of travel do not differ much from those in Case I. But the peak breech pressure can be 10 to 15 percent higher than the corresponding pressure in Case I. This causes the propellant to burn faster. The piston base pressure, however, remains very close to the corresponding pressure in Case I except for a short period towards the end. This accounts for the slight variation in the final piston velocity between the two cases.

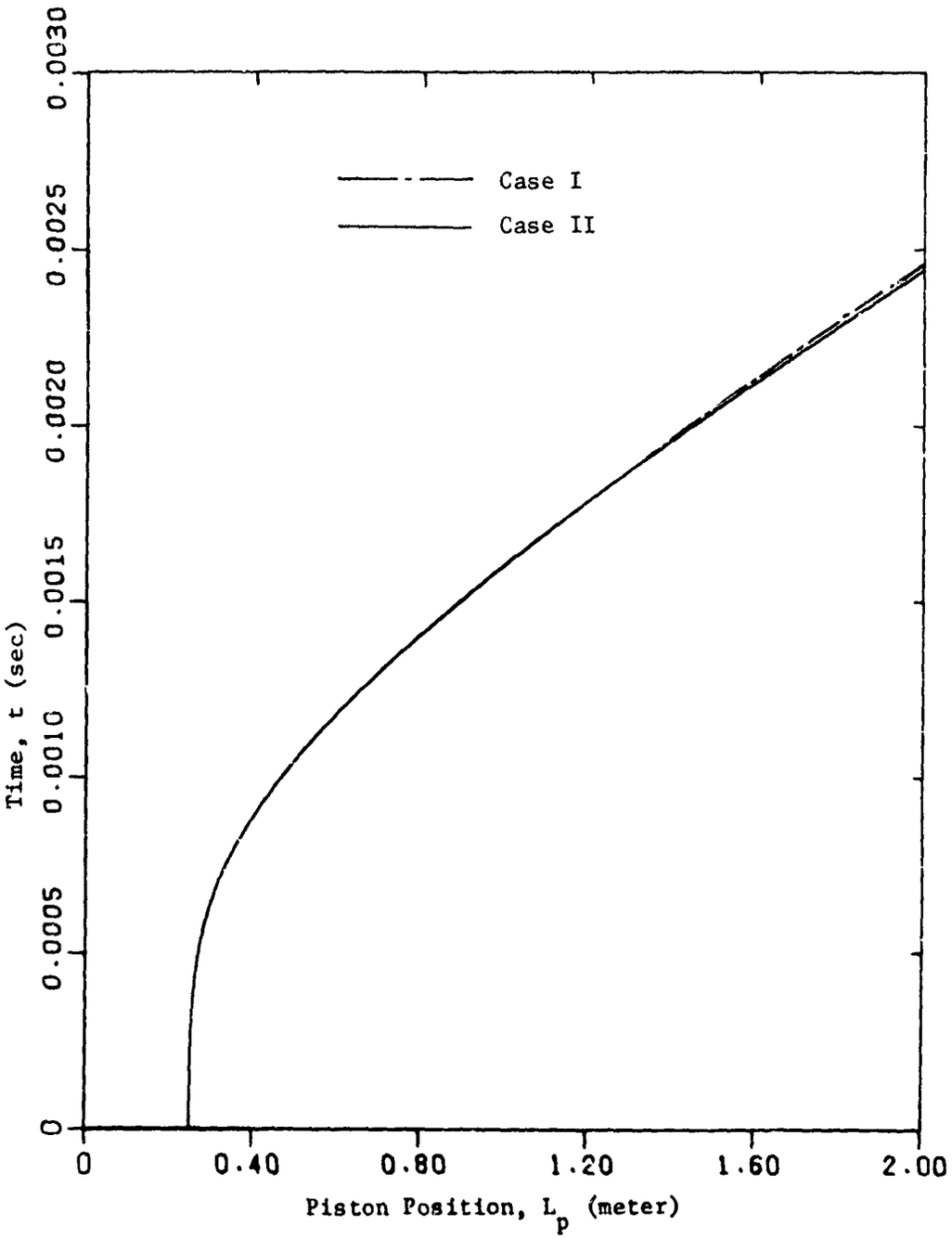

Figure 15. Comparison of Piston Paths in Case I and Case II

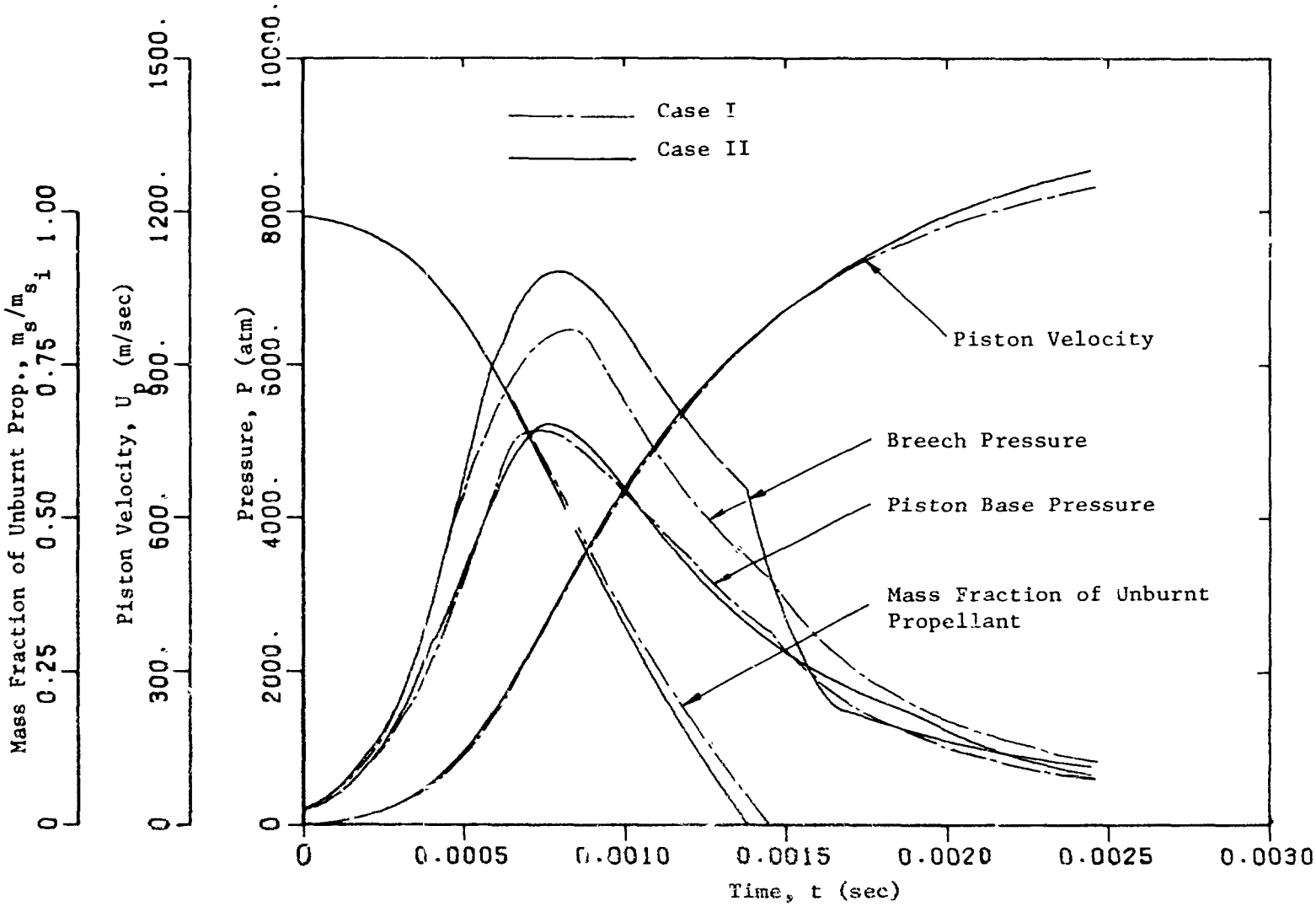

Figure 16. Comparison of End Pressures, Piston Velocities and Mass Fractions of Solids in Case I and Case II

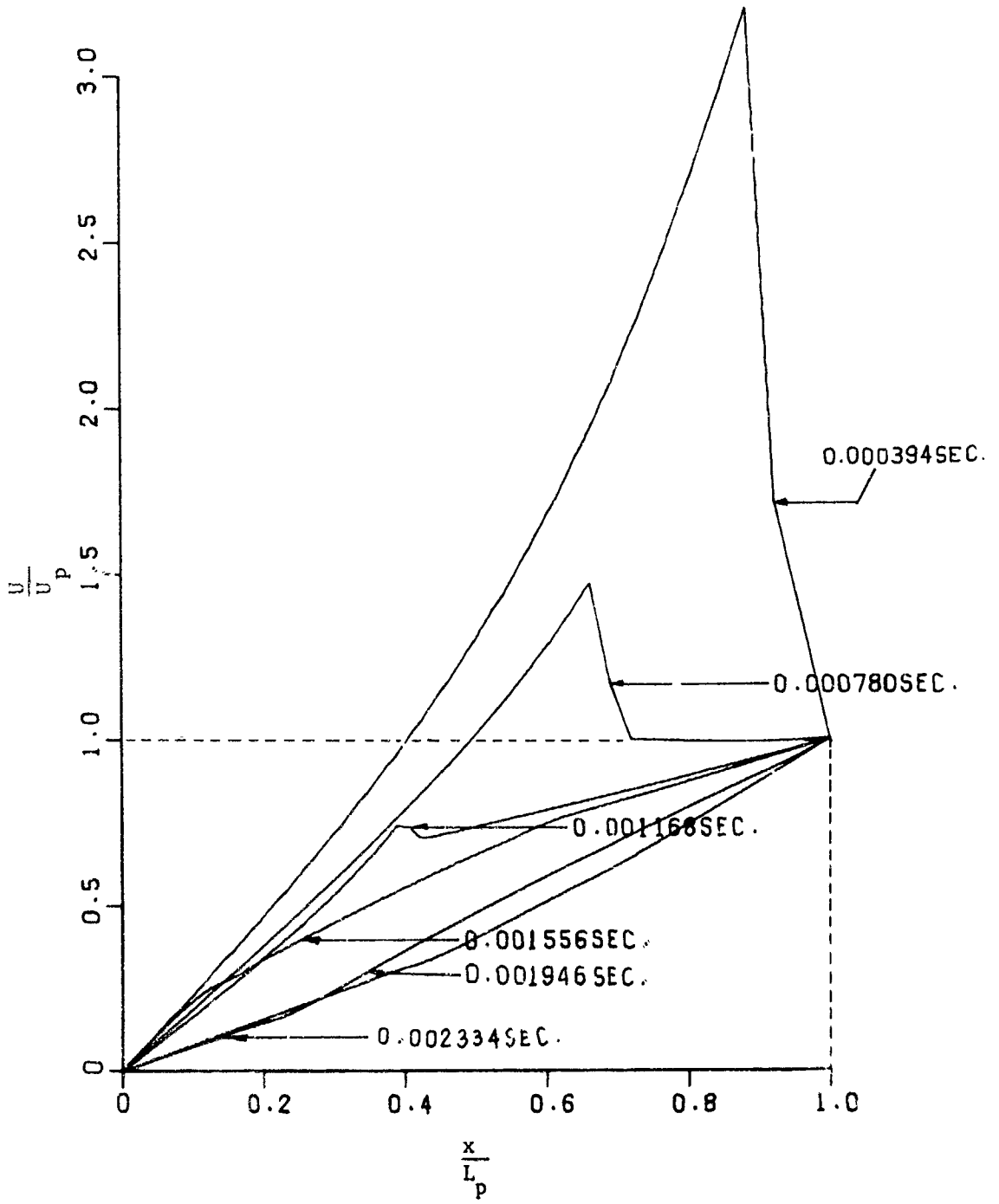

Figure 17. Spacewise Distribution of Gas Velocity at Various Times (Case II)

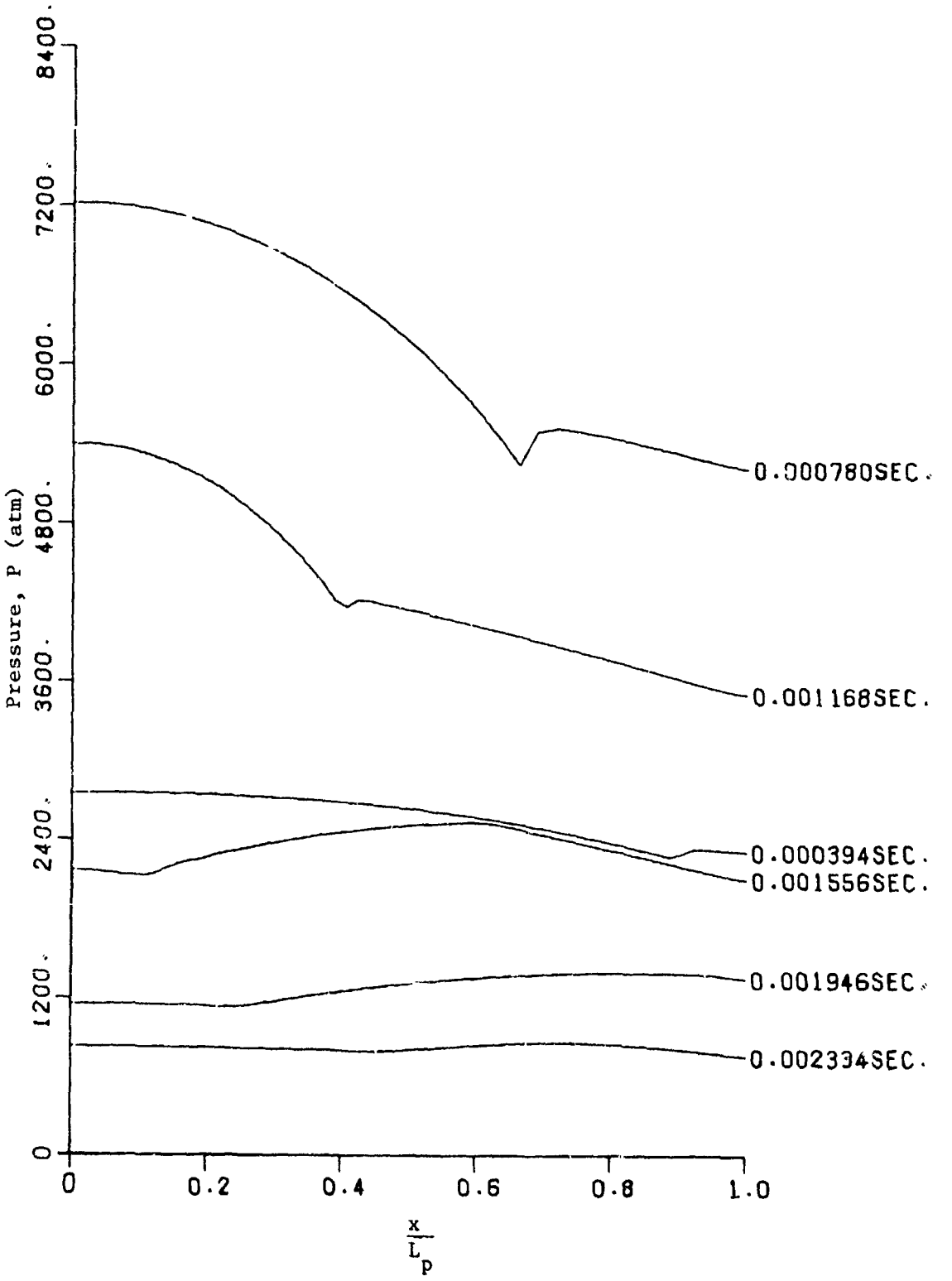

Figure 18. Spacewise Distribution of Pressure at Various Times (Case II)

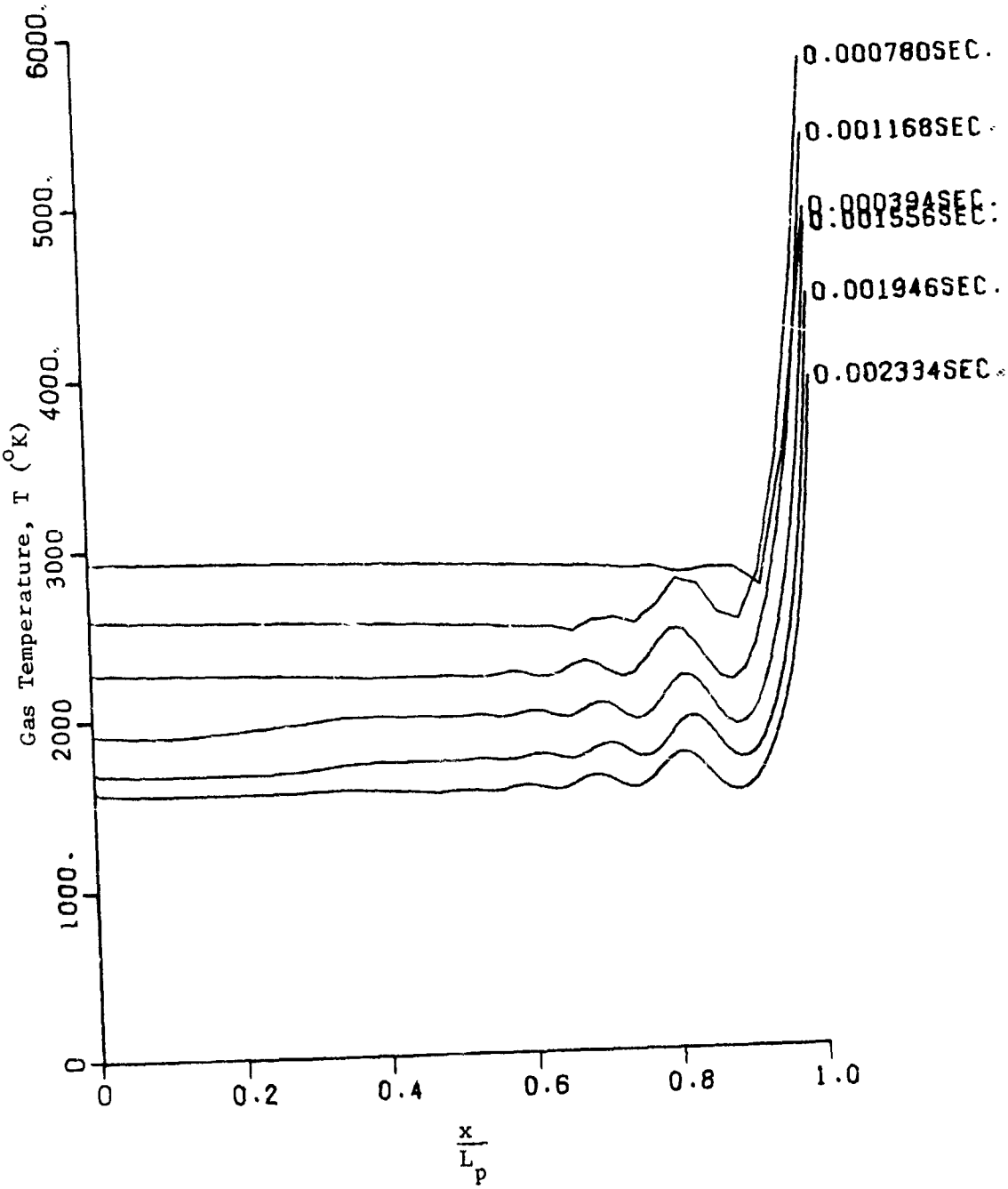

Figure 19. Spacewise Distribution of Gas Temperature at Various Times (Case II)

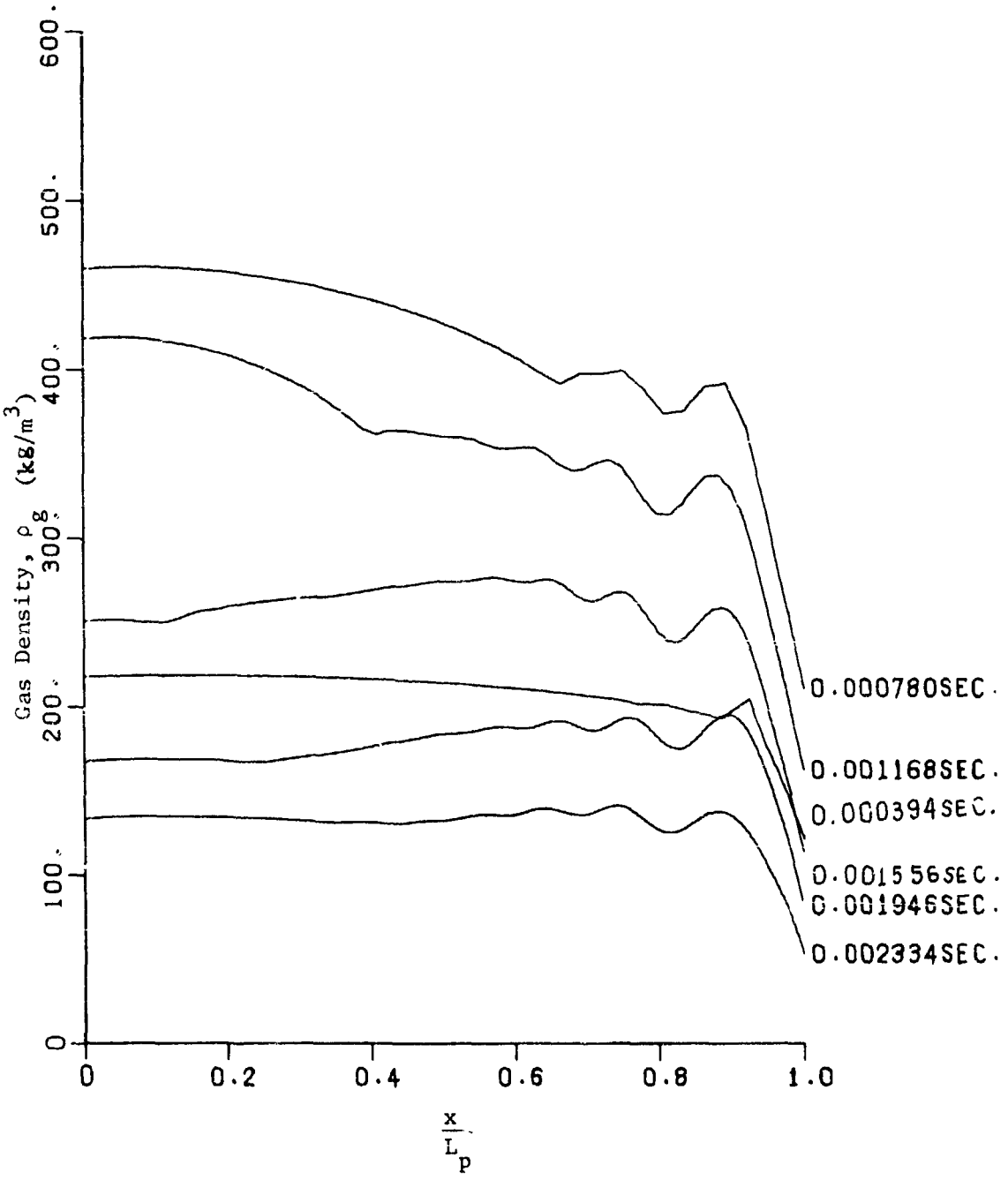

Figure 20. Spacewise Distribution of Gas Density at Various Times (Case II)

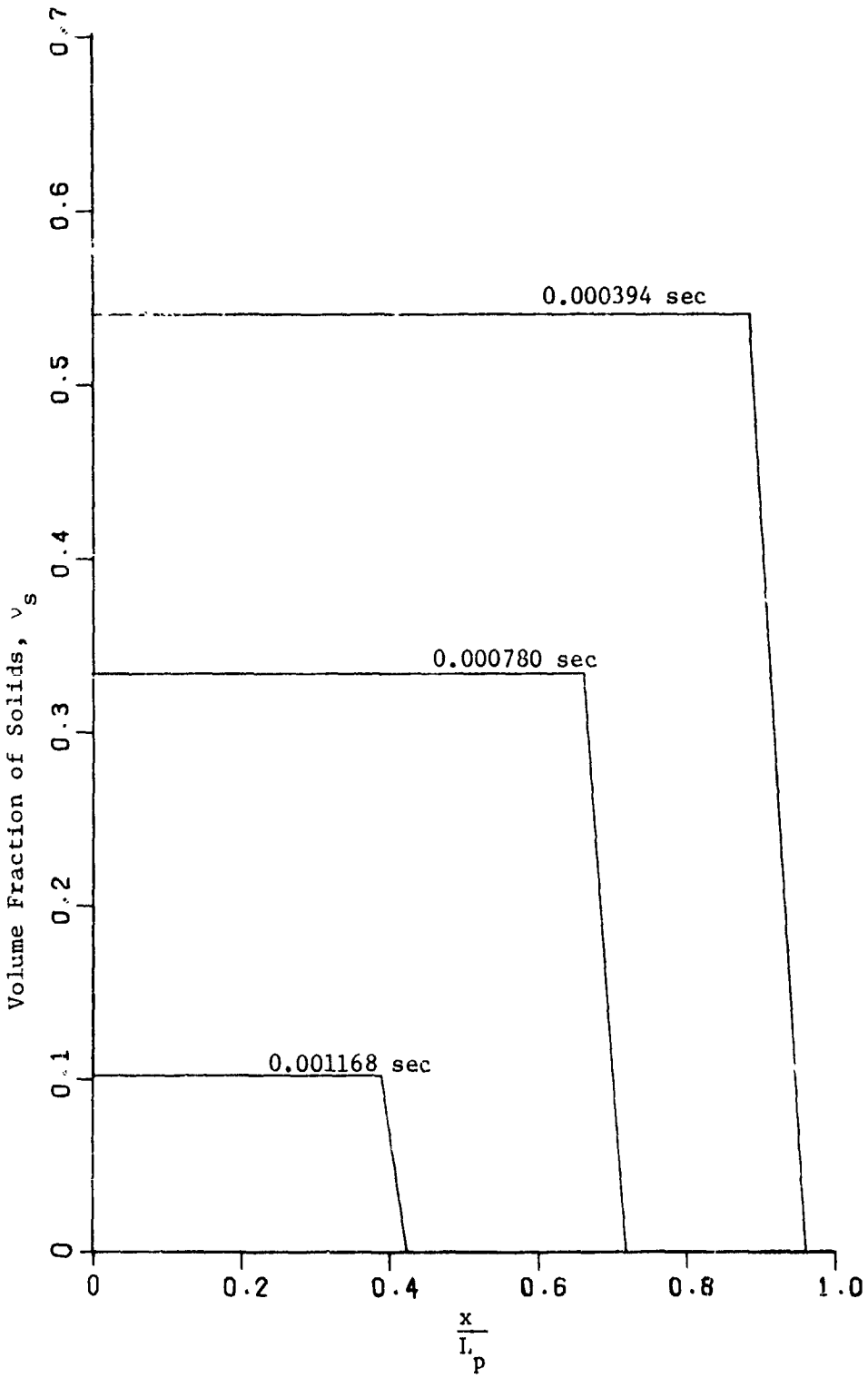

Figure 21. Spacewise Distribution of Volume Fraction of Solids at Various Times (Case II)

A couple of interesting phenomena are observed in this case of stationary solids:

(1) Just after the propellant is completely burnt, the breech pressure falls rapidly and finally becomes less than the piston base pressure. The same phenomenon was also observed by Carriere [5]. This happens because all the solid particles are assumed to stay near the breech end all the time, whereas there are no solids at the piston base. Therefore, when the solids are completely burnt, no sudden change in the pressure slope occurs at the piston base as it is observed at the breech.

(2) Due to the rapid change in the volume fraction of solids ν_s near x equal to L_o, a pressure difference sufficient to produce a local gas velocity higher than the piston velocity is created (Figure 17). The gas having higher velocity slams at the back of the piston and thus increases the temperature (Figure 19). This large temperature rise is confined within a thin layer at the piston base and does not affect the rest of the gas. The oscillations observed in Figures 19 and 20 are not due to the numerical instability, but are most probably due to the sudden area change near x equal to L_o.

Boundary Layer and Heat Transfer Solution

The results showing the boundary layer thickness, heat transfer coefficient, and the wall temperature for moving solids (i.e., Case I) are presented in Figures 22 through 27. As the time increases, the boundary layer thickness increases to a maximum value of approximately 20 percent of the tube radius when the piston reaches the end of the tube. This implies that the maximum value of the displacement thickness

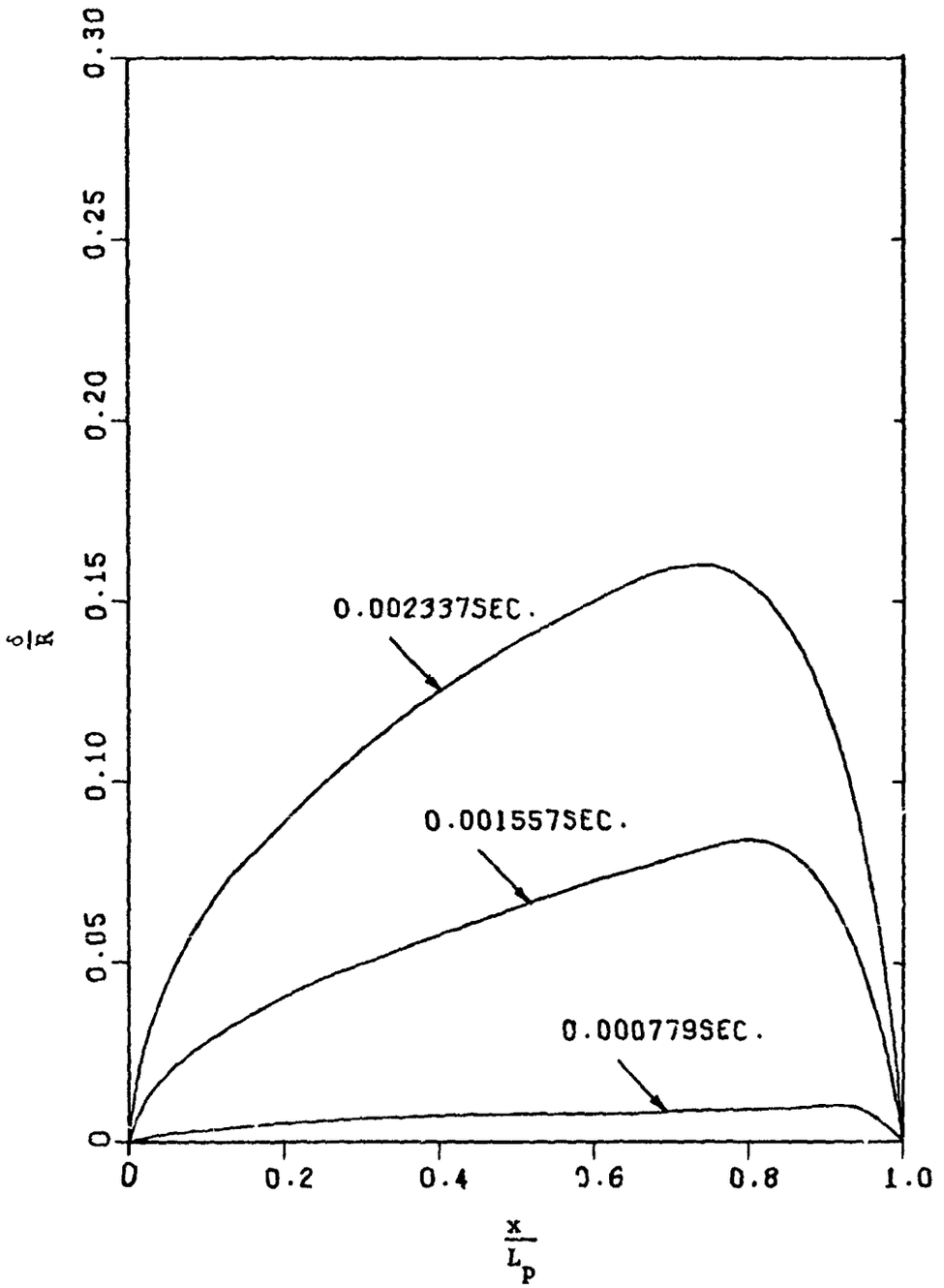

Figure 22. Boundary Layer Growth with Time (Case I)

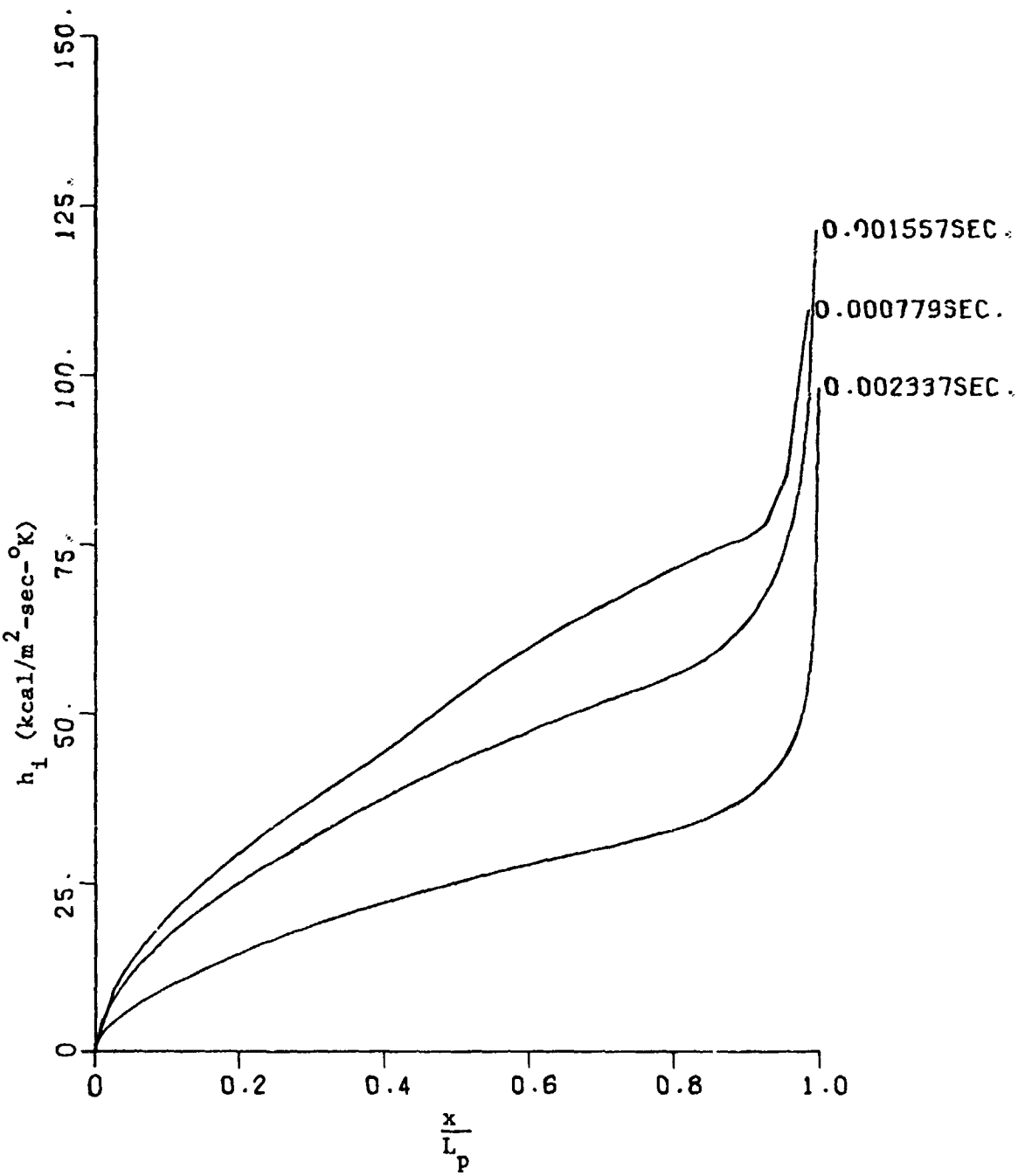

Figure 23. Spacewise Distribution of Heat Transfer Coefficient at Various Times (Case I)

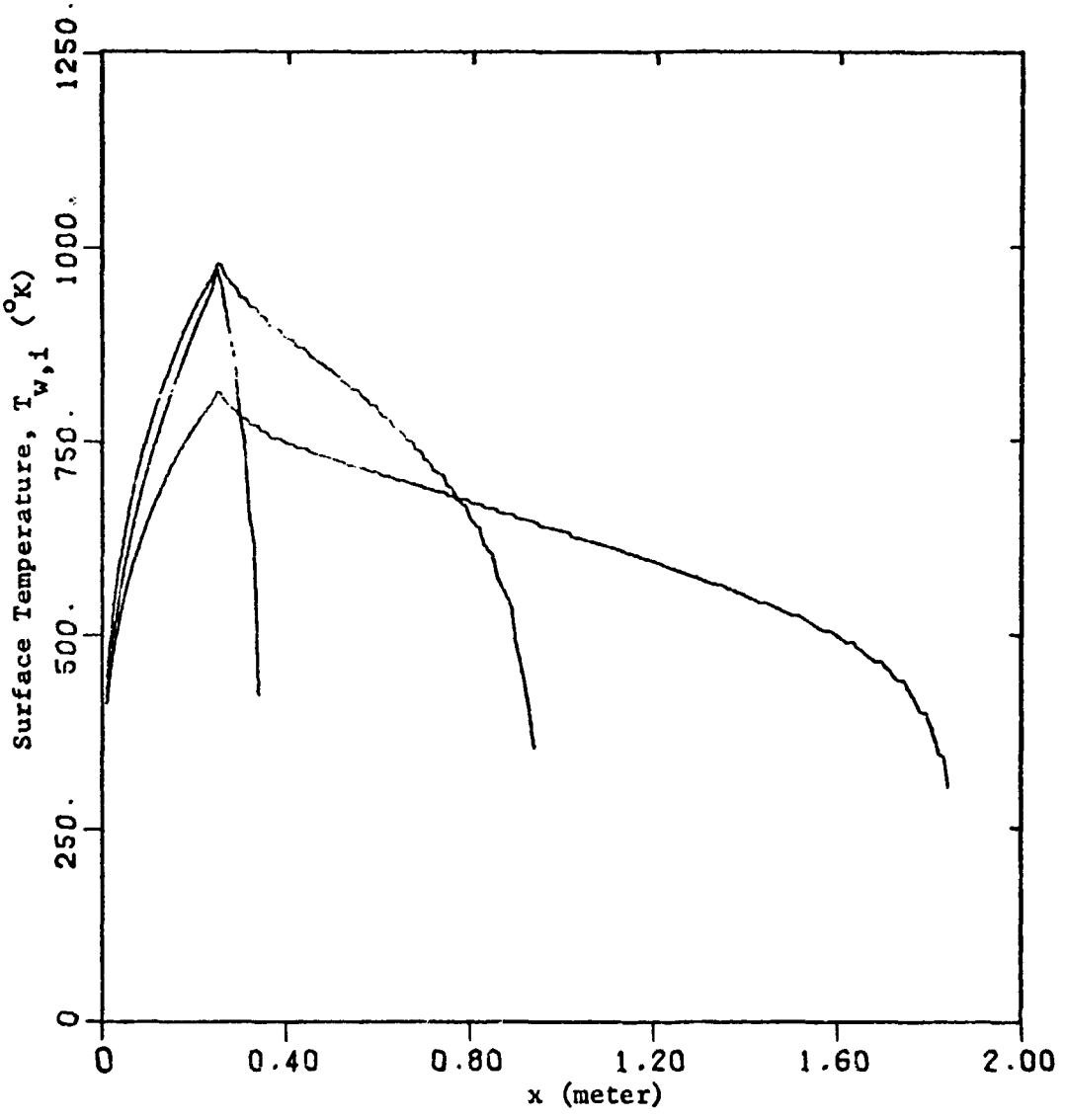

Figure 24. Spacewise Distribution of Wall Surface Temperature at Various Times (Case 1)

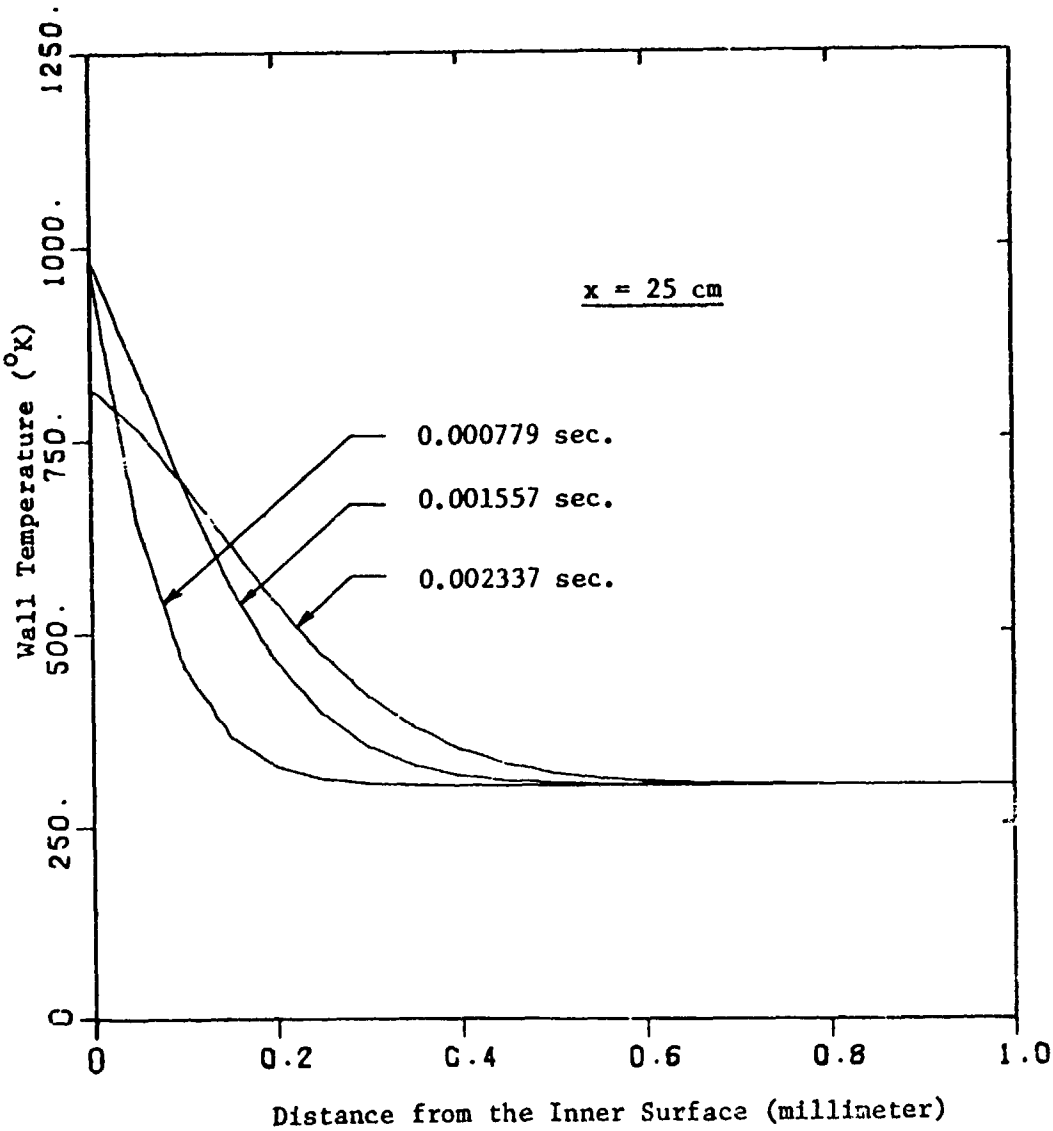

Figure 25. Variation of Wall Temperature at a Particular Position with Depth at Various Times (Case I)

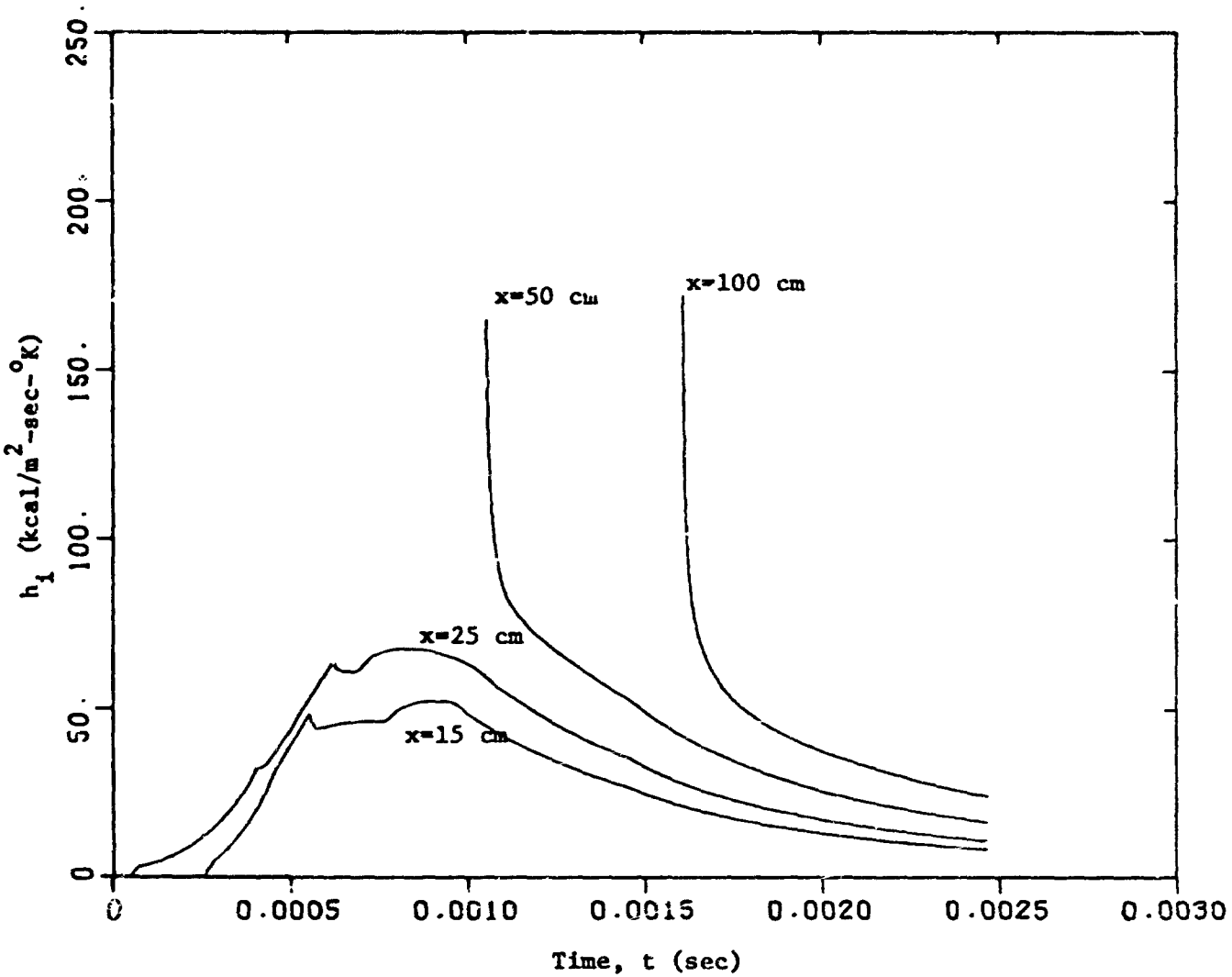

Figure 26. Variation of Heat Transfer Coefficients at Certain Fixed Locations with Time (Case I)

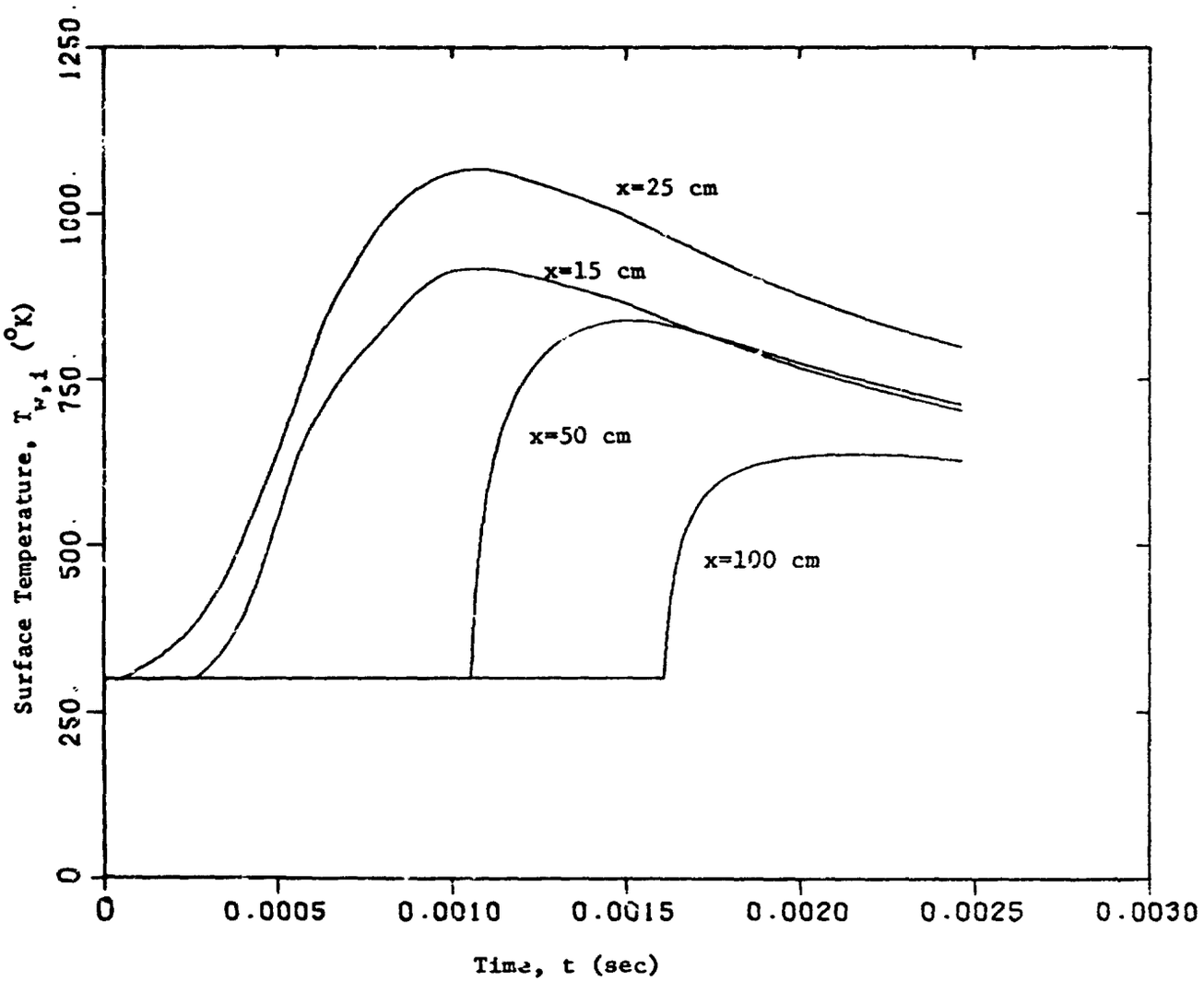

Figure 27. Variation of Wall Surface Temperatures at Certain Fixed Locations with Time (Case I)

is less than three percent of the tube radius and, therefore, the assumption of a thin boundary layer is valid.

The order of magnitude of the heat transfer coefficient is extremely high due to high gas density and velocity (Figures 23 and 26). The surface temperature of the tube wall reaches as high as $1100^{o}K$, and it occurs at the initial piston position (Figures 24 and 27). The total time is so short that in spite of a very steep radial temperature gradient and high thermal diffusivity of the tube material, the temperature wave cannot penetrate more than one millimeter into the tube wall (Figure 25). This justifies the exclusion of equation (140) from the computer program.

The heat flux, $h_i(T-T_{w,i})$ at certain fixed positions along the length of the tube are shown in Figure 28. Although the maximum value of heat flux could be as high as 350,000 $kcal/m^2$-sec, these types of fantastically high values last only for one or two microseconds. The average value of heat flux would be around 50,000 $kcal/m^2$-sec.

The same type of results was also obtained for Case II, and the total heat losses for both the cases are compared in Figure 29. It shows that the heat loss in Case II is about ten percent higher than that in Case I. This is mainly due to the higher gas velocity in the initial period of Case II. After this initial period, the heat transfer coefficients in the two cases are quite close.

The important results of both the cases are tabulated in Table II. A mass and energy balance detailed in Table III shows that the computation error is less than 0.5 per cent. The ballistic efficiency (i.e., the ratio of final kinetic energy of the piston and the propellant energy)

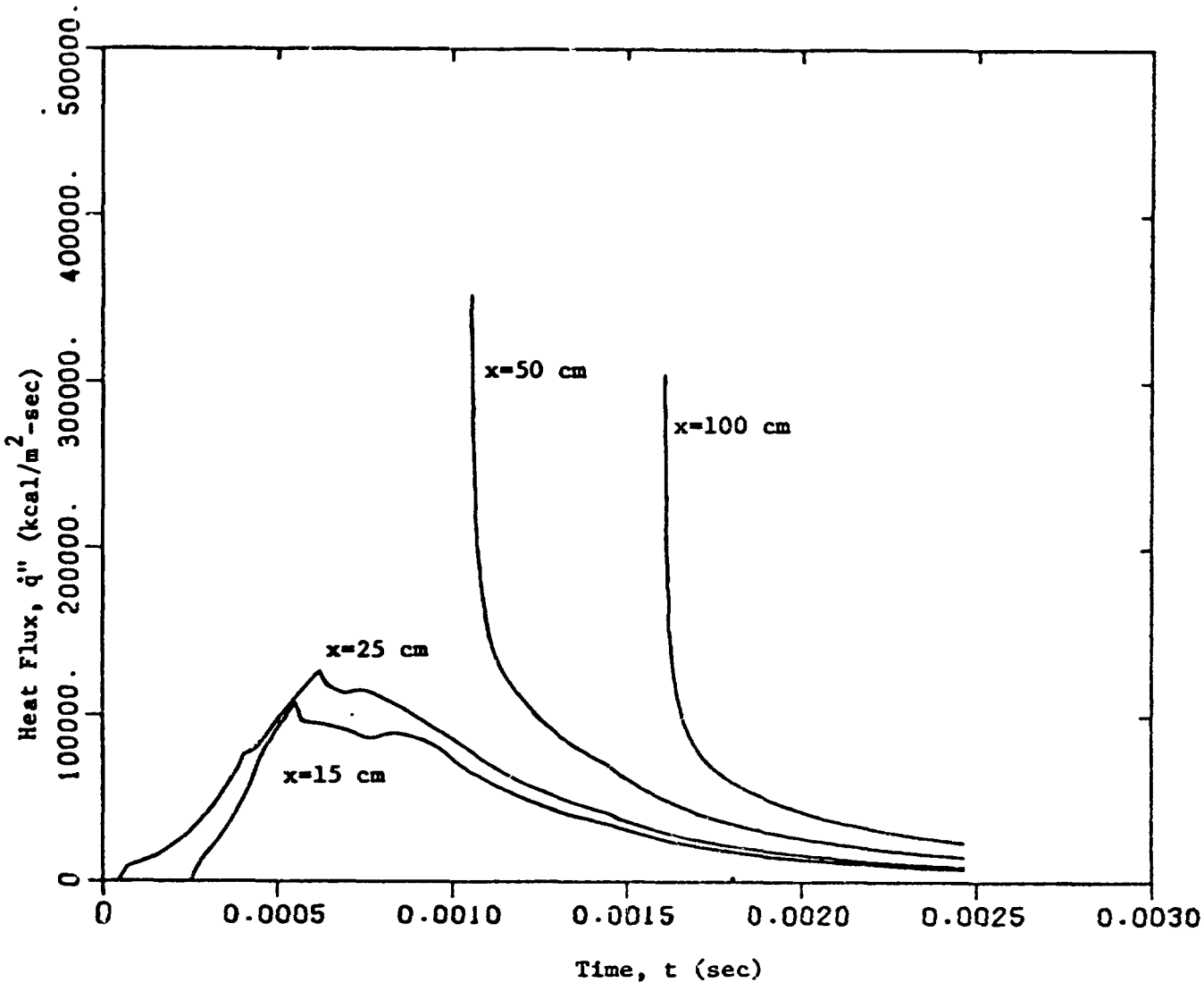

Figure 28. Variation of Heat Fluxes at Certain Fixed Locations with Time (Case I)

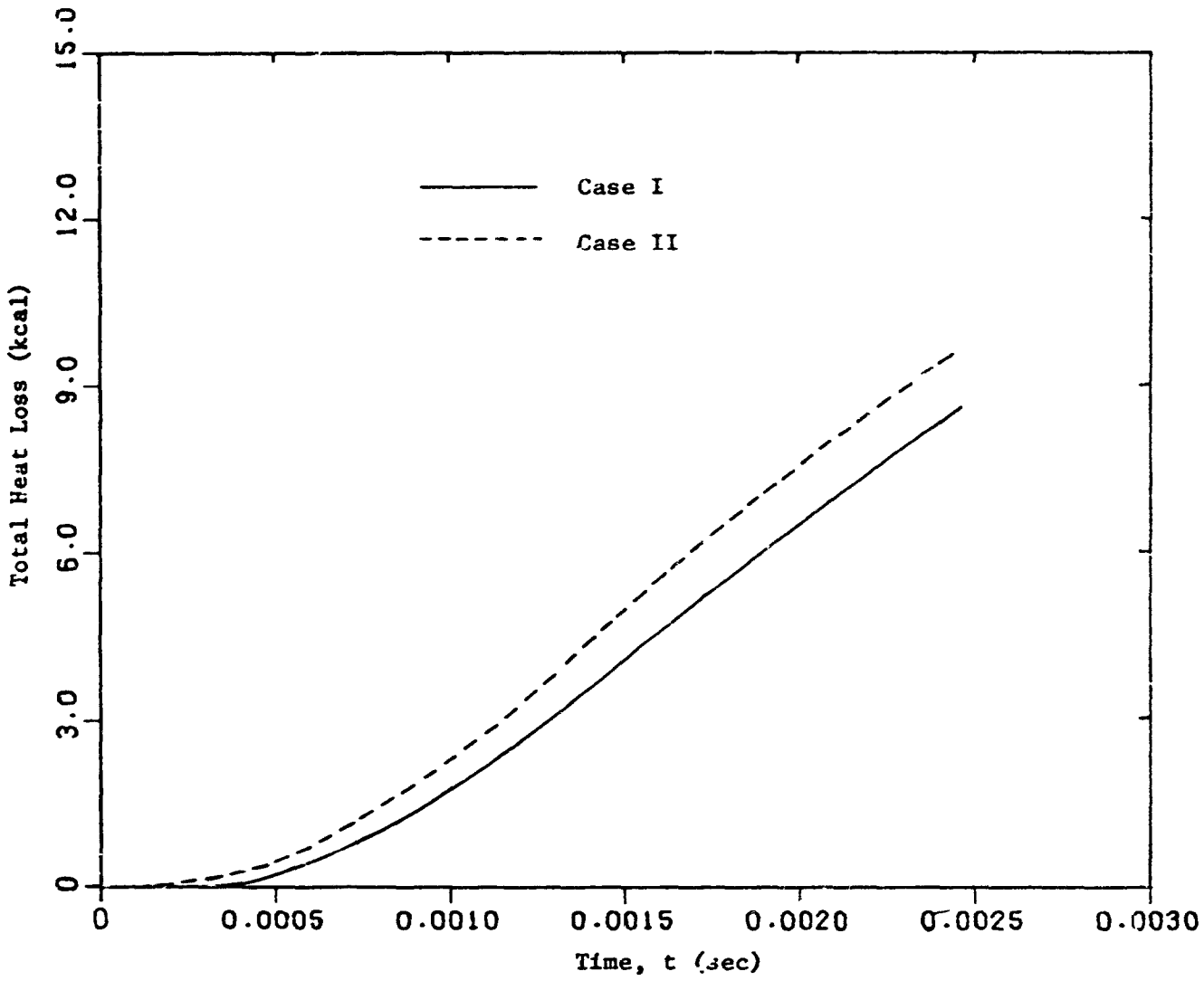

Figure 29. Comparison of Total Heat Losses to the Tube Wall in Case I and Case II

TABLE II. COMPARISON OF RESULTS FOR TWO LIMITING CASES OF SOLIDS VELOCITY

	Case I (solids moving)	Case II (solids stationary)
Time of travel (second)	0.002465	0.002448
Final piston velocity (m/sec)	1242.3	1271.3
Peak breech pressure (atmosphere)	6450	7200
Peak surface temperature (^{o}K)	1067	1270
Ballistic efficiency (%)	35.47	37.14
Total heat loss (kcal)	8.64	9.60
Heat loss in percentage of input energy (%)	5.10	5.66

TABLE III. MASS AND ENERGY BALANCE FOR CASE I and CASE II

	Case I	Case II
Initial Conditions:		
Propellant charge (kg)	0.172	0.172
Propellant energy (kcal)	169.53	169.53
Final Conditions:		
Total gas mass (kg)	0.1716	0.1713
Gas internal energy (kcal)	90.10	87.63
Gas kinetic energy (kcal)	9.90	8.56
Piston kinetic energy (kcal)	60.13	62.96
Heat loss (kcal)	8.64	9.60
Total energy (kcal)	168.77	168.75
Error in Mass Balance (%)	-0.233	-0.407
Error in Energy Balance (%)	-0.450	-0.460

has also been presented. The total heat loss to the tube wall is found to be five to six percent of the input energy and about 15 percent of the final piston kinetic energy.

Parameter Variation

Because of the large number of independent design parameters, no general correlation is attempted here. Only a few important parameters are varied for Case I to study their effect on the ballistic as well as heat transfer solution, and the important results are presented in Table IV.

Initial Chamber Pressure, P_o

The selection of initial chamber pressure, i.e., piston start pressure is quite arbitrary as it is very difficult in practice to determine the exact pressure at which the piston starts to move. Therefore, two different initial chamber pressures (100 atmosphere and 300 atmosphere) other than the standard 200 atmosphere are considered, and the solution neglecting the heat transfer and skin friction is presented in Figure 30. The peak breech pressure and the final piston velocity are very much the same for all the three cases of different piston start pressures. Only the time of travel is prolonged as the initial pressure decreases. It is obvious that the heat transfer solution would be very close for all the three initial pressures because of close ballistic properties. This implies that the piston start pressure has insignificant effect on the overall performance of the device.

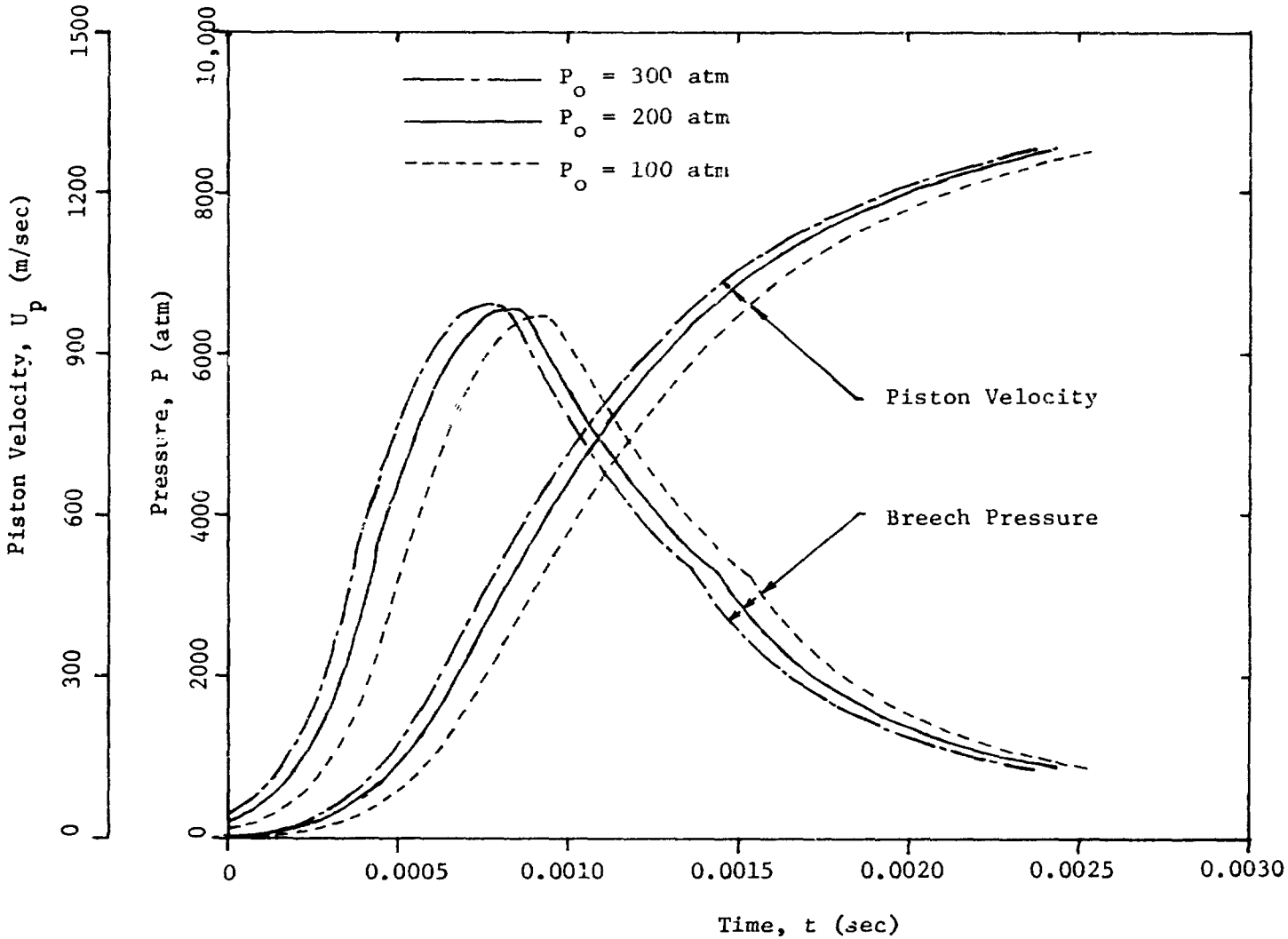

Figure 30. Variation of Breech Pressure and Piston Velocity with Time for Various Piston Start Pressures (Case I)

Profile Shape Factor, H

In this effort the profile shape factor, H, is assumed to be a constant throughout the entire solution; however, this may not be true in the real situation. For non-uniform steady flow, a favorable pressure gradient lowers the value of H [24] whereas in uniform steady flow an increase in flow Mach number increases H [13]. In the present case, however, it is difficult to predict its probable variation. Therefore, two different values of shape factor (1.4 and 1.2222), corresponding to the one-fifth and the one-ninth velocity profile, are taken and the results are compared with those for H equal to 1.2857. It is clear from Figure 31 that lower values of H cause higher values of boundary layer thickness and heat transfer coefficient, i.e. the viscous effect of the fluid is higher. Because of this, the total heat loss to the tube wall and the peak inner surface temperature go up as the shape factor decreases. However, at H equal to 1.2222, these values do not exceed the corresponding values for the standard conditions by more than ten percent. The total heat losses to the tube wall for the three different values of shape factor are compared in Figure 32.

Tube Inside Diameter, D

The tube inside diameter is varied keeping the loading density (m_{s_i}/V_o), and the piston mass per unit area (M_p/A_p) constant. Two tube diameters (2cm and 4cm) are selected with appropriate propellant charge m_{s_i} and piston mass M_p. The results are shown in Figure 33. It can be noted from Table IV that, although an increase in tube diameter means an increase in the total heat loss, the heat loss per unit input energy decreases with larger tube diameter. This is due to decrease in

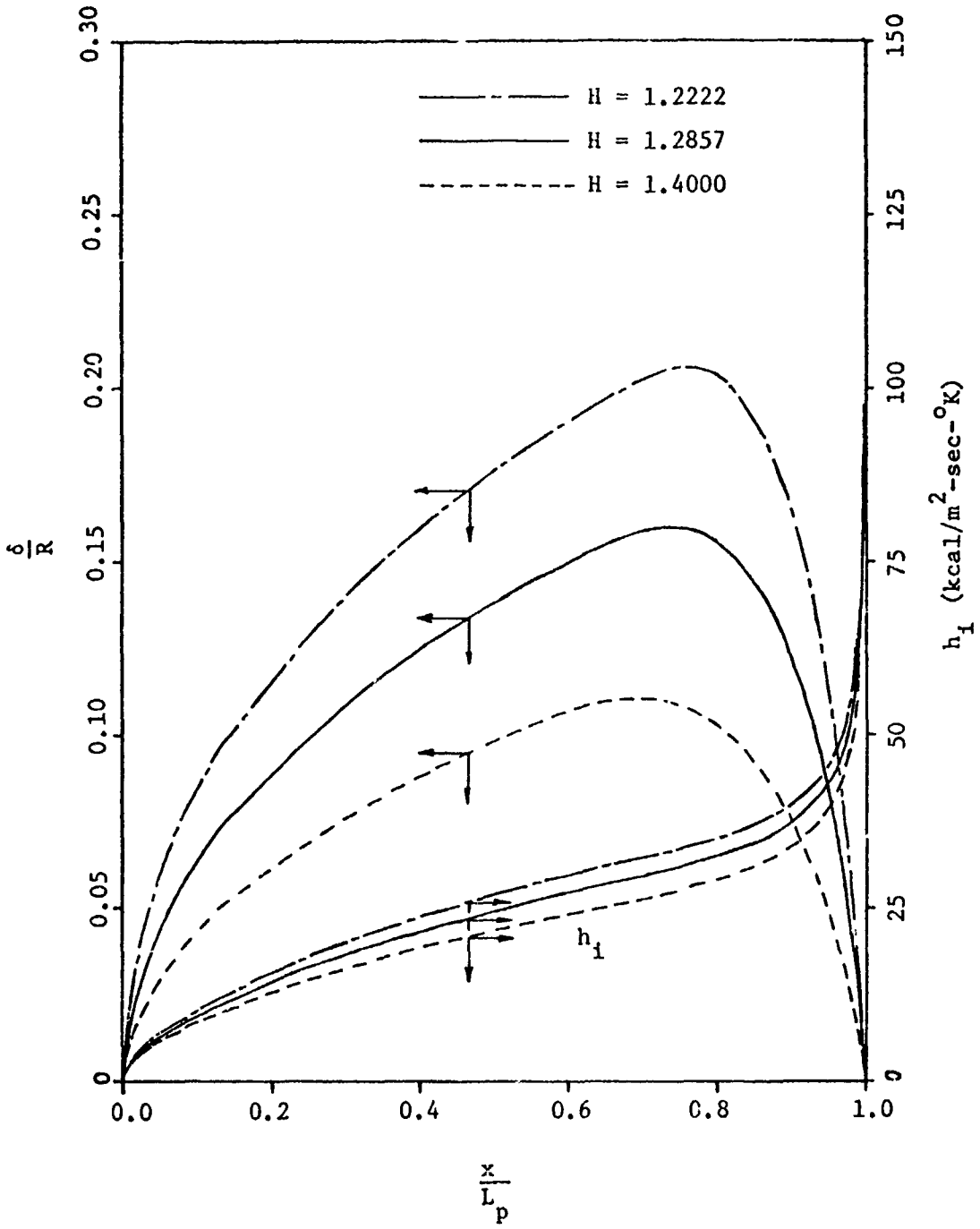

Figure 31. Comparison of Boundary Layer Thickness and Heat Transfer Coefficient for Various Profile Shape Factors at 0.002337 sec (Case I)

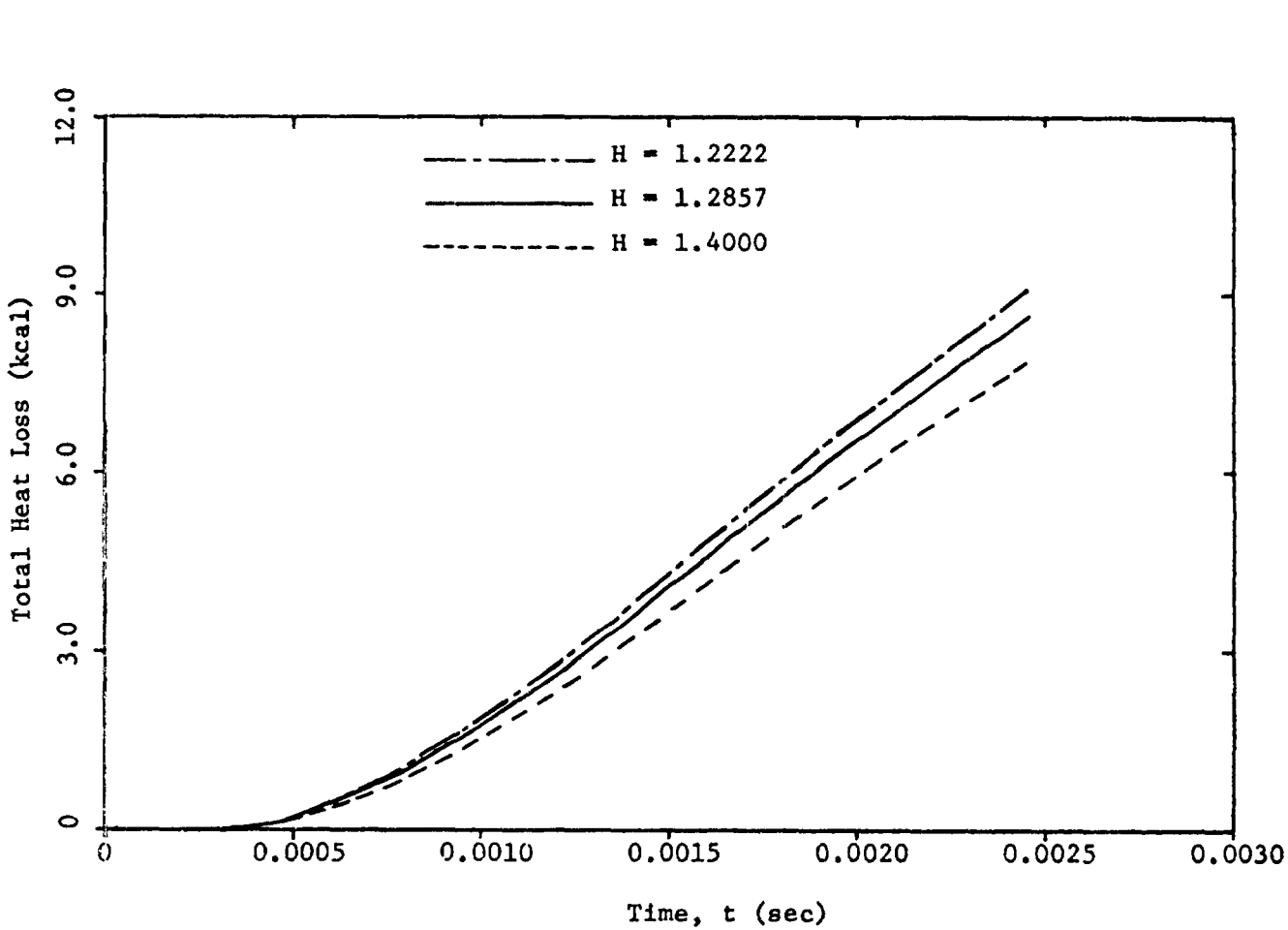

Figure 32. Comparison of Total Heat Loss to the Tube Wall for Various Profile Shape Factors (Case I)

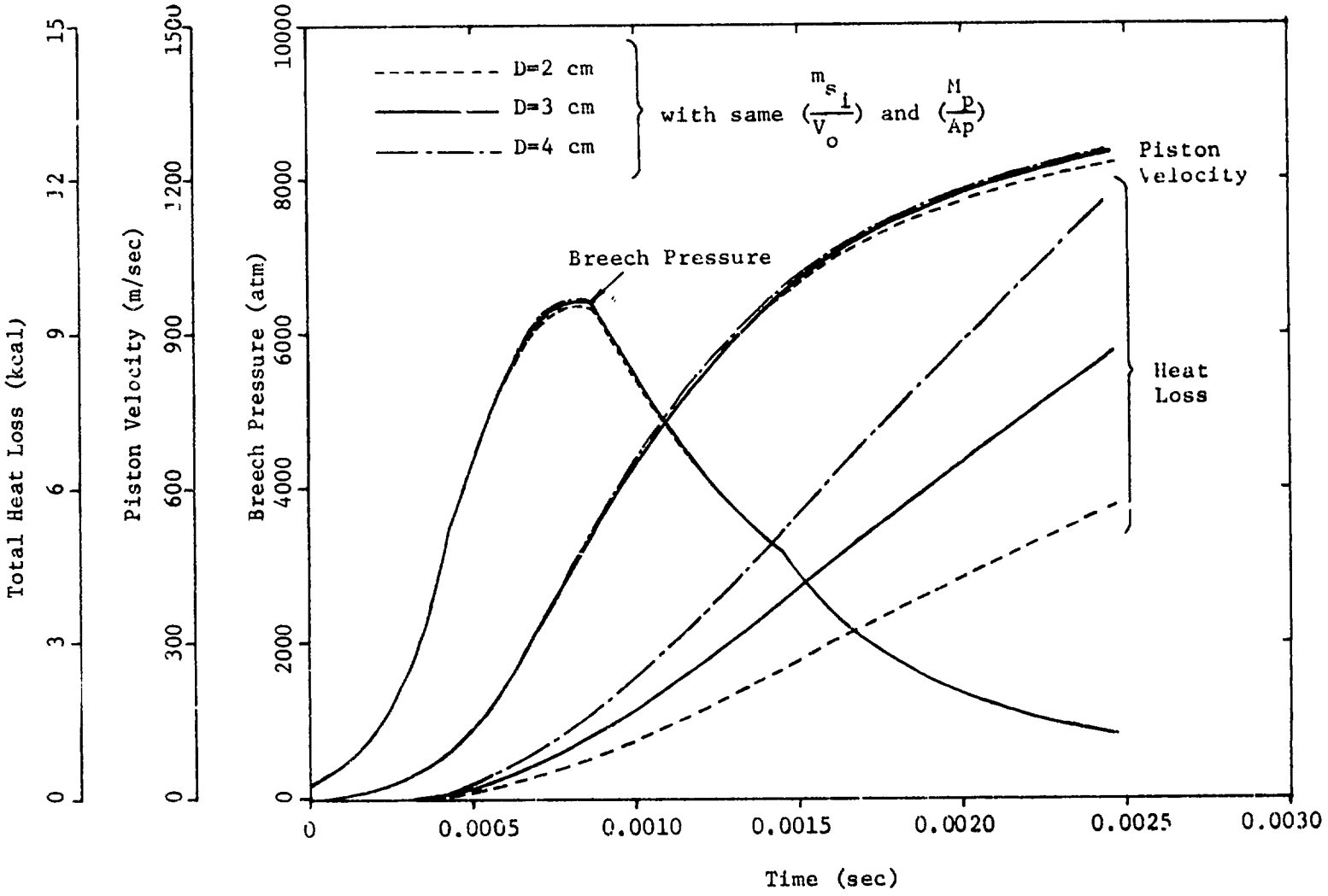

Figure 33. Comparison of Breech Pressure, Piston Velocity, and Total Heat Loss to the Tube Wall for Various Tube Diameters with Same Loading Density and Same Piston Mass per Unit Area (Case I)

the surface to volume ratio. In other words, for ballistically similar devices, the increase in tube diameter reduces the heat loss per unit mass of gas and this accounts for the slightly better ballistic results obtained for the 4-cm-diameter tube.

Propellant Charge, m_{s_i}

Two different values of the propellant charge (0.15 kg and 0.19 kg) are chosen apart from the standard value of 0.172 kg, and the results are presented in Figure 34. It is obvious that an increase in propellant charge improves the ballastic efficiency of the device. At the same time this increases the peak pressure, heat transfer coefficient, and the peak surface temperature which put a limit on the propellant charge.

Piston Mass, M_p

Piston mass plays an important role in the problem of internal ballistics. Therefore, besides the standard mass of 0.326 kg, two other pistons having masses equal to 0.2 kg and 0.5 kg are considered. The results are shown in Figure 35. The heavier the piston, the slower it moves, thereby leaving less room for the combustion gas to expand which causes an increase in the peak pressure. Although the heavier piston moves slower, the ballistic efficiency of the device is improved and therefore suitable for the application where energy conversion is of prime interest. If higher velocity is desired, a lighter piston would be chosen. The surface temperature is also lower in the case of a lighter piston due to lower pressures which lead to lower heat transfer coefficients.

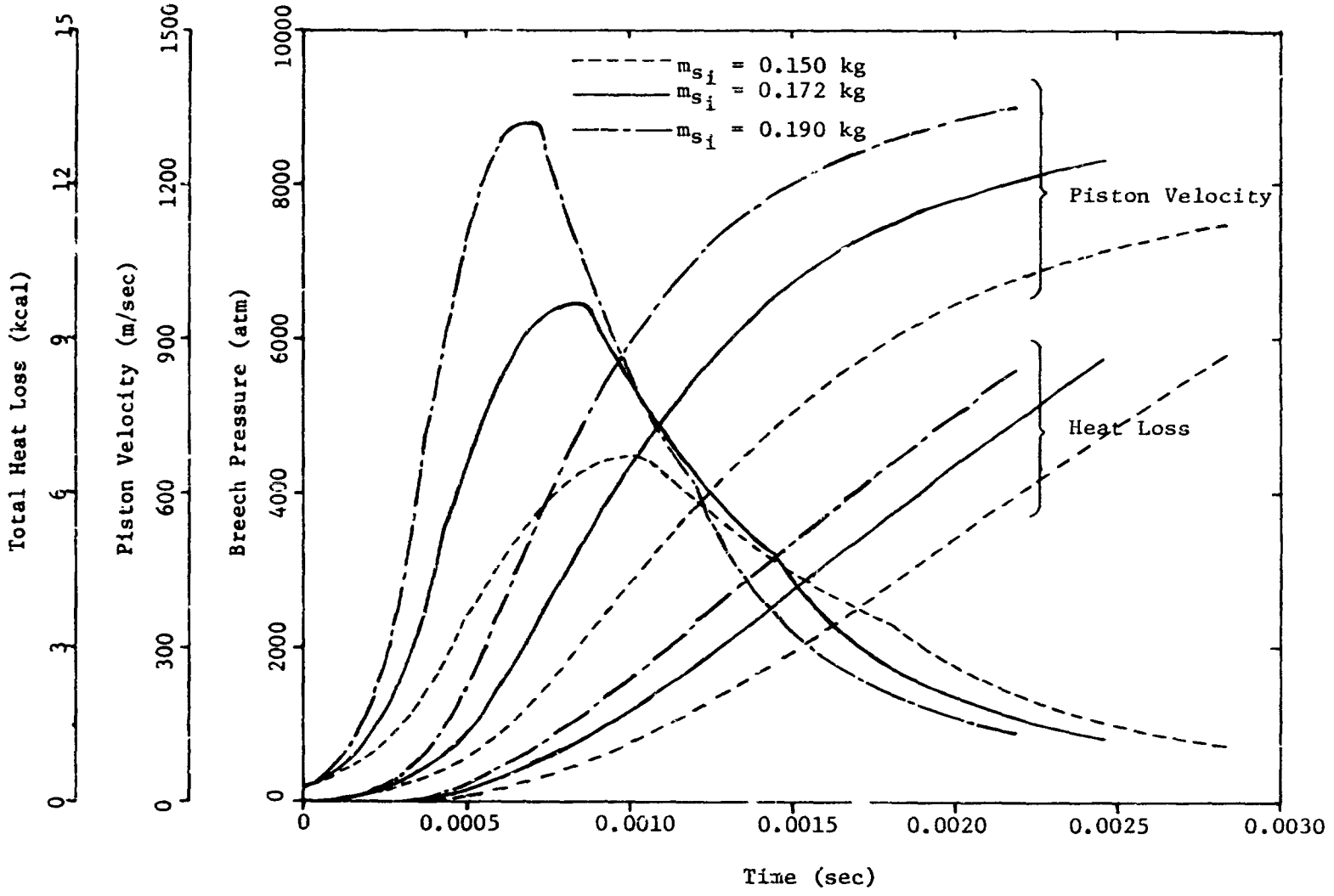

Figure 34. Comparison of Breech Pressure, Piston Velocity and Total Heat Loss to the Tube Wall for Various Propellant Charges (Case I)

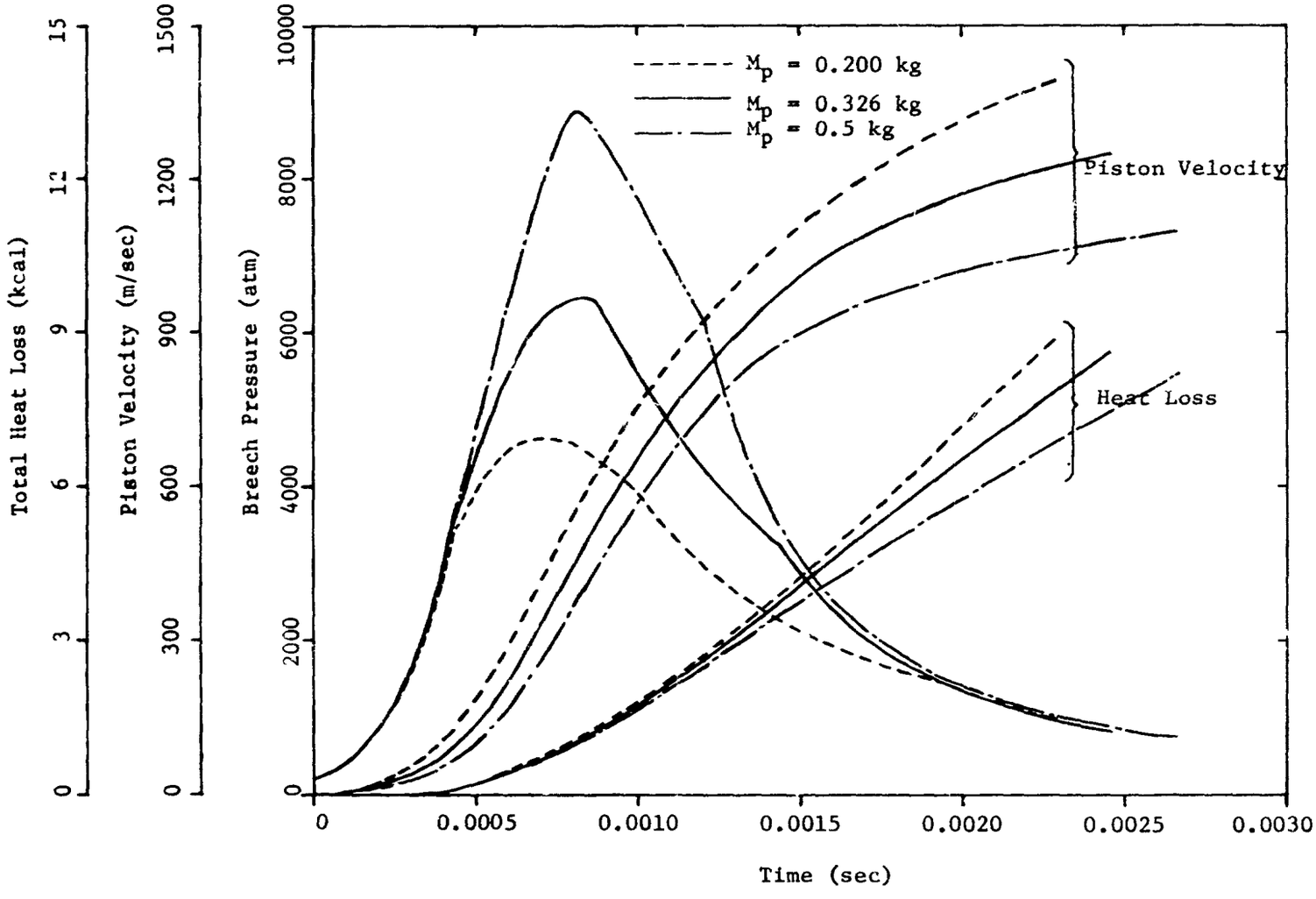

Figure 35. Comparison of Breech Pressure, Piston Velocity and Total Heat Loss to the Tube Wall for Various Piston Masses (Case I)

Web Thickness, w_{s_i}

Although the web thickness is only a geometrical property of the solid particles, it is important because it determines the total burning surface for a given propellant charge. For thinner webs more surface is available for burning and consequently the pressure rise is more rapid. This aspect is clear from Figure 36 where results of three different web thicknesses (0.5mm, 0.711 mm (standard), and 0.9 mm) are presented. A rapid pressure rise naturally accelerates the piston faster and thus improves the ballistic efficiency. This gain is neutralized by a much higher peak pressure and wall surface temperature.

Comparison with Other Work

No analytical work in the past considered the movement of the solid particles in the one-dimensional ballistic solution. Although Carriere [5] studied the problem of internal ballistics assuming the solids to be stationary, it was not possible to determine the input data and final results from his publication. Therefore, a quantitative comparison could not be made. However, an excellent qualitative agreement is observed between his results showing the piston path, piston velocity and end pressures, and the results obtained from the present analysis for the case of stationary solids. Unfortunately, no work presently exists that the spacewise distribution of the ballistic properties; therefore, no comparison can be made.

The boundary layer and heat transfer analysis of Hicks and Thornhill [2] assumed the Lagrange approximation and omitted the zero boundary layer thickness condition at the piston base. The values of

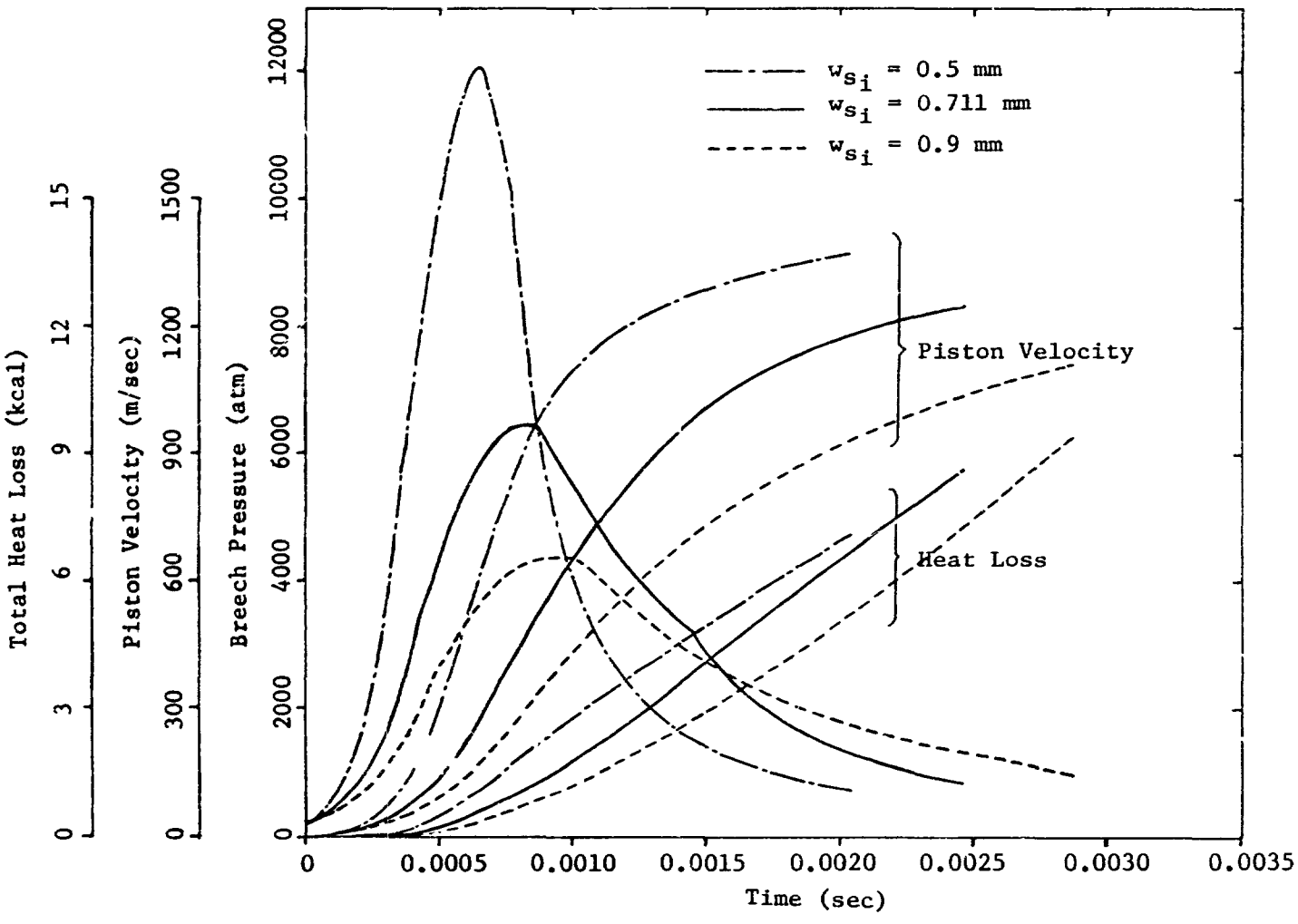

Figure 36. Comparison of Breech Pressure, Piston Velocity and Total Heat Loss to the Tube Wall for Various Web Thicknesses (Case I)

TABLE IV. RESULTS FOR VARIOUS INPUT PARAMETERS

Parameter / Item	H		D		m_{s_i}		M_p		w_{s_i}	
	1.2222	1.40	2.0cm	4.0cm	0.15kg	0.19kg	0.2kg	0.5kg	0.5mm	0.9mm
Time of travel (millisecond)	2.467	2.462	2.484	2.456	2.840	2.196	2.292	2.680	2.047	2.876
Peak breech pressure (atmosphere)	6440	6460	6400	6500	4470	8840	4660	8900	12000	4380
Peak surface temperature (^{o}K)	1114	991	1059	1071	985	1127	1008	1099	1180	984
Ballistic efficiency (%)	35.37	35.63	34.52	35.94	32.86	37.68	27.11	41.85	42.83	28.10
Total heat loss (kcal)	9.09	7.87	5.70	11.60	8.69	8.44	8.85	8.24	7.13	9.43
Heat loss in percentage of input energy (%)	5.36	4.65	7.58	3.85	5.88	4.5	5.21	4.86	4.21	5.56

heat transfer coefficient for a typical case (input data not indicated), as presented in reference 2, are lower than the values obtained for the typical case in the present study, by a factor of approximately two. The reason could be due to entirely different input data and different boundary layer thickness condition at the piston base. However, the value of peak surface temperature and the location when it occurs are in good agreement with the study of Hicks and Thornhill.

A very recent analysis on convective heat transfer in gun barrels [25], which is also based on the Lagrange approximation, indicates that the heat flux at the inside surface of the barrel can be as high as 2.7×10^5 kcal/m^2-sec. This value is quite close to the expected maxima shown in Figure 28 for the typical case.

Eglin Condition

In order to compare results with experimental temperature data gathered at Eglin Air Force Base, Florida, conditions other than the Standard conditions were run with the following input conditions:

Tube length, L_t	2m
Tube inside diameter, D	3 cm
Piston Mass, M_p	.326 kg

Initial conditions:

Piston position, L_o	25 cm
Chamber pressure (Piston start pressure), P_o	200 atm
Gas temperature (explosion temperature, τ_o	3000°K
Change of propellant, m_{si}	0.140 kg

Propellant properties:

Density, ρ_s	1670 kg/m^3
Initial web thickness, w_{s_i}	0.7366 mm
Type	M-10, single perforated

Gas Properties:

Molecular weight, M	24
Ratio of specific heats, γ	1,252
covolume, η	0.00095 m^3/kg
Specific heat at constant Pressure, c_p	0.412 kcal/kg°K
Viscosity (at 3000°K), μ_{go}	0.00007 kg/m/sec
Thermal conductivity (at 3000°K), κ_{go}	0.000034 kcal/m/sec°K

Tube material properties:

Thermal diffusivity, α_w	0.062 cm^2/sec
Thermal conductivity, κ_w	0.0138 kcal/m-sec^oK
Initial tube temperature, T_{amb}	300^oK

The burning rate was again taken from Table I, and only Case I was taken, i.e., the solids move with the gas.

The results of this calculation are shown in Figures 37 through 43, and agree extremely well with experimental data for the peak wall temperature taken by Eglin Air Force Base. The calculated maximum wall temperature shown in Figure 43 is 1020^oK at x = 25 cm. The experimental maximum measured at Eglin was approximately 1000^oK. No measured parameters such as chamber pressures were input to the program to calculate this wall temperature. The only necessary input conditions are propellant, gun, and loading parameters listed at the beginning of this section. These Eglin conditions are obviously more realistic than the original standard conditions due to the smaller propellant loading (140 grams instead of 172 grams). The peak head and chamber pressure is approximately 58,000 psi, as seen from Figure 38.

This excellent agreement verifies the accuracy of the detailed ballistic and heat transfer model developed here and used without the aid of experimental ballistic data.

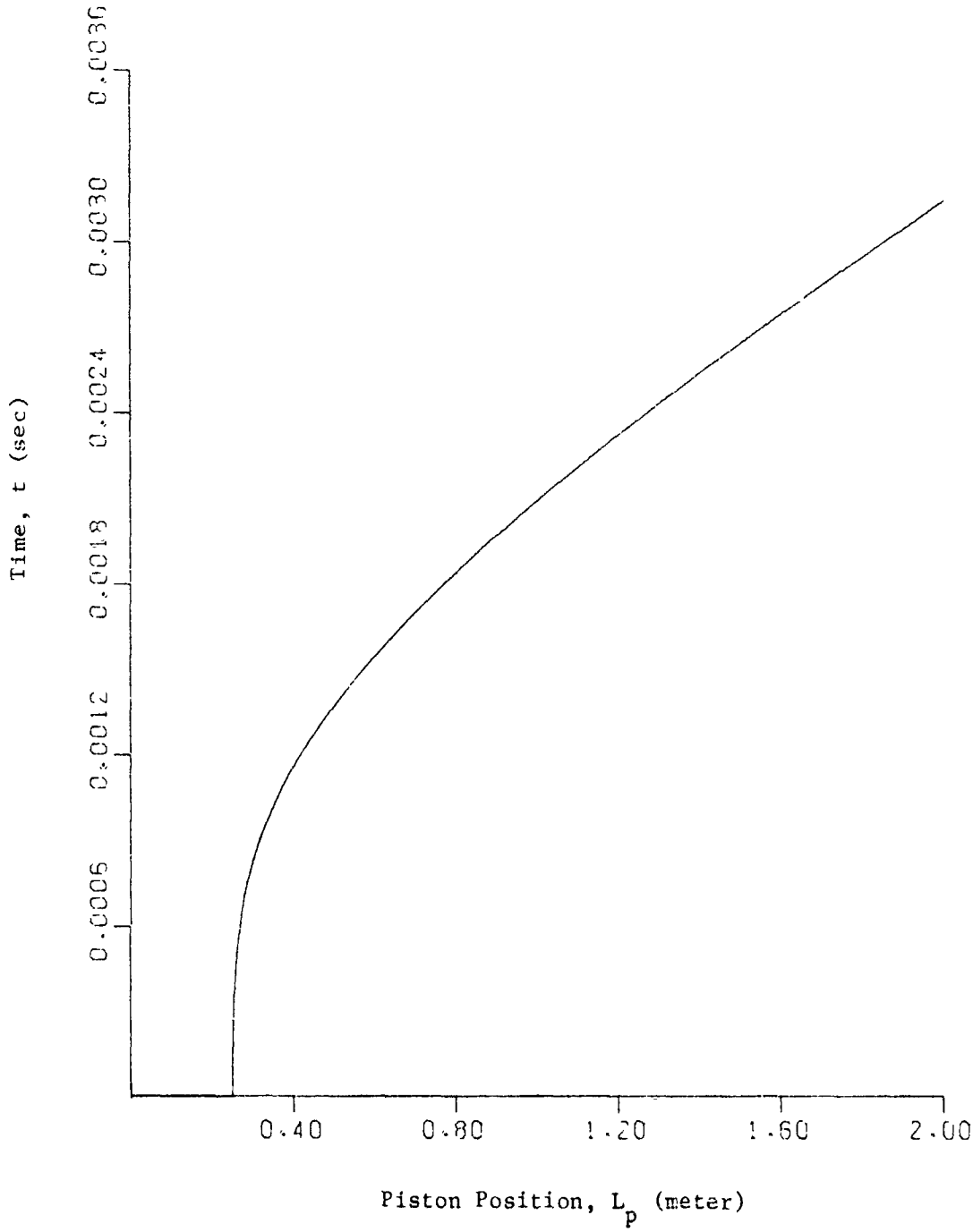

Figure 37. Piston Position Versus Time (Case I, Eglin Conditions)

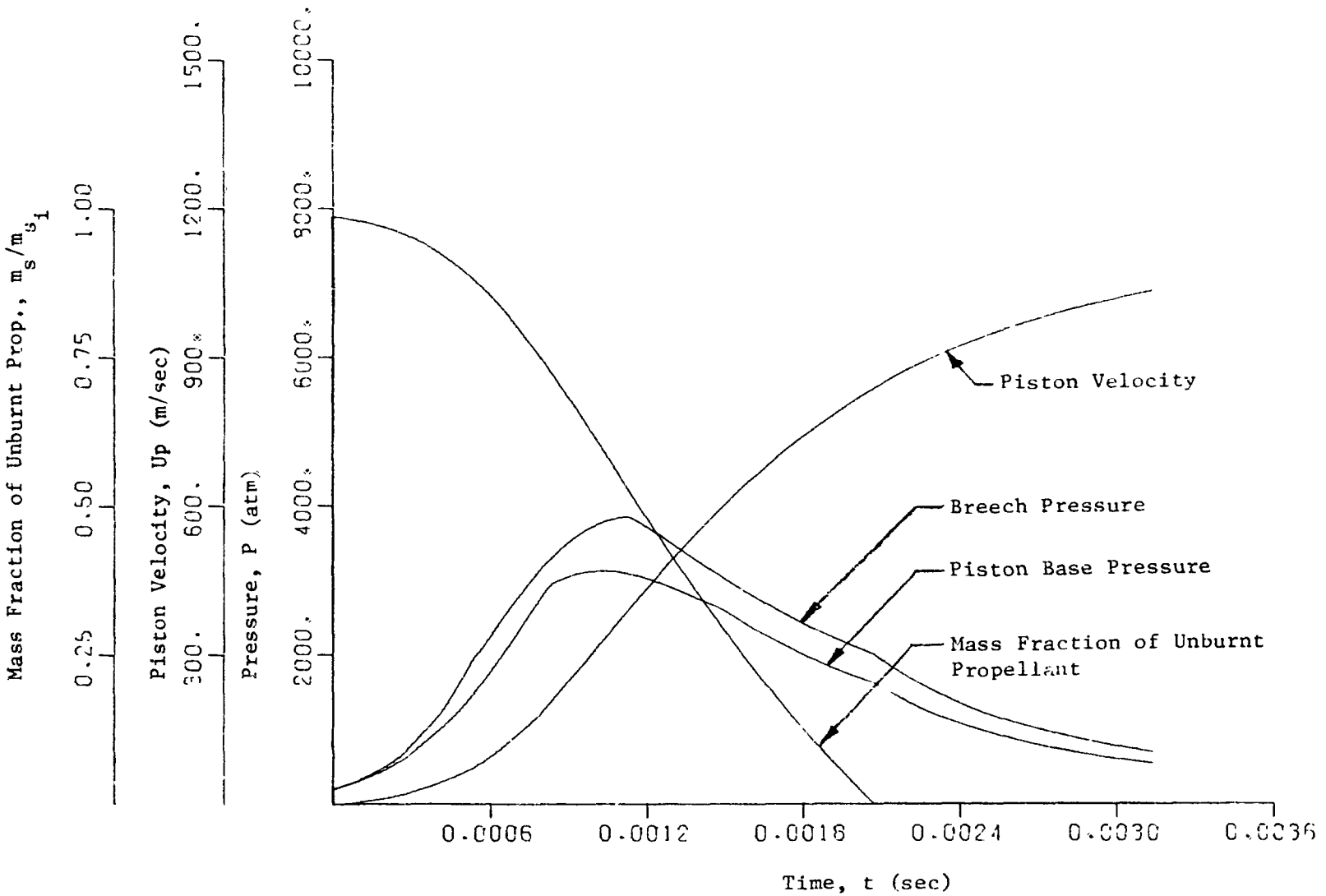

Figure 38. End Pressures, Piston Velocity, and Mass Fractions of Solids (Case I,Eglin Conditions)

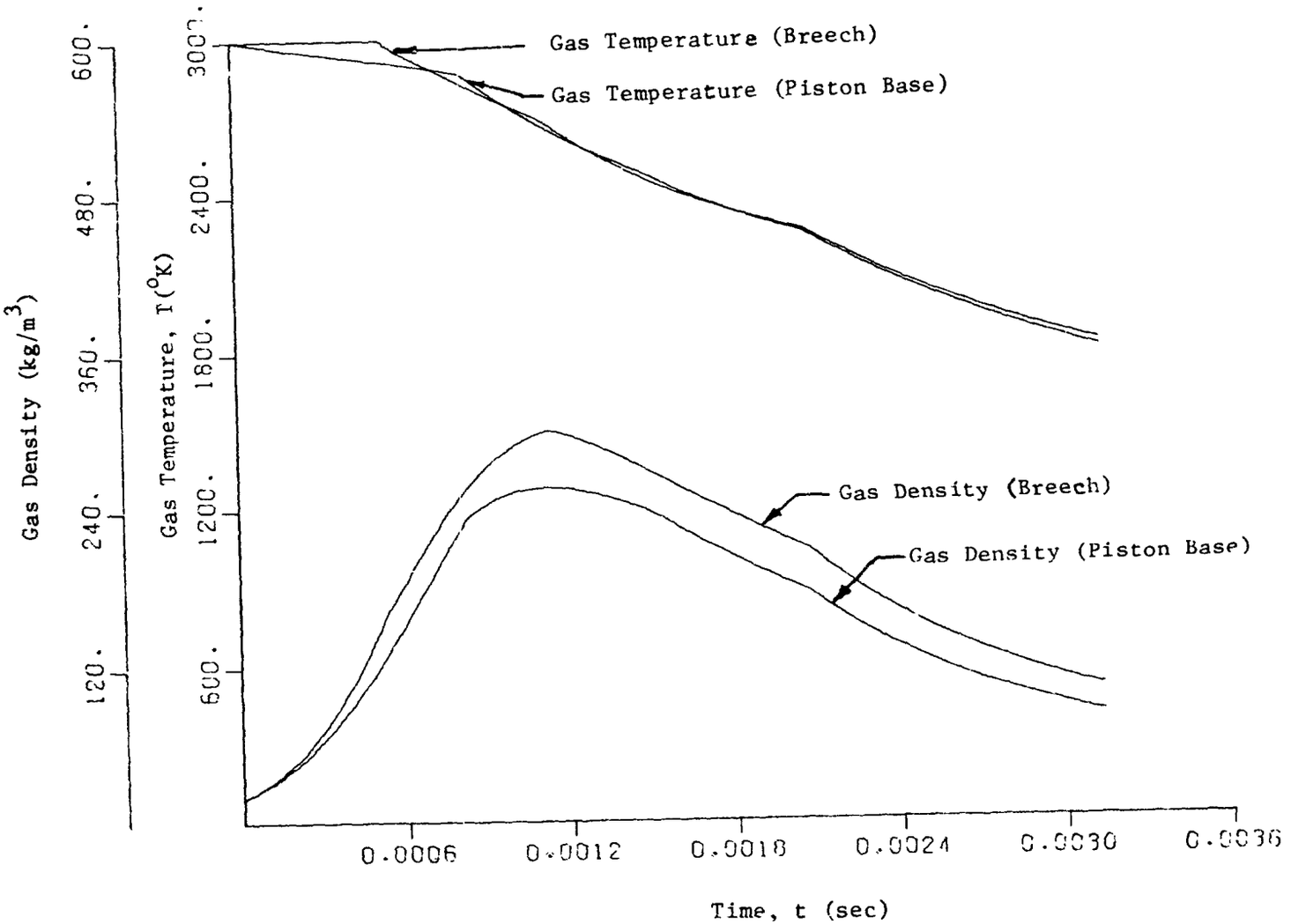

Figure 39. End Gas Densities and Temperatures Versus Axial Location at Various Times (Case I, Eglin Conditions)

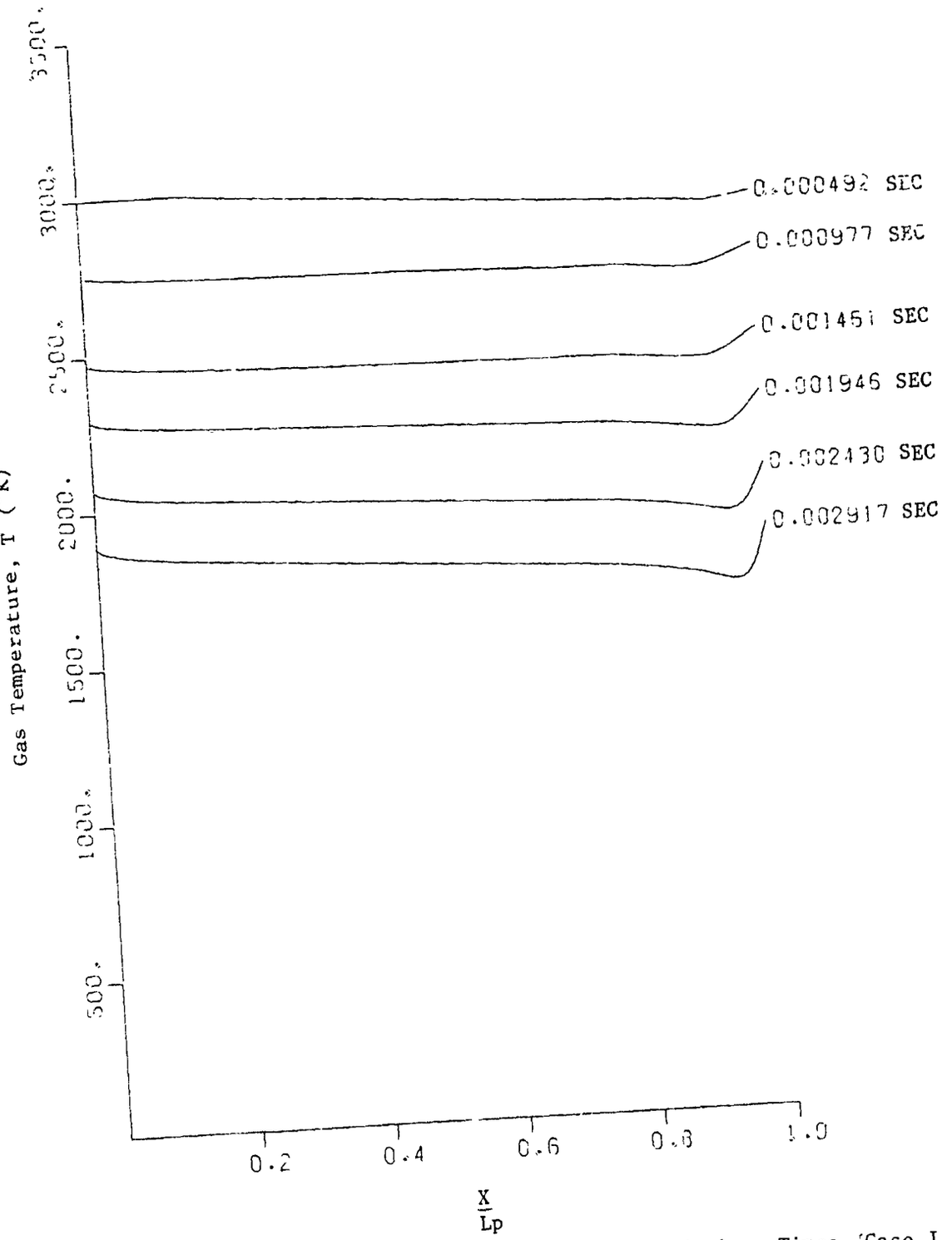

Figure 40. Gas Temperature Versus Axial Location at Various Times (Case I, Eglin Conditions)

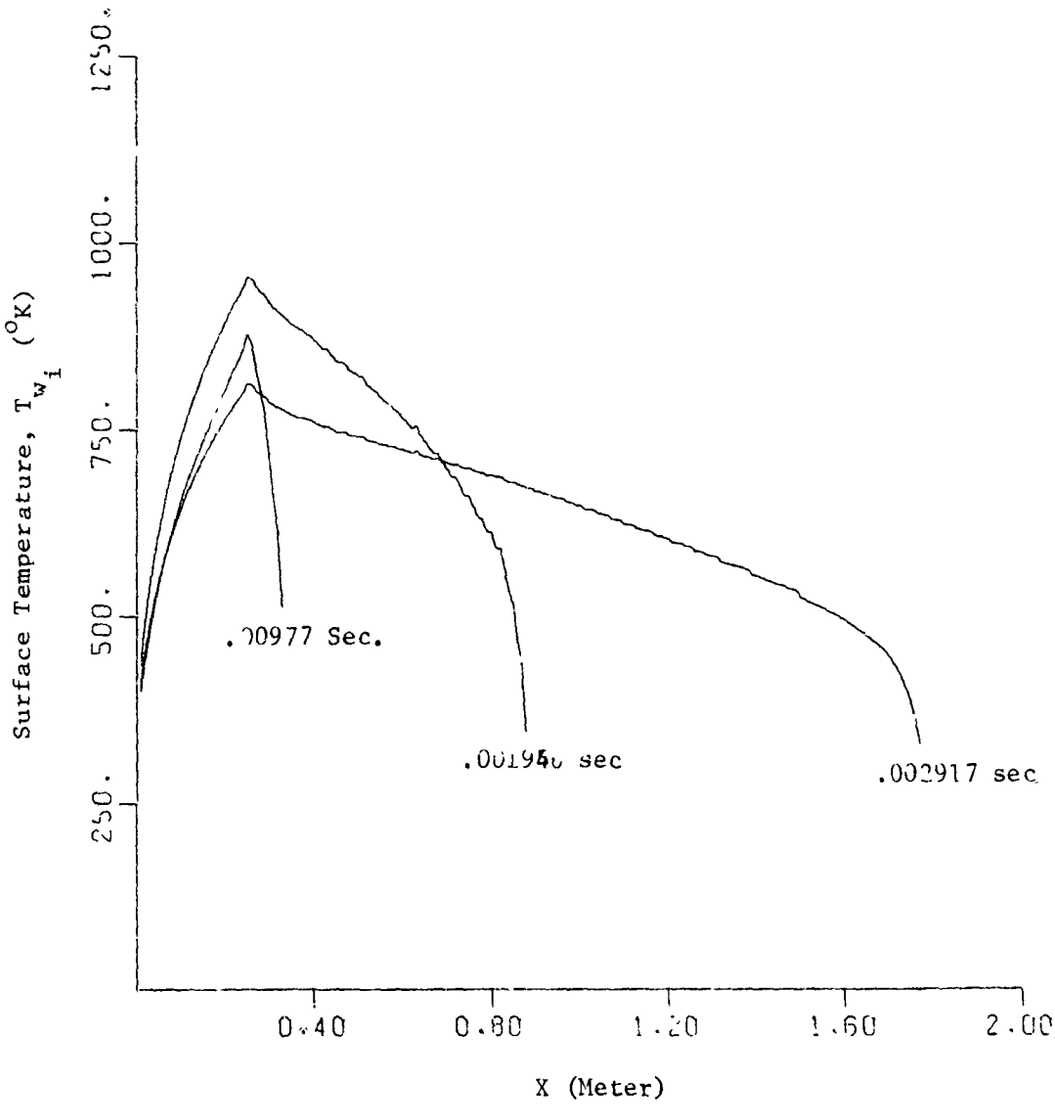

Figure 41. Tube Inside Wall Temperature Versus Axial Distance at Various Times (Case 1, Eglin Conditions)

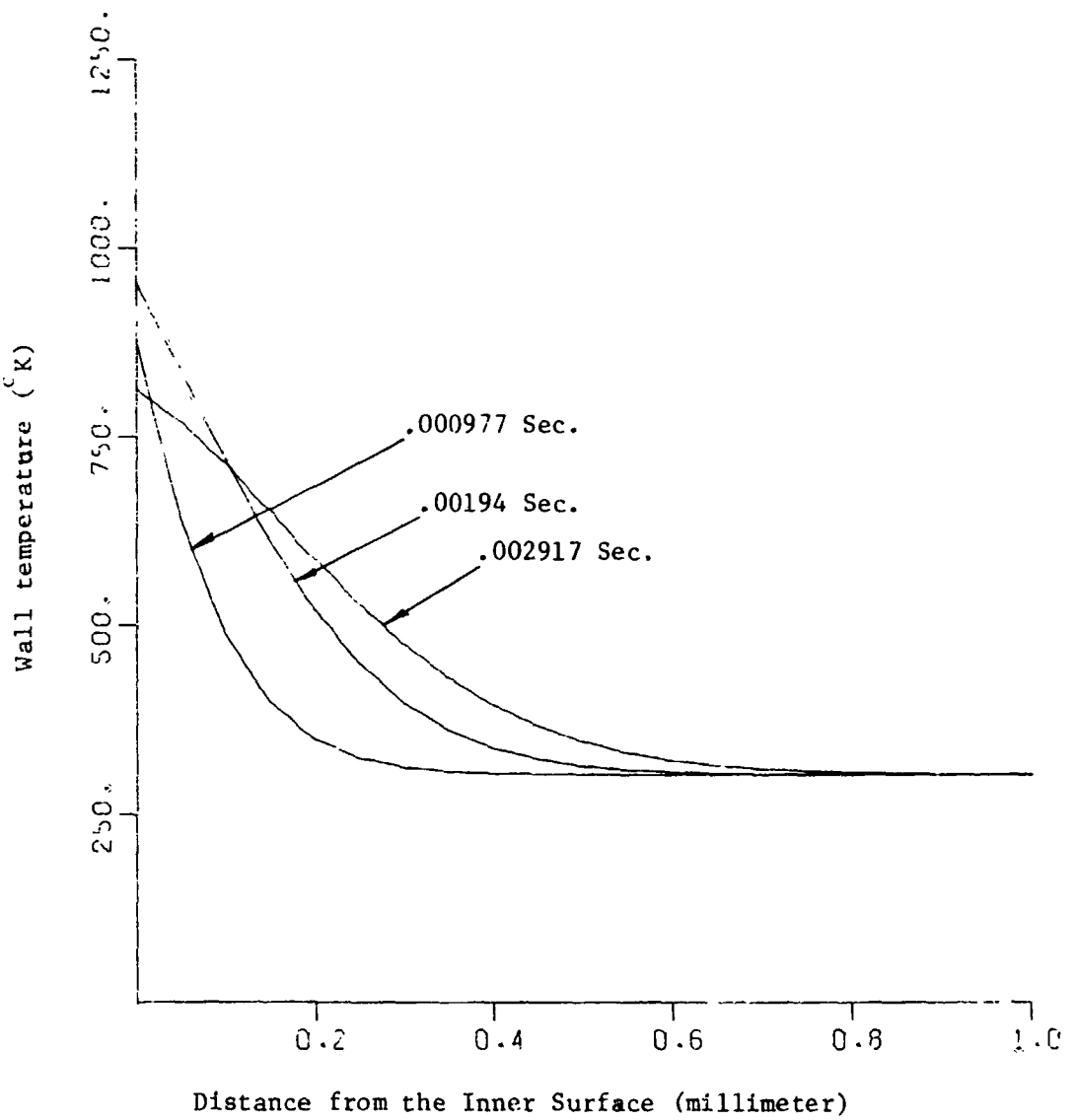

Figure 42. Tube Temperatures Versus Radial Distance at Certain Fixed Times (Case I, Eglin Conditions)

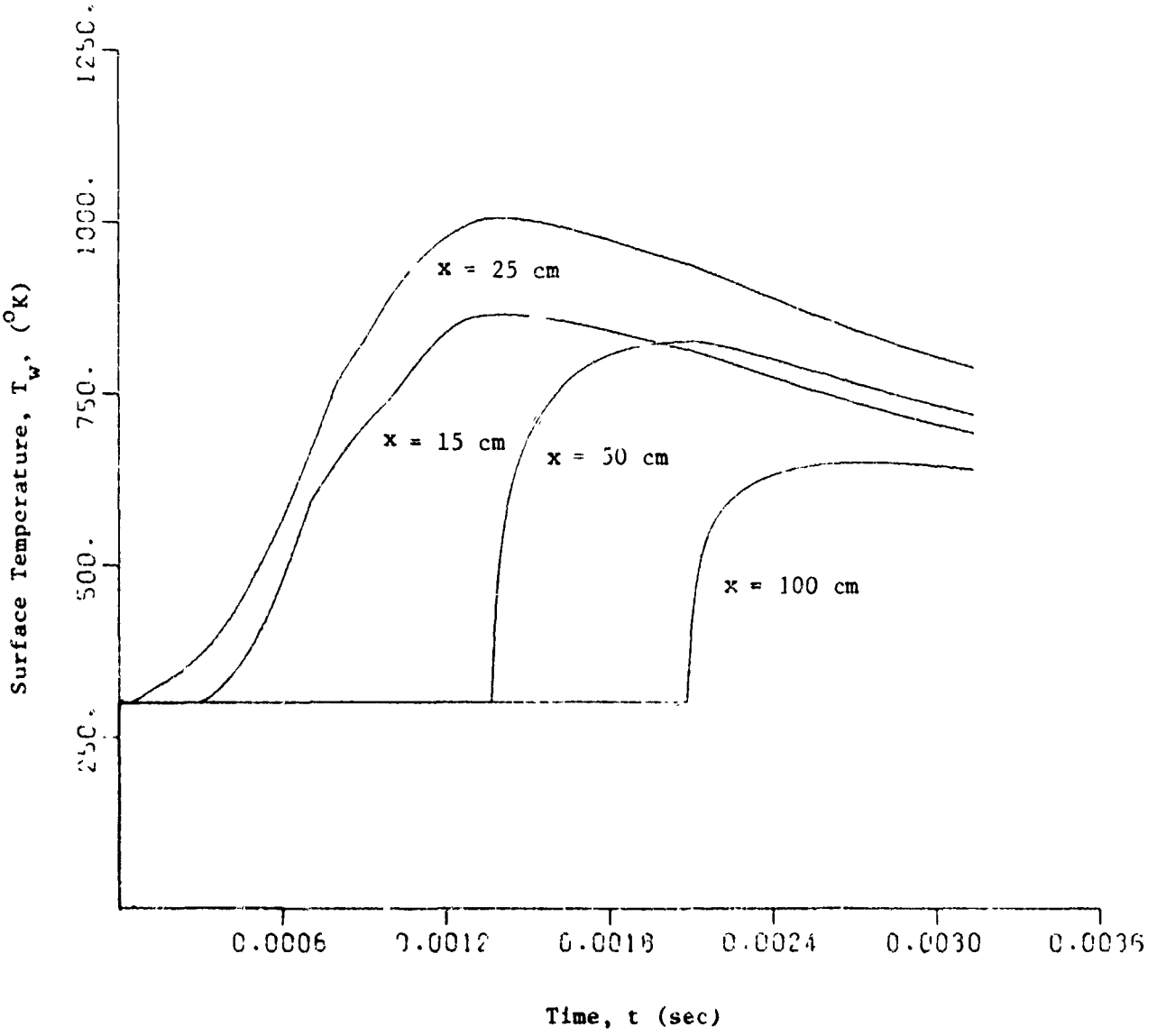

Figure 43. Tube Inside Wall Temperature Versus Time at Several Locations (Case I, Eglin Conditions)

SECTION VI

CONCLUSIONS

The following conclusions can be drawn in the context of the results presented in Part I.

1. The Lagrange approximation of linear velocity distribution and uniform gas density along the length of the tube is not a good representation of the real case. It takes a considerable amount of total time before the velocity distribution can be linear. Furthermore, the gas density cannot be called uniform at any time.

2. There is a large pressure gradient along the length of the tube and at the peak condition the difference between the pressures at the two ends can be as high as 20 to 30 percent of the maximum pressure.

3. As the piston moves, the gas temperature continuously decreases with almost a uniform spacewise distribution. For the case of stationary solids, however, a steep spacewise temperature rise is observed at the back of the piston.

4. While the final ballistic results are essentially the same for the two extreme cases of solids velocity, the peak pressure in the case of stationary solids is about 10 to 15 percent higher than in the case of moving solids.

5. The maximum boundary layer thickness can be on the order of 20 percent of the tube radius in typical cases. For ballistically similar devices the ratio of the maximum boundary layer thickness to the tube radius increases as the tube diameter is reduced. Therefore,

the assumption of a thin boundary layer may not hold good for very small diameter tubes.

6. The order of magnitude of the heat transfer coefficient and the heat flux at the inner surface of the tube is extremely high. Average values of 50 kcal/m^2-sec-^oK and 50,000 kcal/m^2-sec for the heat transfer coefficient and the heat flux, respectively, can be expected for typical cases. The maximum values can be five to six times higher than the average values but the maxima do not last for more than a few microseconds.

7. The tube inner surface temperature can reach 1000^{o}K for typical cases, and it occurs near the initial piston position. The time of travel is so short that, even with the extremely high values of heat fluxes and high thermal properties of tube material, the temperature wave cannot penetrate more than one millimeter into the tube wall.

8. The total heat loss to the tube wall is five to six percent of the input energy for typical cases and has only a minor effect on the final ballistic results. The same conclusion is valid for the skin friction.

9. The piston start pressure, although difficult to determine in practice, does not pose any real problem due to its insignificant effect on the ballistic solution.

10. Improvement in ballistic efficiency can be brought about by increasing the propellant charge and the piston mass or by reducing the web thickness. In each of these cases, there exists an adverse effect of higher peak pressure and higher wall temperature. Therefore,

great care should be taken to obtain the optimum design conditions.

11. The heat transfer model is verified by the limited wall temperature data available at this time. This agreement is gained without the use of experimentally measured interior ballistic data such as chamber pressure versus time, as used in other analysis [25].

PART II - PARTICLE SEEDING EFFECTS ON GUN BARREL HEAT TRANSFER AND EROSION

SECTION VII

INTRODUCTION

The seeding of gun propellants with additives, such as TiO_2 in a wax matrix, appears to be an effective method of reducing gun barrel erosion [26, 27, 28, 29, 30]. The mechanism by which this is accomplished has not, however, been satisfactorily explained. This makes it impossible to optimize the effect or properly predict it without expensive and time consuming trial-and-error experiments.

Since gun barrel erosion has been shown to be primarily tube temperature [31] and thereby heat transfer, sensitive, the quantitative heat transfer model developed in the previous section will be used to test various possible mechanisms by which additives might reduce the temperature of the gun tube.

The fact that the reduced erosion is primarily a temperature phenomena rather than a chemical phenomena is substantiated not only by reference 31 but also by reference 29 which shows an increase in CO due to a wax additive. Reference 31 shows the CO increase should increase rather than reduce chemical erosion. The fact that erosion is actually reduced by the TiO_2 - wax additive causes one to search for a reduced heat transfer mechanism created by the additive.

This is carried out by looking at (1) temperatures reached under repetitive fire conditions, (2) experimental results from dusty gas heat transfer experiments usually related to gas-cooled nuclear reactors, and (3) insulation effects of particles imbedded in valleys of the barrel surface roughness.

SECTION VIII

REPETITIVE FIRE ANALYSIS

Introduction

Since rapid fire aircraft cannons are of primary interest in this effort, the wall temperatures predicted in the foregoing single-shot analysis are not directly applicable. Since this wall temperature is the parameter of most interest, a repetitive fire analysis is carried out here to determine what peak temperatures actually occur in aircraft cannons. This allows one to determine if the temperatures are sufficiently high to cause melting of a thin layer of metal on the inside of the barrel.

Model

In carrying out a repetitive fire analysis, one is immediately confronted with the gun emptying problem, i.e., calculating the gas flow properties and gas to metal heat transfer rates after the projectile leaves the tube but before the next projectile is fired. The previous single-shot analysis is not applicable because it assumes a solid projectile base closes the tube at all times.

Rather than attempt to solve this complex problem, it was decided to carry out the calculations using an upper and lower limit on the heat transfer during this emptying or soaking period. Since the total heat transfer during this time was expected to be small, it was hoped that these two limits would put a rather small bracket on the actual results.

An upper limit is obviously taken if one assumes that the gas temperature and heat transfer coefficient remain at their values which existed at the time the projectile left the tube. After the projectile leaves, the gas temperature will be reduced, the gas pressure will be reduced, and the gas velocity will decay to zero. Each of these factors will tend to reduce the heat transfer to the barrel below this assumed upper limit.

A lower limit is certainly given by assuming that the inside of the barrel is suddenly insulated from the gases at the instant the projectile leaves the barrel. This assumes that no heat is transferred from the hot gases to the barrel during the soak period between shots.

The gas temperature and heat transfer coefficient as a function of axial distance and time were taken from the single shot analysis and repetitively applied during each and every shot while the projectile was moving down the barrel. The conduction analysis was started at the time of the initial shot and successively calculated each Δt during the firing period and the soaking period. Since the metal temperature, T_w, at any $t + \Delta t$ depends on the metal temperature profile $T_w(r)$ at t, this conduction calculation must be carried on continuously with the repetitive heat transfer coefficient, $h_i(t)$, and gas temperature, $T_\infty(t)$, being repeated for each firing cycle, as detailed in Chapter IV, except that the wall temperatures are not reset to T_{amb} at the beginning of each firing.

One should note that this model does not assume that the total heat transferred during each cycle is the same from one cycle to the next because the wall temperature, $T_{w,i}$, is increasing from cycle to cycle, thereby reducing $(T_\infty - T_{w,i})$ and the heat transfer.

Conduction Series Solution During Soaking

For short cyclic firing times (i.e., 0.010 second or less) the conduction solution during soaking was carried out by the finite difference technique detailed in Chapter IV. However, at larger cyclic firing times (i.e., up to 0.060 second), the number of time steps required during the soak period was so large that the computer computation time was excessive. Therefore, a closed form series solution was developed and used during the time period from the instant the projectile left the barrel to the time the next shot was initiated. This series solution was made possible during soaking due to the constant heat transfer coefficient, h_i, with respect to time. This parameter is not constant with time during the firing itself.

Taking the conduction equation and applying it at some specific axial location during the nth soaking period:

$$\frac{\partial T_w}{\partial t} = \alpha_w \left[\frac{\partial^2 T_w}{\partial r^2} + \frac{1}{r} \frac{\partial T_w}{\partial r} \right] \tag{145}$$

and separating variables, one finds that the solution may be expressed as [32,33]

$$T_w - T_{amb} = \sum_{m=1}^{\infty} \left[A_m J_o (\lambda_m r) + B_m Y_o (\lambda_m r) \right] e^{-\lambda_m^2 \alpha_w t} \tag{146}$$

where J_o and Y_o are zero order Bessel functions of the 1st and 2nd kind, respectively, and A_m and B_m must be found from the boundary and initial conditions which, for the lower limit case of zero heat transfer during soaking, are:

$$\frac{\partial T_w}{\partial r} = 0 \text{ at } r = r_i \tag{147}$$

$$\kappa_w \frac{\partial T_w}{\partial r} + h_o (T_w - T_{amb}) = 0 \text{ at } r=r_o \quad (148)$$

$$T_w(r) - T_{amb} = f(r) \text{ at } t = t_n \quad (149)$$

where t_n is the time when the nth projectile leaves the tube and the nth soak period begins and f(r) is the temperature distribution with respect to r existing at that time.

Applying these boundary conditions to (146), one finds:

$$T_w - T_{amb} = \sum_{m=1}^{\infty} C_m \frac{\lambda_m J_1 (\lambda_m r)}{\lambda_m^2 \kappa_w J_1 (\lambda_m r_o) - h_o J_o (\lambda_m r_o)}$$

$$\frac{\lambda_m Y_1(\lambda_m r)}{\lambda_m^2 \kappa_w Y_1 (\lambda_m r_o) - h_o Y_o (\lambda_m r_o)} e^{-\lambda_m \alpha_w t} \quad (150)$$

where U, and Y, are first order Bessel functions of the 1st and 2nd kind, respectively, λ_m is the mth root of the equation:

$$\frac{\lambda_m J_1 (\lambda_m r_i)}{\lambda_m^2 \kappa_w J_1 (\lambda_m r_o) - h_o J_o (\lambda_m r_o)} - \frac{\lambda_m Y_1 (\lambda_m r_i)}{\lambda_m^2 \kappa_w Y_1 (\lambda_m r_o) - h_o Y_o (\lambda_m r_o)} = 0 \quad (151)$$

and C_m is calculated by use of the function in equation (149):

$$C_m = \frac{1}{N_m} \int_{r_i}^{r_o} r R_o (\lambda_m, r) f(r) dr \quad (152)$$

where:

$$R_o (\lambda_m, r) = \frac{J_o (\lambda_m r)}{\lambda_m \kappa_w J_o (\lambda_m r_o) + h_o J_o (\lambda_m r_o)} -$$

$$\frac{Y_o (\lambda_m r)}{\lambda_m \kappa_w Y_o (\lambda_m r_o) + h_o J_o (\lambda_m r_o)} \quad (153)$$

$$N_m = \int_{r_i}^{r_o} r R_o^2 (\lambda_m, r) dr \quad (154)$$

Using an r_i of 3 cm and an r_o of 6 cm the first five roots of equation (151) are:

$$\lambda_1 = 3.1965$$

$$\lambda_1 = 6.3275$$

$$\lambda_1 = 9.4522$$

$$\lambda_1 = 12.5844$$

$$\lambda_1 = 15.7230$$

and only five terms were retained in the series. Accuracy was checked by comparing the results from the series solution containing five and ten terms with the finite difference solution results. This comparison showed that five terms yielded sufficient accuracy.

Results

Results of the repetitive fire calculations were carried out for two firing rates: 0.010 second between firings and 0.060 second between firings. Since the projectile is in the tube for less than 0.003 second, the soaking times are about 0.007 and 0.057 second for the two firing rates, respectively.

The results for three axial locations are shown in Figures 44 through 46 for the 0.010 second firing time with the heat transfer coefficient h_i during soaking at its upper limit which is equal to its value at the time the projectile leaves the tube, devoted by $h_{i_{last}}$. These are for ten repetitive firings.

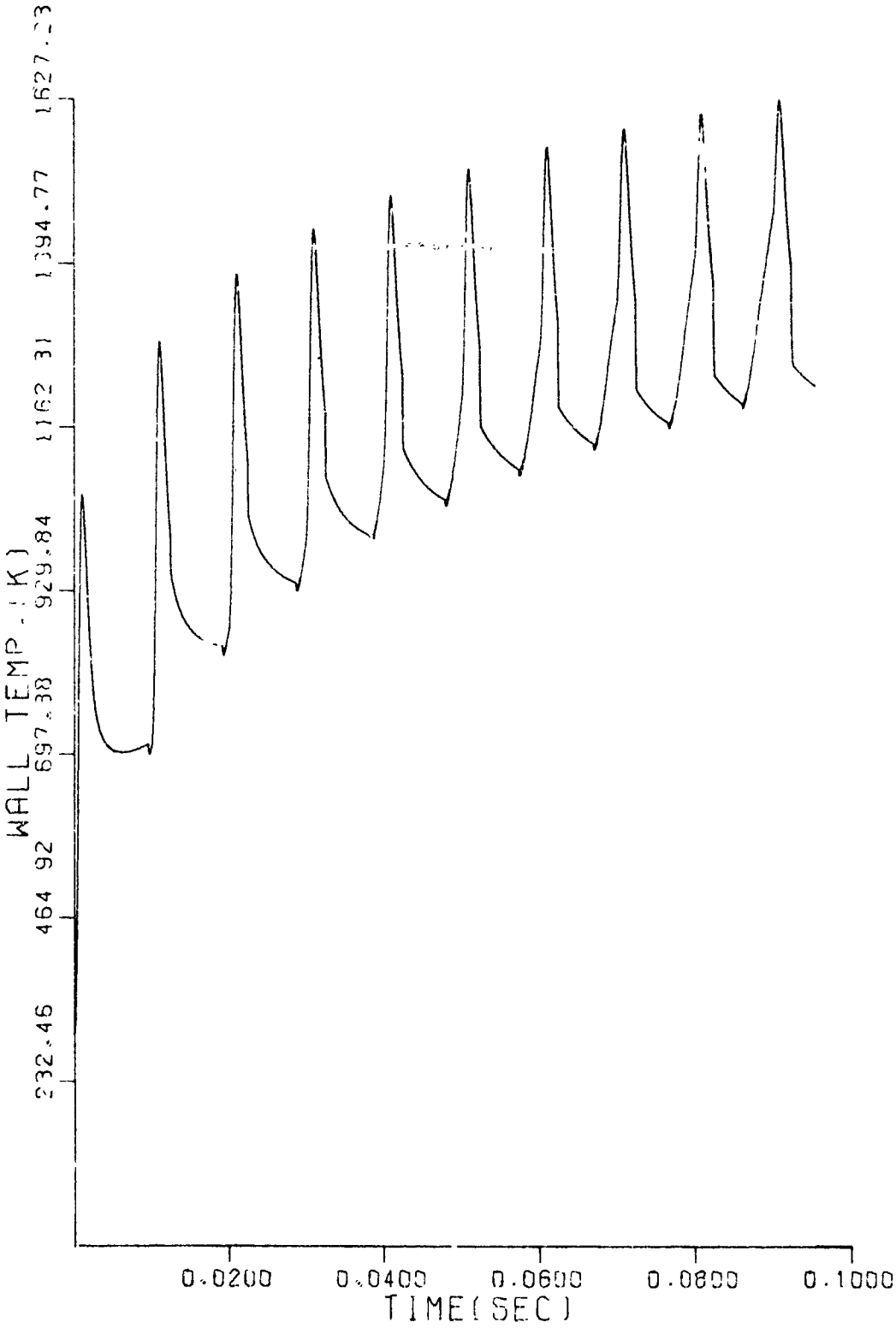

Figure 44. Repetitive Fire Wall Temperature Versus Time at Axial Location of 25 cm (Upper Limit)

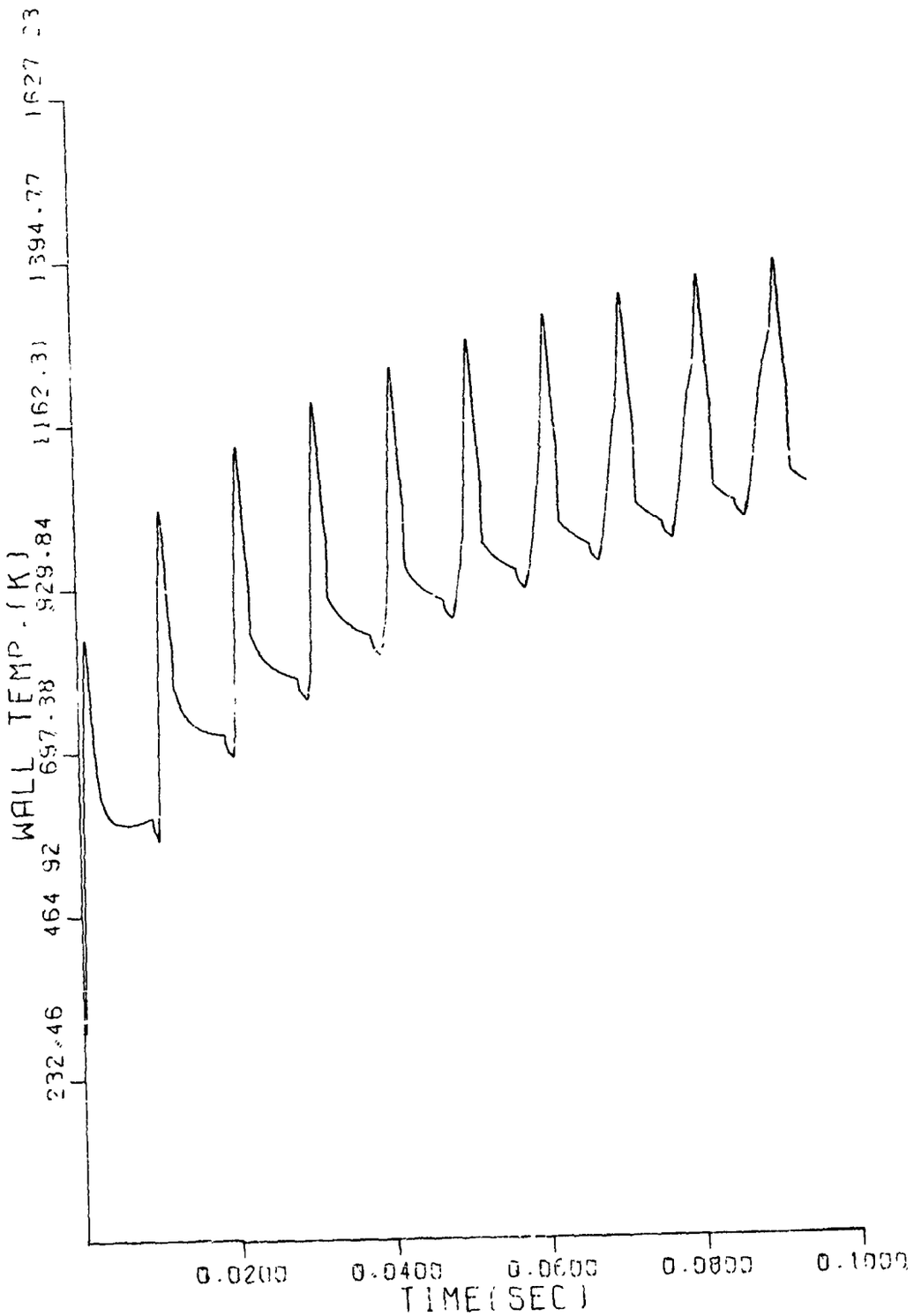

Figure 45. Repetitive Fire Wall Temperature Versus Time at Axial Location of 12 cm (Upper Limit)

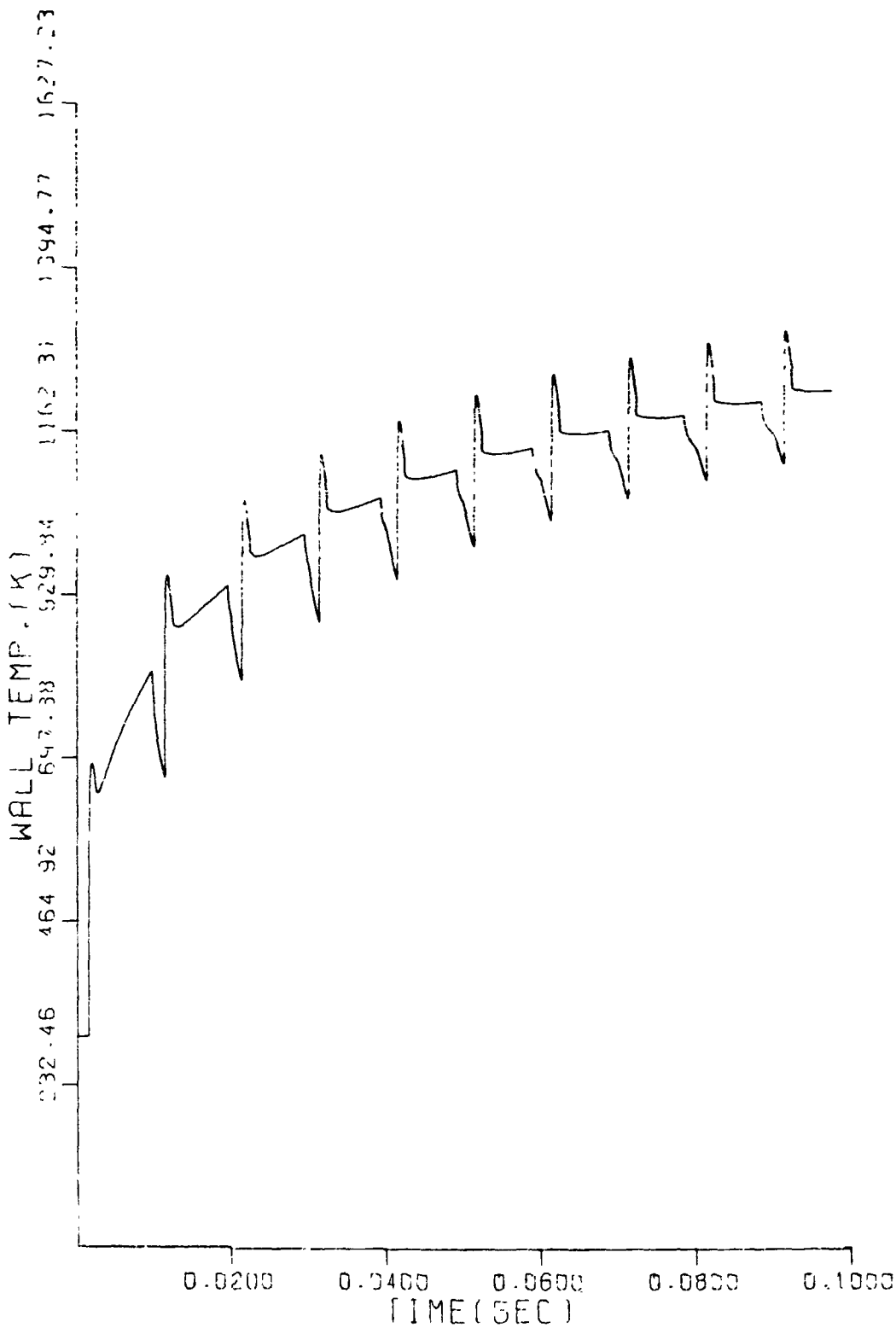

Figure 46. Repetitive Fire Wall Temperature Versus Time at Axial Location of 83 cm. (Upper Limit)

Figures 47 through 49 show the same results assuming zero convective heat transfer during soaking, i.e., h_i equal zero which is the lower limit. These sets of curves then bracket the upper and lower limits for the inside wall temperature. At an axial location of 25 cm, which sees the highest temperature (Figure 24), the upper limit case after ten firings show a maximum temperature of about 1600°K compared with the lower limit case of about 1500°K. This is a small bracket (8 percent) and shows that assumption concerning the heat transfer during the soaking period has little effect on the maximum wall temperature of interest. Therefore, at a given axial position, subsequent calculations assumed zero heat transfer from the combustion gas to the tube walls from the time projectile n leaves the tube to the time projectile n+1 passes that axial position.

Results using this lower limit assumption for the lower cyclic firing time of 0.060 second/round are shown in Figures 50 through 55 for 50 repetitive firings at the same three axial positions as shown for the previous case in Figures 44 through 49.

Figure 50 shows the wall temperature as a function of time at the high temperature axial position of 25 cm. Figure 51 shows the temperature profile inside the tube wall at this same axial position at four different times. These same type of curves are repeated at the two other axial positions of 12 and 84 cm in Figures 52-53 and Figures 54-55, respectively.

With the longer soaking periods between firings, the maximum temperature after 50 cycles is about 1400°K. It is seen from the wall temperature versus time graphs that the peak temperature during each cycle rises very slowly after the initial 10 rounds. Also, it is seen from the radial temperature distribution inside the tube wall that the outside tube temperature has not risen significantly after the 50 rounds.

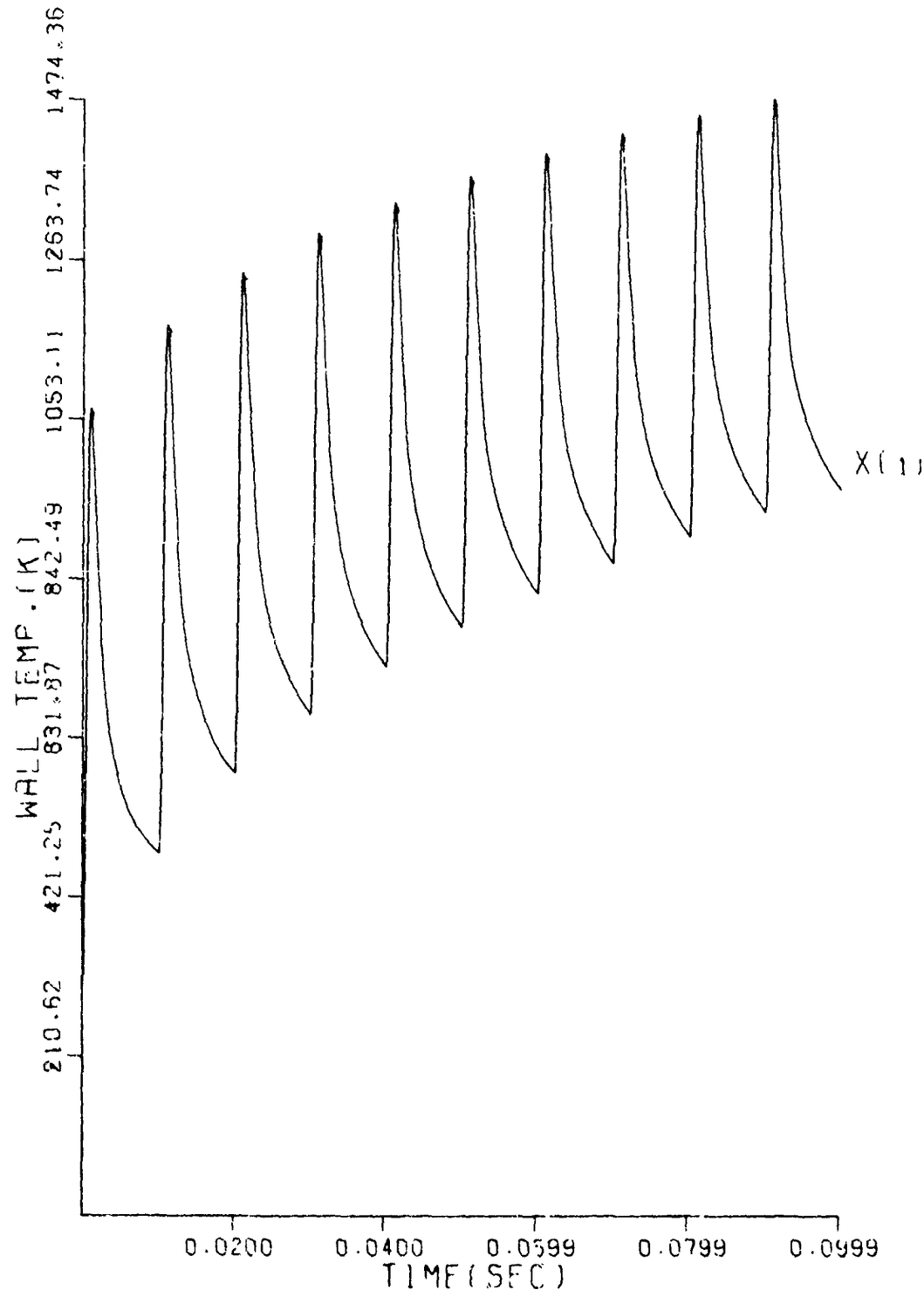

Figure 47. Repetitive Fire Wall Temperature Versus Time at Axial Location of 25 cm (Lower Limit)

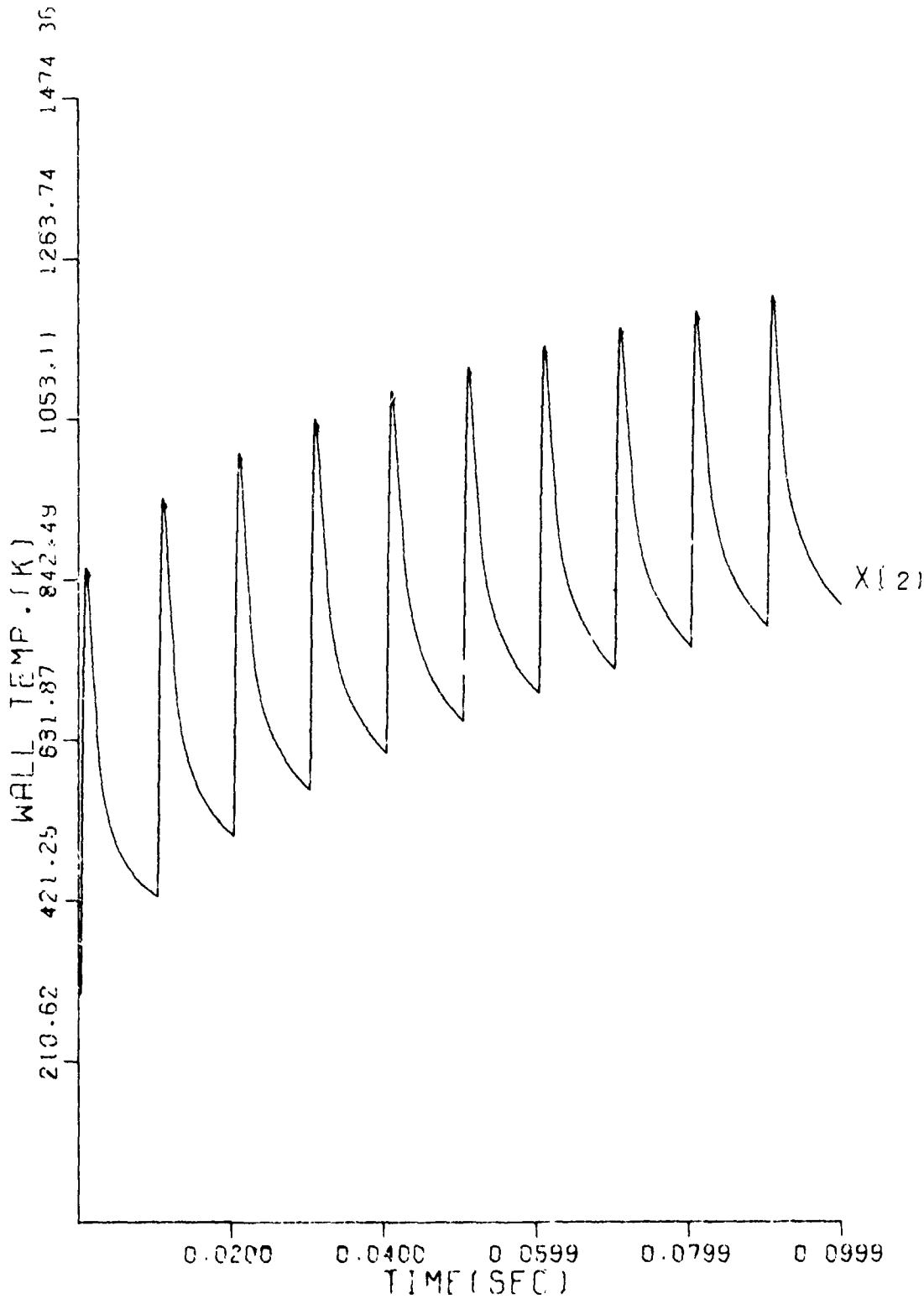

Figure 48. Repetitive Fire Wall Temperature Versus Time at Axial Position of 12 cm (Lower Limit)

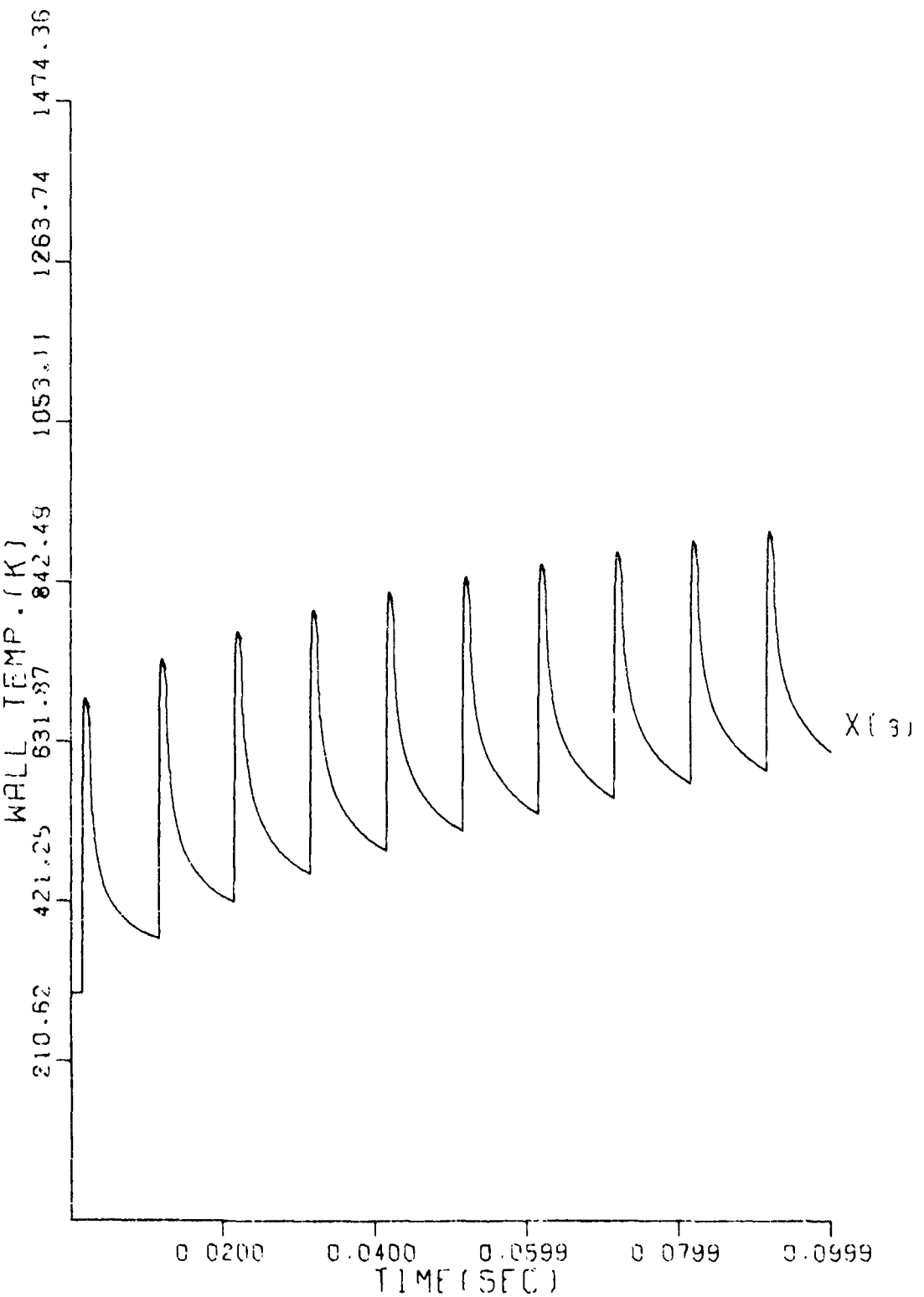

Figure 49. Repetitive Fire Wall Temperature Versus Time at Axial Location of 83 cm (Lower Limit)

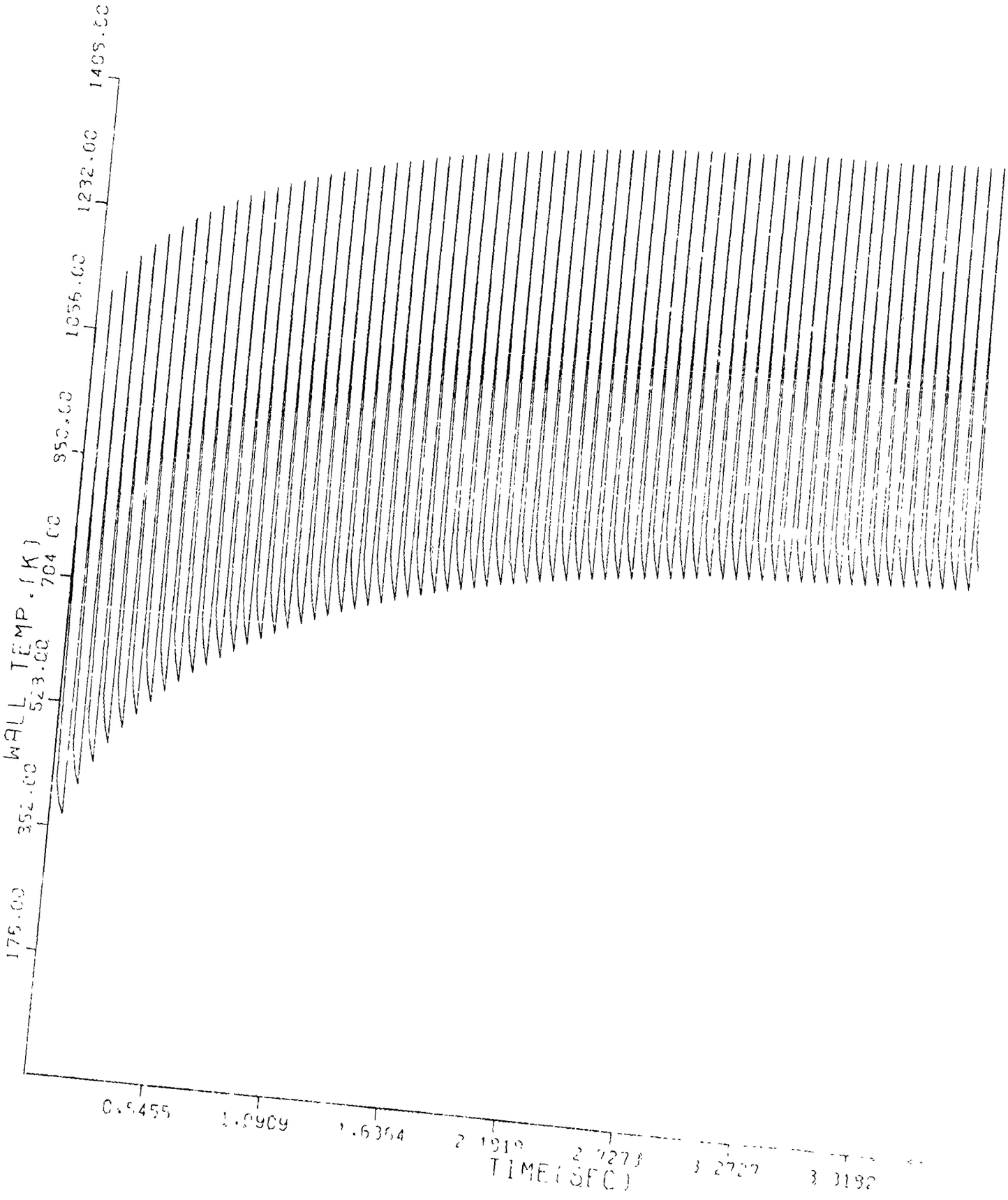

Figure 50. Repetitive Fire Wall Tem
of 25 cm (0.060 second f

(The reverse

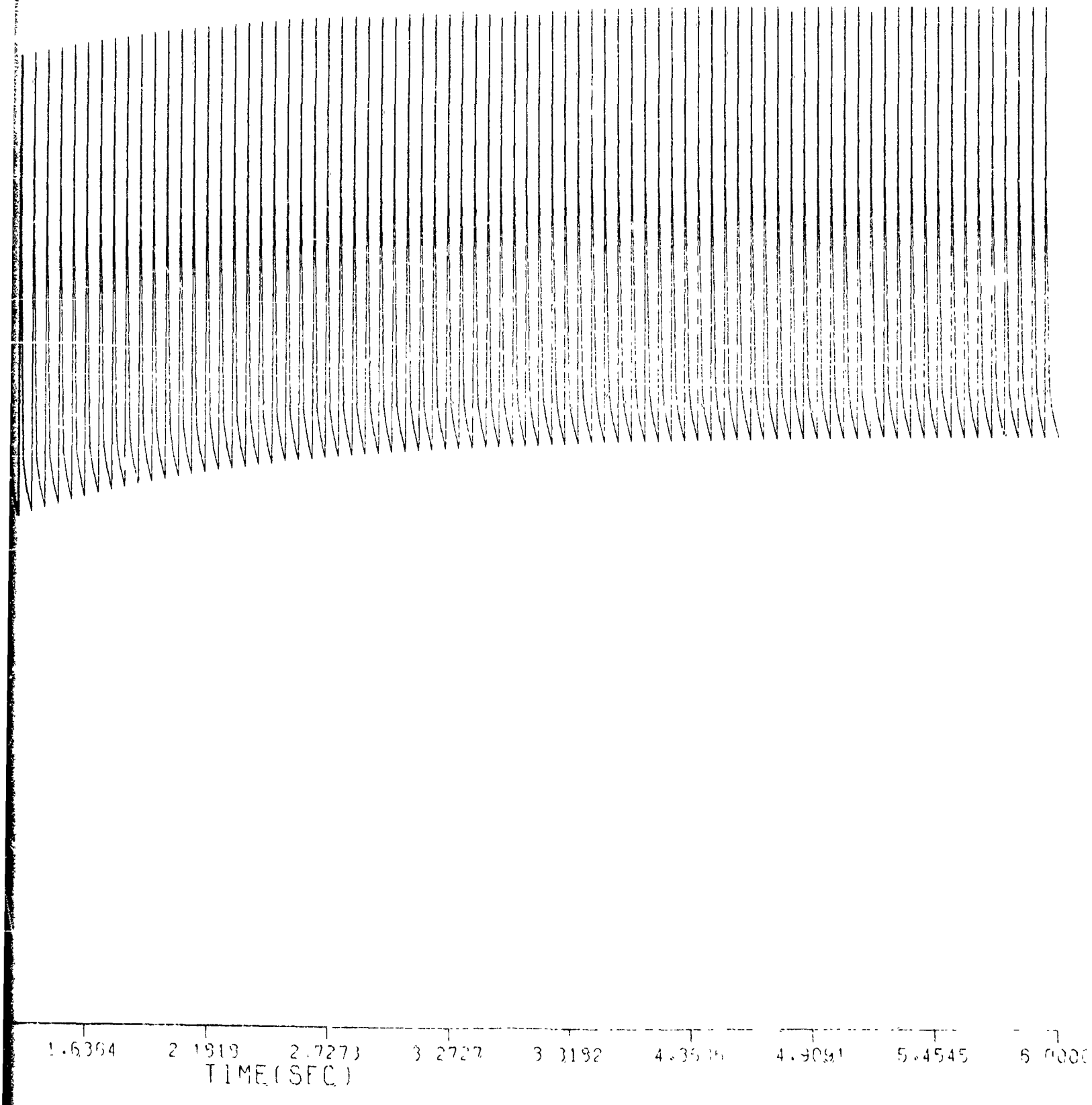

Figure 50. Repetitive Fire Wall Temperature Versus Time at Axial Position of 25 cm (0.060 second firing)

(The reverse of this page is blank.)

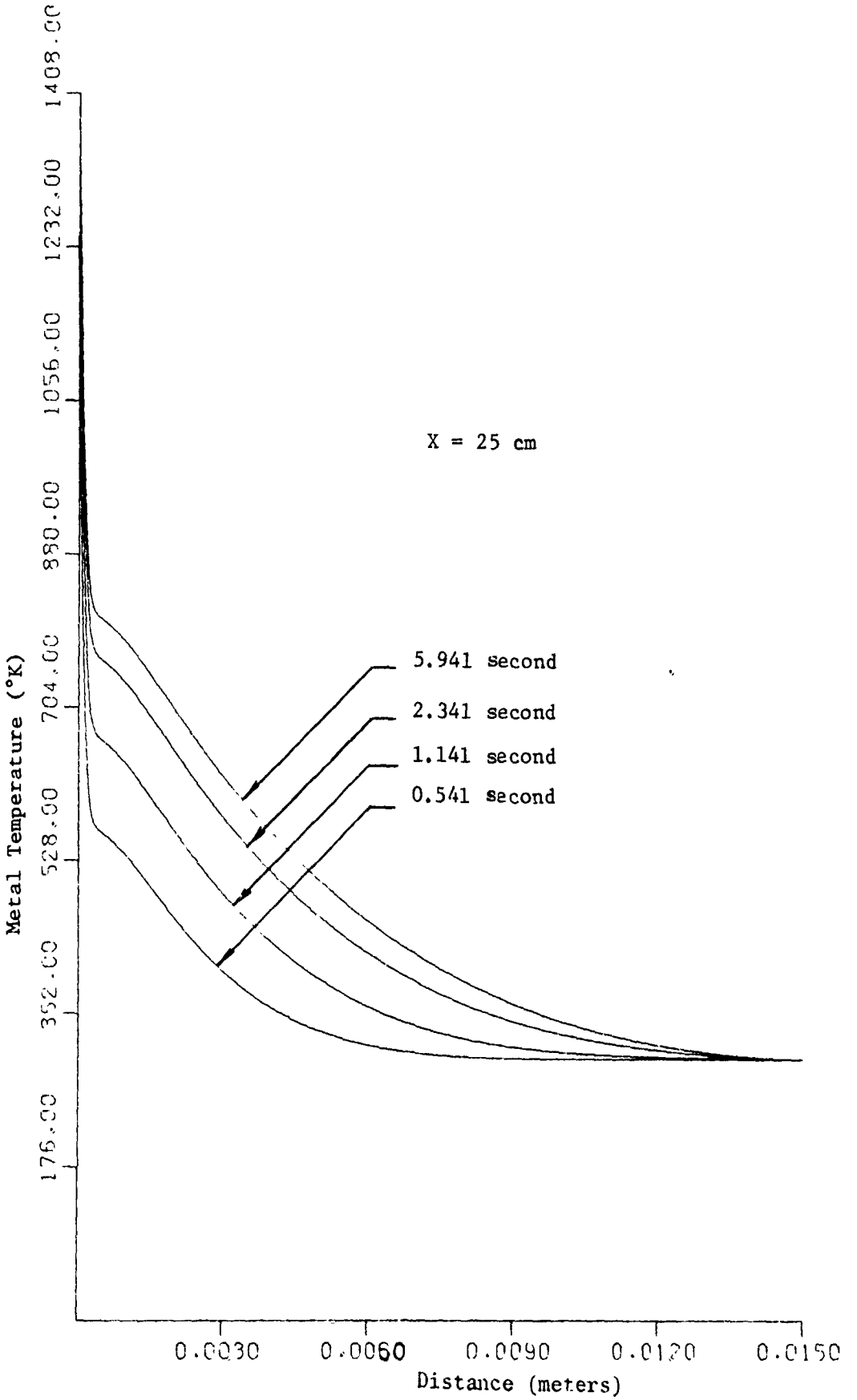

Figure 51. Variation of Repetitive Fire Wall Temperature with Depth at Axial Position of 25 cm at Various Times

(The reverse of this page is blank)

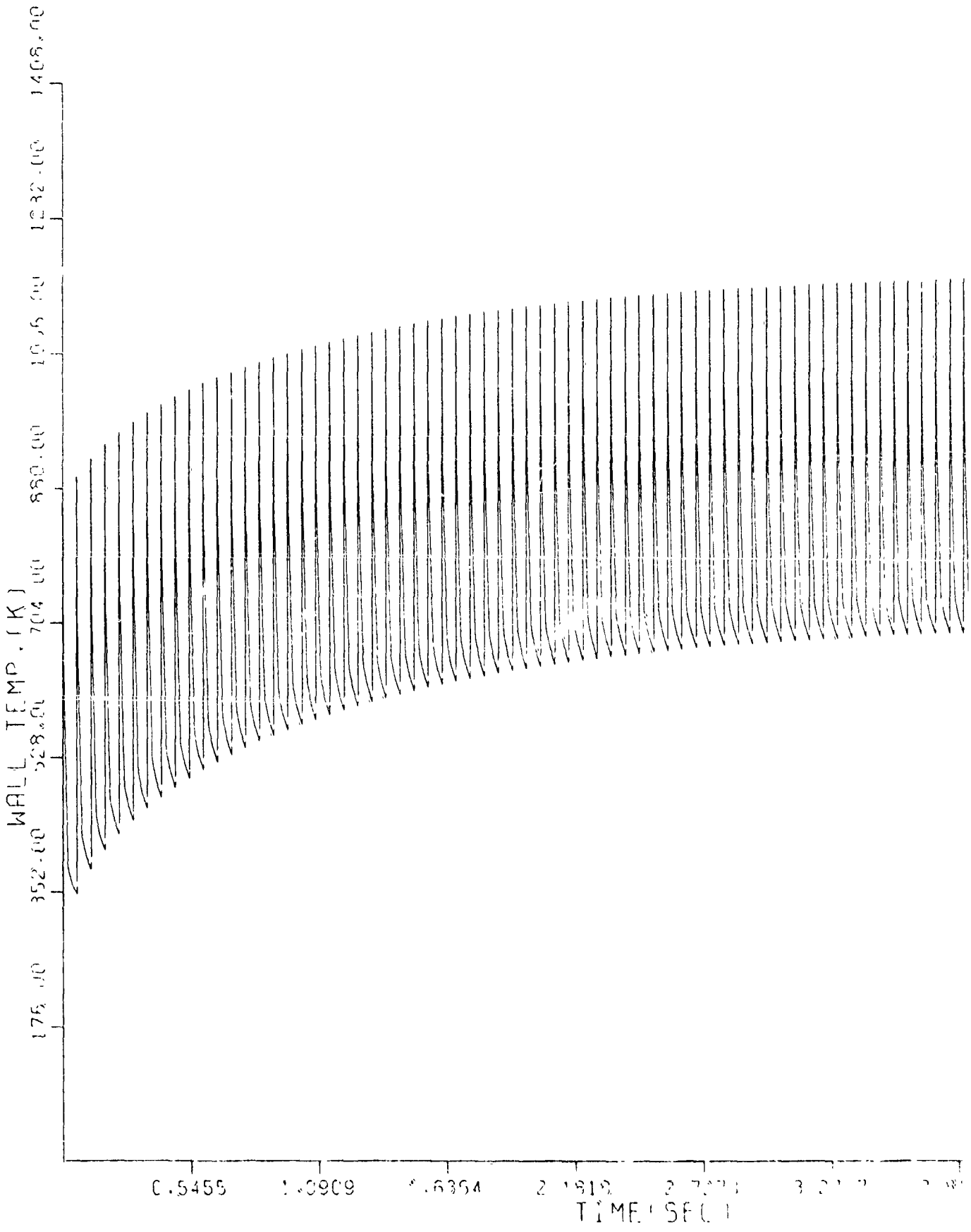

Figure 52. Repetitive Fi
of 12 cm (0.0

(The re

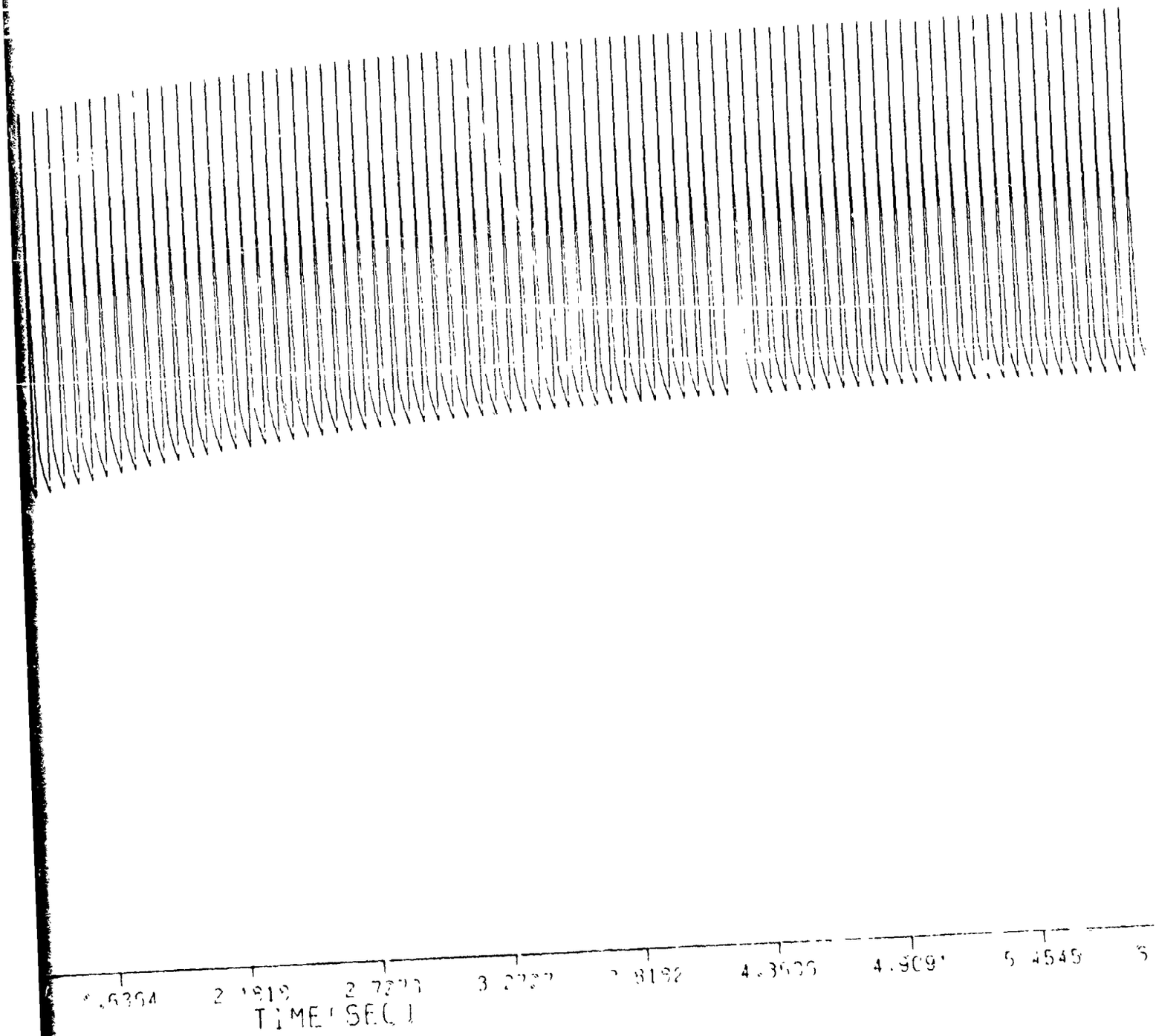

Figure 52. Repetitive Fire Wall Temperature Versus Time at Axial Position of 12 cm (0.060 second firing)

(The reverse of this page is blank.)

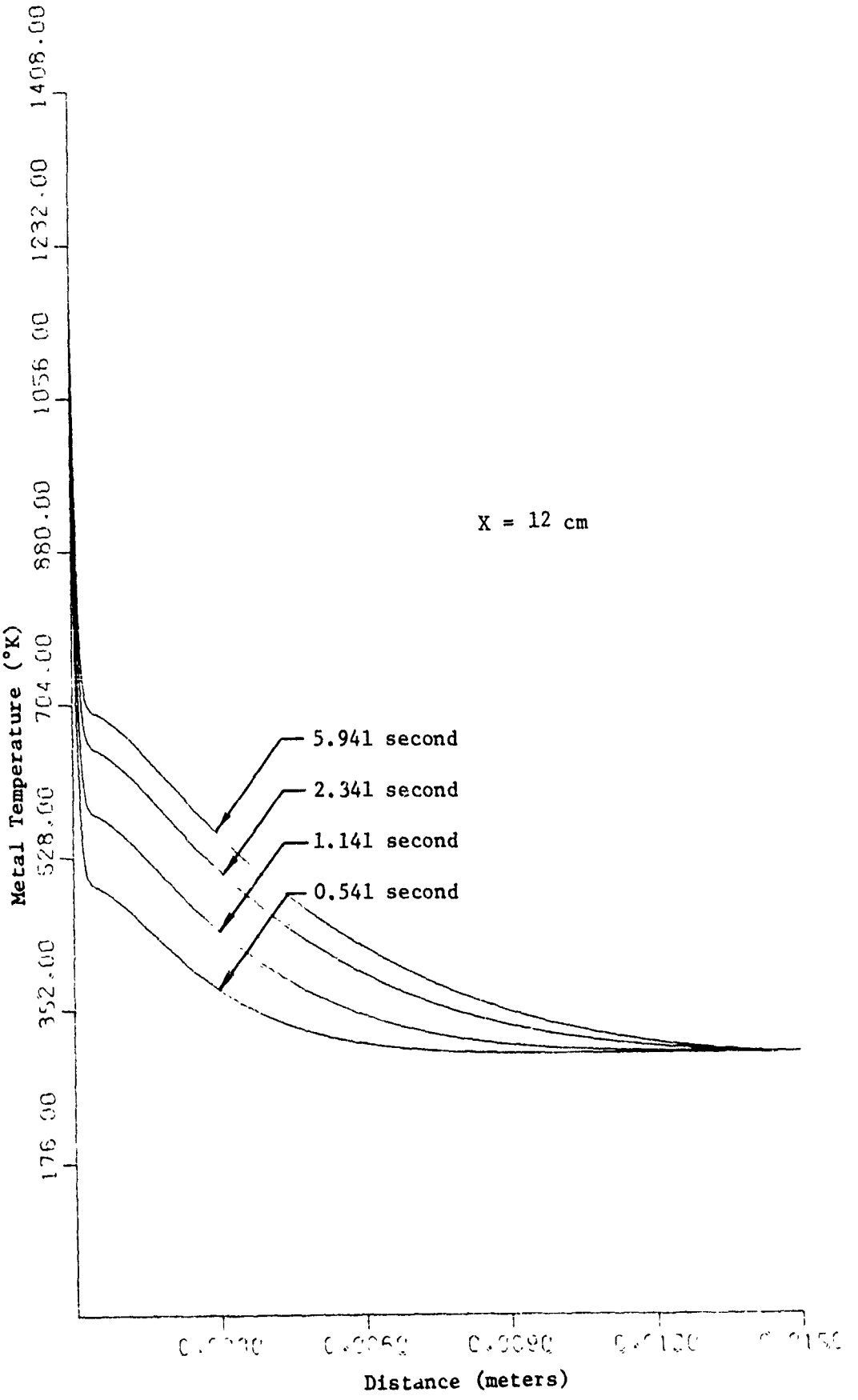

Figure 53. Variation of Repetitive Fire Wall Temperature with Depth at Axial Position of 12 cm at Various Times

(The reverse of this page is blank.)

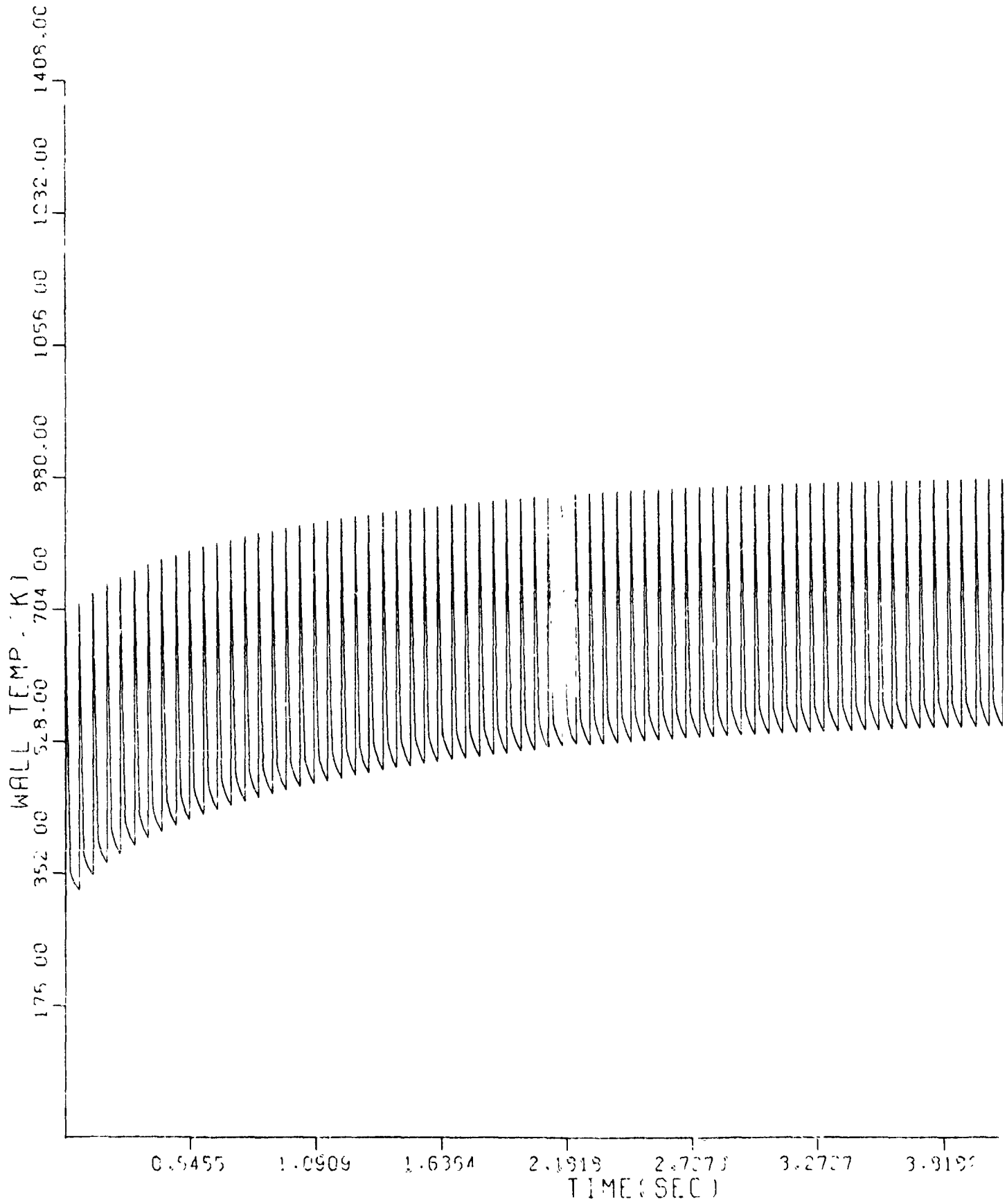

Figure 54. Repetitive Fire W
of 84 cm (0.060 s

(The reverse

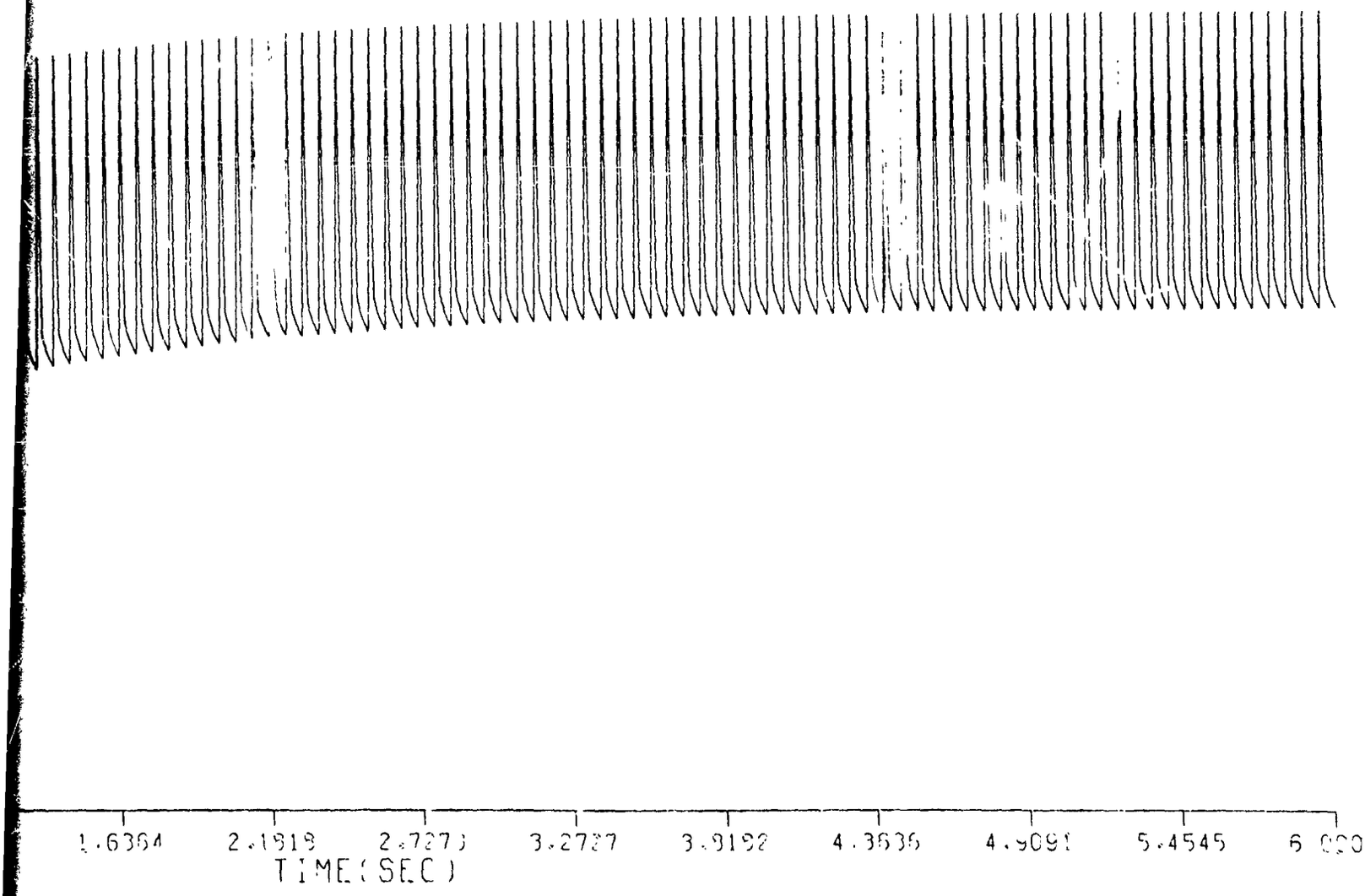

Figure 54. Repetitive Fire Wall Temperature Versus Time at Axial Position of 84 cm (0.060 second firing)

(The reverse of this page is blank.)

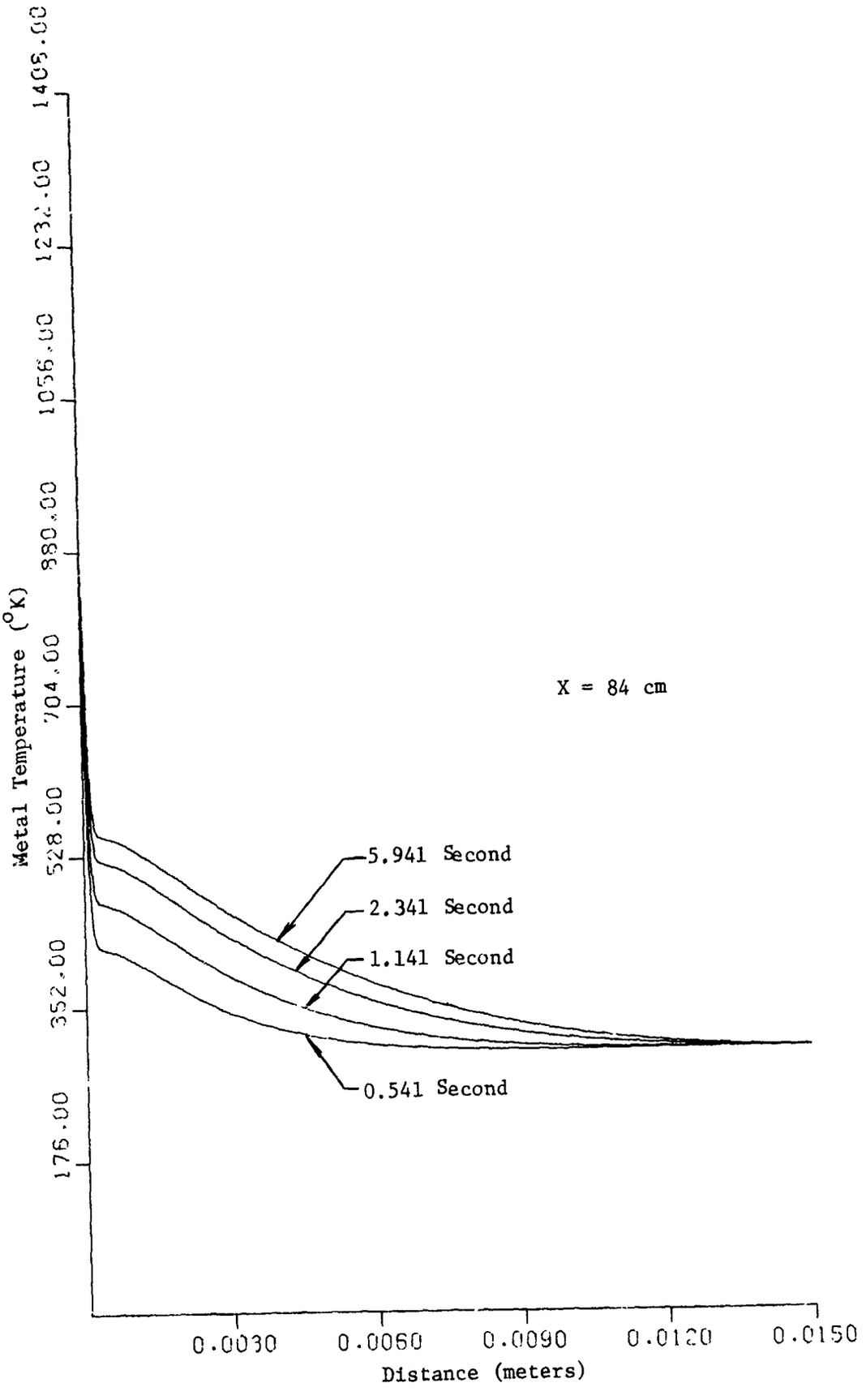

Figure 55. Variation of Repetitive Fire Wall Temperature with Depth at Axial Position of 84 cm at Various Times

Of course, with soaking time between series of 50-round bursts the outside wall temperature would rise and result in higher inside wall temperatures as well.

SECTION IX

PARTICLE SEEDING EFFECT ON TURBULENT BOUNDARY LAYER HEAT TRANSFER

Introduction

The section will be devoted to a discussion of the physical phenomena whereby certain additives (e.g., small titanium dioxide particles in a wax matrix dramatically reduce erosion in gun barrels. The limited open literature documents the effectiveness of several additives; however, no consistent physical explanation is offered, and no satisfactory mathematical model has been proposed.

Since hot gas erosion rates appear to be strongly dependent on temperature level, an effort has been made to relate erosion reduction to a reduction of the barrel inner surface temperatures. Some mechanism must be presented then which attenuates the heat transfer from combustion products to the gun barrel. Three distinct possibilities have been considered:

1. The additive significantly alters combustion gas properties so as to reduce combustion gas temperatures and/or heat transfer coefficients.
2. The additive particles reduce the turbulence level near the wall, thereby reducing the heat transfer coefficient.
3. The particles and/or wax matrix deposit on the wall, forming a protective coating which insulates the metal from the hot gas.

Effects of Additive on Combustion Products

The work by Lenchitz et al [29] indicates that TiO_2 is not involved in the combustion process, as the heat of reaction remains essentially the same when relatively large amounts of the micronized additive are included with the propellant. On the other hand, the addition of about 10 percent by weight of wax decreased the heat of reaction by about 10 percent. This is apparently due to a combination of reaction of wax with the explosion products and prevention of complete combustion of the propellant. Less reduction in heat of reaction is observed when TiO_2 is added to the wax, suggesting that the TiO_2 inhibits the interaction between the wax and combustion products of the propellant. There seems to be a trade-off between heat of reaction and quantity of gas such that the pressure is unaffected by the additives; hence, the interior ballistic properties are observed to be nearly the same.

From the heat transfer standpoint, the effects of interest are a probable lowering of the adiabatic flame temperature and a change in composition of the combustion gases. In addition, the gas temperature could be reduced due to sensible heating of the TiO_2 particles and wax [34].

The magnitude of this cooling due to the inert particles having to be heated to the flame temperature can be approximated by an energy balance on the gas-particle mixture. Since the heat transfer to the particles is equal to the heat transfer from the gas:

$$Q_{part} = -Q_{gas} \tag{155}$$

Using:

$$Q_{part} = Cp_{gas} M_{gas} \Delta T_{part} \tag{156}$$

$$Q_{gas} = c_{p_{gas}} M_{gas} \Delta T_{gas} \quad (157)$$

in Equation (155)

$$\Delta T_{gas} = c_{p_{part}} + M_{part} \Delta T_{part} / c_{p_{part}} M_{gas} \quad (158)$$

Since the combustion gas temperatures are around 2000°K and the particles start out at ambient temperature, ΔT_{part} is about 1700°K. Using $c_{p_{gas}}$ of 0.412 k cal/kg -°K, $c_{p_{part}}$ of 0.23 k cal/kg -°K, and M_{part}/M_{gas} of 0.05:

$$\Delta T_{gas} = -28^{\circ}K$$

This is obviously much too small of a gas temperature drop to result in a significant tube wall temperature reduction.

Effects of Particle Seeding on Turbulent Heat Transfer

There has been considerable interest in recent years in the fluid mechanical and heat transfer characteristics of suspensions, both liquid-solid and gas-solid. Gas-solid flows, for example, have been extensively studied during the past 15 years in connection with pneumatic conveying of solids, coolants for gas-cooled nuclear reactors, etc.

Liquid-Solid Suspensions

The technology of drag reduction phenomena dates back to 1945 when it was discovered that under turbulent flow conditions, gasoline-aluminum soap gels exhibited much less hydraulic resistance than untreated gasoline [35].

Since then, hierarchies of drag reduction effects have been found in liquids containing low molecular weight micelle-type additives, high

molecular weight polymers, and particulates. The decrease in drag or pressure drop is usually attributed to the non-Newtonian nature of the suspension. The solids absorb energy from the stream, thereby decreasing the turbulence level possibly to the point of laminarizing the flow.

In spite of the more than 400 references in the open literature, it seems that practical exploitation of this technology area has not yet been realized. Furthermore, there is relatively little information available regarding the heat transfer characteristics of these suspensions. The natural temptation, however, is to assume that heat transfer will be reduced in accordance with the analogy between heat and momentum transfer.

Alteration of Transport Properties of Particle Seeding.

It is appropriate at first to turn to experience on the dynamics of dense clouds of particles or dusty gases. The classical Einstein relation for an incompressible fluid containing solid spheres gives the viscosity as [36]

$$\mu_m = \mu_g (1 + 2.5\alpha) \tag{159}$$

where μ_m and μ_g are the viscosity of the mixture and pure gas respectively and α is the volume fraction of solids. In order to estimate the increase in viscosity due to solids addition, assume that TiO_2 is added in the large proportion of 20 percent by weight of propellant. Presume that the propellant undergoes complete combustion. The volume fraction of TiO_2, for no relative velocity between phases, is then

$$\alpha = \frac{M_s/P_s}{M_s/P_s + M_g/P_g} = \frac{M_s}{M_g}\frac{P_g}{M_g} \approx 0.2 \times \frac{0.05}{300} \approx 0 \tag{160}$$

where M is the mass of the solids, $(\ )_s$, or gas. $(\ )_g$. In other words, the loading ratio is too low to cause any significant increase in viscosity. Even if the local concentration at the wall were much higher, it is probable that the density would be sufficiently elevated so that the Reynolds number would be increased rather than decreased. The usual description of dusty gas flows is that the particle addition results in a flow of higher effective Reynolds number [37, 38]. The heat transfer coefficient would then be expected to increase.

This is consistent with theoretical and experimental work which suggests that particle-particle interactions, which could increase viscous drag, are negligible for particle volume fractions less than 0.05 [39].

Studies of Gas-Solids Suspensions (>10 μ Particles)

During the past 15 years several studies have been reported of heat transfer to (or from) gas-solid suspensions, with particle sizes generally in the 30 to 200μ range and with relatively large loading ratios. The results have been applied to numerous industrial applications, including coal-fired boilers, heat recovery equipment, solid propellant rockets, and gas-cooled nuclear reactors. Numerous investigators have reported a decrease in local heat transfer coefficients at low solids loading ratios. This observation is of direct interest to the present study.

Farber and Morley [40] made average measurements of heat transfer from a steam-heated tube to air-alumina catalyst mixtures. No consistent trend of decreasing coefficient can be discerned in the data, which exhibit considerable scatter at low loading ratios. It was noted that bulk temperature rises were lower (and ΔT_{lm}'s higher) with the

suspensions than for pure air; however, this effect was more than compensated for by the increased heat transfer coefficient, i.e., the heat transfer rate was always greater with solids addition.

One of the few analytical attempts was reported by Tien [4] who considered the case of mass loading ratios lower than about 1.0. A linear increase in local coefficient with loading ratio was predicted. In addition, the solid particles were expected to have negligible effect on heat transfer far downstream from the thermal entrance. Average predictions compared reasonably well with the data of Farber and Morley.

Farber and Depew [42] took average data which demonstrated a distinct decrease in coefficient at low loading ratios; however, no particular notice was taken of this behavior. The overall technique thus precludes a clear look at what is happening to the local heat transfer coefficient.

Depew and Farber [43] subsequently reported local data which clearly demonstrated decreases in heat transfer coefficients at low loading ratios, as shown in Figure 57. A theoretical analysis qualitatively predicted this decrease; however, the predicted decrease became negligible as the particle size was reduced to 30 microns, a trend which was contrary to the data. Tien and Quan [44] also took local data (Figure 57) which demonstrated the decrease in coefficient at low loading ratios. It was speculated that the particles altered the flow field.

Briller and Peskin [45] reported average measurements of heat transfer to gas-solids mixtures and suggested that there was no observable increase in heat transfer. This conclusion is perhaps justified considering the inordinately large scatter in data; however, a closer examination

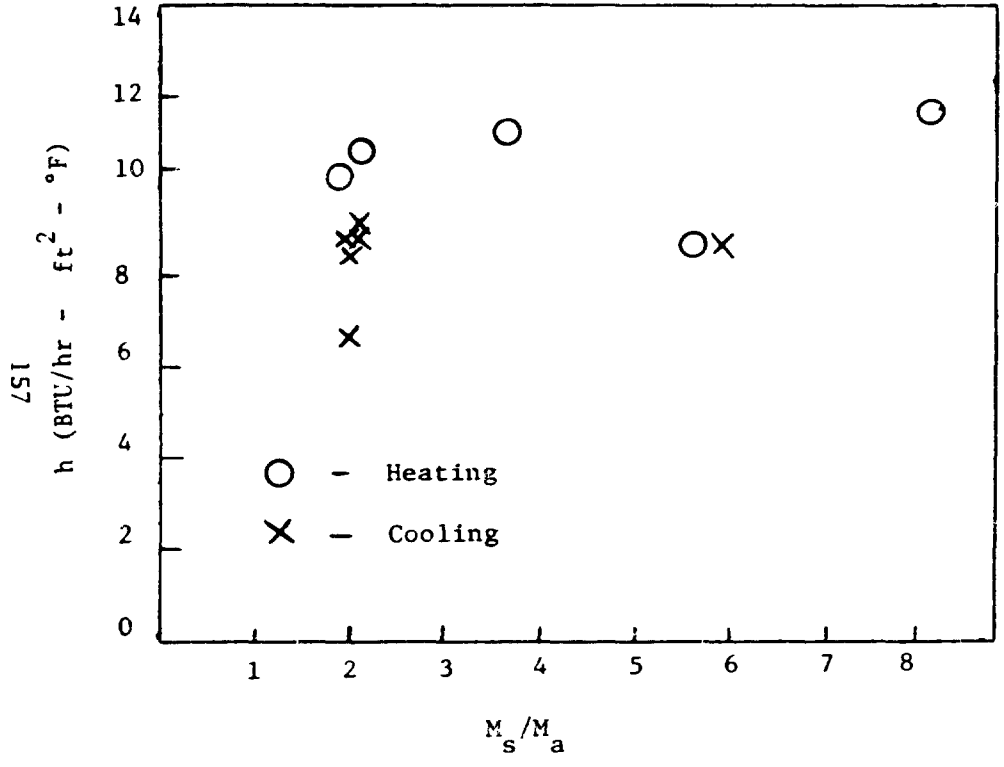

Figure 55. Heat Transfer Coefficient Variation with Particle Loading (Briller and Peskin)

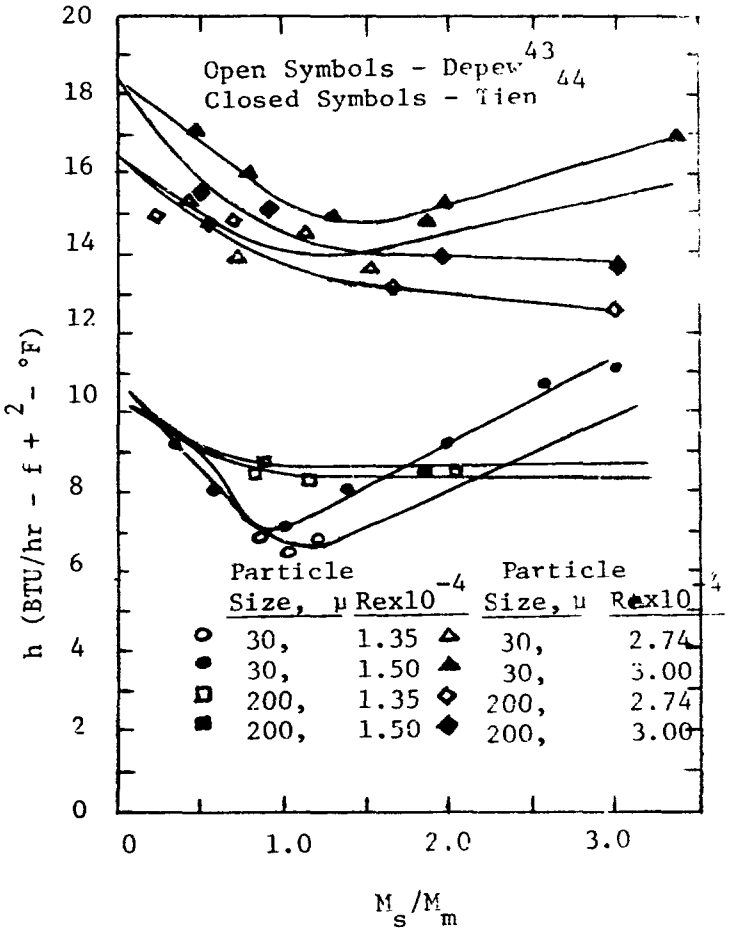

Figure 57. Heat Transfer Coefficient Variation with Particles Loading (Depew and Tien)

of the cooling data shown in Figure 56 suggests a distinct decrease in the coefficient at low loading ratio since the heating data exhibited no particular dependence on M_s/M. This could suggest that decreases are more pronounced with cooling.

Soo [46] has developed an interesting analogy explanation for the effect of solids on heat transfer at low loading ratios. The decrease in friction factor [44] in the presence of solid particles (Figure 58) is attributed to reduced mixing length due to dissipation by the solid particles. Upon introduction of the reduced shear stress into the Reynolds analogy, a Nusselt number - loading ratio expression is determined which is similar to the experimental behavior, as shown in Figure 59. While this approach is interesting, it serves only to express one dependent variable in terms of another; hence, little insight is given into the mechanism of transport process reduction.

Rossetti and Pfeffer [47] have recently reported friction data which are of interest in the application of the analogy concept. As illustrated in Figure 60, when glass beads of 10 to 60μ were added to air at Reynolds numbers of 10,000 to 25,000, friction factor reduction up to 75 percent was observed in horizontal test sections.* In order to clarify this effect, turbulence intensities were measured at the pipe centerline. The intensity of turbulence was always greater with solids addition, an effect which is in direct conflict with the drag reduction. It was postulated that the interaction of particles with the turbulence eddies actually occurs very close to the wall and that at the wall the turbulence decreases.

---

* It is noted that the reduction is real since the suspension friction factor is evaluated on the basis of the gas-phase density. Use of a suspension density will always yield a reduced friction factor.

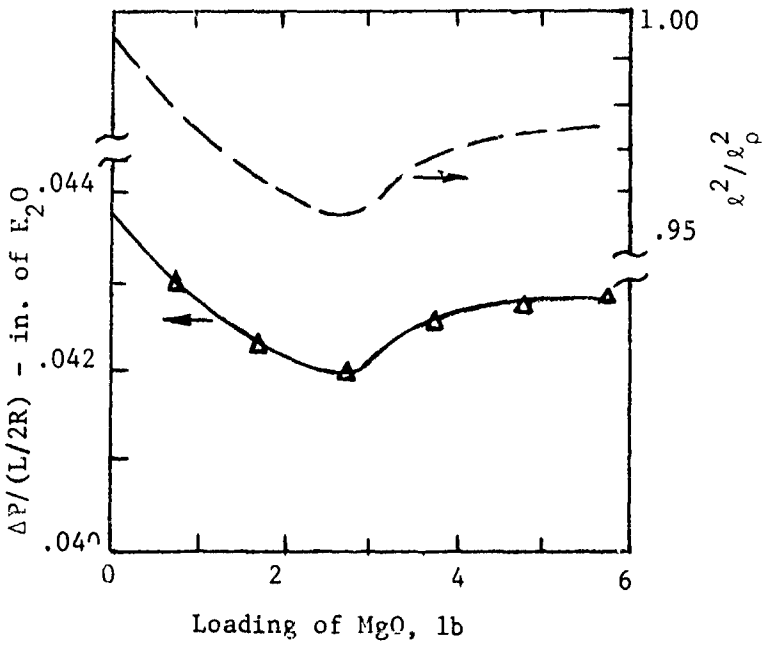

Figure 58. Effect of Particles on Pressure Drop (Soo[46])

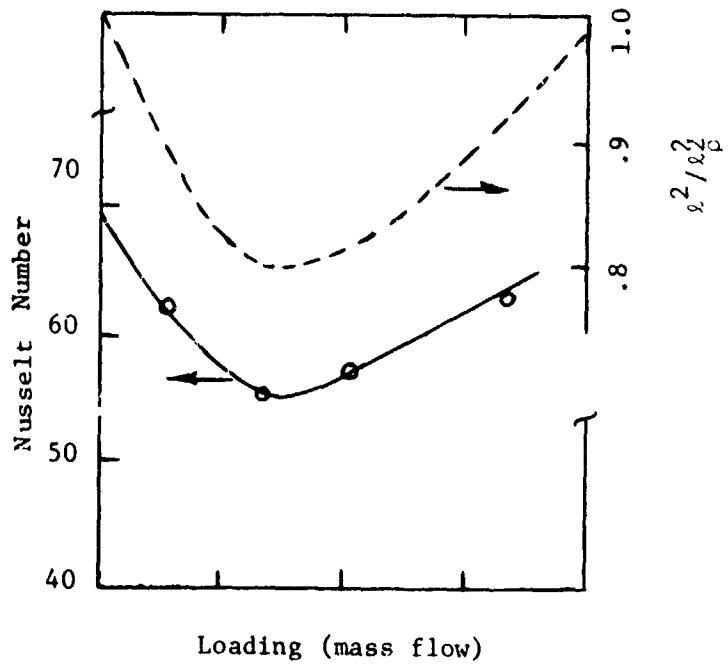

Figure 59. Heat Transfer Correlation for 30-μ Glass Particles at Pipe Flow Reynolds Number $3x10^4$ (Soo)

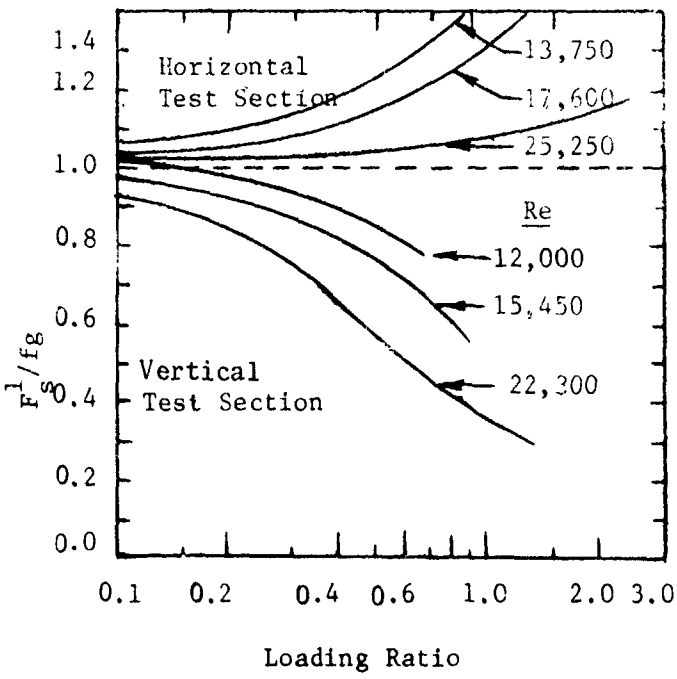

Figure 60. Friction Factor Ratio as a Function of Loading Ratio for 30μ Particles (Rossetti and Pfeffer)

Brandon [48] has also pointed out the need for wall turbulence measurements as a necessary step toward understanding friction and heat transfer behavior of gas-solids suspensions.

Survey Conclusions.

A detailed examination of the data suggests that the following conclusions can be drawn from the experimental studies cited above.

1. The decrease in heat transfer coefficient is generally larger with smaller particles [44].

2. The percentage decrease in h is smaller with higher Reynolds numbers [44].

3. The loading ratio at which the minimum h occurs seems to decrease as particle size is reduced; however, increases in Reynolds number shift the minimum to higher values of loading ratio [44].

4. The decrease in h is greater for lead particles than for glass particles [44].

5. Thermal entrance lengths are larger for glass particles than for lead particles, and are considerably larger for smaller particles. In all cases, however, the entrance length was increased over the pure gas value [44].

6. The decrease in heat transfer coefficient at low loading ratios appears to be more pronounced with cooling than with heating [45].

7. Several available analytical and semi-analytical studies of heat transfer and friction do not satisfactorily account for the observed reduction in heat transfer and friction at low loading ratios [41,46,49].

Observation 1 is encouraging as it suggests that still smaller particles (<30μ) would exhibit greater decreases in h. However, observations 2 through 5 are either nebulous or suggest a trend in the opposite

direction to what is desired to explain reduced heat transfer in gun tubes with seeding. Observation 6 is favorable; however, the data are too limited to draw firm conclusions. Finally, it is noted from observation 7 that the theory is of little help in suggesting what will happen with micron-size additives.

Studies of Gas-Solids Suspensions (~1μ Particles)

Particles in the size range of more direct interest have been employed in studies relating to augmentation of heat transfer in gas-cooled nuclear reactors. The general idea has been to add graphite to the helium coolant in such proportions as to appreciably increase the coolant specific heat and the heat transfer coefficient. Graphite is the normal additive since it will pose few problems for the circulating equipment; regardless of the size of addition, the particles shortly pulverize to an average size less than 1μ.

Schuderberg et al [50] summarized an extensive program at Babcock and Wilcox to study the characteristics of dispersions of micron-size graphite particles. Friction factors at higher Reynolds numbers dropped below the nominal value. It was suggested that flow turbulence was suppressed by the suspended particles. By analogy, heat transfer should be affected to a comparable extent. Unfortunately, the heat transfer tests were done only with loading ratios considerably in excess of unity.

Woodcock and Worley [51] summarized extensive English studies of boiler performance in a gas-cooled nuclear reactor system, where the CO_2 coolant was loaded with graphite. Only loading ratios greater than 4 were considered, and the average heat transfer coefficient for

the tube bank always increased. One interesting aspect of their work was that the effective particle sizes appeared to be much larger than those of the basic particle. It is doubtful, however, that the loading ratios encountered with barrel wear-reducing additives are high enough for the mixture to exhibit this effect.

One of the more serious difficulties encountered with gas-graphite suspensions is the deposition of the solids on cold surfaces [52]. This is apparently due to a combination of Brownion motion and electrostatic effects. For the present application, this observation suggests that particle concentration near the wall will be relatively high. It would seem, however, that the high velocities and short firing times would tend to limit the buildup of as heavy particle layer as is experienced in gas-cooled reactor system tests. The effects of any particle buildup will be examined in the next section of this report.

The IITRI Analysis

In 1966 the Illinois Institute of Technology Research Institute was awarded a contract by Picatinny Arsenal to explain the mechanism by which an additive reduces gun barrel erosion. While the primary emphasis in this investigation was devoted to tests with a vented chamber, an analytical model was also developed as described in the summary report by Remaly and Stanley [52].

The basic premise of this model is that reduced erosion is related to a reduction in heat transfer from the gas to the metal. Following the qualitative explanation offered for reduction of transport rate with solid-liquid and gas-solid suspensions, turbulent damping was hypothesized. The gas particles were assumed to be in simple harmonic motion; the

particles then interact with the gas through a dasnpot that represents the drag. The equations of motion were then solved numerically for various spectra of turbulence. The output parameter of interest is the loss of turbulent kinetic energy due to injection of the particles. The rate of energy loss was then computed for various particle diameters (0.1 to 10 microns), densities (2 to 8 g/cc), and concentration (2 to 9 percent by weight). Computations were limited by computer running time to the first three cycles of gas oscillation (about 100 μsec). Typical increases of 5 percent were found in the boundary layer thickness.

The computations indicated that turbulent damping increases with particle diameter, density, and concentration. Typical results are shown in Figure 61. The experimental program was then designed to provide at least a qualitative verification of the analytical model.

Controlled Firing Tests

IITRI Tests

Remaly and Stanley [52] tested the effects of various propellant additives in a 37 mm vented chamber. Additive effectiveness was by measuring wear of an orifice-type plug.

A variety of additives was tested for multiple firings since weight loss data from single shots were inconclusive. No wax was utilized in tests presented in this report, and the additives were introduced in such a fashion that good mixing with the explosion products was obtained.

All of the additives (TiO_2, talc, WO_3, and microballoons) were found to be effective in reducing erosion of the orifice insert. The data shown in Figure 62 are typical of the results obtained. Low density

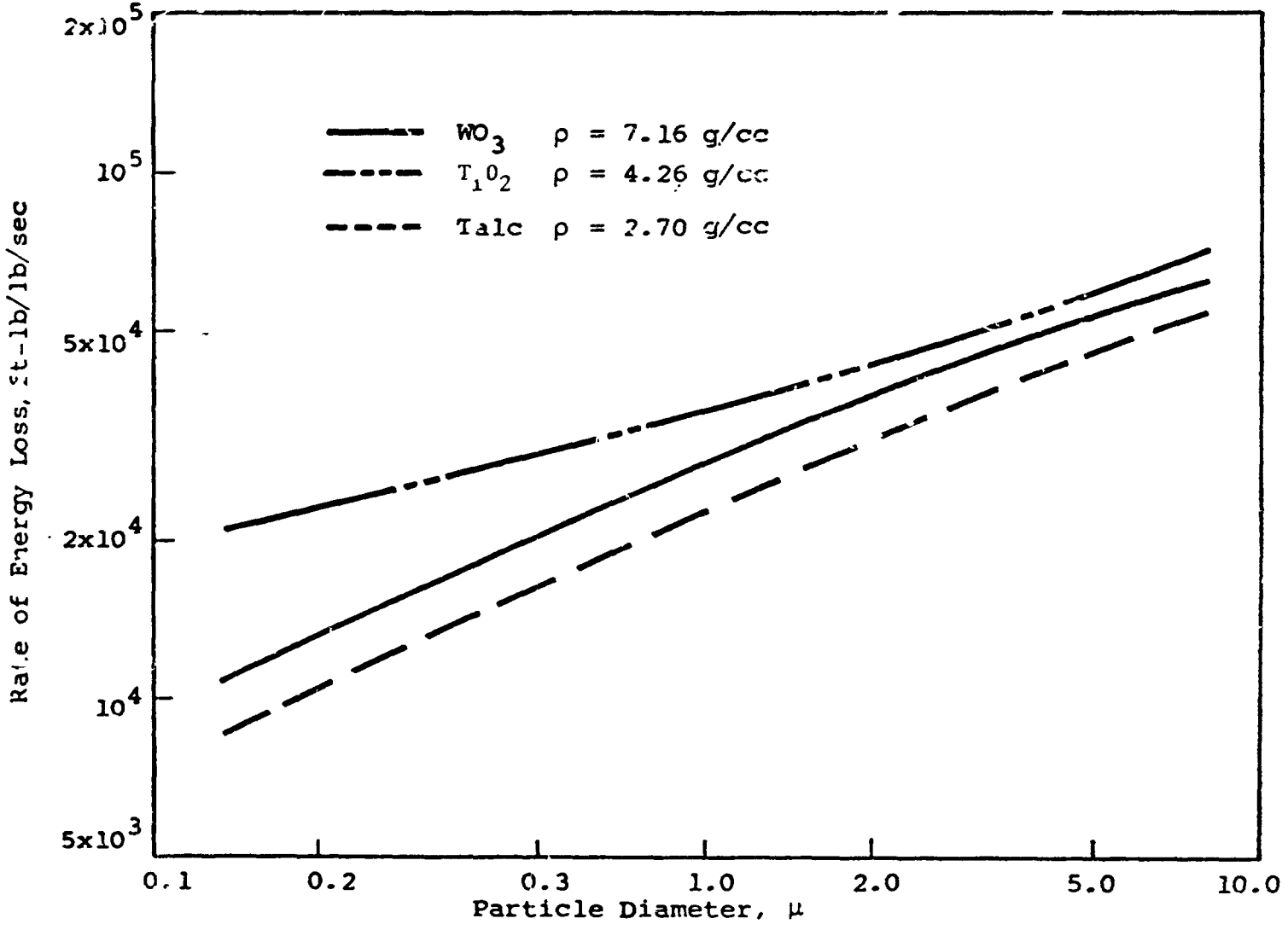

Figure 61. Rate of Energy Loss Versus Particle Diameter With T_iO_2, WO_3 and Talc (Remaly and Stanley)

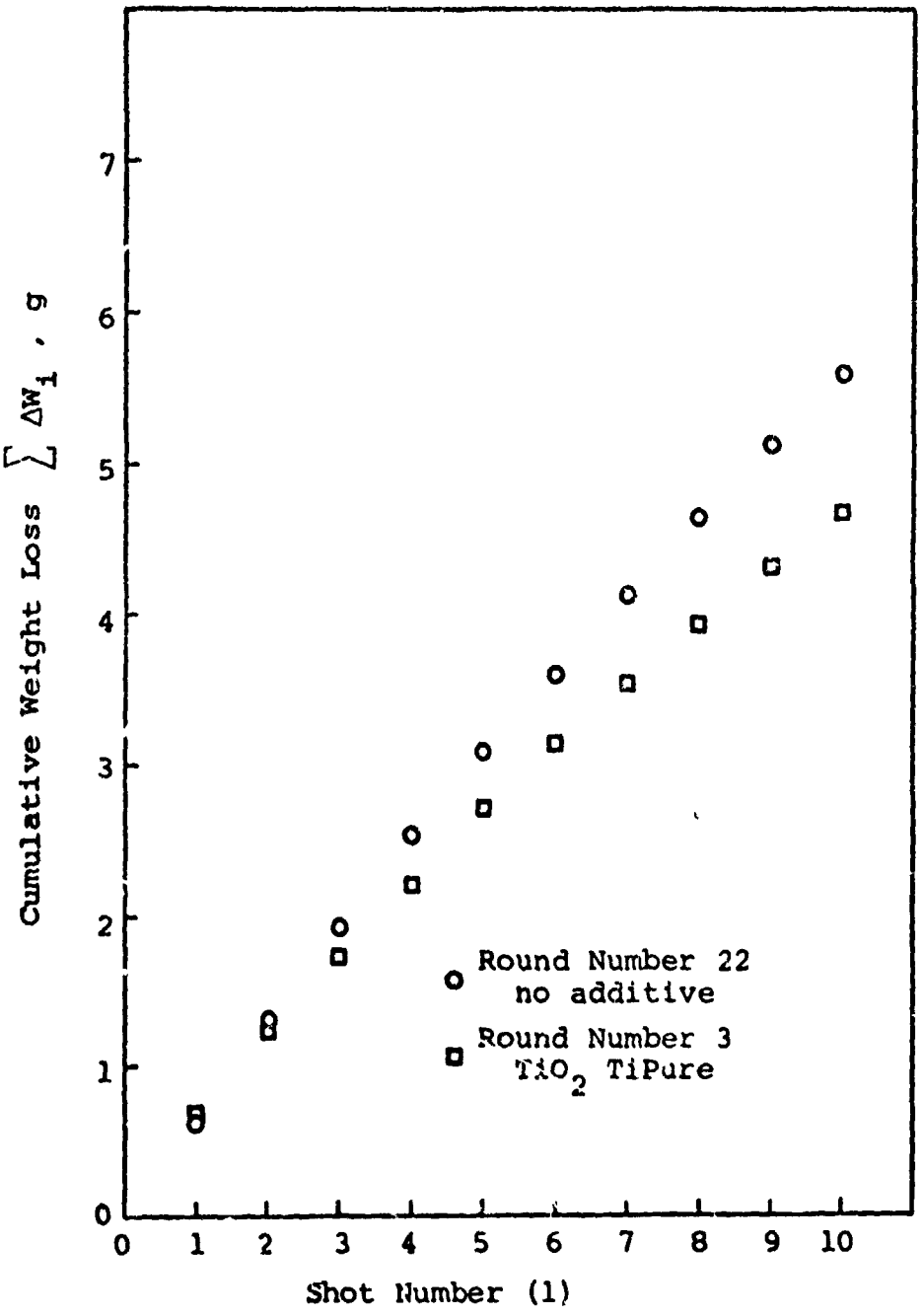

Figure 62. Cumulative Weight Loss Versus Shot Number (Remaly and Stanley)

materials were found to be the most effective in contrast to the results of the model described in the previous section. Furthermore, small particles gave greater erosion reduction, which was again an effect opposite to that predicted (Figure 61). A re-examination of the model was thus suggested. This leads one to suspect that the basic premise of turbulence alteration may not be correct.

One of the incidental observations of these tests was concerned with a residue in the orifice insert. This propellant residue was apparently substantial since soaking in a chlorinated hydrocarbon solvent was necessary to remove it before the weight was recorded. While no indications of the thickness, composition, or influence of the residue on erosion were given, it seems reasonable to expect that the residue could play a role in reducing the erosion.

Picatinny Arsenal Tests

The Swedish Additive, titanium dioxide or tungsten trioxide in a wax matrix, was adopted for U.S. military application in 1961. This additive was highly effective in reducing (up to 90 percent) bore erosion in a variety of gun barrels. The empirical results of previous tests reported by Swedish consultants indicated that many metal compounds have wear-reducing properties. The percentage composition of the metal compound and wax and the location of the coated cloth liner were found to be important.

Several reasons were suggested for the effectiveness of the additive. The wax component vaporizes and forms a cool insulating gas layer along the wall, the metal oxide particles in the flow have a high reflectivity and reduce radiant heat transfer from the propellant gas to the tube, and the metal oxide particles form a protective coating on the tube wall

so as to reflect heat away from the surface.

Extensive tests were undertaken at Picatinny Arsenal to evaluate various additives and suggest a mechanism for reduced erosion which is consistent with the test firing data. The first major report issued is by Wolff [26] who described extensive tests with 90 and 105mm tank ammunition. The results of a preliminary series of tests with WO_3 wax additive and a full series of test with TiO_2 wax additive are summarized in Figure 63. Control tests with no additive and with wax additive only are also indicated. The general conclusion is that any additive is better than ordinary untreated ammunition. The Swedish-type additives are definitely superior to the other laminar coolant. The TiO_2 additive seems to be better than the WO_3 additive; however, a larger number of firings for the WO_3 would seem to be necessary to confirm this finding. Most surprising perhaps is the observation that the plain wax is also reasonably effective.

This report is strictly empirical and does not pursue the mechanism of barrel wear reduction. The mechanism advanced by the Swedish consultants concerning reflection of radiation is not a reasonable explanation because the radiative heat transfer from the gas to the tube is negligible compared to the convective heat transfer. The maximum radiative heat transfer is given by:

$$q_{rad} = \sigma (T_{gas}^4 - T_w^4) \qquad (161)$$

which for T_w of 500°K and T_{gas} of 2000°K yields a q_{rad} of 20.6 kcal/m^2-sec compared with the average convective heat flux calculated in Part I of 50,000 kcal/m^2-sec.

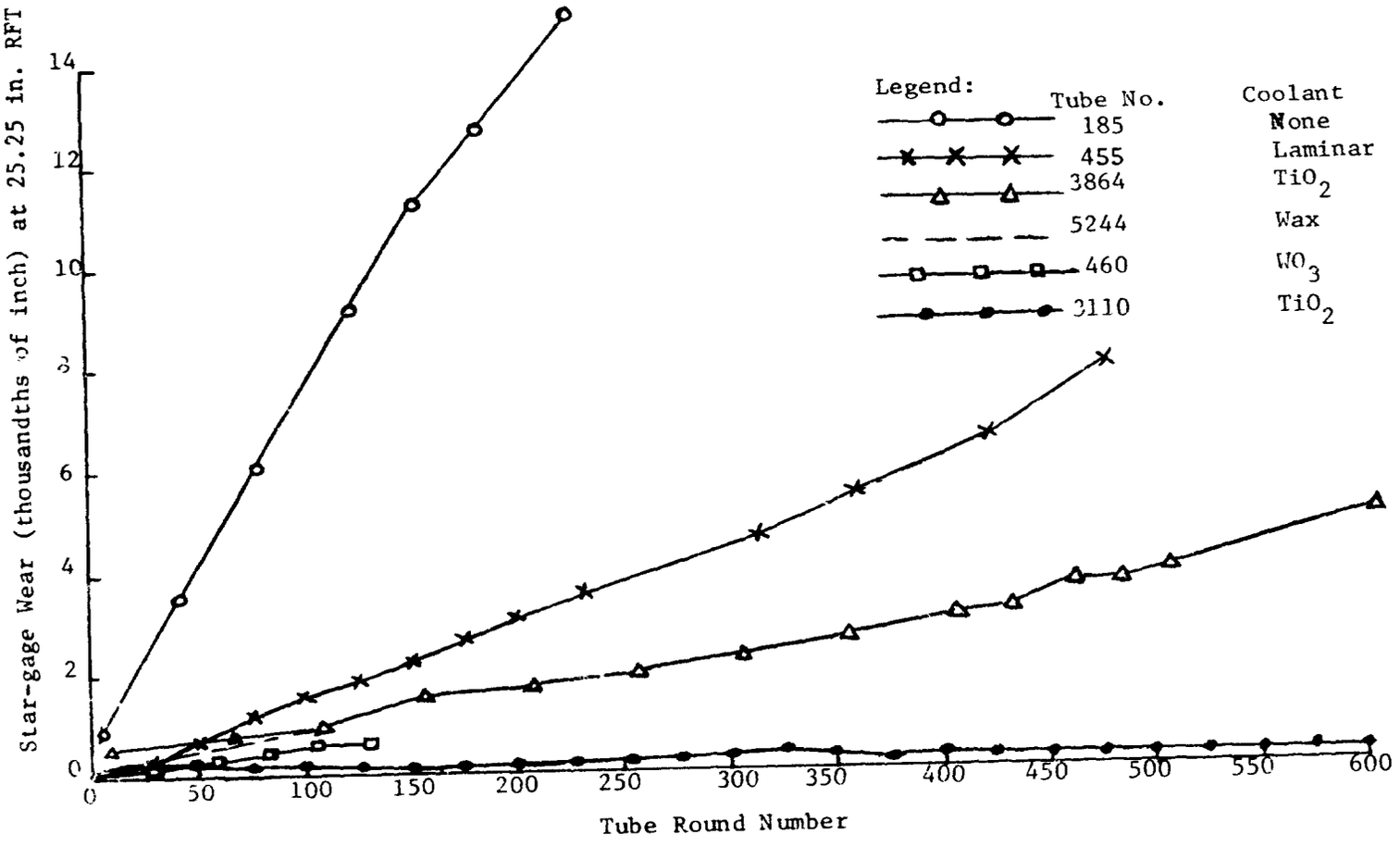

Figure 63. Comparison of Tube Wear Versus Number of 105mm APDS-T, M392 Rounds Fired in M68 Gun Tubes (Wolff)

On the other hand, the existence of a residue on the barrel wall is significant. The coating was readily removed before measurements were made. For the main series of tests a chemical analysis indicated that the coating was mainly TiO_2.

Subsequent tests at the Picatinny Propellants Laboratory were reported by Lenchitz et al [36]. Their conclusions relating to the effect of additives on the combustion products is given early in this section of the report. While this effect tends in the right direction, the coating effect of the additive appears to be of greater significance. Lenchitz and his co-workers suggested that the wax is the prime factor in building up an effective insulating coating. The role of TiO_2 was considered to be that of strengthening and permitting proper dispersion of the wax. The test results with a 3/8-inch vented chamber (see Table V) abstracted from their work was used to justify this conclusion:

TABLE V. EXPERIMENTAL EFFECTS OF ADDITIVES ON EROSIVITY

Sample	Proportions	Erosivity mg at 16,000 psi (5-shot average)
M-2 Propellant	35g	24.1
Propellant + TiO_2	35g + 2g	19.0
Propellant + wax	35g + 2-4g	2.8
Propellant + wax/TiO_2 (55%/45%)	35g + 4g	0.9

The wax is clearly indicated as the major erosion reducer. In addition to small chemical effects, the thermal insulation of the carbonized wax was

considered to be important.

Taking an overall look at the Picatinny Arsenal test, it is reasonable to conclude that barrel wear reducing additives produce a deposit on the tube wall which thermally insulates the metal from the hot combustion gases. This is consistent with the observation that either wax alone, TiO_2 (WO_3) alone, or TiO_2/wax (WO_3/wax) reduces erosion. In all cases a deposit was noticed on the barrel. The IITRI tests mentioned previously are in substantial agreement for the effects of TiO_2 and WO_3 as well as for talc and microballoons. It now remains to demonstrate that thin layers of any of these materials can produce sufficient reduction in metal temperature to inhibit erosion.

SECTION IX

MECHANISMS FOR REDUCED EROSION WITH TiO_2 PARTICLES

Introduction

In light of the repetitive firing analysis and the survey of the dusty gas heat transfer literature, the possible mechanisms by which reduced erosion may result from TiO_2 seeding of the propellant was studied for their plausibility. The fact that the repetitive firing analysis showed that temperatures on the inside surface of the barrel may reach the metal melting temperature plus the findings in the literature led to concentrating efforts on two wall temperature reducing mechanisms. The first to be discussed is the reduced heat transfer coefficient resulting from the particles reducing the turbulence level and the second is the insulation of the tube wall by particles forming a packed bed in the crevices of the tube surface roughness.

Reduced Heat Transfer Coefficient

As shown in the previous section, the literature in the dusty gas area does not include any experimental data for the Reynolds numbers range ($\sim 10^8$) and particle size (<1 micron) applicable to the present gun problem. Also, all experimental work has been carried out at steady conditions, while the gun flow is highly unsteady.

However, it can be seen from Figures 56 through 60 that a reduction in the heat transfer coefficient of around 20 percent has been demonstrated in several cases. There are also indications that the higher Reynolds numbers and smaller particle sizes may lead to an even higher

reductions in the heat transfer coefficient, h, particularly at light loadings. It may thereby be argued that a 20 percent reduction in h might occur with the addition of TiO_2 to gun propellants. There is evidence that it might possibly occur but no experimental proof that it does. The plausibility of a 20 percent reduction in h causing a sufficient reduction in the wall temperature to produce a reduced erosion rate was studied.

The model and program for calculating heat transfer and temperatures in the tube presented in Section II was used for this calculation. The h which the program calculated was reduced by 20 percent and this reduced h was used in the heat conduction analysis to find the tube wall temperature.

The results are shown in Figure 64 where the wall surface temperature is displaced as a function of time. The peak temperature at the hottest location (x=25 cm) is shown to be about 950°K compared to 1050°K from the normal heat transfer coefficient results shown in Figure 27.

This 100°K drop which would result for the 20 percent lower h value would appear to be large enough to substantially reduce the erosion.

This is particularly true when we consider that the temperature-related erosion mechanism would be expected to have somewhat of a threshold temperature. Above this threshold temperature the metal would possibly be liquid so as to erode away easily, whereas below this temperature the metal would be solid with strength to resist erosion. This 100°K reduction could bring the metal surface below this threshold temperature and thereby substantially reduce the temperature-related erosion. The remaining erosion would be primarily related to other mechanisms such as chemical or friction. This could explain the factor of 10 reduction in erosion rate experienced in tests using TiO_2 additives, however, many assumptions would have to be verified to inclusively show this.

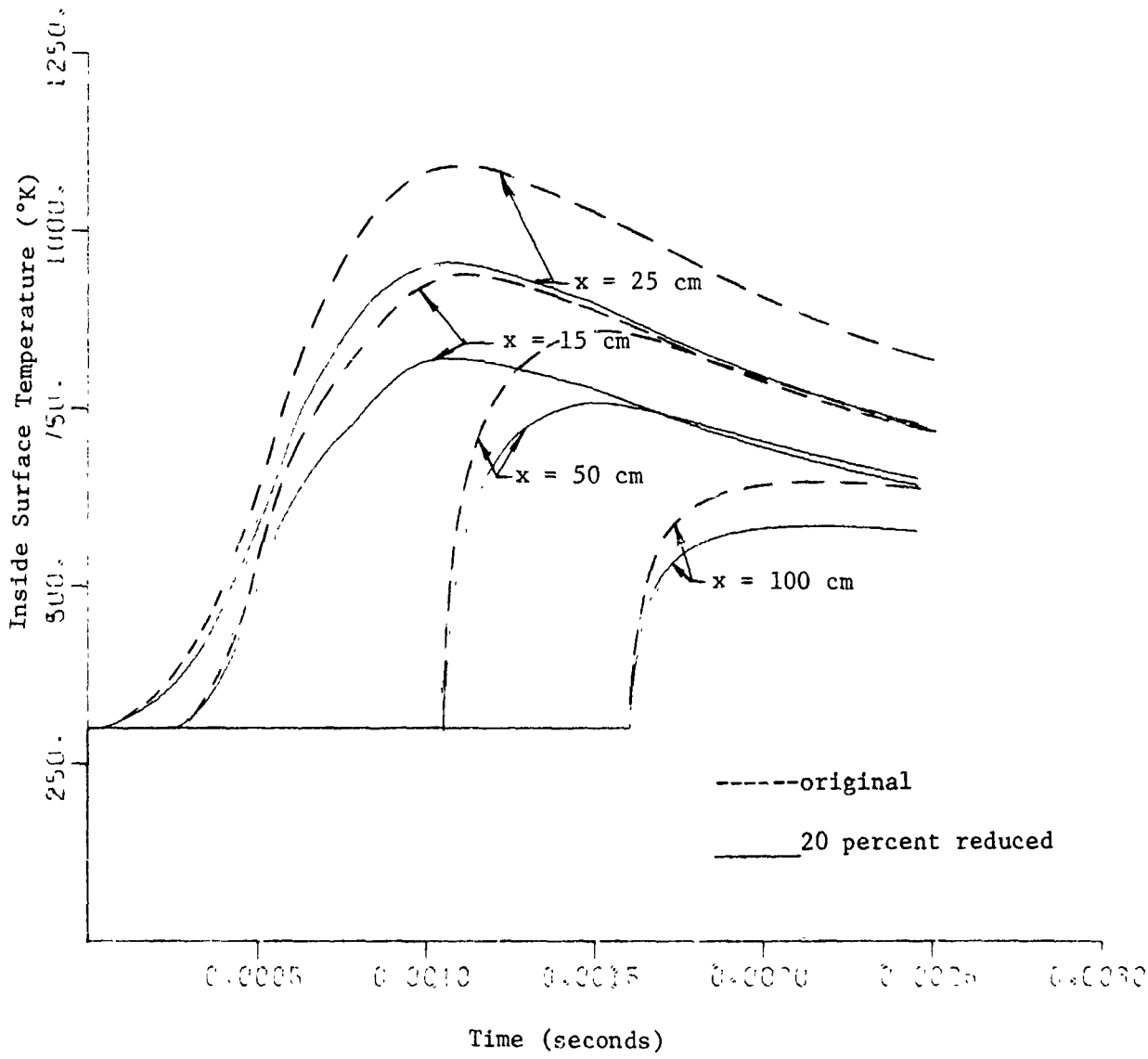

Figure 64. Variation of Wall Surface Temperature at Certain Fixed Locations with Time (Case I, 20 percent Reduced Heat Transfer Coefficient)

Insulation Effect

In order to assess what the effect an insulating layer of TiO_2 particles forming on the tube surface would have on the wall temperature, the model and computer program were modified. The increased thermal resistance was included in a new effective convective heat transfer coefficient h_{eff} given by:

$$h_{eff} = \frac{h}{1 + h(\Delta L/K)_{ins}} \qquad (162)$$

where ΔL is the thickness of the insulating layer and K_{ins} is the thermal conductivity of the insulation.

The order of magnitude of ΔL can be found by considering the surface roughness of the tube wall and assuming the interstices are filled with TiO_2particles. These interstices are on the order of 5 to 10 microns (0.0002 to 0.0004 inches) into which the micron size TiO_2 particles can be packed forming a packed bed 5 to 10 microns thick. The order of magnitude of the thermal conductivity for packed beds is around $4x10^{-4}$ kcal/sec-m-°K. This low value for packed beds is due to the voids existing between the individual packed particles.

The results of the calculations for a single shot firing are shown in Figures 65 and 66 assuming 5 and 10 microns for ΔL, respectively. This calculation should be compared with Figure 27 in Section II which is the identical case without insulation It can be seen that the effect of TiO_2 particles embedded in the surface roughness crevices is to lower the peak metal surface temperature from about 1050°K shown in Figure 27 to

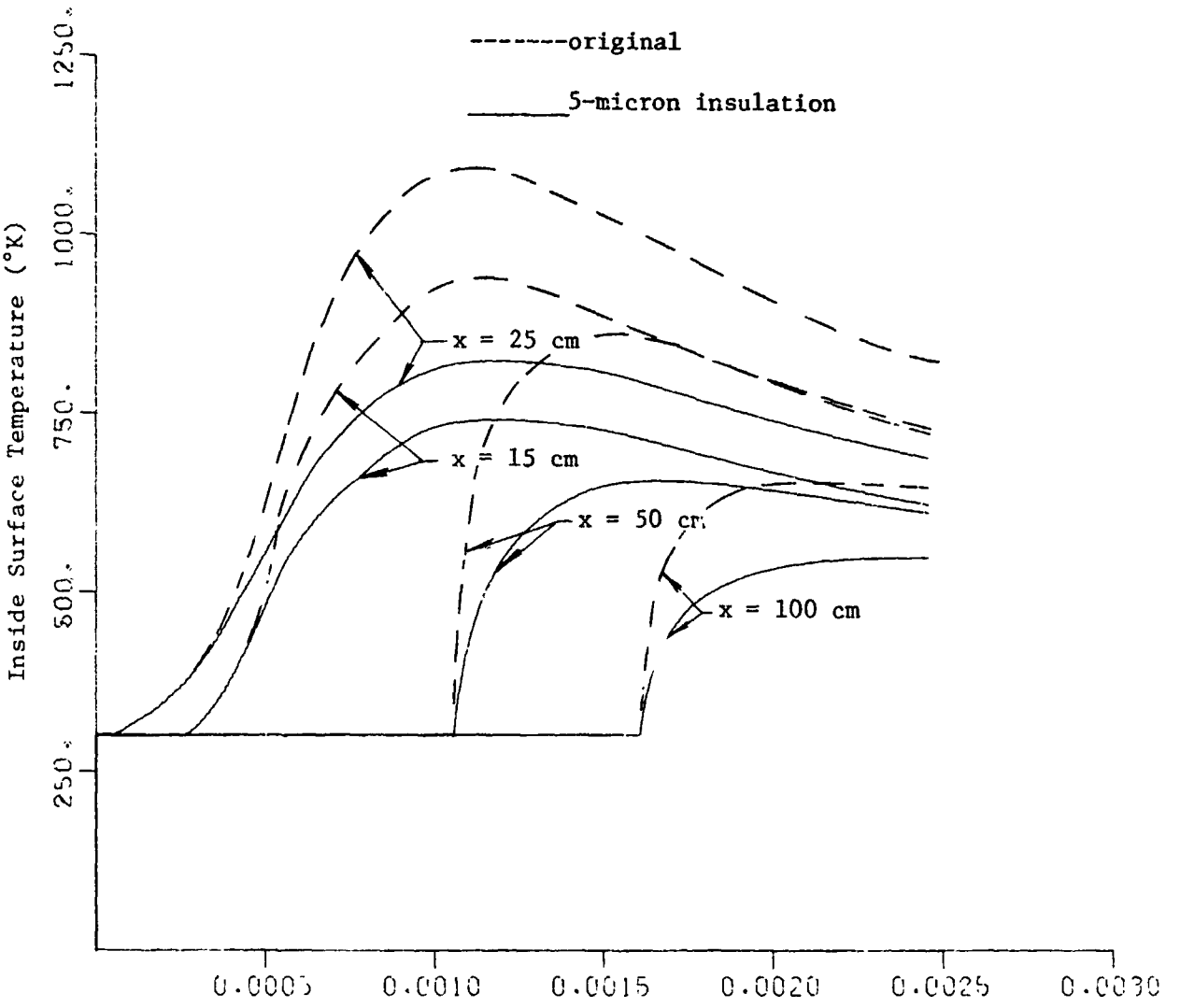

Figure 66. Variation of Wall Surface Temperature at Certain Fixed Locations with Time (Case I, 5-Micron Insulation)

825°K for 5 microns of insluation or 650°K for 10 microns of insulation. This is a very substantial decrease of 225°K and 400°K in the metal temperature and should account for the decreased erosion rate.

In order to further assess the plausibility of this hypothesis, a calculation has been carried out to determine the mass of TiO_2 particles necessary to coat the tube with a 5-micron-thick layer. Taking the barrel dimensions used throughout this work of 200 cm in length and 3cm inside diameter, along with a packed bed TiO_2 density of 4 gm/cm^3, yields a mass of 3.8 gm of TiO_2. For the propellant loading of 172 gm, this is about a 2 percent loading fraction compared to typical loading fractions of 5 percent. Therefore, there are adequate TiO_2 particles in the propellant so that after only a few firings the interstices of the surface roughness can be filled with an insulating layer of TiO_2 particles.

SECTION XI

CONCLUSIONS

The following conclusions can be drawn from the findings presented in Part II of this report.

1. Repeated firings every 60 milliseconds produced increasing gun tube wall temperatures to 1500°K after fifty firings. At this time (3 seconds) the thermal wave does not reach the outside of the 1.5-cm-thick wall. Repeated firing bursts could produce temperatures high enough to cause melting of a very thin layer of metal inside the tube. Even after 50 firings, the temperature drops very rapidly with increasing distance from the inside wall surface, i.e., with a surface temperature of 1500°K, at a depth of 0.1mm below the surface the temperature is typically below 800°K.

2. A review of the existing literature concerning experimental measurements on dusty gases reveal that a reduction in wall friction and convective heat transfer is possible in many cases of lightly loaded dusty gases. Reductions up to 30 percent have been measured in some cases. However, no experimental measures of any kind are available which are applicable to the gun tube gas flow problem.

3. Available experimental data on gun propellant additives containing micron size particles all produce evidence of a deposit on the inside surface of the gun tube.

4. If a reduction of the heat transfer coefficient of 20 percent were caused by the presence of micron-size particles in the

combustion gases, the inside wall temperature would be reduced by about 100°K. This 20 percent reduction is considered possible, but experimental evidence of this reduction applicable to this specific problem is not available.

5. Insulation of the tube wall from the hot combustion gases can result from the micron-size particles becoming packed into the metal surface roughness crevices. These crevices have dimensions on the order of five to ten microns; therefore, the packed bed of particles in these crevices form an insulating layer of five to ten microns thickness between the wall and the gases. Taking typical values, this insulation layer can reduce the tube metal temperature by up to 300°K. This hypothesis is supported in many ways, and it is felt that it represents the mechanism by which gun tube erosion is reduced when TiO_3 particles are added to propellants. Therefore, in order to minimize erosion in gun tubes, this deposition of any insulating particles into the surface roughness crevices should be optimized.

APPENDIX I

DERIVATION OF CONSERVATION EQUATIONS

A control volume approach has been taken for the derivation of the conservation equations. In Figure 37 a control volume having a cross-sectional area A_p and length Δx has been shown. The volume fraction of solids per unit length is ν_s, or in the other words, ν_s is the fraction of the total cross-sectional area A_p occupied by the solids. Therefore, $(1-\nu_s)$ is the fractional area occupied by the gases at any position and time.

Due to the assumptions regarding the burning rate of the solids (same for all the particles at a particular instant) and the constant total burning surface S_{b_t}, it is easy to estimate the burning surface available in the chosen control volume,

$$S_L = S_{b_t} \frac{\nu_s A_p \Delta x}{\int_0^{L_p} \nu_s A_p dx} \qquad (I\text{-}1)$$

Therefore, the rate of gas produced (by mass) from the solids (or, rate of decrease of solids by mass) within the control volume is given by,

$$\rho_s S_L r_b$$

$$= \rho_s S_{b_t} \frac{\nu_s \Delta x \, r_b}{\int_0^{L_p} \nu_s dx} \qquad (I\text{-}2)$$

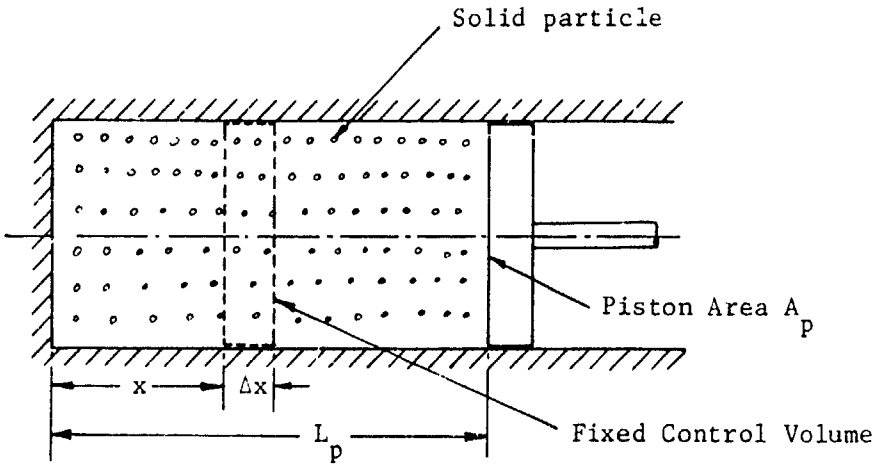

Figure I-1. Schematic of Control Volume Chosen for the Derivation of Conservation Equations.

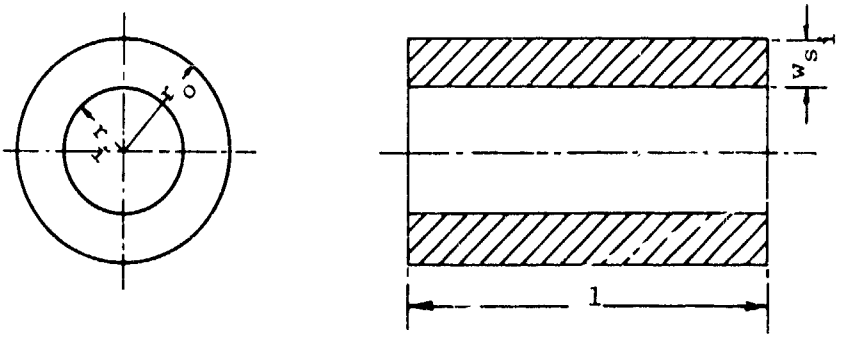

Figure I-2. A Typical Solid Particle Assumed in the Present Study.

Case I (Solid particles moving at gas velocity)

Continuity of solids.

Rate of increase of solid mass in c.v. = Rate of solid flowing in − Rate of solid flowing out − Rate of gas produced in c.v.

$$\frac{\partial}{\partial t}(\rho_s A_p \nu_s \Delta x) = (\rho_s U_s A_p \nu_s)\Big|_x - (\rho_s U_s A_p \nu_s)\Big|_{x+dx} - \rho_s S_{b_t} \frac{\nu_s r_b \Delta x}{\int_0^{L_p} \nu_s dx}$$

or,

$$A_p \rho_s \left[\frac{\partial \nu_s}{\partial t} + \frac{\partial}{\partial x}(\nu_s U_s)\right] + \rho_s S_{b_t} \frac{\nu_s r_b}{\int_0^{L_p} \nu_s dx} = 0$$

with $U_s = U_g = U$,

$$\frac{\partial \nu_s}{\partial t} + U \frac{\partial \nu_s}{\partial x} + \nu_s \frac{\partial U}{\partial x} + \left(\frac{S_{b_t}}{A_p}\right) \frac{\nu_s r_b}{\int_0^{L_p} \nu_s dx} = 0$$

or,

$$\frac{\partial \nu_s}{\partial t} + U \frac{\partial \nu_s}{\partial x} + \nu_s \frac{\partial U}{\partial x} + \dot{v}_{d_s} = 0 \qquad \text{(I-3)}$$

Continuity of Gases.

Rate of increase of mass of gas in c.v. = Rate of gas flowing in − Rate of gas flowing out + Rate of gas produced in c.v.

$$\frac{\partial}{\partial t}\left[(1-\nu_s)\rho_g A_p \Delta x\right] = \left[(1-\nu_s)\rho_g A_p U_g\right]\Big|_x - \left[(1-\nu_s)\rho_g A_p U_g\right]\Big|_{x+dx} + \rho_s S_{b_t} \frac{\nu_s r_b \Delta x}{\int_0^{L_p} \nu_s dx}$$

or,

$$\frac{\partial}{\partial t}\left[(1-\nu_s)\rho_g\right] + \frac{\partial}{\partial x}\left[(1-\nu_s)\rho_g U_g\right] = \rho_s \left(\frac{S_b}{A_p}\right) \frac{\nu_s r_b}{\int_o^{L_p} \nu_s dx}$$

Using equation (I-3) and $U_s = U_g = U$:

$$(1-\nu_s)\frac{\partial \rho_g}{\partial t} + (1-\nu_s)\, U \frac{\partial \rho_g}{\partial x} + \rho_g \frac{\partial U}{\partial x} = (\rho_s - \rho_g)\, \dot{v}_{d_s}$$

or,

$$\frac{\partial \rho_g}{\partial t} + U \frac{\partial \rho_g}{\partial x} + \frac{\rho_g}{(1-\nu_s)} \frac{\partial U}{\partial x} = \frac{(\rho_s - \rho_g)}{(1-\nu_s)}\, \dot{v}_{d_s} \qquad \text{(I-4)}$$

A general equation of continuity can be obtained by considering the gas-solid mixture as a whole which gives,

Rate of increase of mass of gas-solid mixture in c.v.	=	Rate of gas-solid mixture flowing in	-	Rate of gas-solid mixture flowing out

$$\frac{\partial}{\partial t}\left[\nu_s \rho_s A_p \Delta x + (1-\nu_s)\rho_g A_p \Delta x\right] = \left[\nu_s \rho_s U A_p + (1-\nu_s)\rho_g U A_p\right]\Big|_x - \left[\nu_s \rho_s U A_p + (1-\nu_s)\rho_g U A_p\right]\Big|_{x+dx}$$

or,

$$\frac{\partial}{\partial t}\left[\nu_s \rho_s + (1-\nu_s)\rho_g\right] + \frac{\partial}{\partial x}\left[\nu_s \rho_s U + (1-\nu_s)\rho_g U\right] = 0 \qquad \text{(I-5)}$$

Momentum Equation.

Rate of increase of momentum in c.v.	+	Momentum flux out	-	Momentum flux in	=	Σ External forces

$$\frac{\partial}{\partial t}\left[\nu_s\rho_s U + (1-\nu_s)\rho_g U\right] A_p\,\Delta x + \left[\nu_s\rho_s U^2 + (1-\nu_s)\rho_g U^2\right] A_p\Big|_{x+dx}$$

$$- \left[\nu_s\rho_s U^2 + (1-\nu_s)\rho_g U^2\right] A_p\Big|_{x}$$

$$= P\,A_p\Big|_x - P\,A_p\Big|_{x+dx} - 2\pi R\,\Delta x\,\tau_w$$

or,

$$\frac{\partial}{\partial t}\left[\{\nu_s\rho_s + (1-\nu_s)\rho_g\}U\right] + \frac{\partial}{\partial x}\left[\{\nu_s\rho_s U + (1-\nu_s)\rho_g U\}U\right] = -\frac{\partial P}{\partial x} - \frac{2\tau_w}{R}$$

Using equation (I-5):

$$\left[\nu_s\rho_s + (1-\nu_s)\rho_g\right]\left[\frac{\partial U}{\partial t} + U\frac{\partial U}{\partial x}\right] = -\frac{\partial P}{\partial x} - \frac{2\tau_w}{R}$$

Now, mixture density $\rho_m = \nu_s\rho_s + (1-\nu_s)\rho_g$

$$\therefore \quad \frac{\partial U}{\partial t} + U\frac{\partial U}{\partial x} = -\frac{1}{\rho_m}\frac{\partial P}{\partial x} - \frac{2\tau_w}{\rho_m R} \qquad \text{(I-5)}$$

Energy Equation.

Rate of increase of energy in c.v. = Energy flux flowing in − Energy flux flowing out + Rate of increase of energy due to conversion of solids into gases in c.v.

− Rate of work done by the gas-solid mixture − Rate of heat loss to the tube wall

or,

$$\frac{\partial}{\partial t}\left[\{\nu_s\rho_s(e_s + \frac{U_s^2}{2}) + (1-\nu_s)\rho_g(e_g + \frac{U_g^2}{2})\}A_p\,\Delta x\right]$$

$$= \left[\{\nu_s\rho_s(e_s + \frac{U_s^2}{2})U_s + (1-\nu_s)\rho_g(e_g + \frac{U_g^2}{2})U_g\}A_p\right]\Big|_x$$

$$- \left[\{\nu_s\rho_s(e_s + \frac{U_s^2}{2})U_s + (1-\nu_s)\rho_g(e_g + \frac{U_g^2}{2})U_g\}A_p\right]\Big|_{x+dx}$$

$$+ \rho_s S_{b_t}\frac{\nu_s r_b \Delta x}{\int_0^L P\nu_s dx}\Delta E - \left[A_p\left\{\nu_s\rho_s U_s(\frac{P}{\rho_s}) + (1-\nu_s)\rho_g U_g(\frac{P}{\rho_g})\right\}\Big|_{x+dx}\right.$$

$$\left. - A_p\left\{\nu_s\rho_s U_s(\frac{P}{\rho_s}) + (1-\nu_s)\rho_g U_g(\frac{P}{\rho_g})\right\}\Big|_x\right] - 2\pi R\,\Delta x\, h_i(T-T_{w,i})$$

where, ΔE = Additional energy release per unit mass due to conversion of solids into gases,

$$= c_v T_o - c_s T_s \quad = W - c_s T_s \tag{I-6}$$

Using the definition of enthalpy for solids and gas, i.e.

$$h_s = e_s + \frac{P}{\rho_s} \quad ; \qquad h_g = e_g + \frac{P}{\rho_g} \quad :$$

$$\frac{\partial}{\partial t}\left[\nu_s\rho_s(h_s - \frac{P}{\rho_s}) + (1-\nu_s)\rho_g(h_g - \frac{P}{\rho_g})\right] + \frac{\partial}{\partial x}\left[\nu_s\rho_s h_s U_s + (1-\nu_s)\rho_g h_g U_g\right]$$

$$+ \frac{\partial}{\partial t}\left[\nu_s\rho_s\frac{U_s^2}{2} + (1-\nu_s)\rho_g\frac{U_g^2}{2}\right]$$

$$+ \frac{\partial}{\partial x}\left[\nu_s\rho_s\frac{U_s^2}{2}U_s + (1-\nu_s)\rho_g\frac{U_g^2}{2}U_g\right] = \rho_s(\frac{S_{b_t}}{A_p})\frac{\nu_s r_b \Delta E}{\int_0^L P\nu_s dx}$$

$$- \frac{2h_i}{R}(T-T_{w,i})$$

Using $U_s = U_g = U$,

$$\frac{\partial}{\partial t}\left[\nu_s\rho_s h_s + (1-\nu_s)\rho_g h_g\right] - \frac{\partial P}{\partial t} + \frac{\partial}{\partial x}\left[\nu_s\rho_s h_s U + (1-\nu_s)\rho_g h_g U\right]$$

$$+ \frac{U^2}{2}\frac{\partial}{\partial t}\left[\nu_s\rho_s + (1-\nu_s)\rho_g\right] + \left[\nu_s\rho_s + (1-\nu_s)\rho_g\right] U\frac{\partial U}{\partial t}$$

$$+ \frac{U^2}{2}\frac{\partial}{\partial x}\left[\nu_s\rho_s U + (1-\nu_s)\rho_g U\right] + \left[\nu_s\rho_s + (1-\nu_s)\rho_g\right] U^2\frac{\partial U}{\partial x}$$

$$= \rho_s \dot{v}_{d_s} \Delta E - \frac{2h_i}{R}(T-T_{w,i})$$

Using the general equation of continuity (I-4) and the momentum equation (I-5):

$$\frac{\partial}{\partial t}\left[\nu_s\rho_s h_s + (1-\nu_s)\rho_g h_g\right] + \frac{\partial}{\partial x}\left[\nu_s\rho_s h_s U + (1-\nu_s)\rho_g h_g U\right] - \frac{\partial P}{\partial t} + U\frac{\partial P}{\partial x}$$

$$= \rho_s \dot{v}_{d_s} \Delta E - \frac{2h_i}{R}(T-T_{w,i}) + \frac{2\tau_w U}{R}$$

On differentiation and by use of continuity of solids (164) and continuity of gases (I-3):

$$\nu_s\rho_s\left[\frac{\partial h_s}{\partial t} + U\frac{\partial h_s}{\partial x}\right] + (1-\nu_s)\rho_g\left[\frac{\partial h_g}{\partial t} + U\frac{\partial h_g}{\partial x}\right] - \frac{\partial P}{\partial t} + U\frac{\partial P}{\partial x}$$

$$= \rho_s \dot{v}_{d_s}(\Delta E + h_s - h_g) - \frac{2h_i}{R}(T-T_{w,i}) + \frac{2\tau_w U}{R}$$

Using the notation $\frac{D}{Dt} = \frac{\partial}{\partial t} + U\frac{\partial}{\partial x}$

and $h_s = c_s T_s + \frac{P}{\rho_s}$, finally:

$$\nu_s \rho_s \frac{Dh_s}{Dt} + (1-\nu_s)\rho_g \frac{Dh_g}{Dt} - \frac{DP}{Dt} = \rho_s \dot{v}_{d_s} (W + \frac{P}{\rho_s} - h_g) - \frac{2h_i}{R} (T-T_{w,i})$$

$$+ \frac{2\tau_w U}{R} \qquad \text{(I-7)}$$

Case II (Solid particles stationary at their initial positions)

Continuity of Solids.

Rate of increase of solid mass in c.v. = Rate of solids flowing in − Rate of solids flowing out − Rate of gas produced in c.v.

$$\frac{\partial}{\partial t}(\rho_s A_p \nu_s \Delta x) = 0 - 0 - \rho_s S_{b_t} \frac{\nu_s r_b \Delta x}{\int_o^{L_p} \nu_s dx}$$

or,

$$\frac{\partial \nu_s}{\partial t} = - \left(\frac{S_{b_t}}{Ap}\right) \frac{\nu_s r_b}{\int_o^{L_p} \nu_s dx} = - \dot{v}_{d_s} \qquad \text{(I-8)}$$

Continuity of Gases.

Rate of increase of mass of gas in c.v. = Rate of gas flowing in − Rate of gas flowing out + Rate of gas produced in c.v.

$$\frac{\partial}{\partial t}\left[(1-\nu_s)A_p \rho_g \Delta x\right] = \left[(1-\nu_s)A_p \rho_g U_g\right]\Big|_x - \left[(1-\nu_s)A_p \rho_g U_g\right]\Big|_{x+dx}$$

$$+ \rho_s S_{b_t} \frac{\nu_s r_b \Delta x}{\int_o^{L_p} \nu_s dx}$$

or,

$$\frac{\partial}{\partial t}\left[(1-\nu_s)\rho_g\right] + \frac{\partial}{\partial x}\left[(1-\nu_s)\rho_g U_g\right] = \rho_s\left(\frac{S_{b_t}}{A_p}\right)\frac{\nu_s \tau_b}{\int_0^{L_p} \nu_x dx} = \rho_s \dot{v}_{d_s} \quad \text{(I-9)}$$

Putting $U_g = U$ and using equation (I-8):

$$(1-\nu_s)\left[\frac{\partial \rho_g}{\partial x} + U\frac{\partial \rho_g}{\partial x} + \rho_g \frac{\partial U}{\partial x}\right] + \rho_g \dot{v}_{d_s} - \rho_g U \frac{\partial \nu_s}{\partial x} = \rho_s \dot{v}_{d_s}$$

or,

$$\frac{\partial \rho_g}{\partial t} + U\frac{\partial \rho_g}{\partial x} + \rho_g \frac{\partial U}{\partial x} = \frac{(\rho_s - \rho_g)}{(1-\nu_s)}\dot{v}_{d_s} + \frac{\rho_g U}{(1-\nu_s)}\frac{\partial \nu_s}{\partial x} \quad \text{(I-10)}$$

Momentum Equation. As the solids are at rest, the free as volume in the control volume shown in Figure 37 is taken as the new control volume in the following derivation. It is assumed that the solids are at the core of the flow and the skin friction at the surface of the solid particles is negligible.

Rate of increase of momentum in c.v. + Momentum flux out − Momentum flux in = Σ External forces

$$\frac{\partial}{\partial t}\left[(1-\nu_s)A_p \rho_g U_g \Delta x\right] + \left[(1-\nu_s)A_p \rho_g U_g^2\right]\Big|_{x+dx} - \left[(1-\nu_s)A_p \rho_g U_g^2\right]\Big|_x$$

$$= \left[(1-\nu_s)A_p P\right]\Big|_x - \left[(1-\nu_s)A_p P\right]\Big|_{x+dx}$$

$$+ P A_p \Delta x \frac{\partial(1-\nu_s)}{\partial x} - 2\pi R \Delta x \tau_w$$

or,

$$\frac{\partial}{\partial t}\left[(1-\nu_s)\rho_g U_g\right] + \frac{\partial}{\partial x}\left[(1-\nu_s)\rho_g U_g U_g\right] = -\frac{\partial}{\partial x}\left[(1-\nu_s)P\right]$$

$$+ P\frac{\partial(1-\nu_s)}{\partial x} - \frac{2\tau_w}{R}$$

Using equation (I-9) and putting $U_g = U$,

$$(1-\nu_s)\rho_g\left[\frac{\partial U}{\partial t} + U\frac{\partial U}{\partial x}\right] + \rho_s \dot{v}_{d_s} U = -(1-\nu_s)\frac{\partial P}{\partial x} - \frac{2\tau_w}{R}$$

or,

$$\frac{\partial U}{\partial t} + U\frac{\partial U}{\partial x} = -\frac{1}{\rho_g}\frac{\partial P}{\partial x} - \frac{\rho_s U}{(1-\nu_s)\rho_g}\dot{v}_{d_s} - \frac{2\tau_w}{(1-\nu_s)\rho_g R} \qquad \text{(I-11)}$$

Energy Equation. The same control volume as used in the derivation of momentum equation is taken.

Rate of energy increase in c.v. = Energy flux flowing in − Energy flux flowing out + Rate of energy increase due to gas coming into the c.v. from the solids − Rate of work done by the flowing gas − Rate of heat loss to the tube wall

or,

$$\frac{\partial}{\partial t}\left[(1-\nu_s)A_p\rho_g(e_g+\frac{U_g^2}{2})\Delta x\right] = \left[(1-\nu_s)A_p\rho_g U_g(e_g+\frac{U_g^2}{2})\right]\Big|_x$$

$$-\left[(1-\nu_s)A_p\rho_g U_g(e_g+\frac{U_g^2}{2})\right]\Big|_{x+dx}$$

$$+\rho_s S_{b_t}\frac{\nu_s\Delta x\, r_b}{\int_o^{L_p}\nu_s dx}\, W$$

$$-\left[\left\{(1-\nu_s)A_p\rho_g U_g(\frac{P}{\rho_g})\right\}\Big|_{x+dx}\right.$$

$$\left.-\left\{(1-\nu_s)A_p\rho_g U_g(\frac{P}{\rho_g})\right\}\Big|_x\right]-2\pi R\,\Delta x\, h_i(T-T_{w,i})$$

or,

$$\frac{\partial}{\partial t}\left[(1-\nu_s)\rho_g(e_g+\frac{U_g^2}{2})\right]+\frac{\partial}{\partial x}\left[(1-\nu_s)\rho_g U_g(e_g+\frac{P}{\rho_g}+\frac{U_g^2}{2})\right]$$

$$=\rho_s(\frac{S_{b_t}}{A_p})\frac{\nu_s r_b}{\int_o^{L_p}\nu_s dx}\,W-\frac{2h_i}{R}(T-T_{w,i})$$

Put $U_g = U$ and $h_g = e_g + \frac{P}{\rho_g}$,

$$\frac{\partial}{\partial t}\left[(1-\nu_s)\rho_g(h_g-\frac{P}{\rho_g})\right]+\frac{\partial}{\partial x}\left[(1-\nu_s)\rho_g h_g U\right]+\tfrac{1}{2}\frac{\partial}{\partial t}\left[(1-\nu_s)\rho_g U^2\right]$$

$$+\tfrac{1}{2}\frac{\partial}{\partial x}\left[((1-\nu_s)\rho_g U)U^2\right]=\rho_s\dot{v}_{d_s}W$$

$$-\frac{2h_i}{R}(T-T_{w,i})$$

Using equations (I-9) and (I-11)

$$\frac{\partial}{\partial t}\left[(1-\nu_s)\rho_g h_g\right] + \frac{\partial}{\partial x}\left[(1-\nu_s)\rho_g h_g U\right] - \frac{\partial}{\partial t}\left[(1-\nu_s)P\right] + \rho_s \dot{v}_{d_s}\frac{U^2}{2}$$

$$+ U\left[-\rho_s \dot{v}_{d_s} U - (1-\nu_s)\frac{\partial P}{\partial x} - \frac{2\tau_w}{R}\right] = \rho_s \dot{v}_{d_s} W$$

$$- \frac{2h_i}{R}(T-T_{w,i})$$

Using equation (I-8)

$$\frac{\partial}{\partial t}\left[(1-\nu_s)\rho_g h_g\right] + \frac{\partial}{\partial x}\left[(1-\nu_s)\rho_g h_g U\right] - (1-\nu_s)\left[\frac{\partial P}{\partial t} + U\frac{\partial P}{\partial x}\right]$$

$$= \rho_s \dot{v}_{d_s}\left(W + \frac{P}{\rho_s} + \frac{U^2}{2}\right) - \frac{2h_i}{R}(T-T_{w,i}) + \frac{2\tau_w U}{R}$$

or,

$$(1-\nu_s)\rho_g\left[\frac{\partial h_g}{\partial t} + U\frac{\partial h_g}{\partial x}\right] + h_g\left[\frac{\partial}{\partial t}\left\{(1-\nu_s)\rho_g\right\} + \frac{\partial}{\partial x}\left\{(1-\nu_s)\rho_g U\right\}\right]$$

$$- (1-\nu_s)\left[\frac{\partial P}{\partial t} + U\frac{\partial P}{\partial x}\right] = \rho_s \dot{v}_{d_s}\left(W + \frac{P}{\rho_s} + \frac{U^2}{2}\right)$$

$$- \frac{2h_i}{R}(T-T_{w,i}) + \frac{2\tau_w}{R} U$$

Using equation (I-9) and notation $\frac{D}{Dt} = \frac{\partial}{\partial t} + U\frac{\partial}{\partial x}$, finally :

$$(1-\nu_s)\rho_g \frac{Dh_g}{Dt} - (1-\nu_s)\frac{DP}{Dt} = \rho_s \dot{v}_{d_s} \left(W + \frac{P}{\rho_s} + \frac{U^2}{2} - h_g\right)$$

$$- \frac{2h_i}{R}(T-T_{w,i}) + \frac{2\tau_w}{R} U \qquad \text{(I-12)}$$

Computation of Burning Surface

A typical solid particle, a single perforated cylinder in shape, is shown in Figure 38.

Let,

r_i = initial inner radius of the particle

r_o = initial outer radius of the particle

l = length of the particle

n = total number of the particles in the chamber

Therefore, total initial burning surface = $2\pi(r_i+r_o)\, l\, n$. It is assumed that combustion gas is produced from both inner and outer cylindrical surfaces of a particle but not from two ends. If r_b is the linear speed of burning, which is assumed to be same for all the particles at a particular instant, the total burning surface after time Δt is

$$2\pi \left[(r_i+r_b\,\Delta t) + (r_o-r_b\,\Delta t)\right] l\, n$$

$$= 2\pi\,(r_i+r_o) l\, n$$

It is clear that for hollow cylindrical particles the total burning surface is constant and can be given by :

$$S_{b_t} = \frac{2\pi(r_o^2 - r_i^2) l \, n \, \rho_s}{\rho_s (r_o - r_i)}$$

$$= \frac{2m_{s_i}}{\rho_s w_{s_i}} \qquad \text{(I-13)}$$

where

m_{s_i} = initial mass of solids

ρ_s = solid mass density

w_{s_i} = initial web thickness of a solid particle

Expressions for Enthalpies of Solids and Gases

For any pure substance, $h = h(P,T)$

$$dh = \left(\frac{\partial h}{\partial P}\right)_T dP + \left(\frac{\partial h}{\partial T}\right)_P dT \qquad \text{(I-14)}$$

From thermodynamics, $dh = Tds + vdP$

$$\left(\frac{\partial h}{\partial P}\right)_T = T\left(\frac{\partial s}{\partial P}\right)_T + v \qquad \text{(I-15)}$$

Again from Gibb's form of first law of thermodynamics,

$$dG = -s\,dT + v\,dP \qquad \text{(I-16)}$$

As Gibb's function G is a property of the system, dG must be an exact differential

$$\therefore \quad \left(\frac{\partial s}{\partial P}\right)_T = -\left(\frac{\partial v}{\partial T}\right)_P \tag{I-17}$$

Now, coefficient of thermal expansion, $\beta = \frac{1}{v}\left(\frac{\partial v}{\partial T}\right)_P$

$\therefore$ Equation (I-15) becomes,

$$\left(\frac{\partial h}{\partial P}\right)_T = -T\beta v + v = v(1-T\beta)$$

$\therefore$ Equation (I-14) becomes,

$$dh = v(1-T\beta)\ dP + c_p\ dT \tag{I-18}$$

Solids

For solids, c_p is equal to c_s and it has been assumed that the temperature of the solids T_s remains constant throughout the period of burning

$$\therefore \quad dh_s = \frac{1}{\rho_s}(1-T_s\beta_s)\ dP$$

It has also been assumed that the coefficient of expansion for solids β_s is negligible.

$$\therefore \quad dh_s = \frac{dP}{\rho_s} \tag{I-19}$$

$$\text{and} \quad h_s = c_s T_s + \frac{P}{\rho_s} \tag{I-20}$$

Gases

The equation of state for the combustion gas at high pressure can be taken as,

$$P(v_g - \eta) = R_g T \tag{I-21}$$

where, the covolume η is a constant.

Now,

$$P\left(\frac{\partial v_g}{\partial T}\right)_P = R_g$$

$$\therefore \beta_g = \frac{1}{v_g}\left(\frac{\partial v_g}{\partial T}\right)_P = \frac{R_g}{v_g P}$$

From equation (I-18)

$$dh_g = v_g\left[1 - \frac{R_g T}{v_g P}\right]dP + c_p\, dT$$

or,

$$dh_g = \eta\, dP + c_p\, dT \tag{I-22}$$

Now, the specific heat at constant pressure, $c_p = \frac{\gamma}{\gamma-1} R_g$ yields,

$$dh_g = \eta\, dP + \frac{\gamma}{\gamma-1} R_g\, dT \tag{I-23}$$

Differentiating equation (I-21) and using $v_g = 1/\rho_g$:

$$R_g\, dT = \left(\frac{1}{\rho_g} - \eta\right) dP - \frac{P}{\rho_g^2}\, d\rho_g$$

Equation (I-23) becomes,

$$dh_g = \frac{(\gamma - \eta\rho_g)}{\rho_g(\gamma-1)}\, dP - \frac{\gamma P}{(\gamma-1)\rho_g^2}\, d\rho_g \qquad \text{(I-24)}$$

From equation (I-22)

$$h_g = \eta P + c_p T$$

$$= \eta P + \frac{\gamma}{(\gamma-1)} P \left(\frac{1}{\rho_g} - \eta\right)$$

$$= \frac{(\gamma - \eta\rho_g)}{(\gamma-1)\rho_g} P \qquad \text{(I-25)}$$

APPENDIX II

DERIVATION OF BOUNDARY LAYER MOMENTUM EQUATION

With reference to Figure 39, the boundary layer momentum integral equation is derived as follows:

Equation of Continuity

Rate of increase of mass in c.v. = Rate of mass flow into the c.v. through surface AB − Rate of mass flow out through surface CD + Rate of mass flow into the c.v. through surface BC

$$\frac{\partial}{\partial t}\int_{R-\delta}^{R} 2\pi r\,\Delta x\,\rho\,dr = \left[\int_{R-\delta}^{R} 2\pi r\,\rho\,u\,dr\right]\Bigg|_{x} - \left[\int_{R-\delta}^{R} 2\pi r\,\rho\,u\,dr\right]\Bigg|_{x+dx} + \dot{m}_{BC} \qquad \text{(II-1)}$$

Momentum Equation (x-directional)

Rate of increase of momentum in c.v. − Momentum flux in + Momentum flux out = $\sum$ External forces

$$\frac{\partial}{\partial t}\int_{R-\delta}^{R} 2\pi r\,\Delta x\,\rho\,u\,dr - \dot{m}_{BC}\,U_{\infty} - \left[\int_{R-\delta}^{R} 2\pi r\,\rho\,u^{2}\,dr\right]\Bigg|_{x} + \left[\int_{R-\delta}^{R} 2\pi r\,\rho\,u^{2}dr\right]\Bigg|_{x+dx}$$

$$= \left[\int_{R-\delta}^{R} 2\pi r\,P\,dr\right]\Bigg|_{x} - \left[\int_{R-\delta}^{R} 2\pi r\,P\,dr\right]\Bigg|_{x+dx}$$

$$+ 2\pi(R-\delta)\left(\frac{\partial\delta}{\partial x}\Delta x\right)P - 2\pi R\,\Delta x\tau_{w} \qquad \text{(II-2)}$$

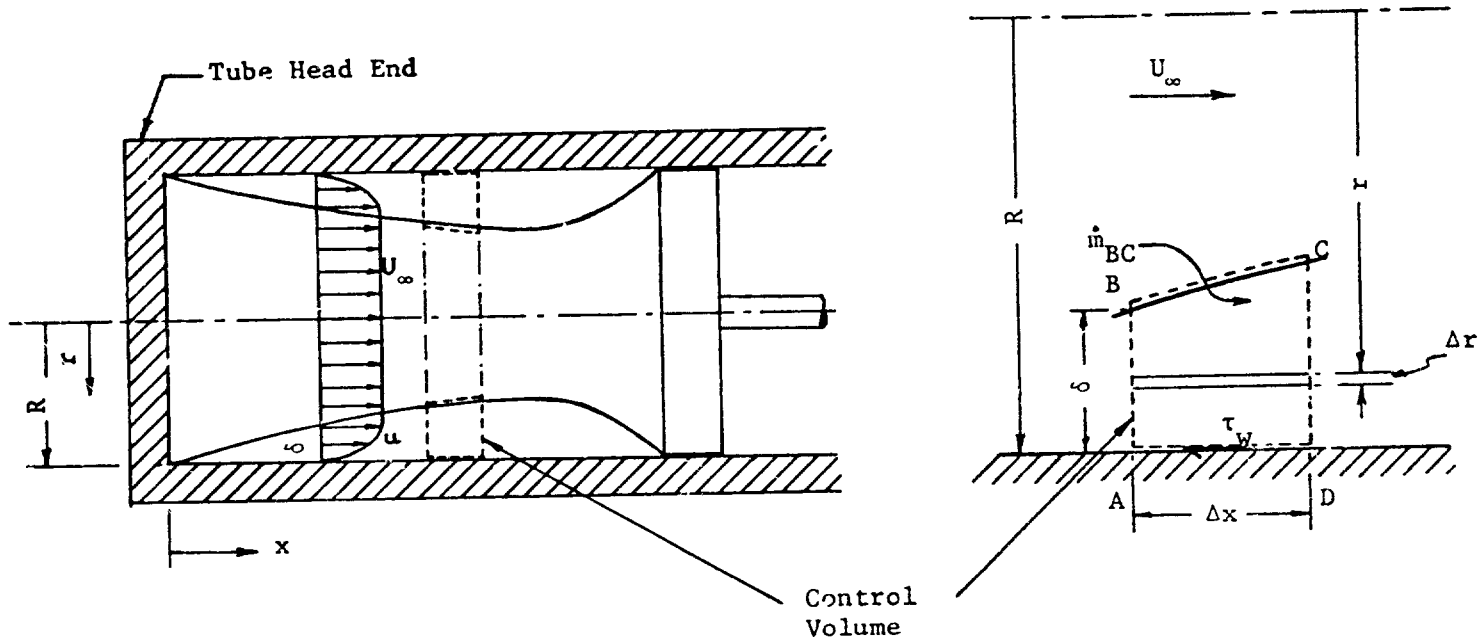

Figure 69. Schematic of Boundary Layer Growth in a Tube With a Sliding Piston at one End

Using the expression for $\dot{m}_{BC}$ from equation (II-1), equation (II-2) becomes,

$$\frac{\partial}{\partial t}\int_{R-\delta}^{R}(\rho u\, r)dr - U_\infty \frac{\partial}{\partial t}\int_{R-\delta}^{R}(\rho r)dr - U_\infty \frac{\partial}{\partial x}\int_{R-\delta}^{R}(\rho u\, r)dr + \int_{R-\delta}^{R}(\rho u^2 r)dr$$
$$= -\frac{\partial}{\partial x}\int_{R-\delta}^{R}(P\, r)dr + (R-\delta)P\frac{\partial \delta}{\partial x} - \tau_w R \qquad \text{(II-3)}$$

Now, for thin boundary layer, radial component of velocity is very small and consequently,

$$\frac{\partial P}{\partial r} \simeq 0 \qquad \text{(II-4)}$$

Also, as $U_\infty \neq f(r)$,

$$\frac{\partial}{\partial t}\int_{R-\delta}^{R} U_\infty \rho r\, dr = U_\infty \frac{\partial}{\partial t}\int_{R-\delta}^{R}\rho r\, dr + \left[\int_{R-\delta}^{R}\rho r\, dr\right]\frac{\partial U_\infty}{\partial t} \qquad \text{(II-5)}$$

and

$$\frac{\partial}{\partial x}\int_{R-\delta}^{R} U_\infty(\rho u r)dr = U_\infty \frac{\partial}{\partial x}\int_{R-\delta}^{R}\rho u r\, dr + \left[\int_{R-\delta}^{R}\rho u r\, dr\right]\frac{\partial U_\infty}{\partial x} \qquad \text{(II-6)}$$

Using relations (II-4), (II-5), and (II-6), finally

$$\frac{\partial}{\partial t}\int_{R-\delta}^{R}\rho(U_\infty - u)r\, dr + \frac{\partial}{\partial x}\int_{R-\delta}^{R}\rho u(U_\infty - u)r\, dr - \left[\int_{R-\delta}^{R}\rho r\, dr\right]\frac{\partial U_\infty}{\partial t}$$
$$-\left[\int_{R-\delta}^{R}\rho u r\, dr\right]\frac{\partial U_\infty}{\partial x} = \left[\int_{R-\delta}^{R} r\, dr\right]\frac{\partial P}{\partial x} + \tau_w R \qquad \text{(II-7)}$$

now,

$$\int_{R-\delta}^{R} r\,dr = R\delta - \frac{\delta^2}{2}$$

and using ρ_f, i.e. gas density corresponding to the film temperature, as the average density in the boundary layer, the equation (II-7) becomes,

$$\frac{\partial}{\partial t}\int_{R-\delta}^{R}\rho(U_\infty-u)r\,dr + \frac{\partial}{\partial x}\int_{R-\delta}^{R}\rho u(U_\infty-u)r\,dr + \left[\int_{R-\delta}^{R}\rho(U_\infty-u)r\,dr\right]\frac{\partial U_\infty}{\partial x}$$
$$= (R\delta - \frac{\delta^2}{2})\left[\frac{\partial P}{\partial x} + \rho_f\frac{\partial U_\infty}{\partial t} + \rho_f U_\infty\frac{\partial U_\infty}{\partial x}\right] + \tau_w R \qquad \text{(II-8)}$$

The equation (II-8) is the required momentum integral equation for a nonsteady, nonuniform, and developing compressible flow in a tube.

APPENDIX III

FLOW CHART FOR THE SINGLE SHOT COMPUTER PROGRAM

Main Program

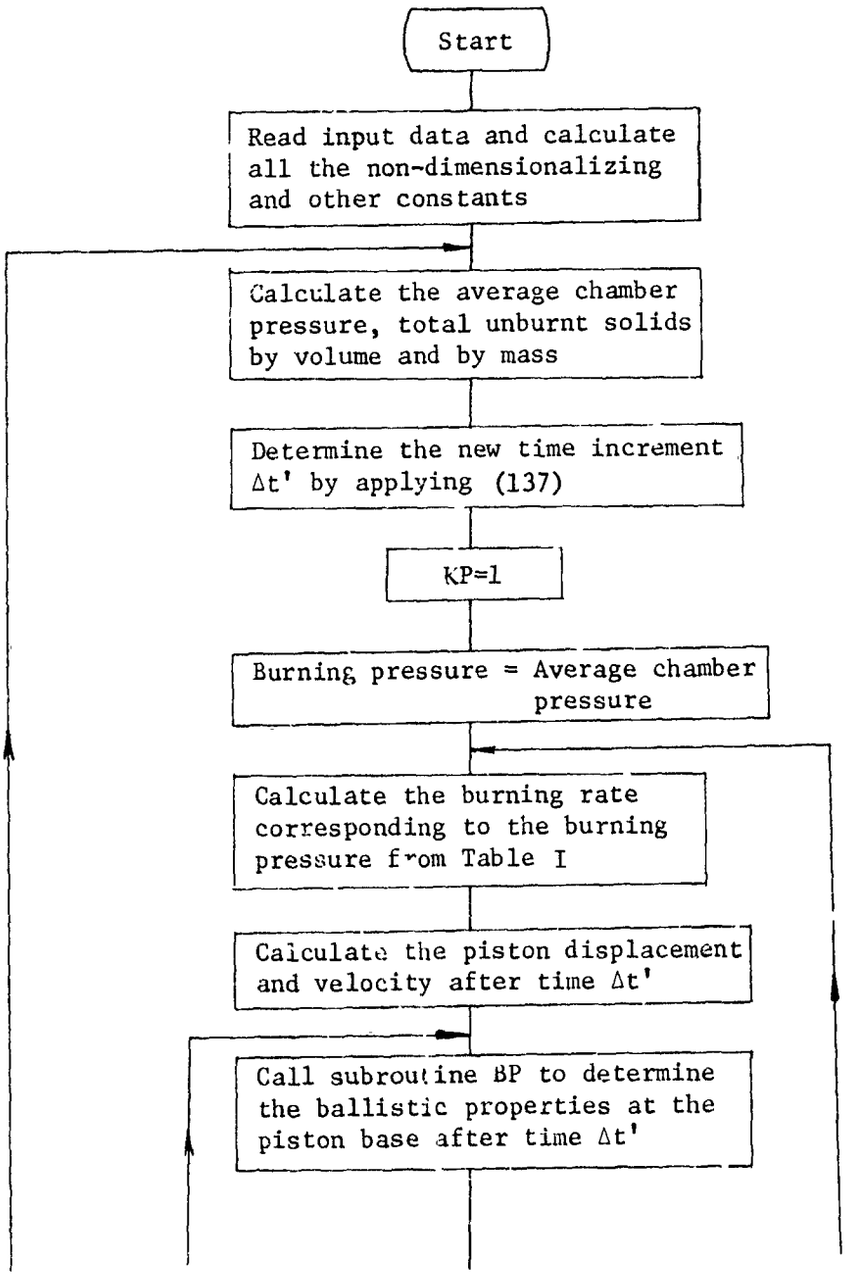

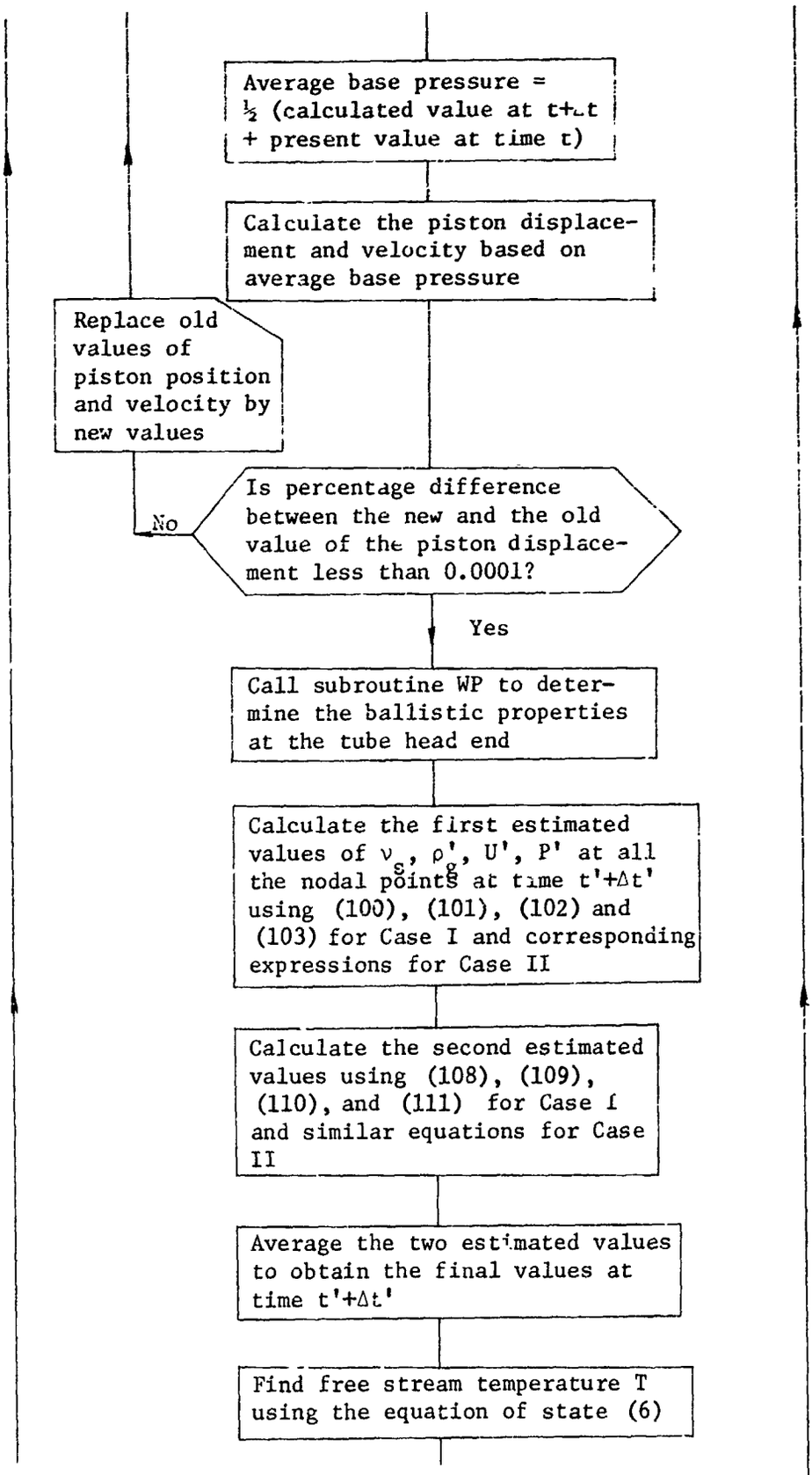
Average base pressure = ½ (calculated value at t+Δt + present value at time t)
Calculate the piston displacement and velocity based on average base pressure
Replace old values of piston position and velocity by new values
No
Is percentage difference between the new and the old value of the piston displacement less than 0.0001?
Yes
Call subroutine WP to determine the ballistic properties at the tube head end
Calculate the first estimated values of ν_s, ρ_g', U', P' at all the nodal points at time t'+Δt' using (100), (101), (102) and (103) for Case I and corresponding expressions for Case II
Calculate the second estimated values using (108), (109), (110), and (111) for Case I and similar equations for Case II
Average the two estimated values to obtain the final values at time t'+Δt'
Find free stream temperature T using the equation of state (6)

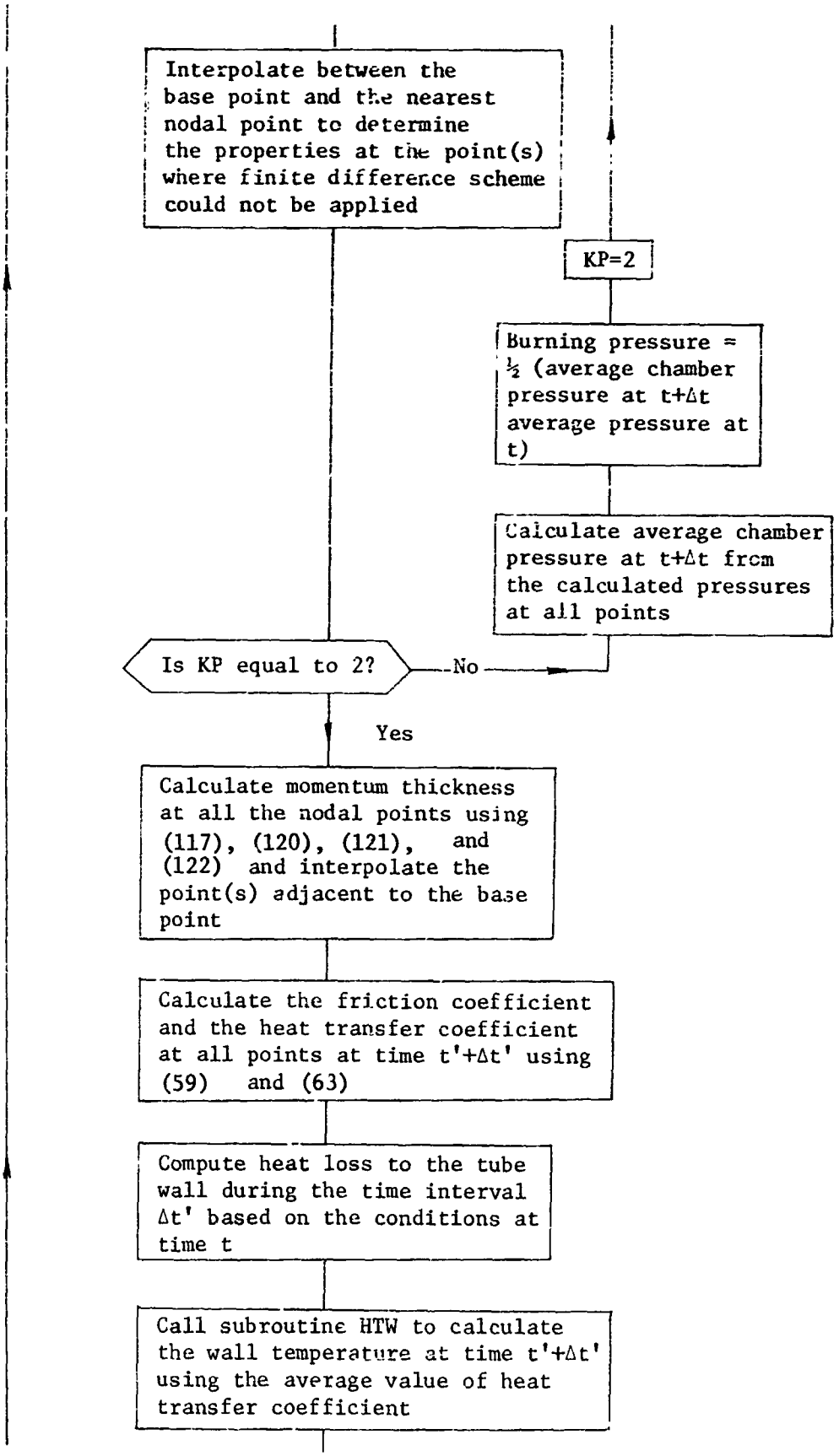
Interpolate between the base point and the nearest nodal point to determine the properties at the point(s) where finite difference scheme could not be applied
KP=2
Burning pressure = ½ (average chamber pressure at t+Δt average pressure at t)
Calculate average chamber pressure at t+Δt from the calculated pressures at all points
Is KP equal to 2?
No
Yes
Calculate momentum thickness at all the nodal points using (117), (120), (121), and (122) and interpolate the point(s) adjacent to the base point
Calculate the friction coefficient and the heat transfer coefficient at all points at time t'+Δt' using (59) and (63)
Compute heat loss to the tube wall during the time interval Δt' based on the conditions at time t
Call subroutine HTW to calculate the wall temperature at time t'+Δt' using the average value of heat transfer coefficient

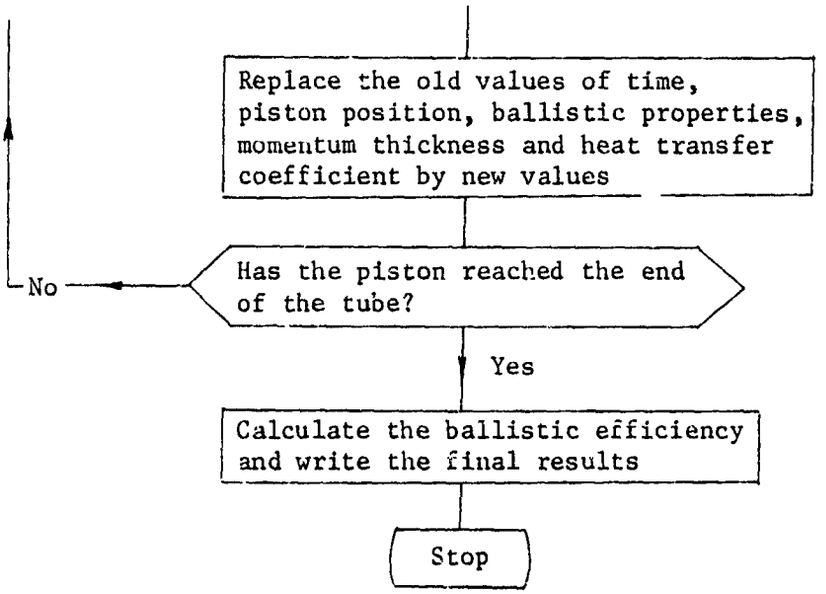
Replace the old values of time, piston position, ballistic properties, momentum thickness and heat transfer coefficient by new values
Has the piston reached the end of the tube?
No
Yes
Calculate the ballistic efficiency and write the final results
Stop

Subroutine BP

The purpose of the subroutine is to calculate the ballistic properties at the piston base at time $t'+\Delta t'$ knowing the properties at all the points at time t', and the velocity and the position of the piston at time $t'+\Delta t'$. The following flow diagram should be read along with Figure 3.

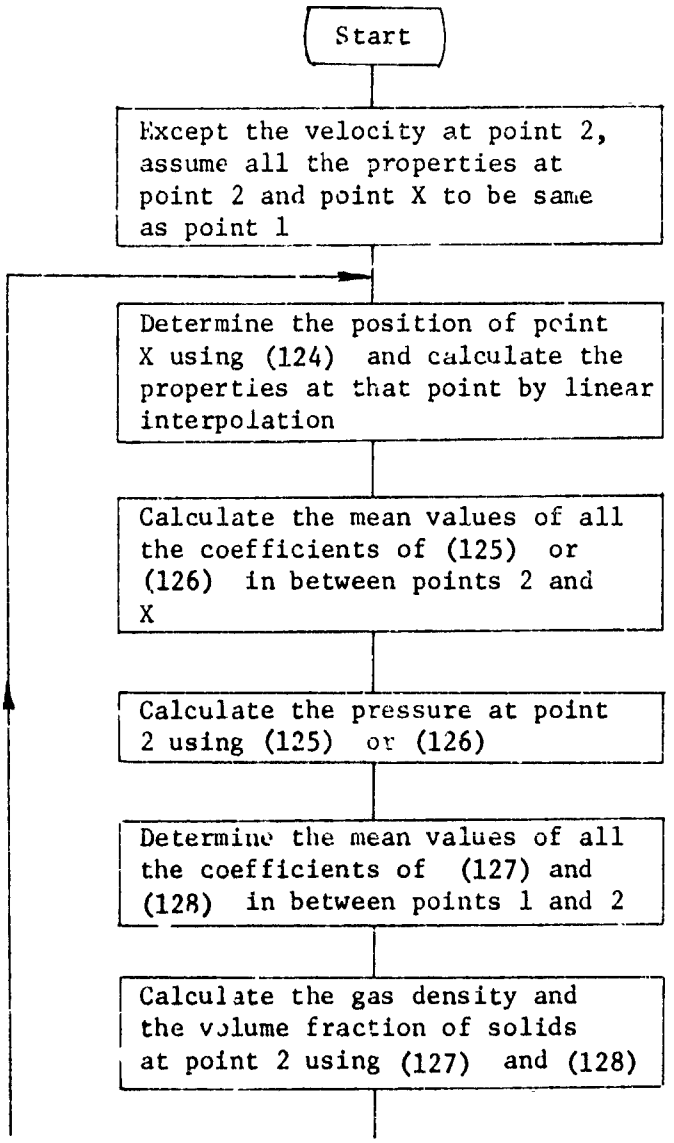

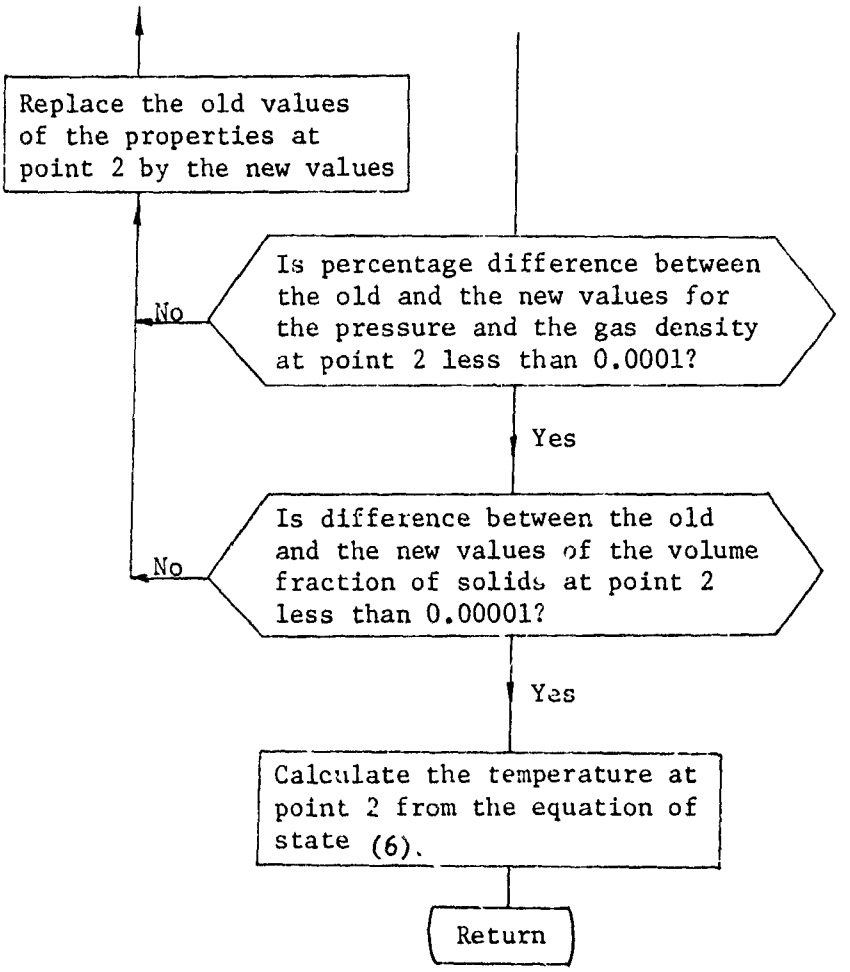
Replace the old values of the properties at point 2 by the new values
Is percentage difference between the old and the new values for the pressure and the gas density at point 2 less than 0.0001?
No
Yes
Is difference between the old and the new values of the volume fraction of solids at point 2 less than 0.00001?
No
Yes
Calculate the temperature at point 2 from the equation of state (6).
Return

Subroutine WP

This subroutine is called to calculate the properties at the tube head end at time $t'+\Delta t'$. The logic is same as that for subroutine BP and the flow diagram should also be read along with Figure 3.

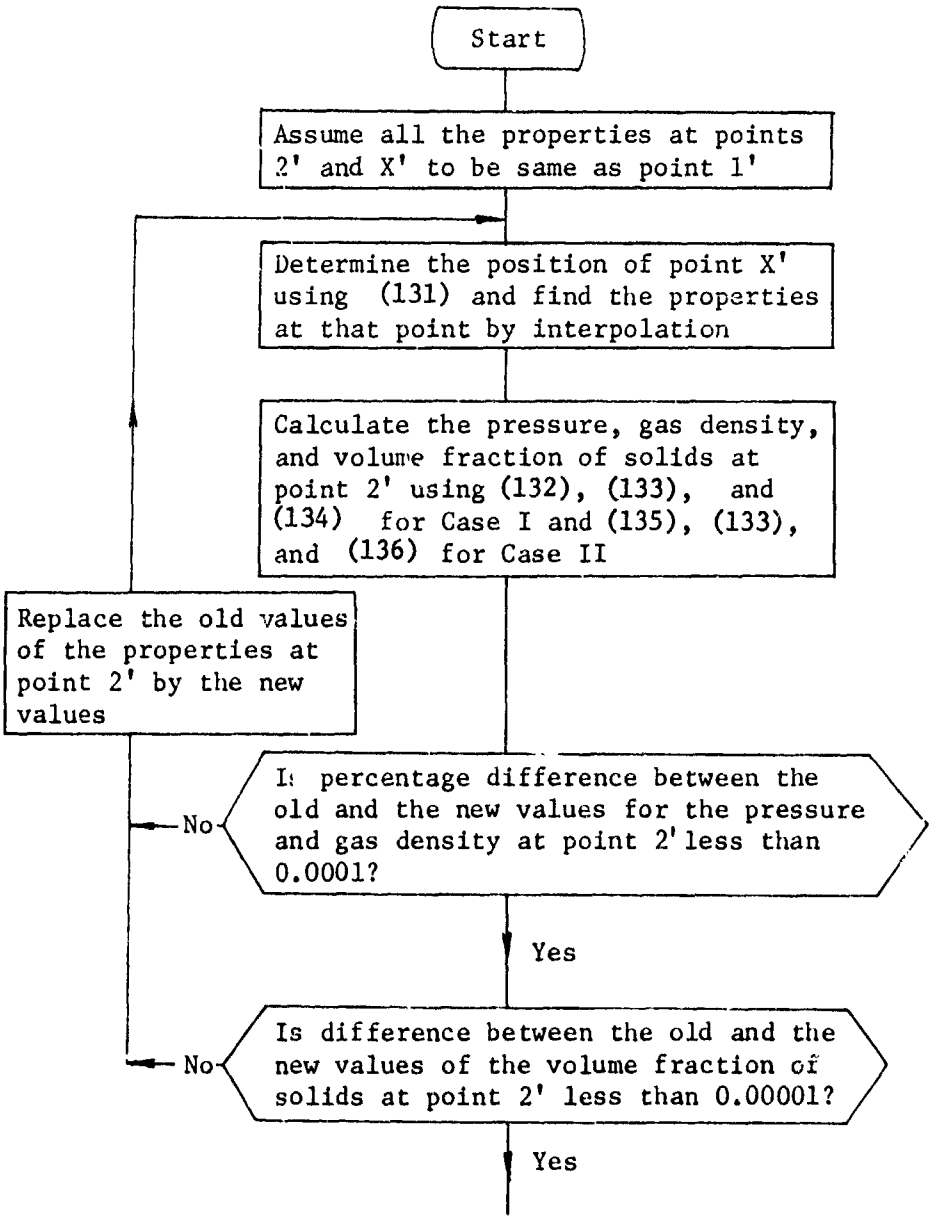

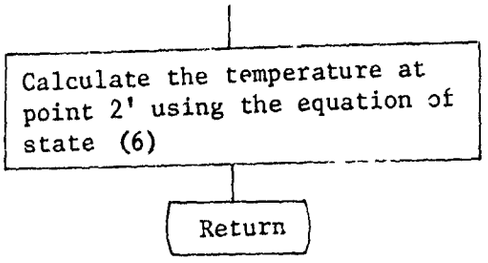
Calculate the temperature at point 2' using the equation of state (6)
Return

Subroutine HTW

The purpose of the subroutine is to calculate the wall temperature at a particular station along the length of the tube at time $t+\Delta t$, knowing the temperature distribution at the present time t, and the mean heat transfer coefficient h_m over the time interval Δt. In the following flow diagram, Δt is the time step selected in the main program whereas $\Delta\bar{t}$ is the time step selected in accordance with the stability condition for the temperature calculation.

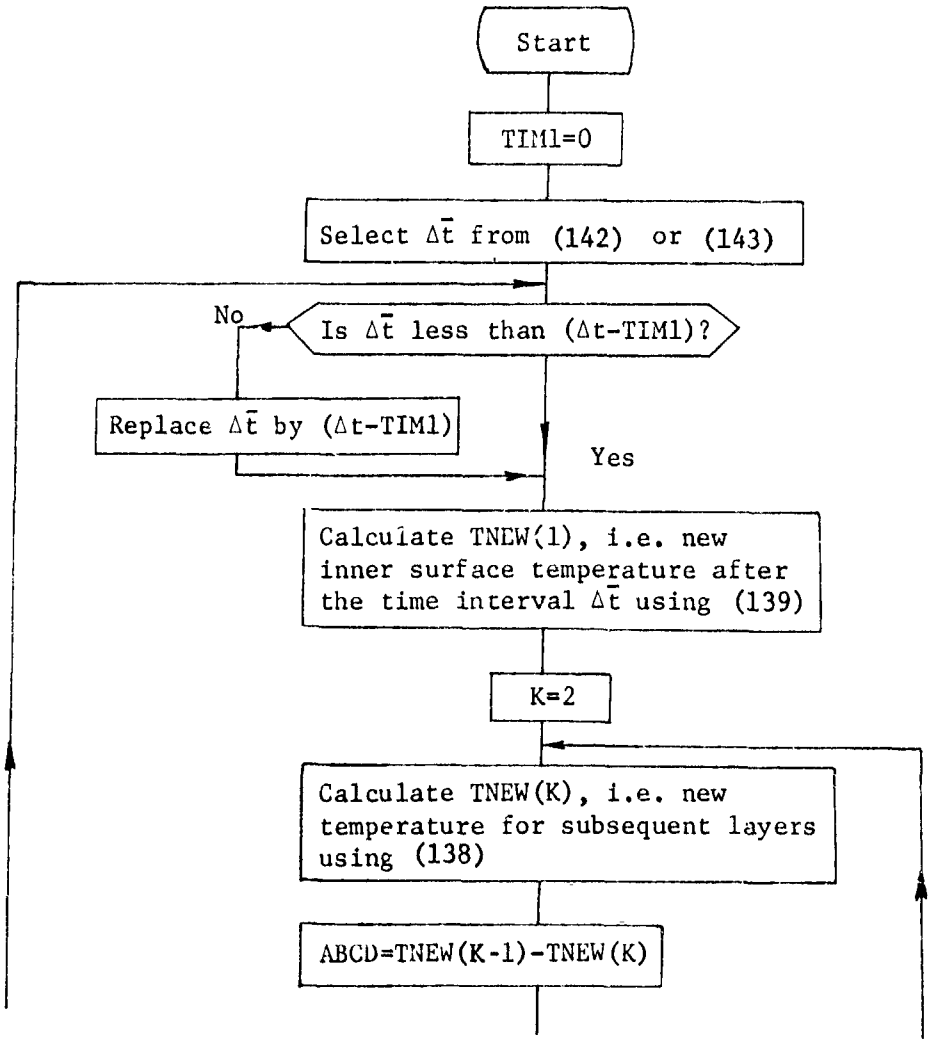

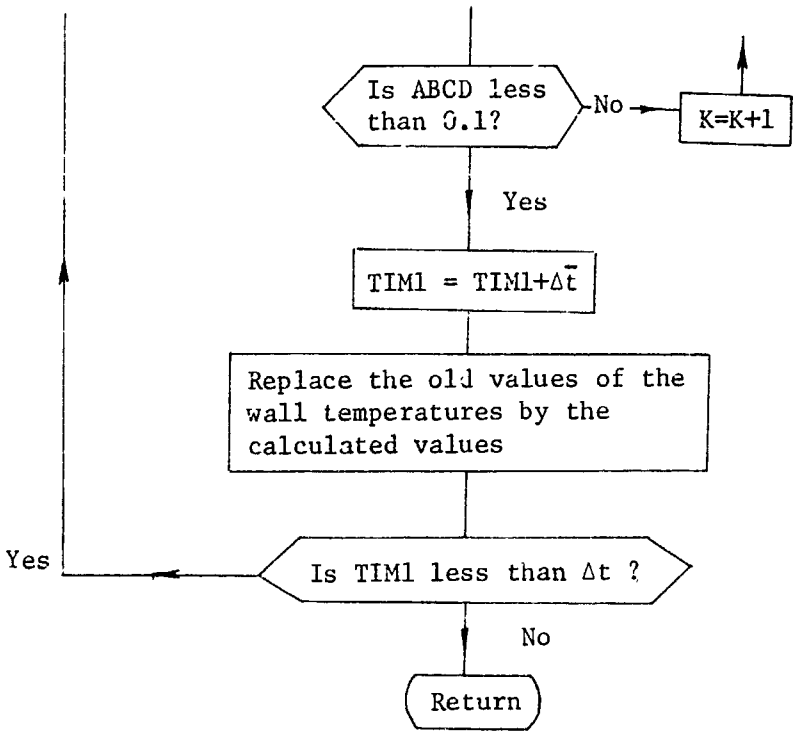
Is ABCD less than 0.1?
No
K=K+1
Yes
TIM1 = TIM1+Δt
Replace the old values of the wall temperatures by the calculated values
Yes
Is TIM1 less than Δt ?
No
Return

APPENDIX IV

SINGLE SHOT COMPUTER PROGRAM INPUT

Input Parameters

PR	-	Pressure at which experimental burning rates are input (nt/m^2)
BUR	-	Burning rate at PR pressure (m/sec)
TUBEL	-	Tube Length, also reference length (m)
XNI	-	Nondimensional projectile starting position
PI	-	Nondimensional axial tube step size
DIAT	-	Tube diameter (m)
MASSP	-	Projectile mass (kg)
PØ	-	Shot start pressure (nt/m^2)
TØ	-	Propellant flame temperature (°K)
RSP	-	Ratio of gas specific heats
WM	-	Propellant molecular weight
ETA	-	Co-volume of gases (m^3/kg)
DENS	-	Propellant solid density (kg/m^3)
CHARØ	-	Initial propellant mass (kg)
BETAS	-	Zero
WEBT	-	Propellant web thickness (m)
MN	-	Gas viscosity at TØ
CPG	-	Specific heat of gas (kcal/kg -°K)
CØNG	-	Thermal conductivity of gas at TØ (kcal/m -sec-°K)
H	-	Boundary layer velocity profile parameter, for one seventh profile = 1.2857

B	-	Ludwig - Tillman friction factor parameter = 0.286
RØUT	-	Tube outside radius (m)
RIN	-	Tube inside radius (m)
DELR	-	Tube wall radial step size for numerical conduction solution (m)
DIFFU	-	Thermal diffusivity of metal (m^2/sec)
CØNDUC	-	Metal thermal conductivity (kcal/m - sec - °K)
TAMB	-	Ambient air temperature (°K)
HØ	-	Heat transfer coefficient for tube outside surface (kcal/m^2 - sec)
UNI	-	Zero
UNBI	-	Zero
PRNI	-	One
PRNBI	-	One
DENNI	-	One
DENNBI	-	One
TEMNI	-	One
TEMNI	-	One

All data is to be input in format form to conform with read and format statements as follows. An example is also shown.

```
    READ 199, (PR(IJ)), BUR(IJ), IJ = 1,20)
199 FORMAT (4(E12.2, F8.3,)
    READ 20C, TUBE2, XN , PI, DIAT, MASSP
200 FORMAT (5F16.4)
    READ 201, PØ, TØ, RSP, WM, ETA
201 FØRMAT (E16.3, F16.1, F16.4, F16.2, F16.6)
    READ 202, DENS, CHARØ, BETAS, WEBT
202 FORMAT (F10.1, 2F10.3, F10.2)
    READ 203, MU, CPG, CØNG, H, B
203 FØRMAT (5F16.7)
    READ 204, RØUT, DELR, DIFFU, CØNDUC, TAMB,HØ
204 FØRMAT  (6F13.7)
    READ 101, UNi(1), UNBI, PRNI(1), PRNB1, DENN1(1),
    DENNBI, TEMN1(1), TEMNB1
101 FØRMAT (8F9.2)
```

Input Data

```
        1         2         3         4         5         6         7         8
        0         0         0         0         0         0         0         0
 20.68E+5  .00330   34.46E+5  .00508   48.25E+5  .00711   68.93E+5  .00965
103.39E+5  .01320  137.86E+5  .01727  172.32E+5  .02057  206.78E+5  .02438
275.71E+5  .03048  344.64E+5  .03683  413.57E+5  .04369  551.43E+5  .05588
689.28E+5  .06858 1378.57E+5  .11684 2067.86E+5  .17018 2757.14E+5  .21082
3446.43E+5 .24384 4825.00E+5  .30988 6892.86E+5  .40132 13785.71E+5 .63500
      2.0000            .1250             .005              .0300          .3260
   202.650E+5           3000.0            1.2520             24.00        .000950
  1670.0     0.172     0.000 0.0007110
     .00007              .412             .000034           1.2857          0.268
  0.03          0.00002         .0000126      .0138      300.0           0.0
  0.00      0.00      1.00      1.00      1.00      1.00      1.00      1.00
```

APPENDIX V

SINGLE SHOT COMPUTER PROGRAM LISTING

```
      DIMENSION UN1(201),PRN1(201),DENN1(201),TEMN1(201),VFS1(201),
     1PR1(201),BUR(201),B1(201),C1(201),DM1(201),UNCAR(201),UN2(201),
     2PRN2(201),DENN2(201),TEMN2(201),VFS2(201),U2E(201),PR2E(201),
     3DEN2E(201),VF2E(201),B2E(201),C2E(201),DM2E(201),U2E2(201),
     4PR2E2(201),DEN2E2(201),VF2E2(201),MTK1(201),MT2E(201),MT2E2(201),
     5MTK2(201),AMTK(201),H1(201),H2(201),TEMM(201,51),REMI(201),
     6E1(201),E2E(201),DENF1(201),DENF2(201),DEN2F(201),DEN2F2(201),
     7RIMF(201)
      DIMENSION HP(4,500),TG(4,500)
      COMMON /MCDEF/DENNS,TBETA,      RIAV
      COMMON /MBPWPC/RSP,ETADO
      COMMON /MBPWP/DIN,PI,PRN1,UN1,DENN1,VFS1,DSV,BUM6,BUM7,
     1H1,REMT,B,DENF1
      COMMON /MBP/PRNB1,DENNB1,UNB1,UNB2,XN1,XN2,    VFSB1
      COMMON /MRAUT/TIMEP(500),TWX1(600),TWX2(600),TWX3(600),TWX4(600),
     1TIMESP(6),JM(6),XWM(51),TWM(6,51)
      COMMON /MBPR/KT
      COMMON /MHTW/ANN,L,RIN,ROUT,DELR,DIFFU,CONDUC,HI,HO,TAMB,DT
      COMMON /MHBPWP/TO,TEMN1,TEMM
      REAL MASSP,MTK1,MT2E,MT2E2,MTK2,MU,MUL,MB
  199 FORMAT(4(E12.2,F8.5))
  200 FORMAT(5E16.4)
  201 FORMAT(E16.3,F16.1,F16.4,F16.2,F16.6)
  202 FORMAT(E10.1,2E10.3,E10.7)
  203 FORMAT(5F16.7)
  204 FORMAT(6E13.7)
  209 FORMAT(17H     MOLECULAR WT=,F6.1,22H     RATIO OF SP.HEATS=,F6.4,/)
  210 FORMAT(11H      TUBLE=,F4.1,10HM      XN1=,F5.4,8H      PI=,F5.4,11H
     1      DIAT=,F5.4,11HM     MASSP=,F5.3,13H KG     COVOL=,F8.7,7HCU.M/K
     2G10H PRANDTL =,F6.4,/)
  211 FORMAT(11H          PO=,E8.4,23HNEWTON PER SQM    DENGO=,F6.2,17HKG P
     1ER CU.M    TO=,F6.1,15HDEG K     UNITV=,F6.1,19HM PER SEC     TIMEC=,
     2F7.5,3HSEC/)
  212 FORMAT (12H      CHARGE=,F6.3,21H KG     WEB THICKNESS=,F6.5,21H M
     1   SOLID DENSITY=,F7.1,22H KG/CU.M     POTENTIAL=,F10.2,8H KCAL/KG/
     2/)
  218 FORMAT(24H  G.VISCOSITY(REF.TEMP)=,F8.6,17HKG/M-SEC- GAS CP=,F6.4,
     21HKCAL/KG-K   GAS COND=,F9.7,23HKCAL/M-SEC-K SHAPE FAC=,F5.3,/)
  219 FORMAT(13H  METL.DIFFU=,F10.8,20HSQM/SEC  METAL COND=,F8.6,23HKCAL
     1/M-SEC-K   AMB.TEMP=,F6.1,5HDEG K/)
  213 FORMAT (//10H TIME(ND)=,F9.6,15H    SOL BY MASS=,F8.6,14H  AV.PRESS
     1URE=,F10.6,18H    PISION VEL(ND)=,F9.6,12H  HEAT LOSS=,F9.6,/)
  214 FORMAT (115H  DIST(ND)  VEL(ND)   PRESS(ND)  SOL BY VOL  GAS D(ND)
     1  MIX D(ND)  TEMP(ND)  M THICK(ND) REYNOLD NO H.T.COEF  TWALL)
  215 FORMAT (7F11.6)
  216 FORMAT (7F11.6,F11.7,2E10.4,F10.2)
  101 FORMAT(8F9.2)
   77 FORMAT(3G16.9)
  250 FORMAT(/7H  TIME=,F8.6,13HSEC  PRO.VEL=,F8.1,15HM/SEC  PRO.K.E=,
     1F8.2,20HKCAL   INPUT ENERGY=,F8.2,22HKCAL   BALLISTIC EFF=,F8.5)
  220 FORMAT(5F15.7)
      READ 199,(PR(IJ),BUR(IJ),IJ=1,20)
      READ 200, TUBEL,XN1,PI,DIAT,MASSP
      READ 201, PO,TO,RSP,WM,ETA
      READ 202, DENS,CHARO,BETAS,WEBT
      READ 203, MU,CPG,CONG,H,B
      READ 204, ROUT,DELR,DIFFU,CONDUC,TAMB,HO
      READ 101,UN1(1),UNB1,PRN1(1),PRNB1,DENN1(1),DENNB1,TEMN1(1),TEMNB1
```

```
      AREAB=2*CHARO/(DENS*WEBT)
      N=XN1/PI+0.0001
      AREAP=3.14159*(DIAT**2)/4.
      RU=8314./WM
      UNITV=SQRT(PO*ETA+RU*TO)
      TIMEC=TUBEL/UNITV
      DENGO=1./(ETA+RU*TO/PO)
      VT=AREAP*XN1*TUBEL
      VFSI=(CHARO/VT-DENGO)/(DENS-DENGO)
      DO 500 I=1,N
  500 VFS1(I)=VFSI
      VFSB1=VFSI
      DENNS=DENS/DENGO
      ETADO=ETA*DENGO
      TEMS=300.
      TBETA=TEMS*BETAS
      RATIOA=AREAB/AREAP
      HVS=RU*TO/((RSP-1)*4184.)
      RTAV=4184.*DENGO*HVS/PO
      CALV=HVS
      RIN=DIAT/2.
      NN=(ROUT-RIN)/DELR+0.000001
      I=NN+1
      DO 251 I=1,201
      DO 251 J=1,50
  251 TEMM(I,J)=TAMB
      DO 252 I=1,N
      MTK1(I)=0.
      AMTK(I)=0.
      REMT(I)=0.
  252 H1(I)=0.
      QT=0.
      PRNDTL=MU*CPG/CONG
      A=0.123/(10.0**(0.678*H))
      BUM=(1./(RIN*UNITV*DENGO))**B
      BUM1=((1+B)*A/H)*(TUBEL/RIN)*BUM
      BUM2=2*A*BUM
      BUM3=DENGO*CPG*UNITV/(2*(PRNDTL**(2./3.)))
      BUM4=1./(1.+B)
      WRITE(6,217) BUM4
  217 FORMAT (F15.6)
      BUM5=DENGO*UNITV*RIN
      BUM6=2*A*(TUBEL/RIN)
      BUM7=2.*4184.0*TUBEL/(PO*UNITV*RIN)
      WRITE(6,210) TUBEL,XN1,PI,DIAT,MASSP,ETA,PRNDTL
      WRITE(6,209) WM,RSP
      WRITE(6,211) PO,DENGO,TO,UNITV,TIMEC
      WRITE(6,212) CHARO,WEBT,DENS,CALV
      WRITE(6,218)MU,CPG,CONG,H
      WRITE(6,219)DIFFU,CONDUC,TAMB
      DO 1 IX=2,N
      UN1(IX)=UN1(1)+(UNB1-UN1(1))*(IX-1)/N
      PRN1(IX)=PRN1(1)+(PRNB1-PRN1(1))*(IX-1)/N
      DENN1(IX)=DENN1(1)+(DENNB1-DENN1(1))*(IX-1)/N
    1 TEMN1(IX)=TEMN1(1)+(TEMNB1-TEMN1(1))*(IX-1)/N
      M=N
      TIME1=0.
      TIMEW=0.
      KI=1
      TIMES=0.2
      IK=0
C     CALCULATION OF AVERAGE CHAMBER PRESSURE AND BURNING RATE
    5 PDUM1=PRN1(1)
```

```
      KK=M-1
      DO 105 I=2,KK
  105 PDUM1=PDUM1+PRN1(I)
      AVPRH=(PDUM1*PI+PRN1(M)*(XN1-(M-1)*PI))/XN1
      PDUM2=PRN1(2)
      DO 106 I=3,M
  106 PDUM2=PDUM2+PRN1(I)
      AVPRL=(PDUM2*PI+PRN1*(XN1-(M-1)*PI))/XN1
      AVPRN=(AVPRH+AVPRL)/2.
      VDUM1=VFS1(1)
      DO 107 I=2,KK
  107 VDUM1=VDUM1+VFS1(I)
      TSVH=VDUM1*PI+VFS1(M)*(XN1-(M-1)*PI)
      VDUM2=VFS1(2)
      DO 108 I=3,M
  108 VDUM2=VDUM2+VFS1(I)
      TSVL=VDUM2*PI+VFS1*(XN1-(M-1)*PI)
      TSV=(TSVH+TSVL)/2.
      PROPM=DENS*AREAP*TUBEL*TSV/CHARQ
      IF (M.LT. 13) GO TO 73
      TG(2,KT)=TEMN1(13)*TO
      GO TO 72
   73 TG(2,KT)=TEMNB1*TO
   72 HP(2,KT)=H1(13)
      IF (M .LT. 26) GO TO 700
      TG(1,KT)=TEMN1(26)*TO
      GO TO 701
  700 TG(1,KT)=TEMNB1*TO
  701 HP(1,KT)=H1(26)
      TIMEP(KT)=TIME1*TIMEC
      IF (M .LT. 84) GO TO 702
      TG(3,KT)=TEMN1(84)*TO
      GO TO 703
  702 TG(3,KT)=TEMNB1*TO
  703 HP(3,KT)=H1(84)
      IF (M .LT. 142) GO TO 705
      TG(4,KT)=TEMN1(142)*TO
      GO TO 706
  705 TG(4,KT)=TEMNB1*TO
  706 HP(4,KT)=H1(142)
      TWX1(KT)=TEMM(16,1)
      TWX2(KT)=TEMM(26,1)
      TWX3(KT)=TEMM(51,1)
      TWX4(KT)=TEMM(101,1)
      IF (TIME1-TIMES) 560,561,561
  561 IK=IK+1
      TIMESP(IK)=TIME1*TIMEC
      DO 623 IJ=1,51
      TWM(IK,IJ)=TEMM(26,IJ)
  623 XWM(IJ)=(IJ-1)*0.02
      JM(IK)=M
      TIMES=TIMES+0.2
  560 IF(TIME1-TIMEW)370,371,371
  371 WRITE(6,213) TIME1,PROPM,AVPRN,UNB1,QT
      PRINT 214
      DO 90 IX=1,M,5
      X=(IX-1)*PI
      DM1(IX)=VFS1(IX)*DENNS+(1-VFS1(IX))*DENN1(IX)
      IF (IX.EQ.1) GO TO 89
      WRITE(6,216) X,UN1(IX),PRN1(IX),VFS1(IX),DENN1(IX),DM1(IX),
     1TEMN1(IX),AMTK(IX),REMT(IX),H1(IX),TEMM(IX,1)
      GO TO 90
   89 WRITE(6,215)X,UN1(IX),PRN1(IX),VFS1(IX),DENN1(IX),DM1(IX),
```

```
     1TEMN1(IX)
   90 CONTINUE
      DMB1=VFSB1*DENNS+(1-VFSB1)*DENNA1
      WRITE(6,215) XN1,UNB1,PRNB1,VFSB1,DENNB1,DMB1,TEMNB1
      TIMEW=TIMEW+0.025
C     SELECTION OF NEW TIME INCREAMENT
  370 DO 2 I=1,M
      RTMF(I)=2*TO*TEMN1(I)/(TO*TEMN1(I)+TEMN(I,1))
      DENE1(I)=RTMF(I)*DENN1(I)/(1.+EIADO*DENN1(I)*(RTMF(I)-1.1)
      CALL COEF(PRN1(I),DENN1(I),VFS1(I),B1(I),C1(I),DM1(I),DUM1,DUM2,
     1E1(I))
    2 UNCAR(I)=UN1(I)+SQRT(B1(I)/DM1(I))
      CALL COEF(PRNB1,DENNB1,VFSB1,BB1,CB1,DMB1,DUM1,DUM2,EB1)
      UNCARB=UNB1+SQRT(BB1/DMB1)
      UMAX=UNCAR(1)
      DO 12 I=2,M
      IF (UMAX-UNCAR(I))11,12,12
   11 UMAX=UNCAR(I)
   12 CONTINUE
      IF (UMAX-UNCARB)13,14,14
   13 UMAX=UNCARB
   14 DTN=PI/UMAX
      DT=DTN*TUBEL/UNITV
      KP=1
      AVPR1=AVPRN*PO
      AVPR2=AVPR1
  120 AVPR=(AVPR1+AVPR2)/2.
      DO 17 IJ=1,20
      IF (AVPR-PR(IJ))18,18,17
   17 CONTINUE
   18 BURD=BUR(IJ-1)+(BUR(IJ)-BUR(IJ-1))*(AVPR-PR(IJ-1))/(PP(IJ)-
      PR(IJ-1))
      BURN=BURD/UNITV
      IF(TSV.LE.0.) GO TO 360
      DSV=RATIOA*BURN/TSV
      GO TO 361
  360 DSV=0.
C  CALCULATION OF NEW PISTON POSITION,ITS VELOCITY AND GAS PROPS AT BASE
  361 ACCL=PO*PRNB1*AREAP/MASSP
      DELS=UNB1*UNITV*DT+ACCL*(DT**2)/2.
      DELSN=DELS/TUBEL
    6 XN2=XN1+DELSN
      UNB2=UNB1+ACCL*DT/UNITV
      CALL BP(PB,DEB,TEB,VSB)
      PNEW=(PRNB1+PB)/2.
      ACNEW=PO*PNEW*AREAP/MASSP
      DNEW=(UNB1*UNITV*DT+ACNEW*(DT**2)/2.)/TUBEL
      IF((ABS(DNEW-DELSN)/DELSN)-0.0001)20,20,25
   25 DELSN=DNEW
      ACCL=ACNEW
      GO TO 6
   20 XN2=XN1+DNEW
      UNB2=UNB1+ACNEW*DT/UNITV
      PRNB2=PB
      DENNB2=DEB
      TEMNB2=TEB
      VFSB2=VSB
C  CALCULATION OF GAS PROPERTIES AT TUBE HEAD END
      UN2(1)=0.
      MTK2(1)=0.
      CALL WP(PRN2(1),DENN2(1),TEMN2(1),VFS2(1))
C    CALCULATION FOR INTERIOR POINTS START
      U2E(1)=UN1(1)-DTN*UN1(1)*(UN1(2)-UN1(1))/PI-DTN*(PRN1(2)-PRN1(1))/
```

```
     1(DM1(1)*PI)
      DEN2E(1)=DENN1(1)-DTN*UN1(1)*(DENN1(2)-DENN1(1))/PI-DTN*DENN1(1)*
     1(UN1(2)-UN1(1))/((1-VFS1(1))*PI)+DTN*(DENNS-DENN1(1))*VFS1(1)*DSV/
     2(1-VFS1(1))
      PR2E(1)=PRN1(1)-DTN*UN1(1)*(PRN1(2)-PRN1(1))/PI-DTN*B1(1)*(UN1(2)-
     1UN1(1))/PI+C1(1)*DSV*VFS1(1)*DTN
      VF2E(1)=VFS1(1)-DTN*UN1(1)*(VFS1(2)-VFS1(1))/PI-DTN*VFS1(1)*
     1(UN1(2)-UN1(1))/PI-DTN*DSV*VFS1(1)
      IF (VF2E(1).LE.0.) VF2E(1)=0.
      CALL COEF(PR2E(1),DEN2E(1),VF2E(1),B2E(1),C2E(1),DM2F(1),DUM1,
     1DUM2,E2E(1))
      MT2E(1)=0.
      XI=XN1/PI
      J=XI+0.00001
      IF(ABS(XI-J)-0.00001)50,50,51
   50 UN1(J+1)=UNB1
      PRN1(J+1)=PRNB1
      DENN1(J+1)=DENNB1
      VFS1(J+1)=VFSB1
      MTK1(J+1)=0.
      H1(J+1)=0.
      RTMF(J+1)=2*TO*TEMNB1/(TO*TEMNB1+TAMB)
      DENF1(J+1)=RTMF(J+1)*DENN1(J+1)/(1.+ETADO*DENN1(J+1)*(RTMF(J+1)-1.
     1))
   51 DO 30 IX=2,J
      MUL=MU*SQRT((TO*TEMN1(IX)+TEMM(IX,1,))/(2*TO))
      MB=MUL**B
      IF(REMT(IX).LE.0.) GO TO 6000
      ULOSSF=BUM6*DENF1(IX)*(UN1(IX)**2.)/(DM1(IX)*(REMT(IX)**B))
      PGAINF=BUM6*E1(IX)*DENF1(IX)*(UN1(IX)**3.)/(REMT(IX)**B)
      GO TO 6001
 6000 ULOSSF=0.
      PGAINF=0.
 6001 U2E(IX)=UN1(IX)-DTN*UN1(IX)*(UN1(IX+1)-UN1(IX))/PI-DTN*(PRN1(IX+1)
     1-PRN1(IX))/(DM1(IX)*PI)-ULOSSF*DTN
      IF (U2E(IX).LE.0.) U2E(IX)=0.
      DEN2E(IX)=DENN1(IX)-DTN*UN1(IX)*(DENN1(IX+1)-DENN1(IX))/PI-DTN*
     1DENN1(IX)*(UN1(IX+1)-UN1(IX))/((1-VFS1(IX))*PI)+DTN*(DENNS-
     2DENN1(IX))*VFS1(IX)*DSV/(1-VFS1(IX))
      DEN2F(IX)=RTMF(IX)*DEN2E(IX)/(1+ETADO*DEN2E(IX)*(RTMF(IX)-1))
      PR2E(IX)=PRN1(IX)-DTN*UN1(IX)*(PRN1(IX+1)-PRN1(IX))/PI-DTN*B1(IX)*
     1(UN1(IX+1)-UN1(IX))/PI+C1(IX)*VFS1(IX)*DSV*DTN-DTN*BUM7*E1(IX)*
     2H1(IX)*(TO*TEMN1(IX)-TEMM(IX,1))+DTN*PGAINF
      VF2E(IX)=VFS1(IX)-DTN*UN1(IX)*(VFS1(IX+1)-VFS1(IX))/PI-DTN*
     1VFS1(IX)*(UN1(IX+1)-UN1(IX))/PI-DTN*DSV*VFS1(IX)
      IF (VF2E(IX).LE.0.) VF2E(IX)=0.
      CALL COEF(PR2E(IX),DEN2E(IX),VF2E(IX),B2E(IX),C2E(IX),DM2E(IX),
     1DUM1,DUM2,E2E(IX))
      U2E2(IX)=UN1(IX)-DTN*U2E(IX)*(U2E(IX)-U2E(IX-1))/PI-DTN*(PR2E(IX)-
     1PR2E(IX-1))/(DM2E(IX)*PI)-ULOSSF*DTN
      DEN2E2(IX)=DENN1(IX)-DTN*U2E(IX)*(DEN2E(IX)-DEN2E(IX-1))/PI-DTN*
     1DEN2E(IX)*(U2E(IX)-U2E(IX-1))/((1-VF2E(IX))*PI)+DTN*(DENNS-
     2DEN2E(IX))*VFS1(IX)*DSV/(1-VF2E(IX))
      DEN2F2(IX)=RTMF(IX)*DEN2E2(IX)/(1+ETADO*DEN2E2(IX)*(RTMF(IX)-1))
      PR2E2(IX)=PRN1(IX)-DTN*U2E(IX)*(PR2E(IX)-PR2E(IX-1))/PI-DTN*
     1B2E(IX)*(U2E(IX)-U2E(IX-1))/PI+C2E(IX)*DSV*VFS1(IX)*DTN-DTN*BUM7*
     2E2E(IX)*H1(IX)*(TO*TEMN1(IX)-TEMM(IX,1))+DTN*PGAINF
      VF2E2(IX)=VFS1(IX)-DTN*U2E(IX)*(VF2E(IX)-VF2E(IX-1))/PI-DTN*
     1VF2E(IX)*(U2E(IX)-U2E(IX-1))/PI-DTN*DSV*VFS1(IX)
      UN2(IX)=(U2E(IX)+U2E2(IX))/2.
      IF(UN2(IX).LE.0.) UN2(IX)=0.
      DENN2(IX)=(DEN2E(IX)+DEN2E2(IX))/2.
      PRN2(IX)=(PR2E(IX)+PR2E2(IX))/2.
```

```
      VFS2(IX)=(VF2E(IX)+VF2E2(IX))/2.
      IF (VFS2(IX).LE.0.) VFS2(IX)=0.
   30 TEMN2(IX)=PRN2(IX)*(1-ETADO*DENN2(IX))/(DENN2(IX)*(1-ETADO))
      XP=XN2/PI
      K=XP
      MM=J+1
      MN=K+1
      DO 80 IX=MM,MN
      UN2(IX)=UN2(J)+(UNB2-UN2(J))*(IX-J)*PI/(XN2-(J-1)*PI)
      PRN2(IX)=PRN2(J)+(PRNB2-PRN2(J))*(IX-J)*PI/(XN2-(J-1)*PI)
      DENN2(IX)=DENN2(J)+(DENNB2-DENN2(J))*(IX-J)*PI/(XN2-(J-1)*PI)
      VFS2(IX)=VFS2(J)+(VFSB2-VFS2(J))*(IX-J)*PI/(XN2-(J-1)*PI)
      IF (VFS2(IX).LE.0.) VFS2(IX)=0.
   80 TEMN2(IX)=PRN2(IX)*(1-ETADO*DENN2(IX))/(DENN2(IX)*(1-ETADO))
      M=K+1
      IF(KP.EQ.2) GO TO 100
      PDUM3=PRN2(1)
      KM=M-1
      DO 110 I=2,KM
  110 PDUM3=PDUM3+PRN2(I)
      AVPRH=(PDUM3*PI+PRN2(M)*(XN2-(M-1)*PI))/XN2
      PDUM4=PRN2(2)
      DO 111 I=3,M
  111 PDUM4=PDUM4+PRN2(I)
      AVPRL=(PDUM4*PI+PRNB2*(XN2-(M-1)*PI))/XN2
      AVPR2=PO*(AVPRH+AVPRL)/2.
      KP=2
      GO TO 120
  100 DO 31 IX=2,J
      MUL=MU*SQRT((TO*TEMN1(IX)+TEMM(IX,1))/(2*TO))
      MB=MUL**B
      IF (UN1(IX).LE.0.001) GO TO 1200
      U=(U2E(IX)-UN1(IX))/UN1(IX)
      UP=8.0*(U+DTN*((PRN1(IX+1)-PRN1(IX))/(DENF1(IX)*UN1(IX)*PI)+
     1(UN1(IX+1)-UN1(IX))/PI))
      GO TO 1201
 1200 U=0.
      UP=0.
 1201 MT2E(IX)=MTK1(IX)-DTN*UN1(IX)*(MTK1(IX+1)-MTK1(IX))/(H*PI)+BUM1*
     1MB*DTN*(UN1(IX)**(1-B))/(DENF1(IX)**B)-(1+B)*MTK1(IX)*(DTN*((H+2)*
     2(UN1(IX+1)-UN1(IX))/(H*PI)+UN1(IX)*(DENF1(IX+1)-DENF1(IX))/(H*PI*
     3DENF1(IX)))+U+(DEN2F(IX)-DENF1(IX))/DENF1(IX))+(1+B)*MTK1(IX)*UP
      IF(MT2E(IX).LE.0.) MT2E(IX)=0.
      IF (U2E(IX).LE.0.001) GO TO 1300
      UU=(U2E2(IX)-UN1(IX))/U2E(IX)
      UK=8.0*(UU+DTN*((PR2E(IX)-PR2E(IX-1))/(DEN2F(IX)*U2E(IX)*PI)+
     1(U2E(IX)-U2E(IX-1))/PI))
      GO TO 1301
 1300 UU=0.
      UK=0.
 1301 MT2E2(IX)=MTK1(IX)-DTN*U2E(IX)*(MT2E(IX)-MT2E(IX-1))/(H*PI)+BUM1*
     1MB*DTN*(U2E(IX)**(1-B))/(DEN2F(IX)**B)-(1+B)*MT2E(IX)*(DTN*((H+2)*
     3(U2E(IX)-U2E(IX-1))/(H*PI)+U2E(IX)*(DEN2F(IX)-DEN2F(IX-1))/(H*PI*
     4DEN2F(IX)))+UU+(DEN2F2(IX)-DENF1(IX))/DEN2F(IX))+(1+B)*MT2E(IX)*UK
      IF(MT2E2(IX).LE.0.)MT2E2(IX)=0.
   31 MTK2(IX)=(MT2E(IX)+MT2E2(IX))/2.
      DO 81 IX=MM,MN
   81 MTK2(IX)=MTK2(J)-MTK2(J)*(IX-J)*PI/(XN2-(J-1)*PI)
      DO 600 I=2,M
      MUL=MU*SQRT((TO*TEMN2(I)+TEMM(I,1))/(2*TO))
      MB=MUL**B
      IF(MTK2(I).LT.0.) WRITE(6,217) MTK2(I)
      AMTK(I)=MTK2(I)**BUM4
```

```
      IF(I.GT.MM) RTMF(I)=2*TO*TEMN2(I)/(TEMN2(I)*TO+TEMM(I,1))
      DENF2(I)=RTMF(I)*DENN2(I)/(1+ETADO*DENN2(I)*(RTMF(I)-1))
      IF(DENF2(I).LE.0.) WRITE(6,77) DENF2(I),RTMF(I),DENN2(I)
      REMT(I)=BUM5*DENF2(I)*UN2(I)*AMTK(I)/MUL
      IF(REMT(I).LE.0.) GO TO 401
      FRIF=2*A/(REMT(I)**B)
      GO TO 402
  401 FRIF=0.
  402 H2(I)=BUM3*DENF2(I)*UN2(I)*FRIF
      IF(I.GT.MM) H1(I)=0.
      H1=(H1(I)+H2(I))/2.
C     COMPUTATION OF HEAT LOSS IN TIME DELTA
      IF (I.EQ.2) GO TO 1000
      IF (I.EQ.MM) GO TO 1001
      IF (I.GT.MM) GO TO 1002
      Q1=2.*3.14159*RIN*PI*TUBEL*H1(I)*(TO*TEMN1(I)-TEMM(I,1))*DT
      GO TO 1003
 1000 Q1=2.*3.14159*RIN*(1.5*PI*TUBEL)*H1(2)*(TO*TEMN1(2)-TEMM(2,1))*DT
      GO TO 1003
 1001 Q1=2.*3.14159*RIN*TUBEL*(0.5*PI+(XN1-J*PI))*H1(I)*(TO*TEMN1(I)-
     1TEMM(I,1))*DT
      GO TO 1003
 1002 Q1=0.
 1003 QT=QT+Q1
      IF (I.GT.MM) GO TO 400
      CALL HTW(I)
  400 CONTINUE
C      REINITIALISATION
      TIME1=TIME1+DTN
      KT=KT+1
      XN1=XN2
      UNB1=UNB2
      PRNB1=PRNB2
      DENNB1=DENNB2
      VFSB1=VFSB2
      TEMNB1=TEMNB2
      DO 96 IX=1,M
      UN1(IX)=UN2(IX)
      PRN1(IX)=PRN2(IX)
      DENN1(IX)=DENN2(IX)
      VFS1(IX)=VFS2(IX)
      MTK1(IX)=MTK2(IX)
   96 TEMN1(IX)=TEMN2(IX)
      DO 53 I=2,M
   53 H1(I)=H2(I)
      IF (XN1-1.) 5,7,7
    7 WRITE(6,213) TIME1,PROPN,AVPRN,UNB1,QT
      PRINT 214
      DO 91 IX=1,M,5
      X=(IX-1)*PI
      DM1(IX)=VFS1(IX)*DENNS+(1-VFS1(IX))*DENN1(IX)
      IF (IX.EQ.1) GO TO 88
      WRITE(6,216) X,UN1(IX),PRN1(IX),VFS1(IX),DENN1(IX),DM1(IX),
     1TEMN1(IX),AMTK(IX),REMT(IX),H1(IX),TEMM(IX,1)
      GO TO 91
   88 WRITE(6,215)X,UN1(IX),PRN1(IX),VFS1(IX),DENN1(IX),DM1(IX),
     1TEMN1(IX)
   91 CONTINUE
      DMB1=VFSB1*DENNS+(1-VFSB1)*DENNB1
      WRITE(6,215) XN1,UNB1,PRNB1,VFSB1,DENNB1,DMB1,TEMNB1
      TG(2,KT)=TEMN1(13)*TO
      HP(2,KT)=H1(13)
      TIMEP(KT)=TIME1*TIMEC
```

```
      TG(1,KT)=TEMN1(26)*TO
      HP(1,KT)=H1(26)
      TG(3,KT)=TEMN1(84)*TO
      HP(3,KT)=H1(84)
      TG(4,KT)=TEMN1(142)*TO
      HP(4,KT)=H1(142)
      DO 709 JD=1,4
      DO 710 JK=1,KT
      WRITE (3) HP(JD,JK),TG(JD,JK),TIMEP(JK)
  710 CONTINUE
  709 CONTINUE
      TWX1(KT)=TEMM(16,1)
      TWX2(KT)=TEMM(26,1)
      TWX3(KT)=TEMM(51,1)
      TWX4(KT)=TEMM(101,1)
      WRITE(6,70) KT
   70 FORMAT(15)
      END

      SUBROUTINE COEF(PRF,DENG,VFS,B,C,D,G,H,E)
      COMMON /MCOEF/DENNS,TBETA,     RTAV
      COMMON /MBPWPC/RSP,ETADO
      D=DENG*(1-VFS)+DENNS*VFS
      ENS=PRE*(1-TBETA)/DENNS
      ENG=PRE*(RSP-ETADO*DENG)/(DENG*(RSP-1))
      Z=(1-VFS)*(1-ETADO*DENG)-(RSP-1)*VFS*TBETA
      B=RSP*PRE/Z
      C=(RSP*PRE*(DENNS-DENG)-(RSP-1)*DENNS*DENG*(ENG-ENS-RTAV))/(DENG*
     1Z)
      G=DENG/((1-VFS)*B)
      H=(RSP-1)*DENNS*DENG*(ENG-ENS-RTAV)/((1-VFS)*RSP*PRE)
      E=(RSP-1)/Z
      RETURN
      END

      SUBROUTINE BP(PR,DEN,TEM,VSM)
      COMMON /MBPWPC/RSP,ETADO
      COMMON /MBPWP/DTN,PI,PRN1(201),UN1(201),DENN1(201),VFS1(201),DSV,
     1BUM6,BUM7,HI(201),REMT(201),B,DENF1(201)
      COMMON /MBP/PRNB1,DENNB1,UNB1,UNB2,XN1,XN2,   VFSB1
      COMMON /MBPR/KT
      COMMON /MHBPWP/TO,TEMN1(201),TEMM(201,51)
      PR2=PRNB1
      DEN2=DENNB1
      VS2=VFSB1
      CALL COEF(PR2,DEN2,VS2,B2,C2,D2,G2,H2,E2)
      CALL COEF(PRNB1,DENNB1,VFSB1,BB1,CB1,DB1,GB1,HB1,EB1)
      SB1=VFSB1*(1-VFSB1)/DENNB1
      TB1=DB1/DENNB1
      PRX=PRNB1
      DENX=DENNB1
      UX=UNB1
      VSX=VFSB1
      DX=DB1
      BX=BB1
      CX=CB1
      EX=EB1
    5 DAV=(D2+DX)/2.
      BAV=(B2+BX)/2.
      UAV=(UNB2+UX)/2.
      IF (KT.EQ.1) GO TO 50
      IF (KT.GT.1) GO TO 52
   50 PRX=1.
```

```
      DENX=1.
      UX=0.
      VSX=VFSB1
      SKIN=0.
      GO TO 8
   52 DXN=(UAV+SQRT(BAV/DAV))*DTN
      XXN=XN2-DXN
      I=XN1/PI
      J=XXN/PI
      IF(I.EQ.J) GO TO 6
      IF(I.GT.J) GO TO 7
    6 PRX=PRN1(J+1)+(PRNB1-PRN1(J+1))*(XXN-J*PI)/(XN1-J*PI)
      DENX=DENN1(J+1)+(DENNB1-DENN1(J+1))*(XXN-J*PI)/(XN1-J*PI)
      UX=UN1(J+1)+(UNB1-UN1(J+1))*(XXN-J*PI)/(XN1-J*PI)
      VSX=VFS1(J+1)+(VFSB1-VFS1(J+1))*(XXN-J*PI)/(XN1-J*PI)
      JJ=J+1
      HIB=HI(J+1)
      TB=TEMN1(J+1)
      TW=TEMM(JJ,1)
      IF (REMT(JJ).LE.0.) GO TO 30
      SKIN=DENF1(JJ)*(UN1(JJ)**2.)/(REMT(JJ)**B)
      GO TO 8
   30 SKIN=0.
      GO TO 8
    7 PRX=PRN1(J+1)+(PRN1(J+2)-PRN1(J+1))*(XXN-J*PI)/PI
      DENX=DENN1(J+1)+(DENN1(J+2)-DENN1(J+1))*(XXN-J*PI)/PI
      UX=UN1(J+1)+(UN1(J+2)-UN1(J+1))*(XXN-J*PI)/PI
      VSX=VFS1(J+1)+(VFS1(J+2)-VFS1(J+1))*(XXN-J*PI)/PI
      JJ=J+2
      HIB=HI(J+2)
      TB=TEMN1(J+2)
      TW=TEMM(JJ,1)
      IF (REMT(JJ).LE.0.) GO TO 40
      SKIN=DENF1(JJ)*(UN1(JJ)**2.)/(REMT(JJ)**B)
      GO TO 8
   40 SKIN=0.
    8 CALL COEF(PRX,DENX,VSX,BX,CX,DX,DUM1,DUM2,EX)
      DAV=(D2+DX)/2.
      BAV=(B2+BX)/2.
      UAV=(UNB2+UX)/2.
      EAV=(EX+E2)/2.
      COEAV=(CX+C2)*(VSX+VFSB1)*DSV/4.
      PRNEW=PRX-DAV*SQRT(BAV/DAV)*(UNB2-UX)+DTN*COEAV-DTN*EAV*BUM7*HIB*
     1(TO*TB-TW)+DTN*BUM6*(EAV*UAV-SQRT(BAV/DAV))*SKIN
      GAV=(GB1+G2)/2.
      DCOE1=HB1*DSV*VFSB1
      DCOE2=H2*DSV*VFSB1
      DCOEAV=(DCOE1+DCOE2)/2.
      DENNEW=DENNB1+GAV*(PRNEW-PRNB1)+DTN*DCOEAV
      S2=VS2*(1-VS2)/DEN2
      T2=D2/DEN2
      SAV=(SB1+S2)/2.
      TAV=DSV*(TB1*VFSB1+T2*VFSB1)/2.
      VFSNEW=VFSB1+SAV*(DENNEW-DENNB1)-TAV*DTN
      IF (VFSNEW.LE.0.) VFSNEW=0.
      IF((ABS(PRNEW-PR2)/PR2)-0.0001)10,10,15
   10 IF((ABS(DENNEW-DEN2)/DEN2)-0.0001)11,11,15
   11 IF(ABS(VFSNEW-VS2)-0.00001)12,12,15
   15 PR2=PRNEW
      DEN2=DENNEW
      VS2=VFSNEW
      CALL COEF(PR2,DEN2,VS2,B2,C2,D2,G2,H2,E2)
      GO TO 5
```

```
12 PR=PRNEW
   DEN=DENNEW
   TLM=PR*(1-ETADO*DEN)/(DEN*(1-ETADO))
   VSM=VFSNEW
   RETURN
   END

   SUBROUTINE WP(PW2,DW2,TW2,VFSW2)
   COMMON /MBPWPC/RSP,ETADO
   COMMON /MBPWP/DEN,PI,PRN1(201),UN1(201),DENN1(201),VFS1(201),DSV,
  1BUM6,BUM7,HI(201),REMT(201),B,DENE1(201)
   COMMON /MHBPWP/TO,TEMN1(201),TEMM(201,51)
   PR2=PRN1(1)
   DEN2=DENN1(1)
   VS2=VFS1(1)
   CALL COEF(PR2,DEN2,VS2,B2,C2,D2,G2,H2,E2)
   CALL COEF(PRN1(1),DENN1(1),VFS1(1),B1,C1,D1,G1,H1,E1)
   SW1=VFS1(1)*(1-VFS1(1))/DENN1(1)
   TW1=D1/DENN1(1)
   PRX=PRN1(1)
   DENX=DENN1(1)
   VSX=VFS1(1)
   BX=B1
   CX=C1
   DX=D1
   EX=E1
   UX=0.
10 DAV=(DX+D2)/2.
   BAV=(BX+B2)/2.
   UAV=UX/2.
   DXN=(SQRT(BAV/DAV)-UAV)*DTN
   X=DXN/PI
   I=X+1
   PRX=PRN1(I)+(PRN1(I+1)-PRN1(I))*((X+1)-I)
   DENX=DENN1(I)+(DENN1(I+1)-DENN1(I))*((X+1)-I)
   UX=UN1(I)+(UN1(I+1)-UN1(I))*((X+1)-I)
   VSX=VFS1(I)+(VFS1(I+1)-VFS1(I))*((X+1)-I)
   CALL COEF(PRX,DENX,VSX,BX,CX,DX,DUM1,DUM2,EX)
   DAV=(D2+DX)/2.
   BAV=(B2+BX)/2.
   UAV=UX/2.
   EAV=(EX+E2)/2.
   COEAV=(CX+C2)*(VSX+VFS1(1))*DSV/4.
   IF (REMT(2).LE.0.) GO TO 40
   SKIN=DENE1(2)*(UN1(2)**2.)/(REMT(2)**B)
   GO TO 15
40 SKIN=0.
15 PRNEW=PRX-DAV*SQRT(BAV/DAV)*UX+DTN*COEAV-DTN*EAV*BUM7*HI(2)*
  1(TO*TEMN1(2)-TEMM(2,1))+DTN*BUM6*(EAV*UAV+SQRT(BAV/DAV))*SKIN
   GAV=(G1+G2)/2.
   DCOE1=H1*DSV*VFS1(1)
   DCOE2=H2*DSV*VFS1(1)
   DCOAV=(DCOE1+DCOE2)/2.
   DENNEW=DENN1(1)+GAV*(PRNEW-PRN1(1))+DTN*DCOAV
   SW2=(1-VS2)*VS2/DEN2
   TW2=D2/DEN2
   SAV=(SW1+SW2)/2.
   TAV=DSV*(TW1*VFS1(1)+TW2*VFS1(1))/2.
   VFSNEW=VFS1(1)+SAV*(DENNEW-DENN1(1))-TAV*DTN
   IF (VFSNEW.LE.0.) VFSNEW=0.
   IF((ABS(PRNEW-PR2)/PR2)-0.0001)5,5,6
 5 IF((ABS(DENNEW-DEN2)/DEN2)-0.0001)7,7,6
 7 IF(ABS(VFSNEW-VS2)-0.00001)8,8,6
```

```
    6 PR2=PRNEW
      DEN2=DENNEW
      VS2=VFSNEW
      CALL COEF(PR2,DEN2,VS2,B2,C2,D2,G2,H2,E2)
      GO TO 10
    8 PW2=PRNEW
      DW2=DENNEW
      TW2=PW2*(1-ETADO*DW2)/(DW2*(1-ETADO))
      VFS2=VFSNEW
      RETURN
      END

      SUBROUTINE HTW(I)
      DIMENSION TNEW(51)
      COMMON /MHTW/IM,L,RIN,ROUT,DELR,DIFFU,CONDUC,HI,HO,TAMB,DT
      COMMON /MHBPWP/TO,TEMN1(201),TEMM(201,51)
      HINNER=HI
      TIM1=0.
      DTT1=(DELR**2.)/(2.*DIFFU*(HINNER*DELR/CONDUC+1.+DELR/(2.*RIN)))
      DTT2=(DELR**2.)/(2.*DIFFU*(HO*DELR/CONDUC+1.-DELR/(2.*ROUT)))
      DTT=DTT1
      IF(DTT-DTT2)5,5,6
    6 DTT=DTT2
    5 IF(DTT-(DT-TIM1))15,15,16
   16 DTT=DT-TIM1
   15 CHNT=2.*DIFFU*DTT/(DELR**2.)
      TNEW(1)=(1.-CHNT*(HI*DELR/CONDUC+1.+DELR/(2.*RIN)))*TEMM(I,1)+
     1CHNT*HI*DELR*TO*TEMN1(I)/CONDUC+CHNT*(1.+DELR/(2.*RIN))*TEMM(I,2)
      K=2
   10 TNEW(K)=(1-CHNT)*TEMM(I,K)+CHNT*(0.5+DELR/(4.*(RIN+(K-1)*DELR)))*
     1TEMM(I,K+1)+CHNT*(0.5-DELR/(4.*(RIN+(K-1)*DELR)))*TEMM(I,K-1)
      ABCD=TNEW(K-1)-TNEW(K)
      IF (ABCD .LT. 0.1) GO TO 8
      K=K+1
      IF(K.GT.NN) GO TO 8
      GO TO 10
    8 TIM2=TIM1+DTT
   17 TIM1=TIM2
      DO 7 M=1,K
    7 TEMM(I,M)=TNEW(M)
```

APPENDIX VI

REPETITIVE FIRE COMPUTER PROGRAM LISTING

This program requires input, from the single shot program, of heat transfer coefficient (HP) and gas temperature (TG) as a function of time after propellant ignition (TIMEP) at a particular x location. It calculates barrel temperatures at that x location as a function of time for repeated firings assuming HP and TG are the same for each cycle. A cyclic time of 0.060 second is taken. All units are in the metric system (meter, kilograms, seconds, kilocalorie, ^{o}Kelvin)

```
2*          DIMENSION ABA(16)/3.19422,6.3105,9.4409,12.576,15.7136,18.8519,21
3*         1,99081,25.1300,28.26952,31.40917,34,54895,37,6888,40.82873,43.9687
4*         21,47.10875,50.24981/
5*          DIMENSION AAP(5,301)
6*          COMMON /ZL/ AAM,AAN,CONDUC,HO,DELR
7*          DIMENSION A1(5000),A2(5000),A3(10,301),A4(10)
8*          DIMENSION AAN(20,301)
9*          READ 300, RIN,ROUT,DELR,DIFFU,CONDUC,HO,KTMAX
10*       300 FORMAT(6F12.6,I5)
11*         TAMB=300.
12*         NN=(ROUT-RIN)/DELR+0.000001
13*         L=NN+1
14*           1 DO 2 I=1,L
15*           2 TEMM(I)=TAMB
16*         JK=1
17*           4 DO 3 J=1,KTMAX
18*         READ(3) HP(J),TG(J),TIMEP(J)
19*           3 CONTINUE
20*         JK=JK+1
21*         IF (JK.EQ. 2) GO TO 4
22*        98 IPT=1
23*         TIME1=0.
24*         KD=1
25*         KE=1
26*         KR=1
27*          91 KT=1
28*         KP=1
29*           9 IF(KT.GE.KTMAX) GO TO 100
30*         IF (KD.EQ.1) GO TO 41
31*         IF (KR.NE. 10*KD) GO TO 202
32*          41 A1(KD)=TEMM(1)
33*         A2(KD)=TIME1
34*         KD=KD+1
35*          202 HI=(HP(KT)+HP(KT+1))/2.
36*         DT=TIMEP(KT+1)-TIMEP(KT)
37*        1000 TIM1=0.
38*         DTT1=(DELR**2.)/(2.*DIFFU*(HI     *DELR/CONDUC+1.+DELR/(2.*RIN)))
39*         DTT2=(DELR**2.)/(2.*DIFFU*(HO*DELR/CONDUC+1.-DELR/(2.*ROUT)))
40*         DTT=DTT1
41*         IF(DTT-DTT2)5,5,6
42*           6 DTT=DTT2
43*           5 IF(DTT-(DT-TIM1))15,15,16
44*          16 DTT=DT-TIM1
45*          15 CHNT=2.*DIFFU*DTT/(DELR**2.)
46*         TNEW(1)=(1.-CHNT*(HI*DELR/CONDUC+1.+DELR/(2.*RIN)))*TEMM(  1)+
47*          1CHNT*HI*DELR*TG(KT)     /CONDUC+CHNT*(1.+DELR/(2.*RIN))*TEMM(  2)
48*         K=2
49*           10 TNEW(K)=(1-CHNT)*TEMM(  K)+CHNT*(0.5+DELR/(4.*(RIN+(K-1)*DELR)))*
```

```
1*          SUBROUTINE RUM(B,AAJ)
2*          COMMON/RL/ AAI
3*          AB=22./(7.*180.)
4*          AAE=.7979/SQRT(B)
5*          AAF=1./(8*B)
6*          AAG=SIN((57.296*(B)-45)*AB)
7*          AAH=SIN((57.296*(B)+45)*AB)
8*          AAI=AAE*(AAH+AAF*AAG)
9*          AAJ=AAE*(AAG-AAF*AAH)
10*         RETURN
11*         END

1*          SUBROUTINE CUM(C,Z)
2*          COMMON /RL/A
3*          G=0.
4*          J=1
5*          D=1.
6*          E=1.
7*        1 F=((C/2.)**(2.*J))*(-E)*((-1.)**J)/D
8*          IF (ABS(F) .LT. 0.0001) GO TO 2
9*          J=J+1
10*         D=D*(J**2)
11*         E=E+(1./J)
12*         G=G+F
13*         GO TO 1
14*       2 Z=(2.*7./22.)*(A*(.57721+ALOG(C/2.))+G)
15*         RETURN
16*         END

1*          SUBROUTINE MUM(C)
2*          COMMON /RL/G
3*          J=1
4*          D=1.
5*          G=1.
6*        1 F=((C/2.)**(2*J))*((-1.)**J)/D
7*          IF (ABS(F).LT. 0.00001) GO TO 2
8*          J=J+1
9*          D=D*(J**2)
10*         G=G+F
11*         GO TO 1
12*       2 RETURN
13*         END

1*          SUBROUTINE TAI(TEMM,A,AAC,AAD)
2*          COMMON / YL/AAK
3*          COMMON /RL/ AZ
4*          DIMENSION TEMM(301),AAK(301)
5*          DO 10 J=1,301
6*          B=A*TEMM(J)/0.015
7*          IF (B .LE. 6) GO TO 20
8*          CALL RUM(B,AY)
9*          GO TO 30
10*      20 CALL MUM(B)
11*         CALL CUM(B,AY)
12*      30 AAK(J)=AZ/AAC-AY/AAD
13*      10 CONTINUE
14*         RETURN
15*         END
```

```
     1TEMM(  K+1)+CHNT*(0.5-DELR/(4.*(RIN+(K-1)*DELR)))*TEMM(  K-1)
      ABCD=TNEW(K-1)-TNEW(K)
      IF (ABCD .LT. 0.1) GO TO 8
      K=K+1
      IF(K.GT.NN) GO TO 80
      GO TO 10
   80 TNEW(K)=(1.-CHNT*(HO*DELR/CONDUC+1.-DELR/(2.*ROUT)))*TEMM(K)+CHNT*
     1HO*DELR*TAMB/CONDUC+CHNT*(1.-DELR/(2.*ROUT))*TEMM(K-1)
    8 TIM2=TIM1+DTT
      TIM1=TIM2
      IF (TNEW(1) .GT. TEMM(1)) GO TO 912
      KP=KP+1
      IF (KP .NE. 3) GO TO 912
      APKR=TEMM(1)
      A1(KD)=TEMM(1)
      A2(KD)=TIME1+TIM2-DTT
      KD=KD+1
      IF (IPT .NE. 10*KE) GO TO 912
      DO 913 LK=1,L
      A3(KE,LK)=TEMM(LK)
  913 CONTINUE
      A4(KE)=TIME1+TIM2-DTT
      KE=KE+1
  912 DO 7 M=1,K
    7 TEMM(M)=TNEW(M)
 1003 IF(TIM2.LT.DT) GO TO 5
      KT=KT+1
      KR=KR+1
      TIME1=TIME1+DT
      GO TO 9
  100 HI=0.
  910 WRITE (6,90) APKR
      TGAF=TG(KTMAX)
      DO 996 LK=1,L
      R(LK)=(LK-1)*DELR+RIN
      TEMM(LK)=TEMM(LK)-300.
      DO 996 KY=1,5
      AAP(KY,LK)=0.
  996 CONTINUE
      TIME2=0.06*IPT-TIME1
      AAS=DIFFU/((0.015)**2)
      DO 221 KZ=1,16
      TIME3=TIME2/3.
      TIME4=TIME3
      AAM=0.
      BA=ABA(KZ)
      IF (IPT.NE. 1) GO TO 20
      CALL PADA(R,BA,TEMM,KZ)
   20 CALL DADA (R,TEMM,KZ)
      AAR=(BA**2)*AAS
      DO 995 KY=1,3
      AAT=AAM*EXP(-AAR*TIME3)
      DO 997 J=1,301
      AAP(KY,J)=AAP(KY,J)+AAN(KZ,J)*AAT
  997 CONTINUE
      TIME3=TIME3+TIME4
  995 CONTINUE
  221 CONTINUE
      DO 914 KY=1,3
      IF (AAP(KY,301) .GT. 0.) GO TO 112
      BPK= -AAP(KY,301)
      GO TO 113
  112 BPK=0.
  113 A1(KD)=AAP(KY,1)+300.+BPK
      A2(KD)=TIME1+KY*TIME4
      KD=KD+1
```

```
116*        914 CONTINUE
117*         90 FORMAT(1H ,11E11.5)
118*            DO 998 LK=1,L
119*        998 TEMM(LK)=AAP(3,LK)+300.+BPK
120*            TIME1=TIME1+TIME2
121*            GO TO 11
122*        901 DTT1=(DELR**2.)/(2.*DIFFU*(HI     *DELR/CONDUC+1.+DELR/(2.*RIN)))
123*            DTT2=(DELR**2.)/(2.*DIFFU*(HO*DELR/CONDUC+1.-DELR/(2.*ROUT)))
124*            DTT=DTT1*.9
125*            IF(DTT-DTT2) 25,25,26
126*         26 DTT=DTT2*.9
127*         25 CHNT=2.*DIFFU*DTT/(DELR**2.)
128*            TNEW(1)=(1.-CHNT*(HI*DELR/CONDUC+1.+DELR/(2.*RIN)))*TEMM(  1)+
129*           1CHNT*HI*DELR*TGAF       /CONDUC+CHNT*(1.+DELR/(2.*RIN))*TEMM(  2)
130*            K=2
131*        210 TNEW(K)=(1-CHNT)*TEMM(  K)+CHNT*(0.5+DELR/(4.*(RIN+(K-1)*DELR)))*
132*           1TEMM(  K+1)+CHNT*(0.5-DELR/(4.*(RIN+(K-1)*DELR)))*TEMM(  K-1)
133*            ABCD=TNEW(K-1)-TNEW(K)
134*            IF (ABCD .LT. .01) GO TO 28
135*            K=K+1
136*            IF(K.GT.NN) GO TO 280
137*            GO TO 210
138*        280 TNEW(K)=(1.-CHNT*(HO*DELR/CONDUC+1.-DELR/(2.*ROUT)))*TEMM(K)+CHNT*
139*           1HO*DELR*TAMB/CONDUC+CHNT*(1.-DELR/(2.*ROUT))*TEMM(K-1)
140*         28 DO 27 M=1,K
141*         27 TEMM(M)=TNEW(M)
142*            TIME1=TIME1+DTT
143*            KD=KD+1
144*         99 IF (TIME1-IPT*0.06) 901,11,11
145*         11 IPT=IPT+1
146*            WRITE (6,90) TIME1,TEMM(1)
147*            WRITE (6,90) TEMM(301)
148*            IT1=ITIME(IT2,IT3)
149*            IF (IT2 .GT. 1.40E+6) GO TO 994
150*            IF (IPT.LE.100) GO TO 91
151*        994 WRITE (11) IPT,TIME1,KD,KE,KR
152*            WRITE (11) (A1(J),A2(J),J=1,KD)
153*            WRITE (11) ((A3(I,J),J=1,301),I=1,10)
154*            WRITE (11) (A4(I),I=1,10)
155*            WRITE (11) (TEMM(I),I=1,301)
156*            WRITE (11) ((AAN(I,J),J=1,301),I=1,15)
157*       9999 END
```

```
 1*          SUBROUTINE PADA(TEMM,A,SIGMA,KZ)
 2*          COMMON / YL/AAK
 3*          COMMON /ZL/ AAM,AAN,COND,HO,DELR
 4*          DIMENSION TEMM(301),AAK(301),AAN(20,301),SIGMA(301)
 5*          AAA=-(.7979)/SQRT(2*A)
 6*          AAB=3./(8*2*A)
 7*          AA=57.296*2*A
 8*          AB=22./(7.*180.)
 9*          AAC=(COND*A/.015)*AAA*(SIN((AA-45)*AB)+AAB*SIN((AA+45)*AB))+HO*(-
10*         1AAA)*(SIN((AA+45)*AB)+(AAB/3.)*SIN((AA-45)*AB))
11*          AAD=(COND*A/.015)*AAA*(SIN((AA-135)*AB)+AAB*SIN((AA-45)*AB))+HO*(-
12*         1AAA)*(SIN((AA-45)*AB)+(-AAB/3)*SIN((AA+45)*AB))
13*          IF (A.GT. 6.) GO TO 5
14*          CALL TAI(TEMM,A,AAC,AAD)
15*          GO TO 11
```

```
16*          5 DO 10 J=1,301
17*            B=A*TEMM(J)/.015
18*            AAE=.7979/SQRT(B)
19*            AAF=1./(8*B)
20*            AAG=SIN((57.296*(B)-45)*AB)
21*            AAH=SIN((57.296*(B)+45)*AB)
22*            AAI=AAE*(AAH+AAF*AAG)
23*            AAJ=AAE*(AAG-AAF*AAH)
24*            AAK(J)=AAI/AAC-AAJ/AAD
25*         10 CONTINUE
26*         11 AAL=(TEMM(301)**2/2.)*(AAK(301)**2)*(1+((HO*.015)/(COND*A))**2)-(
27*           1TEMM(1)**2/2.)*(AAK(1)**2)
28*            DO 30 J=1,301
29*            AAN(KZ,J)=AAK(J)/SQRT(AAL)
30*         30 CONTINUE
31*            RETURN
32*            END

 1*            SUBROUTINE DATA(TEMM,SIGMA,KZ)
 2*            COMMON /ZL/ AAM,AAN,COND,HO,DELR
 3*            DIMENSION TEMM(301),SIGMA(301),AAN(20,301),AAA(301)
 4*            DO 10 J=1,301
 5*       1    AAA(J)=TEMM(J)*AAN(KZ,J)*SIGMA(J)
 6*         10 CONTINUE
 7*            AAM=(1./2.)*(AAA(1)+AAA(301))
 8*            DO 20 J=2,300
 9*            AAM=AAM+AAA(J)
10*         20 CONTINUE
11*            AAM=DELR*AAM
12*         90 FORMAT(1H ,2E10.4)
13*            RETURN
14*            END
```

BIBLIOGRAPHY

1. Hunt, F. R. W. ed., Internal Ballistics, Philosophical Library, New York, 1951.

2. Corner, J. Theory of the Interior Ballistics of Guns, John Wiley & Sons, Inc., New York, 1950.

3. Brode, H. L. and Enstrom, J. E. "A Numerical Method for Calculating Interior Ballistics," AD-712-846, The RAND Corporation, Santa Monica, California, September 1970.

4. Love, A. E. H. and Pidduck, F. B., "The Lagrange Ballistic Problem," Philosophical Transaction of Royal Society (London), 222A, 1921-22, pp. 167.

5. Carriere, P., "The Method of Characteristics Applied to the Problem of Internal Ballistics," Proceedings of 7th International Congress of Applied Mechanics, London, 1948, pp. 139.

6. Ludwieg, H. and Tillmann, W., "Investigations of the Wall Shearing Stress in Turbulent Boundary Layers," NACA Technical Memorandum 1285, 1950.

7. Colburn, A. P., "A Method of Correlating Forced Convection Data and A Comparison with Fluid Friction," Transaction-American Institute of Chemical Engineers, 1933, pp. 174.

8. Vincenti, W. G. and Kruger, C. H., Introduction to Physical Gas Dynamics, John Wiley and Sons, Inc., New York, 1965, pp. 300-305.

9. Bergles, A. E., "Survey and Evaluation of Techniques to Augment Convective Heat and Mass Transfer," Progress in Heat and Mass Transfer, Vol. 1, Pergamon Press, Oxford and New York, 1969, pp. 405-406.

10. Tien, C. L., "Heat Transfer by a Turbulently Flowing Fluid-Solids Mixture in a Pipe," Journal of Heat Transfer, Transaction of the ASME, May 1961, pp. 183-188.

11. Depew, C. A. and Farber, L., "Heat Transfer to Pneumatically Conveyed Glass Particles of Fixed Size," Journal of Heat Transfer, Transaction of the ASME, May 1963, pp. 164-172.

12. Simpson, A. V., et. al., "Heat and Mass Transfer in Dispersed, Two-Phase, Single-Component Flow," International Journal of Heat and Mass Transfer, Vol. 12, Pergamon Press, Oxford, 1969, pp. 1141-1155.

13. Reshotko, E. and Tucker, M., "Approximate Calculation of the Compressible Turbulent Boundary Layer with Heat Transfer and Arbitrary Pressure Gradient," NACA TN-4154, 1957.

14. Reynolds, W. C., "A Morphology of the Prediction Methods," Proceedings-Computation of Turbulent Boundary Layer-1968, AFOSR-IFP-STANFORD Conference, Vol. I, pp. 1-15.

15. Eckert, E. R. G. and Drake, R. M. Jr., Heat and Mass Transfer, 2nd ed., McGraw-Hill Book Company, Inc., 1959, pp. 31-32.

16. Lomax, H., "An Analysis of Finite Difference Technique Applied to Equation Governing Convective Transfer," Analytical Methods in Aircraft Aerodynamics, NASA SP-228, 1970, pp. 245-264.

17. Richtmyer, R. D. and Morton, K. W., Difference Methods for Initial Value Problem, 2nd ed., Chapter 12, Interscience Publishers (a division of John Wiley and Sons, Inc.), New York, 1967.

18. Holman, J. P., Heat Transfer, McGraw-Hill Book Company, Inc., New York, 1968, pp. 98-103.

19. Schneider, P. J., Conduction Heat Transfer, Chapter 12, Addison-Wesley Publishing Company, Inc., Massachusetts, 1955.

20. Heiney, D. K., "Analytical and Experimental Interior Ballistics of Closed Breach Guns", AFATL-TR-69-42, Air Force Armament Laboratory, Eglin Air Force Base, May 1969.

21. Schlichting, H., Boundary Layer Theory, 6th ed., McGraw-Hill Book Company, Inc., New York, 1968.

22. Bartz, D. R., "An Approximate Solution of Compressible Turbulent Boundary Layer Development and Convective Heat Transfer in Convergent Divergent Nozzles," Transaction of the ASME, Vol. 77, No. 8, 1955, pp. 1235-1245.

23. Kays, W. M., Convective Heat and Mass Transfer, McGraw-Hill Book Company, Inc., New York, 1966, pp. 95.

24. Daily, J. W. and Harleman, D. R. F., Fluid Dynamics, Addison-Wesley Publishing Company, Inc., Reading, Massachusetts, 1966, pp. 252.

25. Dahm, T. J. and Anderson, L. W., "Propellant Gas Convective Heat Transfer in Gun Barrels," Aerotherm Project 7028, Aerotherm Corporation, California, August 1970.

26. Wolff, R.O., "Reduction of Gun Erosion, Part II, Barrel Wear - Reducing Additive", Picatinny Arsenal Report 3096, August 1963

27 Remaly, R. and Stanley, T., "The Role of Titanium Dioxid in the Reduction of Gun Barrel Erosion", Report No. IITRI - C6090-8 (Technical Summary Report) Contract No. DA-28-017-AMC-3189(A), IIT Research Insitute, Technology Center, Chicago, Illinois, February 21, 1969.

28. Norton, E.S., "Analysis of Gun-Barrel Wear-Reducing Additives and Development of Improved Materials", C.I. Memorandum No. 199, Chemical Inspectorate, Headquarters Building, Royal Arsenal, London.

29. Lenchitz, C., "Same Aspects of the Erosion Reducing Characteristics of the Titanium Dioxide-Wax Additive", Picatinny Arsenal Technical Memorandum No. 1768, Propellants Laboratory, Picatinny Arsenal, Dover, N.J., November 1965.

30. Nelson, C.W. and Ward, J., "Unsteady Heat Transfer in Erosinity Experiments", BRL Memorandum Report No. 2176, Ballistic Research Laboratories, Aberdeen Proving Ground, Maryland, April 1972 .

31. Evans, R., Hom, F., Shapiro, Z, and Wagner, R., "The Chemical Erosion of Steel by Hot Gases under Pressure", NRDC contract OEMsr - 463 and W-36-034-ORD-4126, John Hopkins University, June, 1947.

32. Bowman, F., Introduction to Bessel Functions, Dover Publications, Inc., New York, N.Y., 1958.

33. Jakob, M., Heat Transfer, John Wiley & Son, Inc., New York, N.Y., 1949.

34. Nelson, C. W., and Ward, J. R., "Unsteady Heat Transfer in Erosivity Experiments", Memorandum Report No. 2176, U.S. Army Aberdeen Research and Development Center, Ballistic Research Laboratories, Aberdeen Proving Ground, Md.

35. Savins, J. G. and Virls, P. S., Co-editors, Drag Reductions, Chem. Eng. Prog. Symp. Series 111, 67, 1971.

36. Soo, S. L., Fluid Dynamics of Multiphase Systems, Blaisdell Publishing Co., Waltham, Mass. 1967.

37. Marble, F. E., "Dynamics of Dusty Gases", Annual Review of Fluid Mechanics, Vol. 2, 1970, pp. 397-446.

38. Boyce, M. P. and Blick, E. F., "Fluid Flow Phenomena Dusty Air", J. Basic Engineering, 1970, pp. 495.

39. Probstein, R. F. and Fassio, F., "Dusty Hypersonic Flows", AIAA J., 8, 772-779, 1970.

40. Farber, L. and Morley, M. J., "Heat Transfer to Flowing Gas-Solids Mixtures in a Circular Tube", Ind. and Eng. Chem., 1143-1150, 1957.

41. Tien, C. L., "Heat Transfer by a Turbulent Flowing Fluids-Solids Mixture in a Pipe," J. Heat Transfer, Vol.83, pp. 183-188, 1961.

42. Farber, L. and Depew, C. A., "Heat Transfer Effects to Gas-Solids Mixtures using Solid Spherical Particles of Uniform Size", I&EC Fundamentals, 2, 130-135, 1963.

43. Depew, C. A. and Farber L., "Heat Transfer to Pneumatically Conveyed Glass Particles of Fixed Size", J. Heat Transfer, (64-172, 1963.

44. Tien, C. L. and Quan, V., "Local Heat Transfer Characteristics of Air-Glass and Air-Lead Mixtures in Turbulent Pipe Flow", ASME Paper No. 62-HT-15, 1962.

45. Briller, R. and Peskin, R. L., "Gas Solids Suspension Convective Heat Transfer as a Reynolds Number of 130,000, J. Heat Transfer, 464-468, 1968.

46. Sco, S. L., "Gas-Solid Flow", Proc. of Symp. on Single and Multicomponent Flow Processes, Eng. Res. Pub. No. 45, Rutgers University, 1965.

47. Rossetti, S. J. and Pfeffer, R., "Drag Reduction in Dilute Flowing Gas-Solids Suspensions", AIChE J., 18, 31-39, 1972.

48. Brandon, C. A. and Grizzle, T. A., "A Test Similarity Variable for Dilute Fluid-Solid Heat Transfer", Proceedings of the International Symposium on Two-Phase Systems, Haifa, Israel, 1971.

49. Depew, C. A., "Heat Transfer to Flowing Gas-Solids Mixtures in a Vertical Circular Duct", Ph. D. Thesis, University of California, 1960.

50. Schluderberg, D. C., Whitelaw, R. L., and Carlson, R. W., "Gaseous Suspensions - A New Reactor Coolant", Nucleonics, 19, 67-76.

51. Woodcock, M. T. and Worley, N. G., "Gas-Solids Suspensions as Heat Transfer Media", Proceedings of the Symposium on High Pressure Gases a Heat Transport Medium, London, Inst. Mech. E., March 1967.

52. Remaly, R. and Stanley, T., "The Role of Titanium Dioxide in the Reduction of Gun Barrel Erosion," Report No. IITRI-C6090-8, February 1969.

53. Abel, W. T., Bluman, D. E., and O'Leary, J. P., "Gas-Solids Suspensions as Heat-Carrying Mediums," ASME Paper No. 63-WA-210 (1963).

54. Wolff, R. O., "Reduction of Gun Erosion, Part II, Barrel Wear-Reducing Additive", Picatinny Arsenal Report 3096, August 1963.

55. Ward, J. R., "Unsteady Heat Transfer in Erosion Experiments", BRL MR 2176, April 1972.

INITIAL DISTRIBUTION

Hq USAF (SAMID)	1	AFATL/DLDG	10
AFSC (DLTW)	1	AFATL/DLDL	30
AFSC (SDWM)	1		
ASD (ENYS)	1		
ASD (ENVW)	1		
FTD (PDXA)	1		
AFML (LNP)	1		
TAC (DRFM)	1		
TAC (DMAM)	1		
WRAMA (MMEBL)	1		
AEDC (ARO, INC.)	1		
AUL (AUL-LSE-70-239)	1		
CH R&D, ATTN: CRDAM	1		
Redstone Sci Info Ctr	2		
USA Wpns Comd (AMSWEREW)	1		
Army Matrl Sys Anal Agcy (AMXRD-AA)	1		
USA Aberdeen R&D Ctr (AMXRD-BTL)	2		
Picatinny Ars Attn: SMUPA-RT-S	1		
Nav Air Sys Cmd (Code AIR-350B)	2		
USN Wpns Lab (Code TR)	1		
USN Ord Lab (Code 730)	2		
Nav Ord Sta, Tech Lib	1		
Nav Sys Cen, Newprt Lab	1		
USNWC (Code 753)	2		
USNWC (Code 4585)	1		
USN Wpns Eval Fac (Code WE)	1		
57 Ftr Wpn Wg (FWOA)	1		
Off Ch Nav Opns	1		
USN Rsch Lab (Code 2027)	1		
Los Alamos Sci Lab	1		
Battelle Mem Inst	1		
Inst for Def Analyses	1		
Sandia Corp	2		
Rand Corp	1		
USAFTFWC (CRDC)	1		
Harry Diamond Lab	1		
DDC	2		
TAWC-AY	1		
Frankford ARS, Attn: LIB	1		
ASD (YFM)	10		
TRADOC/ADTC/DO	1		
ADTC/WE	1		
AFATL/DL	1		
AFATL/DLB	1		
AFATL/DLOSL	2		
AFATL/DLY	2		
AFATL/DLR	1		
	237		

(The reverse of this page is blank.)

UNCLASSIFIED

Security Classification

DOCUMENT CONTROL DATA - R & D

(Security classification of title, body of abstract and indexing annotation must be entered when the overall report is classified)

1 ORIGINATING ACTIVITY (Corporate author)

School of Mechanical Engineering
Georgia Institute of Technology
Atlanta, Georgia

2a. REPORT SECURITY CLASSIFICATION: Unclassified

2b. GROUP:

3 REPORT TITLE

STUDY OF HEAT TRANSFER AND EROSION IN GUN BARRELS

4 DESCRIPTIVE NOTES (Type of report and inclusive dates)

Final Report - 15 July 1970 to 15 July 1972

5 AUTHOR(S) (First name, middle initial, last name)

S. Shelton
A. Bergles
P. Saha

6 REPORT DATE: March 1973

7a. TOTAL NO OF PAGES: 248

7b. NO OF REFS: 54

8a. CONTRACT OR GRANT NO: F08635-70-C-0129

b. PROJECT NO: 670A

c. Task No. 02

d Work Unit No. 036

9a. ORIGINATOR'S REPORT NUMBER(S)

9b. OTHER REPORT NO(S) (Any other numbers that may be assigned this report): AFATL-TR-73-69

10 DISTRIBUTION STATEMENT

Distribution limited to U. S. Government agencies only; this report documents test and evaluation; distribution limitation applied March 1973 . Other requests for this document must be referred to the Air Force Armament Laboratory (DLDL), Eglin Air Force Base, Florida 32542.

11 SUPPLEMENTARY NOTES

Available in DDC

12 SPONSORING MILITARY ACTIVITY

Air Force Armament Laboratory
Air Force Systems Command
Eglin Air Force Base, Florida 32542

13 ABSTRACT

This study models the combustion, solid propellant movement, gas dynamics, projectile dynamics, transient boundary layer, heat transfer, and barrel metal temperatures in a gun barrel. This is accomplished by rigorous development of the coupled partial differential equations and carrying out a detailed numerical solution to these equations. Comparison of barrel temperature solutions to experimental data is shown. Erosion mechanisms are discussed in the light of these solutions. This model is then used to study hypotheses concerning the heat transfer, temperature, and erosion effects of submicron size solid particle additives (TiO_2) to gun propellants. A mechanism not previously studied offers excellent theoretical results in explaining the reduced erosion.

DD FORM 1 NOV 65 1473

UNCLASSIFIED

Security Classification

14 KEY WORDS	LINK A		LINK B		LINK C	
	ROLE	WT	ROLE	WT	ROLE	WT
Gun Barrel Heat Transfer						
Gun Barrel Erosion						